





**Développement de modèles d'apprentissage automatique guidés par la théorie en hydrogéologie**

**(Development of theory-guided machine learning models in hydrogeology)**

**Par**

**Adoubi Vincent De Paul Adombi**

**Sous la direction de Romain Chesnaux et Marie-Amélie Boucher**

**Thèse présentée à l'Université du Québec à Chicoutimi en vue de l'obtention du grade de  
Philosophiæ Doctor (Ph. D.) en Sciences de la Terre et de l'atmosphère**

Jury :

Julien Walter, Professeur, Ph.D., UQAC, Président du Jury

Jan Franklin Adamowski, Professeur, Ph.D., McGill University, Membre externe

Maxime Claprood, Professeur, Ph.D., UQAC, Membre interne

Romain Chesnaux, Professeur, Ph.D., UQAC, Directeur

Marie-Amélie Boucher, Professeure, Ph.D., Université de Sherbrooke, Co-directrice

Renée-Luce Simard, Professeur, Ph.D., UQAC, Directrice de programme

Québec, Canada

© Adoubi Vincent De Paul Adombi, Mars 2024

## RÉSUMÉ

La modélisation est l'approche couramment utilisée pour résoudre les problèmes d'hydrogéologie compte tenu de la nécessité de conceptualiser un monde souterrain invisible. Cependant, les approches traditionnelles de modélisation en hydrogéologie, c'est-à-dire la modélisation basée sur la physique, semi-empirique ou empirique, ont montré leurs limites dans la résolution des problèmes hydrogéologiques, soit parce qu'elles sont trop complexes à mettre en œuvre, qu'elles nécessitent beaucoup de données, qu'elles fournissent des modèles dont la justesse n'est pas toujours satisfaisante, soit parce que leur capacité à aider à comprendre les systèmes d'eaux souterraines ainsi que leur capacité d'aide à la prise de décision sont limitées.

Récemment, l'exploration du continuum entre les différentes approches traditionnelles de modélisation a récemment été initiée, donnant lieu à un nouveau paradigme appelé apprentissage automatique guidé par la théorie. L'apprentissage automatique guidé par la théorie (ou theory-guided machine learning, TgML en anglais) est un domaine de recherche qui se concentre sur le développement d'algorithmes d'apprentissage qui intègrent des éléments de connaissance scientifique (par exemple les lois de conservation de masse) dans leur architecture ou pendant leur entraînement.

Cette thèse a cherché à tester l'hypothèse selon laquelle les modèles d'apprentissage automatique guidés par la théorie peuvent bénéficier des forces combinées des approches traditionnelles de modélisation. Pour ce faire, des modèles d'apprentissage automatique guidés par la théorie ont été développés et testés sur des problèmes hydrogéologiques réels, et leurs performances ont été comparées à celles des approches traditionnelles de modélisation. Ceci a eu pour but d'identifier les forces et les faiblesses de l'apprentissage automatique guidé par la théorie et de proposer des solutions pour surmonter ces faiblesses dans le cadre de la modélisation hydrogéologique. La thèse s'est concentrée uniquement sur les problèmes d'écoulements distribués et localisés.

Dans le contexte de la modélisation distribuée, un modèle TgML a été développé et ses performances ont été comparées à celles d'un modèle à base physique et un modèle traditionnel d'apprentissage. Le modèle TgML présentait la meilleure justesse de simulation tout en obéissant à la physique qui régit les écoulements d'eau souterraine, ce qui exprime le fait que le modèle TgML est capable de fédérer les atouts individuels des approches traditionnelles de modélisation. En revanche, le modèle TgML a nécessité des coûts de calculs considérablement importants pour son entraînement comparativement à ceux du modèle à base physique et du modèle traditionnel d'apprentissage.

Dans le contexte de la modélisation localisée, Jiang et al. (2020) ont proposé la première approche de développement d'algorithmes TgML pour la modélisation localisée en hydrologie. Cette approche a ensuite été adaptée par Cai et al. (2022) à l'hydrogéologie pour la modélisation localisée de l'écoulement des eaux souterraines. Dans ce projet de recherche, les approches de Jiang et al. (2020) et de Cai et al. (2022) sont considérées comme des formulations traditionnelles de modèles TgML pour la modélisation localisée. Cette thèse a permis de montrer que les formulations traditionnelles de Jiang et al. (2020) et de Cai et al. (2022) ne permettent pas de construire des modèles TgML qui satisfont au principe de cause à effet entre les variables d'entrée et de sortie, indispensable à tout modèle. Une nouvelle formulation a ensuite été proposée dans cette thèse pour permettre aux modèles TgML d'apprendre des relations causales. Les modèles dérivés à partir de la

nouvelle formulation proposée dans cette thèse présentent des performances plus ou moins similaires à celles des modèles traditionnels d'apprentissage automatique et supérieures à celles de modèle dérivé selon la formulation de Jiang et al. (2020), tout en affichant des propriétés causales. Cependant, les coûts requis pour leur entraînement restent supérieurs à ceux des modèles traditionnels d'apprentissage automatique.

En résumé, l'hypothèse de recherche selon laquelle l'apprentissage automatique guidé par la théorie peut bénéficier des atouts des approches traditionnelles de modélisation a été vérifiée, à l'exception des coûts de calcul en phase d'entraînement, qui peuvent être beaucoup plus élevés.

## TABLE DES MATIÈRES

RÉSUMÉ .....	i
TABLE DES MATIÈRES .....	iii
LISTE DES TABLEAUX .....	vii
LISTE DES FIGURES .....	viii
DÉDICACE .....	xi
REMERCIEMENTS .....	xii
INTRODUCTION .....	1
CHAPITRE 1 .....	25
GÉNÉRALITE SUR L'APPRENTISSAGE AUTOMATIQUE .....	25
1.1    INTELLIGENCE ARTIFICIELLE ET APPRENTISSAGE AUTOMATIQUE .....	25
1.2    RÉSOUTRE UN PROBLÈME PAR L'APPRENTISSAGE AUTOMATIQUE .....	26
1.2.1    POSER LE PROBLÈME HYDROGÉOLOGIQUE .....	27
1.2.2    DU PROBLÈME D'HYDROGÉOLOGIE À UN PROBLÈME D'APPRENTISSAGE .....	28
1.2.3    CHOISIR UN ALGORITHME D'APPRENTISSAGE .....	30
1.2.4    ENTRAINER, ÉVALUER, SÉLECTIONNER UN MODÈLE .....	32
1.3    PROBLÈME DE RÉGRESSION ET RÉSEAUX DE NEURONES ARTIFICIELS .....	33
1.3.1    PROBLÈME DE RÉGRESSION .....	33
1.3.2    RÉSEAUX DE NEURONES ARTIFICIELS .....	38
RÉFÉRENCES .....	44
CHAPITRE 2 .....	47
THEORY-GUIDED MACHINE LEARNING APPLIED TO HYDROGEOLOGY: STATE OF THE ART, OPPORTUNITIES AND FUTURE CHALLENGES – A REVIEW .....	47
2.1    ABSTRACT .....	48
2.2    INTRODUCTION .....	49
2.3    THEORY-GUIDED MACHINE LEARNING VS MACHINE LEARNING LIMITING FACTORS IN HYDROGEOLOGY .....	55
2.3.1    THEORY-GUIDED CONSTRAINED OPTIMIZATION .....	55
2.3.2    THEORY-GUIDED ARCHITECTURE .....	61
2.3.3    THEORY-GUIDED REFINEMENT OF OUTPUTS .....	64
2.4    CHALLENGES OF THEORY-GUIDED MACHINE LEARNING METHODS .....	69
2.5    CONCLUSION .....	71
REFERENCES .....	73
CHAPITRE 3 .....	82

<b>COMPARING NUMERICAL MODELLING, TRADITIONAL MACHINE LEARNING AND THEORY-GUIDED MACHINE LEARNING IN INVERSE MODELING OF GROUNDWATER DYNAMICS: A FIRST STUDY CASE APPLICATION.....</b>	82
3.1 ABSTRACT .....	83
3.2 INTRODUCTION .....	84
3.3 STUDY AREA AND DATA.....	89
3.3.1 STUDY AREA.....	89
3.3.2 DATA .....	91
3.4 METHODS AND MODELS .....	93
3.4.1 NUMERICAL MODEL.....	93
3.4.2 MACHINE LEARNING MODELS.....	97
3.4.3 PERFORMANCE ASSESSMENT METRICS .....	108
3.5 RESULTS .....	108
3.5.1 MODEL CALIBRATION / TRAINING - VALIDATION.....	109
3.5.2 MODEL TESTING .....	113
3.5.3 CAPTURE OF GROUNDWATER DYNAMICS BY THE MODELS .....	114
3.5.4 EFFECTS OF PDE VIOLATION BY THE TGMLP MODEL .....	117
3.6 DISCUSSION .....	121
3.7 CONCLUSION .....	123
<b>REFERENCES.....</b>	126
<b>CHAPITRE 4.....</b>	131
<b>A CAUSAL PHYSICS-INFORMED DEEP LEARNING FORMULATION FOR GROUNDWATER FLOW MODELING AND CLIMATE CHANGE EFFECTS ANALYSIS .....</b>	131
4.1 ABSTRACT .....	133
4.2 INTRODUCTION .....	134
4.3 STUDY AREA AND DATA.....	138
4.3.1 STUDY AREA.....	138
4.3.2 DATA AND PROCESSING.....	139
4.4 METHODS.....	144
4.4.1 CONCEPTUAL HYDROLOGIC MODELS, DEEP LEARNING MODELS, TRADITIONAL THEORY-GUIDED DEEP LEARNING MODELS AND THE PROPOSED THEORY-GUIDED DEEP LEARNING MODELS .....	144
4.4.2 MODEL DEVELOPMENT .....	150
4.5 RESULTS .....	150
4.5.1 COMPARISON OF MODEL RESULTS .....	151
4.5.2 CLIMATE CHANGE EFFECT ANALYSIS .....	158
4.6 DISCUSSION .....	162

4.6.1	GENERAL DISCUSSION OF THE STUDY RESULTS.....	162
4.6.2	PREVIOUS STUDIES ON THE EFFECTS OF CLIMATE CHANGE ON GWL DEVELOPMENT IN NORTH AMERICA.....	164
4.7	CONCLUSION.....	166
<b>REFERENCES</b>		169
<b>CHAPITRE 5</b>		180
<b>DISCUSSIONS ET PERSPECTIVES DE RECHERCHE</b>		180
5.1	CONTRIBUTIONS ET IMPLICATIONS DU PROJET DE RECHERCHE .....	180
5.1.1	APPORT DE L'APPRENTISSAGE AUTOMATIQUE GUIDÉ PAR LA THÉORIE A LA MODÉLISATION HYDROGÉOLOGIQUE .....	180
5.1.2	ETUDE PRÉLIMINAIRE DE L'IMPACT DU CHANGEMENT CLIMATIQUE SUR L'EVOLUTION DES NIVEAUX D'EAU SOUTERRAINE AU QUÉBEC .....	182
5.2	LIMITES DU PROJET DE RECHERCHE ET RECOMMANDATIONS .....	182
5.2.1	MODÉLISATION DISTRIBUÉE ET APPRENTISSAGE AUTOMATIQUE GUIDÉ PAR LA THÉORIE .....	182
5.2.2	MODÉLISATION LOCALISÉE ET APPRENTISSAGE AUTOMATIQUE GUIDÉ PAR LA THÉORIE .....	185
5.2.3	ÉTUDE DE L'IMPACT DU CHANGEMENT CLIMATIQUE SUR LA RESSOURCE EN EAU SOUTERRAINE .....	186
5.3	AUTOMATIQUE GUIDÉ PAR LA THEORIE EN PRATIQUE .....	187
5.4	BRÈVE OUVERTURE SUR LES AVANTAGES TECHNIQUES DE L'APPRENTISSAGE AUTOMATIQUE GUIDÉ PAR LA THÉORIE PAR RAPPORT A LA MODÉLISATION NUMÉRIQUE	
	190	
<b>CONCLUSION</b>		194
<b>LISTE DE RÉFÉRENCES</b>		196
<b>ANNEXES</b>		233
<b>TOWARD A METHODOLOGY TO EXPLORE HISTORICAL GROUNDWATER LEVEL TRENDS AND THEIR ORIGIN: THE CASE OF QUEBEC, CANADA</b>		233
1.1	ABSTRACT .....	233
1.2	INTRODUCTION .....	234
1.3	METHODOLOGY .....	238
1.3.1	LOCAL GROUNDWATER LEVEL TRENDS: SITE SIGNIFICANCE .....	239
1.3.2	REGIONAL GROUNDWATER LEVEL TRENDS: FIELD SIGNIFICANCE .....	240
1.3.3	ORIGIN OF TRENDS: THE REFERENCE HYDROGRAPH METHOD .....	242
1.4	CASE STUDY: THE GROUNDWATER MONITORING NETWORK OF QUEBEC, CANADA	
	244	
1.4.1	STUDY AREA.....	244
1.4.2	GROUNDWATER MONITORING NETWORK AND DATA USED .....	246

1.5	RESULTS .....	248
1.5.1	LOCAL GROUNDWATER LEVEL TRENDS: SITE SIGNIFICANCE .....	249
1.5.2	REGIONAL GROUNDWATER LEVEL TRENDS: FIELD SIGNIFICANCE .....	251
1.5.3	ORIGIN OF THE TRENDS .....	252
1.6	DISCUSSION: LIMITATIONS OF THE PROPOSED METHODOLOGY AND FUTURE WORK	258
1.6.1	THE MANN-KENDALL TEST .....	259
1.6.2	EFFECTS OF CLIMATE VARIABLES ON GROUNDWATER LEVEL TRENDS ....	260
1.6.3	LIMITATIONS OF FIELD OBSERVATIONS .....	260
1.6.4	QUESTIONING THE BASIS OF THE REFERENCE HYDROGRAPH METHOD...	261
1.7	CONCLUSION.....	261
<b>REFERENCES</b> .....		265

## LISTE DES TABLEAUX

<b>Table 1</b> Some situations in which the theory-guided ML methods presented in this study may be applied. A dash indicates the absence of a supporting published study. ....	68
<b>Table 2</b> Comparison of efficiency of the different methods of theory-guided machine learning with respect to ML limiting factors. Question marks indicate an absence of available factual evidence. ....	68
<b>Table 3</b> Range of values of physical properties of hydrogeological layers. ....	92
<b>Table 4</b> Cross-correlation coefficients between groundwater levels at the six piezometers of the study area and the 30-day moving averages of precipitation and mean temperature.	106
<b>Table 5</b> Distribution of the number of observation wells by trend magnitude and aquifer type. UC: unconfined, SC: semi-confined, C: confined, UNK: unknown. Based on the absolute value of the slope, three trend categories have been defined: (1) stable when $ S  < 3 \text{ cm/year}$ , (2) moderate rate when $3 \text{ cm/year} \leq  S  < 10 \text{ cm/year}$ , and (3) significant rate when $ S  \geq 10 \text{ cm/year}$ .....	250
<b>Table 6</b> Analysis of residual hydrographs and corresponding field observations for the 18 observation wells with moderate to large trends .....	257

## LISTE DES FIGURES

<b>Figure 1</b> Flux de travail simplifié pour la résolution de problèmes par l'apprentissage automatique .....	27
<b>Figure 2</b> Topologie du perceptron multicouche et procédure d'apprentissage. Les données d'entrée et de sortie sont bidimensionnelles : la forme des données d'entrée est $(p, n)$ et celle des données de sortie est $(p, m)$ , où $p$ est le nombre d'exemples, $n$ est le nombre de variables d'entrée et $m$ est le nombre de variables de sortie. ....	40
<b>Figure 3</b> Topologie d'un réseau de neurones convolutifs simple. $p$ est le nombre d'exemples, $r$ est la longueur de la séquence de données et $n$ est le nombre de variables d'entrée. $m$ représente le nombre de variables de sortie. ....	41
<b>Figure 4</b> Exemple de topologie d'un réseau de neurones cyclique .....	43
<b>Figure 5</b> Part of the ML process modified by the TGCO method, that is, at the level of cost function (solid blue circle).....	58
<b>Figure 6</b> Example of theory-guided design of architecture by means of decomposition of a problem into theoretically related sub-problems in modelling groundwater flow. $R$ , $qw$ , $K$ , $Ss$ , $hx \pm \Delta xt$ , $hy \pm \Delta yt$ , $ht - 1$ , $ht$ , $ht$ represent respectively the recharge rate, pumping rate, hydraulic conductivity, storativity, hydraulic head in the neighbourhood of the point of interest, previous, current, and estimated hydraulic head at the point of interest. ....	63
<b>Figure 7</b> Part of the ML process modified by the TGRO method, that is, at the level of model outputs (solid blue oval circle) .....	67
<b>Figure 8</b> Geographic location of the study area, geological outcrops consisting of deltaic sediments, sands and gravels, clays, tills, rocks and location of the Valin River, Caribou River and tributaries of interest. Created in part from figures in Boumaiza et al. (2021)....	89
<b>Figure 9</b> Stratigraphic units, from the most superficial (S. Unit 1) to the deepest (S. Unit 4), each composed of a combination of at least three of the hydrogeological layers of coarse, medium and fine sands and clays. Location of the six monitored piezometers and seven pumping wells. ....	91
<b>Figure 10</b> Synthesis of the conceptual model used for the Saint-Honoré aquifer. ....	95
<b>Figure 11</b> The architecture of the (a) MLP and (b) TgMLP models and the corresponding learning process. The $\theta$ parameters of the neural networks need to be optimized; $\lambda$ is the learning rate and $\nabla LTOT\theta$ is the gradient of the cost function $LTOT$ . $t$ , $x$ , $y$ represent time and spatial coordinates respectively; $PMA30$ and $TMA30$ are the 30-day moving average of precipitation and mean temperature respectively; $\varphi sim$ is the groundwater level simulated. ....	103
<b>Figure 12</b> Summary of the methodology used for numerical model calibration, training and validation of machine learning models and their testing. ....	104
<b>Figure 13</b> (a) Convergence of total cost functions during learning as a function of epochs for the MLP model and (b) convergence of the components of the TgMLP total cost function. ....	110
<b>Figure 14</b> Comparison of observed groundwater levels in the four calibration/training piezometers ((a) LA-2, (b) Pz-16, (c) Pz-1 and (d) Pz-20) against groundwater levels simulated by the different models. ....	111
<b>Figure 15</b> Comparison of performance criteria ((a) percentage of normalized RMSE (b) Nash-Sutcliffe Efficiency) during the calibration/training stage. ....	111

<b>Figure 16</b> Comparison of observed and simulated groundwater levels in the two test piezometers ((a) Pz-18 and (b) Pz-21) by the different models.....	113
<b>Figure 17</b> Comparison of performance criteria ((a) percentage of normalized RMSE (b) Nash-Sutcliffe Efficiency) during the test stage.....	113
<b>Figure 18</b> Comparison of groundwater level fields over the entire study area between the numerical model (NumMod) and the TgMLP model and between the NumMod and the MLP model on 09/11/2016.....	115
<b>Figure 19</b> Comparison of groundwater level fields over the entire study area between the numerical model (NumMod) and the TgMLP model and between the NumMod and the MLP model on 04/11/2017.....	115
<b>Figure 20</b> Temporal evolution of the mean and standard deviation calculated on the differences of GWL simulated over the entire aquifer between the numerical model (NumMod) and the TgMLP model (a and c respectively) and between the NumMod and the MLP model (b and d respectively). .....	116
<b>Figure 21</b> Illustration of the spatial consistency of the GWL fields simulated by the TgMLP model with the conceptual model over time.....	117
<b>Figure 22</b> Distribution of the PDE residual given the GWL simulated by TgMLP at different dates. The red dotted line represents the physical inconsistency threshold set during TgMLP training. And at the top left of each figure is displayed the proportion of points where the residual is below the threshold (BT). .....	118
<b>Figure 23</b> The unobserved locations where the effects of PDE violation was examined .	119
<b>Figure 24</b> Illustration of GWLs at unobserved locations for different values of the absolute mean of the PDE residual. The threshold below which the PDE residual was considered acceptable to stop the training is 0.0125 m/d.....	120
<b>Figure 25</b> Location of the study area and the observation wells from the Quebec groundwater monitoring network, (a) the state of confinement of the aquifers observed by each well and (b) the geological nature of these aquifers. ....	140
<b>Figure 26</b> A schematic structure of the proposed formulation of hybrid algorithms. CRC stands for causal relationship constraints; $W_j$ is the $j - th$ component of the kernel (or weight) of a layer and $\sigma'$ is the derivative of the $\sigma$ activation function.....	150
<b>Figure 27</b> Performance of 15-member ensembles, each associated with one of the four algorithms (1D-CNN, H-HBVo, H-Lin and H-HBV), for all observation wells in each of the 6 clusters. Clusters C1 to C6 each contain 24, 6, 7, 11, 13 and 9 observation wells respectively. ....	152
<b>Figure 28</b> Groundwater levels observed and simulated by the four models, namely 1D-CNN, H-HBVo, H-Lin and H-HBV at observation well 02000002 during the testing stage. Further illustrations are provided in the Supplementary Material 2 (Adombi 2023e).....	154
<b>Figure 29</b> Impact of vertical inflow (vi) and potential evapotranspiration (ep) on groundwater levels using the SHAP summary plot for the four algorithms studied. Only the first 8 most decisive variables are shown. The number associated with each variable represents an observation well number in the cluster to which well 02000002 belongs. ....	155
<b>Figure 30</b> Computation time (CPU) required for a single model member per run in (a) the training stage and (b) the projection stage.....	157
<b>Figure 31</b> Mean change and associated standard deviation in vertical inflow and potential evapotranspiration based on trends from 2011 to 2090 over the entire study area. Trends	

were calculated using the TFPW-MK method, and the percentage of significant trends is indicated.....	159
<b>Figure 32</b> Change in groundwater levels over the period 2011 - 2090 for each well, for all 15-member H-HBV ensembles, for all RCP8.5 scenario simulations, based on trend analysis with the TFPW-MK method on projected GWLs: <b>a</b> 2.5% percentile, <b>b</b> mean and <b>c</b> 97.5% percentile. Each observation well is represented by a band which is a boxplot providing from bottom to top the minimum GWL change value, the 25% percentile value, the median, the 75% percentile and the maximum value. <b>d</b> Boxplots of the percentage of significant trends and (e) boxplots of significant changes in GWL for <b>a - c</b> . Note that the adoption of the 2.5% and 97.5% percentiles allows 95% of the uncertainties associated with the climate data and machine learning models used to be covered.....	160
<b>Figure 33</b> Change in groundwater levels over the period 2011 - 2090 for each well, for all 15-member H-HBV ensembles, for all SSP5-8.5 scenario simulations, based on trend analysis with the TFPW-MK method: <b>a</b> 2.5% percentile, <b>b</b> mean and <b>c</b> 97.5% percentile. <b>d</b> Boxplots of the percentage of significant trends and (e) boxplots of significant changes in GWL for <b>a - c</b> .....	162
<b>Figure 34</b> Flowchart of the methodology.....	243
<b>Figure 35</b> Location of the study area including the main cities.....	244
<b>Figure 36</b> Location of the groundwater level observation stations analyzed in this study, as well as (a) the state of confinement and (b) the nature of the geological material. The three observation wells that will be used as illustrations in the rest of this work are located by their identifiers .....	247
<b>Figure 37</b> Spatial distribution of trends in the monitoring network. Based on the absolute value of the slope, three trend categories can be defined: (1) stable when $ S  < 3 \text{ cm/year}$ , (2) moderate rate when $3 \text{ cm/year} \leq  S  < 10 \text{ cm/year}$ , and (3) significant rate when $ S  \geq 10 \text{ cm/year}$ . This classification is based on a combination of statistical and environmental significance criteria, developed by Environmental Reporting BC (2019) and used to focus further investigations on wells where trends are considered more critical ( $ S  > 3 \text{ cm/year}$ ). .....	249
<b>Figure 38</b> Bootstrap empirical cumulative distributions (BECD) of upward (a) and downward (b) trend numbers from the TFPW-MK method.....	251
<b>Figure 39</b> Spatial distribution of trends in (a) vertical inflow (vi) and (b) potential evapotranspiration (pe).....	253
<b>Figure 40</b> Spatial and temporal stability analysis of PCs. <b>(a)</b> Correlation of eigen vector based on the random subsampling of the measurement dates to assess the stability of spatial patterns. <b>(b)</b> Correlation of scores based on the random selection of observation wells, i.e. complete series, to assess the stability of temporal patterns.....	255
<b>Figure 41</b> (a) Time series of GWL and reference hydrograph for well 02000003 located near Gaspé (see <b>Figure 36</b> ). (b) Time series of residuals. The correlation of the observed series with the reference hydrograph and with the residuals is given by $R^2$ . The trend line and slope of the trend are also shown.....	256

## **DÉDICACE**

A mon frère cadet...

## REMERCIEMENTS

Je tiens à exprimer mes plus sincères remerciements et ma gratitude à mon superviseur, le Professeur Romain Chesnaux, et à ma co-superviseure, la Professeure Marie-Amélie Boucher, pour leurs conseils et suggestions, ainsi que pour le temps qu'ils m'ont consacré tout au long de mon aventure dans ce doctorat.

Je tiens également à remercier les organismes suivants pour leur contribution financière à mon projet de recherche :

- Le Conseil de recherche en sciences naturelles et en génie (CRSNG) du Canada pour l'appui financier accordé au Prof. Romain Chesnaux dans le cadre du programme de subvention individuelle à la découverte, qui a contribué à financer mon projet de recherche
- La Fondation de l'Université du Québec à Chicoutimi
- Rio Tinto par l'entremise de son programme de bourses d'études supérieures
- Les Fonds de recherche du Québec - Nature et Technologie, par le biais du programme des bourses d'excellence pour étudiants étrangers (PBEEE)

Je remercie tout spécialement le Ministère de l'Environnement, de la Lutte contre les changements climatiques, de la Faune et des Parcs (MELCCFP) et en particulier Nadine Roy, ingénierie au MELCCFP, pour ses suggestions lors de la rédaction de mon devis de recherche et tout au long de mon projet de recherche, ainsi que pour sa disponibilité. Je tiens à remercier le consortium Ouranos et ses membres Marco Braun, Juliette Lavoie et Rondeau-Genesse Gabriel pour les idées, les pistes de recherche et les données climatiques qu'ils ont fournies pour mon projet de recherche. Je souhaite remercier le groupe de recherche Risque Ressource Eau (R2Eau), qui a été pour moi une seconde école, où j'ai appris à vulgariser mes travaux de recherche et où j'ai également pu acquérir des notions dans des domaines plus ou moins éloignés de l'hydrogéologie ou de l'apprentissage automatique. Je ne saurais remercier le groupe R2Eau sans exprimer ma franche sympathie aux professeurs impliqués dans la bonne marche du groupe : Merci aux Professeurs Julien Walter, Ali Saedi, Alain Rouleau, Mathieu Fiset, Pierre Cousineau, Romain Chesnaux.

Mes remerciements vont également à l'endroit du Professeur Réal Daigneault, directeur des programmes des sciences de la Terre, pour le suivi de mon parcours de doctorat.

Je remercie tout particulièrement Son Excellence la très honorable Mary May Simon, Gouverneure générale du Canada, pour la Médaille d'Or académique que j'ai reçue.

Enfin, je tiens à exprimer ma gratitude à toutes les personnes qui de près ou de loin m'ont apporté leur soutien tout au long de cette riche expérience.

## INTRODUCTION

Les eaux souterraines s'écoulent à travers des matériaux géologiques suffisamment perméables appelés aquifères. Cet écoulement, conditionné par les propriétés physiques de l'aquifère, est également influencé par divers facteurs exogènes tels que l'extraction d'eau, l'utilisation des sols et la variabilité climatique à court et à long terme (Wu and Zeng 2013). Afin de comprendre la dynamique de l'écoulement des eaux souterraines et l'impact des facteurs exogènes sur cette dynamique, les hydrogéologues ont souvent recours à la modélisation.

La modélisation désigne toute approche visant à fournir une représentation plus ou moins simpliste des systèmes réels afin de mieux comprendre leur fonctionnement et, éventuellement, de prévoir leur évolution (Schichl 2004). En modélisation hydrogéologique, les aquifères sont représentés comme des systèmes physiques (modèles), caractérisés par un certain nombre de paramètres, qui interagissent avec leur environnement (par exemple, l'atmosphère, les cours d'eau et les lacs) et dont l'état à un instant donné et en tout point de l'espace est considéré comme entièrement décrit par ses variables d'état. Pour les problèmes d'écoulement souterrain, la variable d'état est le niveau piézométrique ; pour les problèmes de transport, la variable d'état est la concentration des entités chimiques étudiées ; et pour les problèmes de transfert de chaleur, la variable d'état est la température. Dans ce qui suit, seuls les problèmes d'écoulement sont abordés. Plus formellement, l'état  $\varphi$  du système à un instant  $t$  donné et en tout point  $x$  ( $N$ -dimensions  $\leq 3$ ) de l'espace est lié aux entrées  $s$  et aux paramètres  $\theta$  du modèle par la relation  $F$  (Équation 1).

$$F(t, x, s, \theta, \varphi) = 0 \quad (1)$$

Selon le degré d'intégration des principes physiques dans la formulation de la relation  $F$ , on peut distinguer trois types de modèles utilisés en hydrogéologie : les modèles à base physique, les modèles semi-empiriques et les modèles empiriques (Devia et al. 2015; Wu et al. 2005).

- MODÉLISATION A BASE PHYSIQUE

Dans la modélisation à base physique, la relation entre les variables du système (niveaux piézométriques), les paramètres du système et les variables d'entrée est décrite par des équations différentielles connues sous le nom d'équation de diffusivité (Van Geer and Van Der Kloet 1985). Les équations de diffusivité sont dérivées de la loi de Darcy et de l'équation de continuité sous diverses hypothèses comme l'incompressibilité de l'eau, la négligence de la déformation du milieu ou l'absence d'échange de masse entre le milieu et l'eau souterraine (Atangana 2018; Preziosi and Farina 2002). Les équations décrivent comment l'eau s'écoule dans les milieux poreux saturés et résument plusieurs propriétés des eaux souterraines, comme le fait que l'écoulement se produit des charges hydrauliques élevées vers les charges hydrauliques faibles. C'est pourquoi ces équations sont appelées « équations directrices », car l'écoulement des eaux souterraines en milieu poreux est régi par ces équations. Par exemple, l'équation de diffusivité en milieu poreux saturé est donnée par :

$$S_s \frac{\partial \varphi}{\partial t} - \nabla(K\nabla\varphi) - w = 0 \quad (2)$$

où  $(S_s, K) = \theta$  représentent les paramètres du modèle et désignent respectivement l'emmagasinement spécifique et la conductivité hydraulique;  $\varphi$  est la charge hydraulique;  $w$ , un terme de source/puits (injection d'eau / extraction d'eau, respectivement);  $t$ , la variable temps;  $\nabla$ , l'opérateur gradient.

Pour certains problèmes d'écoulement, des hypothèses raisonnables peuvent être formulées pour simplifier la forme de l'équation de diffusivité afin de dériver des solutions analytiques au problème d'écoulement (Li and Jiao 2002; Mathon et al. 2008; Tracy 1995). Cependant, dans un grand nombre de situations réelles, où la complexité du système aquifère ne permet pas une conceptualisation trop simpliste, il n'est pas possible d'obtenir des solutions analytiques de l'équation de diffusivité (Tracy 1995). Tel est le cas, par exemple, lors de l'étude d'aquifères présentant une

hétérogénéité et des conditions aux limites complexes, ou lorsque l'on étudie des écoulements multiphasiques. Dans ces cas, la modélisation numérique est envisagée.

En modélisation numérique, le système aquifère est divisé en petites unités (mailles) sur lesquelles une solution à l'équation de diffusivité est approximée à l'aide de méthodes numériques telles que les différences finies (Larson 2005; Sabat and Kundu 2020). Comme chaque maille possède ses propres variables d'état, ses propres paramètres et ses propres entrées, les hétérogénéités inhérentes aux aquifères peuvent être prises en compte et des problèmes réels de complexité variable peuvent être abordés (Brunner et al. 2010; Sloan 2000; Zhao et al. 2005).

L'élaboration d'un modèle numérique d'écoulement est un processus séquentiel. Quel que soit l'objectif de la modélisation, quatre étapes essentielles sont définies. Tout d'abord, un modèle conceptuel, soit l'ensemble des hypothèses faites sur le fonctionnement de l'aquifère, doit être établi (Enemark et al. 2019). Ces hypothèses concernent, entre autres, la géométrie de l'aquifère, la succession des couches géologiques qui le composent, les propriétés hydrauliques et la distribution de l'hétérogénéité de ces couches, les limites hydrauliques, les relations possibles entre l'aquifère, les systèmes hydrogéologiques voisins et les eaux atmosphériques et de surface (Barzegar et al. 2017b; Cai et al. 2022). Une fois que le modèle conceptuel est jugé raisonnable, une méthode d'analyse numérique est employée pour discréteriser le modèle conceptuel en petites unités sur lesquelles l'équation de diffusivité sera approximée. Ensuite vient l'étape de la calibration où le modèle conceptuel est ajusté afin que le modèle numérique qui en résulte soit capable de reproduire de manière raisonnable les observations de terrain. Enfin, le modèle calibré est validé par de nouvelles observations de terrain avant de servir à la simulation.

Les modèles numériques présentent plusieurs avantages. Premièrement, ils peuvent être utilisés pour valider les solutions analytiques (l'inverse est également possible) (Lin et al. 2022; Tang

et al. 2023; Ying et al. 2018). Deuxièmement, ils peuvent aider à valider ou réfuter des hypothèses afin d'améliorer les modèles conceptuels qui sous-tendent notre compréhension des systèmes d'eau souterraine (Husic et al. 2017; Rodríguez et al. 2013). Ils peuvent être utilisés pour estimer les valeurs des paramètres hydrodynamiques des aquifères (Neuman 1973; Solomatine et al. 1999). Troisièmement, les modèles numériques ont la capacité de simuler des processus complexes qui ne peuvent être représentés de manière réaliste d'aucune autre manière (Abbs 1999). C'est le cas lorsqu'il s'agit de simuler des systèmes karstiques caractérisés par des réseaux de fissures, de grottes et de cours d'eau souterrains. Quatrièmement, les modèles numériques peuvent servir à combler les lacunes de données lorsque des stations d'observation piézométrique ne sont pas disponibles (Husic et al. 2017).

Les modèles numériques ont également leurs limites. Ces modèles sont mathématiquement complexes (Schwartz 2006) et leur mise en œuvre est coûteuse en temps de calcul (Al Aamery et al. 2021) et en données (Yadav et al. 2020). De plus, la complexité de certains problèmes d'écoulement peut conduire à une instabilité numérique importante et à une non-convergence du modèle lors de la calibration (Gao 2011). Dans ce dernier cas, il peut être nécessaire d'affiner la discrétisation spatiale ou temporelle, voire de reconsiderer le modèle conceptuel (Enemark et al. 2019), ce qui prolonge le temps alloué à la tâche de modélisation. Par ailleurs, l'utilisation de modèles numériques dans l'analyse de problèmes d'écoulement à grande échelle est considérée comme peu pratique, notamment en raison de la quantité et de la résolution des données requises (Sloan 2000). Enfin, compte tenu des incertitudes associées aux modèles conceptuels et de la complexité du problème étudié, les modèles numériques peuvent être sujets à une faible justesse (Chen et al. 2020a). Ainsi, lorsque les exigences en matière de données d'un modèle numérique ne sont pas satisfaites (densité et répartition de la donnée), ou pour des applications à grande échelle, une approche de modélisation semi-empirique peut être adoptée (Yu 2015).

- MODÉLISATION SEMI-EMPIRIQUE

Un modèle semi-empirique décrit les systèmes hydrogéologiques à l'aide d'une série d'équations simples qui approximent les lois régissant leur dynamique (Arora et al. 2018). Dans ce type de modèle, l'aquifère est assimilé à une succession de réservoirs communicants (Devia et al. 2015). Chaque réservoir représente un élément physique du système aquifère, tel que la zone racinaire, la zone vadose ou la zone saturée, et possède une capacité de stockage décrite par une équation différentielle ordinaire exprimant le principe de conservation de masse de manière semi-empirique. Les connexions entre les réservoirs correspondent à des processus physiques réels comme le ruissellement, l'infiltration et la percolation. Ces processus physiques sont décrits par des équations paramétriques simples. Ainsi, la relation entre les variables du système, les paramètres du système et les variables d'entrée pour les modèles semi-empiriques peut se résumer aux Équations 3 et 4.

$$\varphi = f(\theta_\varphi, S_n) \quad (3)$$

$$\frac{dS_n}{dt} = \sum_i \pm p_i^n(\theta_i^n) \quad (4)$$

où  $S_n$  est la capacité de stockage du  $n$ ème réservoir;  $p_i^n$  est le  $i$ -ème processus physique de paramètre  $\theta_i^n$  associé au  $n$ ème réservoir;  $f$  est une fonction de paramètre  $\theta_\varphi$  qui permet de transformer la capacité de stockage du dernier réservoir en niveau piézométrique. Utilisé pour résoudre un problème d'écoulement, les paramètres du modèle semi-empirique sont calibrés sur la base d'observations de terrain, car ces paramètres ne sont généralement pas mesurables sur le terrain.

Les modèles semi-empiriques présentent plusieurs avantages. Ces modèles sont beaucoup plus simples d'un point de vue mathématique que leurs équivalents à base physique, sont plus rapides et plus faciles à mettre en œuvre, et nécessitent peu de données comparativement aux

modèles à base physique tout en offrant un certain degré d'interprétabilité physique (Coron et al. 2017; Khakbaz et al. 2012; Lampert and Wu 2015). Un modèle est dit interprétable lorsqu'il permet à l'hydrogéologue de comprendre la physique sous-jacente au phénomène étudié ou d'expliquer ses résultats. De plus, la formulation et la structure généralement simples des modèles empiriques les rendent moins sujettes aux problèmes de sur-paramétrage (Merritt et al. 2003; Vigiak et al. 2006). On parle de sur-paramétrage lorsqu'il y a plus de paramètres de modèle que nécessaire.

Cependant, la principale limite des modèles semi-empiriques est également leur formulation simpliste qui peut atténuer l'importance des processus physiques simulés dans le bilan hydrique (Martina et al. 2011; Parra et al. 2018). De plus, étant donné que tout ou partie des paramètres des modèles empiriques ne peuvent être mesurés, leur interprétation physique peut quelques fois s'avérer difficile et limitée (Devia et al. 2015).

- **MODÉLISATION EMPIRIQUE**

La troisième catégorie de modèles utilisés en hydrogéologie est celle des modèles empiriques dont la mise en œuvre est entièrement basée sur des données, par opposition, en principe, aux modèles à base physique ou semi-empirique (Aldrich 2015). Dans ce type de modèle, les principes fondamentaux et les mécanismes physiques qui sous-tendent les écoulements dans les systèmes aquifères sont ignorés (Ashoor et al. 2019), et la relation entre les variables du système et les variables d'entrée est dérivée en ajustant les données de terrain à la courbe d'une fonction  $F$ , généralement paramétrique (Équations 5 et 6) (Cugnet et al. 2009).

$$\varphi = F(\theta_s, s) \quad (5)$$

$$\theta_s = \operatorname{argmin}_{\theta} \{\|\varphi_{obs} - F(\theta, s)\|\} \quad (6)$$

où  $\theta_s$  est la valeur optimale du paramètre  $\theta$  de la fonction de corrélation  $F$  entre la variable d'état  $\varphi$  du système et les variables d'entrées  $S$ , qui permet de minimiser l'écart entre les sorties du modèle et les observations de terrain  $\varphi_{obs}$ ;  $\|\cdot\|$  est la fonction « norme ».

Il existe diverses approches de la modélisation empirique. Parmi celles-ci, l'intelligence artificielle et sa sous-branche, l'apprentissage automatique, ont connu une croissance exponentielle dans un large éventail de domaines scientifiques (Ezugwu et al. 2022; Huang et al. 2020; Martínez-Santos et al. 2021; Reddy et al. 2020). L'apprentissage automatique a pour objet le développement d'algorithmes permettant d'analyser des données et d'en extraire des modèles comportementaux pouvant ensuite être utilisés pour faire des prédictions sur de nouvelles données (Azodi et al. 2020). Ces dernières années, la communauté hydrogéologique universitaire s'est de plus en plus impliquée dans le développement de modèles d'apprentissage automatique en tant qu'outils de modélisation complémentaires pour une variété de problèmes pratiques, tels que l'évaluation de la qualité des eaux souterraines (Bedi et al. 2020; El Bilali et al. 2021; Singha et al. 2021), la vulnérabilité des eaux souterraines (Elzain et al. 2022; Elzain et al. 2023; Sajedi-Hosseini et al. 2018) et la simulation des niveaux piézométriques (Pham et al. 2022; Rahman et al. 2020; Tao et al. 2022).

Plusieurs raisons expliquent l'attrait que suscite l'apprentissage automatique. Premièrement, les algorithmes d'apprentissage automatique ont une grande capacité à traiter des données multidimensionnelles et multivariées, et à établir des liens entre ces données (Köksal et al. 2011; Wuest et al. 2016). Cette capacité explique pourquoi les algorithmes d'apprentissage automatique sont bien adaptés à la résolution de problèmes complexes. Deuxièmement, les modèles d'apprentissage automatique offrent des performances inégalées par rapport aux modèles à base physique ou semi-empiriques (Chen et al. 2020a). En effet, ces modèles sont spécifiquement entraînés pour minimiser les écarts par rapport aux observations de terrain, comme le montrent les Équations 5 et 6. Troisièmement, le développement de modèles d'apprentissage automatique a été

facilité par la mise à disposition du grand public de codes sources, de bibliothèques et d'applications conviviales (Wuest et al. 2016; Xu and Liang 2021). Dans la plupart des cas, cela permet de réduire considérablement le temps consacré à la tâche de modélisation.

Cependant, l'apprentissage automatique a ses propres limites. La dérivation des modèles d'apprentissage reposant entièrement sur l'analyse des données, leur succès dépend fortement de la disponibilité, de la qualité et de la composition de celles-ci (Pham and Afify 2005; Wuest et al. 2016). C'est pourquoi beaucoup de temps est souvent consacré à l'acquisition et au traitement des données. En hydrogéologie, bien que de plus en plus de données (principalement temporelles plutôt que spatiales) soient acquises, elles sont quelques fois insuffisantes et inconsistantes pour une utilisation efficace de l'apprentissage automatique dans des applications réelles. Il convient également de noter que, bien que les modèles d'apprentissage automatique puissent simuler le comportement d'un système avec un degré élevé de justesse dans des conditions similaires aux données utilisées pour leur entraînement, la justesse de la simulation peut être considérablement altérée lors de l'extrapolation sur des données statistiquement différentes des données d'entraînement (Lawrence and Giles 2000; Montesinos López et al. 2022). Ce comportement est généralement dû à ce que l'on appelle le surapprentissage (analogique au sur-paramétrage). Enfin, la grande majorité des modèles d'apprentissage automatique est considérée comme une boîte noire (Lipton 2018), est généralement incapables de capturer la physique sous-jacente au problème d'écoulement étudié (Chen et al. 2020a) et peine à capturer correctement les relations de cause à effet (Sanchez et al. 2022). En conséquence, la plupart des modèles d'apprentissage automatique ne sont pas physiquement interprétables, ce qui est pourtant essentiel pour qu'un modèle soit opérationnel.

Une comparaison des forces et des faiblesses de la modélisation à base physique, semi-empirique et empirique montre qu'aucune de ces trois approches de modélisation ne peut résoudre tous les problèmes d'écoulement des eaux souterraines avec une grande efficacité. En effet, aucune

de ces approches ne combine toutes les forces des deux autres. Au contraire, les faiblesses de l'une sont compensées par les forces des deux autres, et vice versa, ce qui les rend complémentaires dans une certaine mesure. Ces raisons ont conduit à l'émergence récente d'une exploration des liens entre les modèles basés sur la physique ou semi-empiriques et l'apprentissage automatique, dans le but de trouver des approches hybrides qui combinent le meilleur des deux mondes (Vadyala et al. 2022), donnant lieu à un nouveau concept appelé apprentissage automatique guidé par la théorie (Esterhuizen et al. 2020; Karpatne et al. 2017; Wagner and Rondinelli 2016) ou la physique (Karniadakis et al. 2021; Raissi et al. 2019). Ce concept vise à intégrer des connaissances physiques (e.g., équations directrices, loi de conservations, expertise de terrain) dans la construction des algorithmes d'apprentissage automatique, de sorte que ces algorithmes soient capables non seulement de dériver des modèles à partir de l'analyse de données, mais aussi permettre à ces modèles de satisfaire aux principes physiques qui régissent le phénomène étudié (Karniadakis et al. 2021; Karpatne et al. 2017). L'objectif de ce paradigme est double : il s'agit de réduire l'opacité des modèles d'apprentissage automatique et de bénéficier de la justesse qu'ils offrent mais aussi de leur donner la capacité de servir d'outil d'aide à la compréhension de la physique sous-jacente au phénomène étudié, et in fine d'outil d'aide à la décision. Dans ce qui suit, le terme "apprentissage automatique traditionnel" fait référence à l'apprentissage automatique purement empirique qui n'intègre aucun principe régissant l'écoulement des eaux souterraines.

## ✓ PROBLÉMATIQUE GÉNÉRALE

L'apprentissage automatique guidé par la théorie est apparu comme un moyen de surmonter les limitations des modèles à base physique, semi-empiriques et de l'apprentissage automatique traditionnel en combinant ces types de modélisation pour bénéficier de leurs potentiels respectifs. Cette approche a été employée dans diverses disciplines scientifiques (Li et al. 2023; Li et al. 2021; Ma et al. 2022; Misyris et al. 2020; Wang et al. 2020a; Zobeiry and Humfeld 2021). Par exemple, Li et al. (2023) ont développé un modèle d'apprentissage automatique guidé par la théorie pour simuler

la dynamique à long terme des inondations dues aux ruptures de barrage. Appliqué à une variété de cas traditionnels d'inondation par rupture de barrage en 2D, les résultats montrent que le modèle d'apprentissage automatique guidé par la théorie simule bien la dynamique des inondations par rupture de barrage, fournit des simulations comparables à un modèle numérique, surpassé le modèle d'apprentissage automatique traditionnel et réduit les coûts de calcul de plus de 3 à 4 ordres de grandeur par rapport au modèle numérique.

Si l'apprentissage automatique guidé par la théorie (TgML) semble prometteur en tant qu'outil de modélisation et d'aide à la décision, son développement dans les sciences physiques en général et l'hydrogéologie en particulier n'en est encore qu'à ses débuts. En hydrogéologie, l'apprentissage automatique guidé par la théorie est actuellement principalement utilisé pour résoudre les problèmes d'écoulement des eaux souterraines (Chen et al. 2023; Cuomo et al. 2023; Depina et al. 2022; Guo et al. 2023; Shadab et al. 2023; Wang et al. 2021a, 2021b; Wang et al. 2020b; Xu et al. 2021). Wang et al. (2021b) ont développé un modèle d'apprentissage automatique guidé par la théorie en intégrant le schéma de différences finies de l'équation de diffusivité en milieu poreux saturé dans le processus d'apprentissage. Les auteurs ont ensuite appliqué le modèle à plusieurs cas-types d'écoulement des eaux souterraines et ont pu montrer qu'il peut approximer avec justesse la relation entre les entrées du modèle et les réponses à partir d'une quantité de données d'apprentissage relativement limitées. Wang et al. (2021a) ont proposé une méthodologie pour une quantification efficace de l'incertitude dans les problèmes d'écoulement des eaux souterraines, basée sur un modèle de substitution d'un modèle numérique. Ce modèle de substitution a été construit via le paradigme de l'apprentissage automatique guidé par la théorie et évalué avec des cas-type d'écoulement saturé bidimensionnel en milieu poreux. Les résultats montrent que le modèle de substitution peut améliorer de manière significative l'efficacité des tâches de quantification de l'incertitude par rapport à une mise en œuvre basée sur la simulation à l'aide d'un modèle numérique. D'autres auteurs comme Chen et al. (2023) ou Depina et al. (2022) ont utilisé avec succès l'apprentissage automatique guidé par la théorie pour simuler l'écoulement des eaux souterraines en zone non saturée.

La plupart des études utilisant ce paradigme en hydrogéologie se sont focalisées sur la résolution de problèmes d'écoulement des eaux souterraines dans des contextes hypothétiques. Un contexte hypothétique représente un problème d'écoulement délibérément construit de manière très simpliste dans le but de l'utiliser pour tester, expliquer ou démontrer une méthodologie. Dans de tels contextes, tous les paramètres et données disponibles sont contrôlés par le modélisateur.

Or, la viabilité de l'apprentissage automatique guidé par la théorie ne peut être rigoureusement évaluée qu'en la confrontant à des problèmes hydrogéologiques réels, ce qui n'est pas le cas à ce jour. Dans les problèmes hydrogéologiques réels, les données ne sont pas toujours disponibles en quantité, en qualité et en résolution suffisantes, les propriétés physiques du milieu sont seulement connues en quelques points de la zone d'étude, et de nombreuses incertitudes sont omniprésentes, comme la connaissance partielle de la géologie souterraine.

Le développement et la confrontation de l'apprentissage automatique guidé par la théorie à des problèmes hydrogéologiques réels et sa comparaison avec des approches traditionnelles telles que la modélisation à base physique, la modélisation semi-empirique ou l'apprentissage automatique traditionnel sont essentiels pour mettre en évidence ses forces et ses faiblesses. À ce jour, cela demeure non documenté.

Enfin, aucune étude n'a examiné la question de savoir si les modèles construits selon le paradigme de l'apprentissage automatique guidé par la théorie répondent aux critères nécessaires à leur applicabilité dans des contextes réels, dans le but de les rendre opérationnels. Ces critères sont, entre autres, la capacité d'extrapoler en dehors des données utilisées pour l'entraînement, la justesse de simulation, la transférabilité, la capacité à apprendre la physique sous-jacente au problème d'écoulement étudié et la capacité d'apprendre les relations de cause à effet. La transférabilité d'un

modèle est sa capacité à être utilisé pour résoudre un problème à peu près similaire à celui pour lequel il a été entraîné.

#### ✓ HYPOTHÈSE DE RECHERCHE

Cette thèse vise à tester l'hypothèse selon laquelle les modèles d'apprentissage automatique guidés par la théorie (TgML) peuvent bénéficier des forces combinées des approches traditionnelles de modélisation.

#### ✓ OBJECTIFS DE RECHERCHE

Les deux objectifs de cette thèse sont de tester l'hypothèse de recherche en comparant un modèle TgML avec des modèles traditionnels :

- Dans un contexte de modélisation distribuée de l'écoulement des eaux souterraines.
- Dans un contexte de modélisation localisée de l'écoulement des eaux souterraines.

La comparaison sera basée sur trois critères : la performance des modèles, leur capacité à obéir à la physique qui régit l'écoulement des eaux souterraines, et les coûts de calcul nécessaires pour les entraîner/calibrer. De cette manière, il est possible de déterminer comment les modèles TgML se comparent aux modèles traditionnels, d'identifier leurs forces et leurs faiblesses, et par conséquent de valider ou d'invalider l'hypothèse de recherche.

Les zones et les études de cas utilisées pour tester l'hypothèse recherche de cette thèse concernent les ressources en eau de la province du Québec au Canada.

## ✓ METHODOLOGIE DE RECHERCHE

La méthodologie employée dans cette thèse se décompose en trois étapes. Premièrement, des modèles TgML et traditionnels sont développés. Ensuite, ces modèles sont soumis à des problèmes hydrogéologiques réels. Dans cette thèse, deux problèmes d'écoulement, distribué et localisé, ont été étudiés. Troisièmement, une comparaison de ces modèles est faite sur la base de leur performance, de leur capacité à obéir à la physique régissant l'écoulement des eaux souterraines, et des coûts de calcul nécessaires pour les entraîner/calibrer. Cette comparaison permet d'identifier les forces et les faiblesses des modèles TgML par rapport à celles des modèles traditionnels, afin de réfuter ou de valider l'hypothèse de recherche.

## ✓ STRUCTURE DE LA THÈSE

Outre l'introduction et la conclusion, cette thèse est organisée en cinq chapitres. Le Chapitre 1 explique les concepts généraux sur l'apprentissage automatique. Dans ce chapitre, les concepts spécifiques à l'apprentissage automatique sont définis, différentes approches d'apprentissage sont passées en revue et une exploration de quelques algorithmes populaires d'apprentissage automatique est effectuée, avec un accent particulier sur les réseaux neuronaux artificiels. Le Chapitre 2 est consacré à une revue de la littérature sur les différentes méthodes de mise en œuvre des modèles d'apprentissage automatique guidés par la théorie. Ces méthodes sont évaluées en fonction de leur capacité à surmonter les faiblesses de l'apprentissage automatique traditionnel, sur la base de la littérature actuelle. Cette revue de la littérature identifie également les lacunes de la littérature actuelle, dont certaines sont étudiées dans cette thèse. Dans le Chapitre 3, un modèle d'apprentissage automatique guidé par la théorie est développé dans le cadre d'une modélisation distribuée et ses performances sont comparées avec celles d'un modèle numérique et d'un modèle d'apprentissage automatique traditionnel pour la modélisation et la simulation inverse des écoulements d'eau souterraine. La zone d'étude représente l'aquifère de Saint-Honoré dans la région

du Saguenay-Lac-Saint-Jean au Québec (Canada). Les modèles ont été comparés sur la base de leur justesse de simulation, de leur capacité d'interpolation temporelle, de leur capacité d'extrapolation spatiale, de leur temps de calcul et de leur coût, ainsi que de leur capacité à comprendre la physique qui régit l'écoulement des eaux souterraines. Dans le Chapitre 4, il est démontré que certaines constructions de modèles d'apprentissage automatique guidés par la théorie ne parviennent pas à apprendre les relations de causalité entre les variables d'entrée et de sortie. Ensuite une formulation mathématiquement viable est proposée, permettant d'obtenir des modèles d'apprentissage automatique guidés par la théorie capable de satisfaire aux propriétés de causalité essentielles pour tout modèle en hydrogéologie. Enfin, la formulation proposée est utilisée pour construire et calibrer des modèles afin d'étudier l'impact du changement climatique sur l'évolution du niveau des eaux souterraines au Québec. Le Chapitre 5 porte sur la discussion des résultats obtenus dans le cadre de cette thèse, les limites et les perspectives de recherche.

Les Chapitres 2 à 4 ont fait ou feront l'objet d'une publication dans des revues à comité de lecture. Par conséquent, ils sont présentés dans cette thèse sous la forme d'un article. L'article 1 (Chapitre 2) a été publié dans la revue *Hydrogeology Journal*. L'article 2 (Chapitre 3) a été publié dans la revue *Journal of Hydrology*. Enfin, le manuscrit 3 (Chapitre 4) a été accepté avec correction dans la revue *Journal of Hydrology*.

Il est à noter que durant mon doctorat, j'ai également réalisé une étude qui a conduit à l'acceptation d'un quatrième manuscrit, actuellement en phase de production dans la revue *Environmental Earth Sciences*. Ce manuscrit est présenté en annexe de cette thèse, car il traite d'un sujet différent.

## RÉFÉRENCES

- Abbs, D.J. 1999. A numerical modeling study to investigate the assumptions used in the calculation of probable maximum precipitation. *Water Resources Research*, **35**: 785-796. doi:<https://doi.org/10.1029/1998WR900013>.
- Al Aamery, N., Adams, E., Fox, J., Husic, A., Zhu, J., Gerlitz, M., Agouridis, C., and Bettel, L. 2021. Numerical model development for investigating hydrologic pathways in shallow fluviokarst. *Journal of Hydrology*, **593**: 125844. doi:<https://doi.org/10.1016/j.jhydrol.2020.125844>.
- Aldrich, C. 2015. Chapter One - Hydrocyclones. *In Progress in Filtration and Separation*. Edited by S. Tarleton. Academic Press, Oxford. pp. 1-24.
- Arora, R., Toffolon, M., Tockner, K., and Venohr, M. 2018. Thermal discontinuities along a lowland river: The importance of urban areas and lakes. *Journal of Hydrology*, **564**: 811-823. doi:<https://doi.org/10.1016/j.jhydrol.2018.05.066>.
- Ashoor, B.B., Giwa, A., and Hasan, S.W. 2019. Chapter 5 - Full-Scale Membrane Distillation Systems and Performance Improvement Through Modeling: A Review. *In Current Trends and Future Developments on (Bio-) Membranes*. Edited by A. Basile and E. Curcio and Inamuddin. Elsevier. pp. 105-140.
- Atangana, A. 2018. Chapter 2 - Principle of Groundwater Flow. *In Fractional Operators with Constant and Variable Order with Application to Geo-Hydrology*. Edited by A. Atangana. Academic Press. pp. 15-47.
- Azodi, C.B., Tang, J., and Shiu, S.-H. 2020. Opening the Black Box: Interpretable Machine Learning for Geneticists. *Trends in Genetics*, **36**: 442-455. doi:<https://doi.org/10.1016/j.tig.2020.03.005>.
- Barzegar, R., Fijani, E., Asghari Moghaddam, A., and Tziritis, E. 2017b. Forecasting of groundwater level fluctuations using ensemble hybrid multi-wavelet neural network-based models. *Science of the Total Environment*, **599-600**: 20-31. doi:<https://doi.org/10.1016/j.scitotenv.2017.04.189>.
- Bedi, S., Samal, A., Ray, C., and Snow, D. 2020. Comparative evaluation of machine learning models for groundwater quality assessment. *Environmental monitoring and assessment*, **192**: 776. doi:10.1007/s10661-020-08695-3.

- Brunner, P., Simmons, C.T., Cook, P.G., and Therrien, R. 2010. Modeling Surface Water-Groundwater Interaction with MODFLOW: Some Considerations. *Groundwater*, **48**: 174-180. doi:<https://doi.org/10.1111/j.1745-6584.2009.00644.x>.
- Cai, H., Liu, S., Shi, H., Zhou, Z., Jiang, S., and Babovic, V. 2022. Toward improved lumped groundwater level predictions at catchment scale: Mutual integration of water balance mechanism and deep learning method. *Journal of Hydrology*, **613**: 128495. doi:<https://doi.org/10.1016/j.jhydrol.2022.128495>.
- Chen, C., He, W., Zhou, H., Xue, Y., and Zhu, M. 2020a. A comparative study among machine learning and numerical models for simulating groundwater dynamics in the Heihe River Basin, northwestern China. *Scientific reports*, **10**: 1-13. doi:<https://doi.org/10.1038/s41598-020-60698-9>.
- Chen, Y., Xu, Y., Wang, L., and Li, T. 2023. Modeling water flow in unsaturated soils through physics-informed neural network with principled loss function. *Computers and Geotechnics*, **161**: 105546. doi:<https://doi.org/10.1016/j.compgeo.2023.105546>.
- Coron, L., Thirel, G., Delaigue, O., Perrin, C., and Andréassian, V. 2017. The suite of lumped GR hydrological models in an R package. *Environmental Modelling & Software*, **94**: 166-171. doi:<https://doi.org/10.1016/j.envsoft.2017.05.002>.
- Cugnet, M., Dubarry, M., and Liaw, B.Y. 2009. SECONDARY BATTERIES – LEAD–ACID SYSTEMS | Modeling. In *Encyclopedia of Electrochemical Power Sources*. Edited by J. Garche. Elsevier, Amsterdam. pp. 816-828.
- Cuomo, S., De Rosa, M., Giampaolo, F., Izzo, S., and Schiano Di Cola, V. 2023. Solving groundwater flow equation using physics-informed neural networks. *Computers & Mathematics with Applications*, **145**: 106-123. doi:<https://doi.org/10.1016/j.camwa.2023.05.036>.
- Depina, I., Jain, S., Mar Valsson, S., and Gotovac, H. 2022. Application of physics-informed neural networks to inverse problems in unsaturated groundwater flow. *Georisk: Assessment and Management of Risk for Engineered Systems and Geohazards*, **16**: 21-36. doi:10.1080/17499518.2021.1971251.

- Devia, G.K., Ganasri, B.P., and Dwarakish, G.S. 2015. A Review on Hydrological Models. *Aquatic Procedia*, **4**: 1001-1007. doi:<https://doi.org/10.1016/j.aqpro.2015.02.126>.
- El Bilali, A., Taleb, A., and Brouziyne, Y. 2021. Groundwater quality forecasting using machine learning algorithms for irrigation purposes. *Agricultural water management*, **245**: 106625. doi:<https://doi.org/10.1016/j.agwat.2020.106625>.
- Elzain, H.E., Chung, S.Y., Senapathi, V., Sekar, S., Lee, S.Y., Roy, P.D., Hassan, A., and Sabarathinam, C. 2022. Comparative study of machine learning models for evaluating groundwater vulnerability to nitrate contamination. *Ecotoxicology and Environmental Safety*, **229**: 113061. doi:<https://doi.org/10.1016/j.ecoenv.2021.113061>.
- Elzain, H.E., Chung, S.Y., Venkatramanan, S., Selvam, S., Ahemd, H.A., Seo, Y.K., Bhuyan, M.S., and Yassin, M.A. 2023. Novel machine learning algorithms to predict the groundwater vulnerability index to nitrate pollution at two levels of modeling. *Chemosphere*, **314**: 137671. doi:<https://doi.org/10.1016/j.chemosphere.2022.137671>.
- Enemark, T., Peeters, L.J.M., Mallants, D., and Batelaan, O. 2019. Hydrogeological conceptual model building and testing: A review. *Journal of Hydrology*, **569**: 310-329. doi:<https://doi.org/10.1016/j.jhydrol.2018.12.007>.
- Esterhuizen, J.A., Goldsmith, B.R., and Linic, S. 2020. Theory-guided machine learning finds geometric structure-property relationships for chemisorption on subsurface alloys. *Chem*, **6**: 3100-3117. doi:<https://doi.org/10.1016/j.chempr.2020.09.001>.
- Ezugwu, A.E., Ikotun, A.M., Oyelade, O.O., Abualigah, L., Agushaka, J.O., Eke, C.I., and Akinyelu, A.A. 2022. A comprehensive survey of clustering algorithms: State-of-the-art machine learning applications, taxonomy, challenges, and future research prospects. *Engineering Applications of Artificial Intelligence*, **110**: 104743. doi:<https://doi.org/10.1016/j.engappai.2022.104743>.
- Gao, H. 2011. Groundwater Modeling for Flow Systems with Complex Geological and Hydrogeological Conditions. *Procedia Earth and Planetary Science*, **3**: 23-28. doi:<https://doi.org/10.1016/j.proeps.2011.09.061>.

- Guo, Q., Zhao, Y., Lu, C., and Luo, J. 2023. High-dimensional inverse modeling of hydraulic tomography by physics informed neural network (HT-PINN). *Journal of Hydrology*, **616**: 128828. doi:<https://doi.org/10.1016/j.jhydrol.2022.128828>.
- Huang, J.-C., Ko, K.-M., Shu, M.-H., and Hsu, B.-M. 2020. Application and comparison of several machine learning algorithms and their integration models in regression problems. *Neural Computing and Applications*, **32**: 5461-5469. doi:10.1007/s00521-019-04644-5.
- Husic, A., Fox, J., Ford, W., Agouridis, C., Currens, J., and Taylor, C. 2017. Sediment carbon fate in phreatic karst (Part 2): Numerical model development and application. *Journal of Hydrology*, **549**: 208-219. doi:<https://doi.org/10.1016/j.jhydrol.2017.03.059>.
- Karniadakis, G.E., Kevrekidis, I.G., Lu, L., Perdikaris, P., Wang, S., and Yang, L. 2021. Physics-informed machine learning. *Nature Reviews Physics*, **3**: 422-440. doi:<https://doi.org/10.1038/s42254-021-00314-5>.
- Karpatne, A., Atluri, G., Faghmous, J.H., Steinbach, M., Banerjee, A., Ganguly, A., Shekhar, S., Samatova, N., and Kumar, V. 2017. Theory-Guided Data Science: A New Paradigm for Scientific Discovery from Data. *IEEE Transactions on Knowledge and Data Engineering*, **29**: 2318-2331. doi:<https://doi.org/10.1109/TKDE.2017.2720168>.
- Khakbaz, B., Imam, B., Hsu, K., and Sorooshian, S. 2012. From lumped to distributed via semi-distributed: Calibration strategies for semi-distributed hydrologic models. *Journal of Hydrology*, **418-419**: 61-77. doi:<https://doi.org/10.1016/j.jhydrol.2009.02.021>.
- Köksal, G., Batmaz, İ., and Testik, M.C. 2011. A review of data mining applications for quality improvement in manufacturing industry. *Expert Systems with Applications*, **38**: 13448-13467. doi:<https://doi.org/10.1016/j.eswa.2011.04.063>.
- Lampert, D.J., and Wu, M. 2015. Development of an open-source software package for watershed modeling with the Hydrological Simulation Program in Fortran. *Environmental Modelling & Software*, **68**: 166-174. doi:<https://doi.org/10.1016/j.envsoft.2015.02.018>.
- Larson, M. 2005. Numerical Modeling. In *Encyclopedia of Coastal Science*. Edited by M.L. Schwartz. Springer Netherlands, Dordrecht. pp. 730-733.

- Lawrence, S., and Giles, C.L. Overfitting and neural networks: conjugate gradient and backpropagation. In Proceedings of the IEEE-INNS-ENNS International Joint Conference on Neural Networks. IJCNN 2000. Neural Computing: New Challenges and Perspectives for the New Millennium. 27-27 July 2000 2000. Vol. 1, pp. 114-119 vol.111.
- Li, C., Han, Z., Li, Y., Li, M., Wang, W., Dou, J., Xu, L., and Chen, G. 2023. Physical information-fused deep learning model ensembled with a subregion-specific sampling method for predicting flood dynamics. Journal of Hydrology, **620**: 129465. doi:<https://doi.org/10.1016/j.jhydrol.2023.129465>.
- Li, H., and Jiao, J.J. 2002. Analytical solutions of tidal groundwater flow in coastal two-aquifer system. Advances in Water Resources, **25**: 417-426. doi:[https://doi.org/10.1016/S0309-1708\(02\)00004-0](https://doi.org/10.1016/S0309-1708(02)00004-0).
- Li, W., Bazant, M.Z., and Zhu, J. 2021. A physics-guided neural network framework for elastic plates: Comparison of governing equations-based and energy-based approaches. Computer Methods in Applied Mechanics and Engineering, **383**: 113933. doi:<https://doi.org/10.1016/j.cma.2021.113933>.
- Lin, Y.-F., Chang, C.-H., and Tsai, J.-P. 2022. Analytical solution for estimating transient vertical groundwater flux from temperature-depth profiles. Journal of Hydrology, **610**: 127920. doi:<https://doi.org/10.1016/j.jhydrol.2022.127920>.
- Lipton, Z.C. 2018. The mythos of model interpretability: In machine learning, the concept of interpretability is both important and slippery. Queue, **16**: 31-57.
- Ma, Y., Zheng, J., Liang, Y., Klemeš, J.J., Du, J., Liao, Q., Lu, H., and Wang, B. 2022. Deppipe: Theory-guided neural network method for predicting burst pressure of corroded pipelines. Process Safety and Environmental Protection, **162**: 595-609. doi:<https://doi.org/10.1016/j.psep.2022.04.036>.
- Martina, M.L.V., Todini, E., and Liu, Z. 2011. Preserving the dominant physical processes in a lumped hydrological model. Journal of Hydrology, **399**: 121-131. doi:<https://doi.org/10.1016/j.jhydrol.2010.12.039>.

- Martínez-Santos, P., Díaz-Alcaide, S., De la Hera-Portillo, A., and Gómez-Escaloniella, V. 2021. Mapping groundwater-dependent ecosystems by means of multi-layer supervised classification. *Journal of Hydrology*, **603**: 126873. doi:<https://doi.org/10.1016/j.jhydrol.2021.126873>.
- Mathon, B.R., Ozbek, M.M., and Pinder, G.F. 2008. Transmissivity and storage coefficient estimation by coupling the Cooper–Jacob method and modified fuzzy least-squares regression. *Journal of Hydrology*, **353**: 267-274. doi:<https://doi.org/10.1016/j.jhydrol.2008.02.004>.
- Merritt, W.S., Letcher, R.A., and Jakeman, A.J. 2003. A review of erosion and sediment transport models. *Environmental Modelling & Software*, **18**: 761-799. doi:[https://doi.org/10.1016/S1364-8152\(03\)00078-1](https://doi.org/10.1016/S1364-8152(03)00078-1).
- Misyris, G.S., Venzke, A., and Chatzivasileiadis, S. Physics-Informed Neural Networks for Power Systems. In 2020 IEEE Power & Energy Society General Meeting (PESGM). 2-6 Aug. 2020 2020, pp. 1-5.
- Montesinos López, O.A., Montesinos López, A., and Crossa, J. 2022. Overfitting, Model Tuning, and Evaluation of Prediction Performance. In Multivariate Statistical Machine Learning Methods for Genomic Prediction. Edited by O.A. Montesinos López and A. Montesinos López and J. Crossa. Springer International Publishing, Cham. pp. 109-139.
- Neuman, S.P. 1973. Calibration of distributed parameter groundwater flow models viewed as a multiple-objective decision process under uncertainty. *Water Resources Research*, **9**: 1006-1021. doi:<https://doi.org/10.1029/WR009i004p01006>.
- Parra, V., Fuentes-Aguilera, P., and Muñoz, E. 2018. Identifying advantages and drawbacks of two hydrological models based on a sensitivity analysis: a study in two Chilean watersheds. *Hydrological Sciences Journal*, **63**: 1831-1843. doi:10.1080/02626667.2018.1538593.
- Pham, D.T., and Afify, A.A. 2005. Machine-learning techniques and their applications in manufacturing. *Proceedings of the Institution of Mechanical Engineers, Part B: Journal of Engineering Manufacture*, **219**: 395-412. doi:10.1243/095440505x32274.
- Pham, Q.B., Kumar, M., Di Nunno, F., Elbeltagi, A., Granata, F., Islam, A.R.M.T., Talukdar, S., Nguyen, X.C., Ahmed, A.N., and Anh, D.T. 2022. Groundwater level prediction using machine

- learning algorithms in a drought-prone area. *Neural Computing and Applications*, **34**: 10751-10773. doi:10.1007/s00521-022-07009-7.
- Preziosi, L., and Farina, A. 2002. On Darcy's law for growing porous media. *International Journal of Non-Linear Mechanics*, **37**: 485-491.
- Rahman, A.T.M.S., Hosono, T., Quilty, J.M., Das, J., and Basak, A. 2020. Multiscale groundwater level forecasting: Coupling new machine learning approaches with wavelet transforms. *Advances in Water Resources*, **141**: 103595. doi:<https://doi.org/10.1016/j.advwatres.2020.103595>.
- Raissi, M., Perdikaris, P., and Karniadakis, G.E. 2019. Physics-informed neural networks: A deep learning framework for solving forward and inverse problems involving nonlinear partial differential equations. *Journal of Computational physics*, **378**: 686-707. doi:<https://doi.org/10.1016/j.jcp.2018.10.045>.
- Reddy, G.T., Reddy, M.P.K., Lakshmanna, K., Kaluri, R., Rajput, D.S., Srivastava, G., and Baker, T. 2020. Analysis of Dimensionality Reduction Techniques on Big Data. *IEEE Access*, **8**: 54776-54788. doi:10.1109/ACCESS.2020.2980942.
- Rodríguez, L., Vives, L., and Gomez, A. 2013. Conceptual and numerical modeling approach of the Guarani Aquifer System. *Hydrol. Earth Syst. Sci.*, **17**: 295-314. doi:10.5194/hess-17-295-2013.
- Sabat, L., and Kundu, C.K. 2020. History of finite element method: a review. *Recent Developments in Sustainable Infrastructure: Select Proceedings of ICRDSI 2019*: 395-404.
- Sajedi-Hosseini, F., Malekian, A., Choubin, B., Rahmati, O., Cipullo, S., Coulon, F., and Pradhan, B. 2018. A novel machine learning-based approach for the risk assessment of nitrate groundwater contamination. *Science of the Total Environment*, **644**: 954-962. doi:<https://doi.org/10.1016/j.scitotenv.2018.07.054>.
- Sanchez, P., Voisey, J.P., Xia, T., Watson, H.I., O'Neil, A.Q., and Tsafaris, S.A. 2022. Causal machine learning for healthcare and precision medicine. *Royal Society Open Science*, **9**: 220638.

- Schichl, H. 2004. Models and the history of modeling. Modeling languages in mathematical optimization: 25-36.
- Schwartz, M.O. 2006. Numerical modelling of groundwater vulnerability: the example Namibia. *Environmental Geology*, **50**: 237-249. doi:10.1007/s00254-006-0204-6.
- Shadab, M.A., Luo, D., Hiatt, E., Shen, Y., and Hesse, M.A. 2023. Investigating steady unconfined groundwater flow using Physics Informed Neural Networks. *Advances in Water Resources*, **177**: 104445. doi:<https://doi.org/10.1016/j.advwatres.2023.104445>.
- Singha, S., Pasupuleti, S., Singha, S.S., Singh, R., and Kumar, S. 2021. Prediction of groundwater quality using efficient machine learning technique. *Chemosphere*, **276**: 130265. doi:<https://doi.org/10.1016/j.chemosphere.2021.130265>.
- Sloan, W.T. 2000. A physics-based function for modeling transient groundwater discharge at the watershed scale. *Water Resources Research*, **36**: 225-241. doi:<https://doi.org/10.1029/1999WR900221>.
- Solomatine, D.P., Dibike, Y.B., and Kukuric, N. 1999. Automatic calibration of groundwater models using global optimization techniques. *Hydrological Sciences Journal*, **44**: 879-894. doi:10.1080/02626669909492287.
- Tang, Y., Lu, C., and Luo, J. 2023. An Analytical solution for groundwater lens pumping in a three-dimensional rectangular island. *Journal of Hydrology*, **617**: 128928. doi:<https://doi.org/10.1016/j.jhydrol.2022.128928>.
- Tao, H., Hameed, M.M., Marhoon, H.A., Zounemat-Kermani, M., Heddam, S., Kim, S., Sulaiman, S.O., Tan, M.L., Sa'adi, Z., Mehr, A.D., Allawi, M.F., Abba, S.I., Zain, J.M., Falah, M.W., Jamei, M., Bokde, N.D., Bayatvarkeshi, M., Al-Mukhtar, M., Bhagat, S.K., Tiyasha, T., Khedher, K.M., Al-Ansari, N., Shahid, S., and Yaseen, Z.M. 2022. Groundwater level prediction using machine learning models: A comprehensive review. *Neurocomputing*, **489**: 271-308. doi:<https://doi.org/10.1016/j.neucom.2022.03.014>.
- Tracy, F.T. 1995. 1-D, 2-D, and 3-D analytical solutions of unsaturated flow in groundwater. *Journal of Hydrology*, **170**: 199-214. doi:[https://doi.org/10.1016/0022-1694\(94\)02674-Z](https://doi.org/10.1016/0022-1694(94)02674-Z).

- Vadyala, S.R., Betgeri, S.N., Matthews, J.C., and Matthews, E. 2022. A review of physics-based machine learning in civil engineering. *Results in Engineering*, **13**: 100316. doi:<https://doi.org/10.1016/j.rineng.2021.100316>.
- Van Geer, F., and Van Der Kloet, P. 1985. Two algorithms for parameter estimation in groundwater flow problems. *Journal of Hydrology*, **77**: 361-378.
- Vigiak, O., Sterk, G., Romanowicz, R.J., and Beven, K.J. 2006. A semi-empirical model to assess uncertainty of spatial patterns of erosion. *CATENA*, **66**: 198-210. doi:<https://doi.org/10.1016/j.catena.2006.01.004>.
- Wagner, N., and Rondinelli, J.M. 2016. Theory-guided machine learning in materials science. *Frontiers in Materials*: 28. doi:<https://doi.org/10.3389/fmats.2016.00028>.
- Wang, J., Li, Y., Zhao, R., and Gao, R.X. 2020a. Physics guided neural network for machining tool wear prediction. *Journal of Manufacturing Systems*, **57**: 298-310. doi:<https://doi.org/10.1016/j.jmsy.2020.09.005>.
- Wang, N., Chang, H., and Zhang, D. 2021a. Efficient uncertainty quantification for dynamic subsurface flow with surrogate by Theory-guided Neural Network. *Computer Methods in Applied Mechanics and Engineering*, **373**: 113492. doi:<https://doi.org/10.1016/j.cma.2020.113492>.
- Wang, N., Chang, H., and Zhang, D. 2021b. Theory-guided Auto-Encoder for surrogate construction and inverse modeling. *Computer Methods in Applied Mechanics and Engineering*, **385**: 114037. doi:<https://doi.org/10.1016/j.cma.2021.114037>.
- Wang, N., Zhang, D., Chang, H., and Li, H. 2020b. Deep learning of subsurface flow via theory-guided neural network. *Journal of Hydrology*, **584**: 124700. doi:<https://doi.org/10.1016/j.jhydrol.2020.124700>.
- Wu, J., and Zeng, X. 2013. Review of the uncertainty analysis of groundwater numerical simulation. *Chinese Science Bulletin*, **58**: 3044-3052. doi:10.1007/s11434-013-5950-8.
- Wu, Q., Zhou, W., Li, S., and Wu, X. 2005. Application of grey numerical model to groundwater resource evaluation. *Environmental Geology*, **47**: 991-999. doi:10.1007/s00254-005-1229-y.

- Wuest, T., Weimer, D., Irgens, C., and Thoben, K.-D. 2016. Machine learning in manufacturing: advantages, challenges, and applications. *Production & Manufacturing Research*, **4**: 23-45. doi:10.1080/21693277.2016.1192517.
- Xu, R., Zhang, D., Rong, M., and Wang, N. 2021. Weak form theory-guided neural network (TgNN-wf) for deep learning of subsurface single- and two-phase flow. *Journal of Computational Physics*, **436**: 110318. doi:<https://doi.org/10.1016/j.jcp.2021.110318>.
- Xu, T., and Liang, F. 2021. Machine learning for hydrologic sciences: An introductory overview. *WIREs Water*, **8**: e1533. doi:<https://doi.org/10.1002/wat2.1533>.
- Yadav, B., Gupta, P.K., Patidar, N., and Himanshu, S.K. 2020. Ensemble modelling framework for groundwater level prediction in urban areas of India. *Science of the Total Environment*, **712**: 135539. doi:<https://doi.org/10.1016/j.scitotenv.2019.135539>.
- Ying, H.-w., Zhu, C.-w., Shen, H.-w., and Gong, X.-n. 2018. Semi-analytical solution for groundwater ingress into lined tunnel. *Tunnelling and Underground Space Technology*, **76**: 43-47. doi:<https://doi.org/10.1016/j.tust.2018.03.009>.
- Yu, Z. 2015. HYDROLOGY, FLOODS AND DROUGHTS | Modeling and Prediction. In *Encyclopedia of Atmospheric Sciences* (Second Edition). Edited by G.R. North and J. Pyle and F. Zhang. Academic Press, Oxford. pp. 217-223.
- Zhao, C., Wang, Y., Chen, X., and Li, B. 2005. Simulation of the effects of groundwater level on vegetation change by combining FEFLOW software. *Ecological Modelling*, **187**: 341-351. doi:<https://doi.org/10.1016/j.ecolmodel.2004.10.019>.
- Zobeiry, N., and Humfeld, K.D. 2021. A physics-informed machine learning approach for solving heat transfer equation in advanced manufacturing and engineering applications. *Engineering Applications of Artificial Intelligence*, **101**: 104232. doi:<https://doi.org/10.1016/j.engappai.2021.104232>.

# **CHAPITRE 1**

## **GÉNÉRALITE SUR L'APPRENTISSAGE AUTOMATIQUE**

Ce chapitre vise à présenter les bases de l'intelligence artificielle (IA) et de l'apprentissage automatique (ML) aux hydrogéologues qui lisent cette thèse et qui ne sont pas familiers avec les concepts associés à l'IA et au ML, étant donné que ces deux domaines sont encore émergents en hydrogéologie.

### **1.1 INTELLIGENCE ARTIFICIELLE ET APPRENTISSAGE AUTOMATIQUE**

On perçoit généralement comme caractéristiques de l'intelligence le fait de penser, d'imaginer, de créer, de mémoriser, de comprendre, de reconnaître des modèles, de faire des choix, de s'adapter au changement et d'apprendre par l'expérience (Colom et al. 2010; Khanzode and Sarode 2020). En ce sens, l'intelligence artificielle est définie comme l'intelligence dont font preuve les machines (programmes informatiques) pour répondre à une problématique donnée en beaucoup moins de temps qu'un humain (Ongsulee 2017). L'intelligence artificielle est également un domaine de recherche dans lequel les machines sont entraînées à mimer le comportement des êtres humains (Gupta et al. 2021). Elle comprend plusieurs branches telles que la vision par ordinateur, le traitement automatique des langues ou l'apprentissage automatique (Hashimoto et al. 2018).

La vision par ordinateur a pour objectif de donner aux machines la capacité de voir comme les humains. En particulier, elle permet aux machines d'extraire des informations utiles à partir de données visuelles telles que les images numériques et les vidéos et de prendre des mesures sur la base de ces informations (IBM 2023). En ce qui concerne le traitement automatique des langues, il s'agit de la branche de l'intelligence artificielle qui vise à développer des machines capables de comprendre, de produire et de lire des textes de la même manière que les êtres humains (Hirschberg

and Manning 2015). Enfin, l'apprentissage automatique s'intéresse à l'étude et au développement d'algorithmes que les machines peuvent utiliser pour effectuer une tâche spécifique de manière efficace, sans avoir été explicitement programmées pour le faire (Bishop and Nasrabadi 2006). Dans cette thèse, l'intérêt est exclusivement porté à l'apprentissage automatique.

## 1.2 RÉSOUDRE UN PROBLÈME PAR L'APPRENTISSAGE AUTOMATIQUE

L'apprentissage automatique est la branche de l'intelligence artificielle qui se concentre sur le développement d'algorithmes dont le rôle est de dériver des modèles à partir de données ; les modèles obtenus peuvent ensuite être utilisés soit pour améliorer notre compréhension des données, soit pour faire des prédictions sur de nouvelles données. De ce point de vue, l'apprentissage automatique apparaît comme un outil permettant de résoudre des problèmes. La résolution d'un problème à l'aide de l'apprentissage automatique implique un flux de travail qui est synthétisé dans la **Figure 1** et détaillé dans les paragraphes suivants.

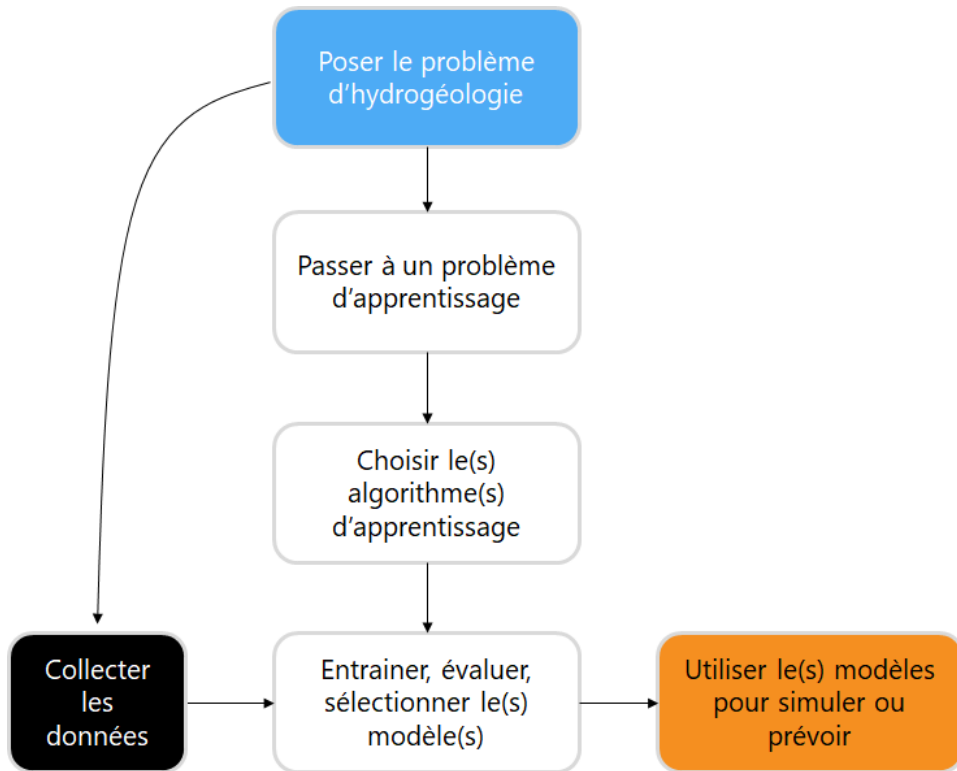


**Figure 1** Flux de travail simplifié pour la résolution de problèmes par l'apprentissage automatique

### 1.2.1 POSER LE PROBLÈME HYDROGÉOLOGIQUE

Pour utiliser l'apprentissage automatique, il faut d'abord définir le problème à résoudre, les objectifs visés, puis examiner les données disponibles. L'objectif peut être de réaliser des simulations ou des prévisions relatives à une certaine grandeur, comme les niveaux piézométriques ou la concentration de polluant dans un aquifère, ou d'analyser une quantité importante de données (géospatiales par exemple) afin d'en extraire des informations utiles. Une fois l'objectif défini, l'étape suivante consiste à collecter et à examiner les données. À ce stade, il convient de déterminer si les données disponibles sont suffisantes pour être utilisées dans le cadre d'un problème d'apprentissage automatique, puis d'examiner le type de données (continues ou non, catégorielles ou non) et de déterminer si elles sont entièrement, partiellement ou non étiquetées.

La notion de données étiquetées intervient lorsque l'on souhaite établir une relation entre une variable  $y$  (appelée étiquette) et une variable  $x$  (appelée caractéristique). Un jeu de données est dit étiqueté lorsqu'il est décrit par des paires caractéristique-étiquette ; dans le cas contraire, lorsque les caractéristiques ne sont pas associées à des étiquettes, le jeu de données est dit non étiqueté. La paire  $(x_i, y_i)$  est également appelée exemple, observation ou instance du couple de variables  $x$  et  $y$ . En fonction de l'objectif visé, de la disponibilité des données et de leur étiquetage ou non, le problème hydrogéologique à résoudre peut être transformé en un problème spécifique d'apprentissage automatique.

### **1.2.2 DU PROBLÈME D'HYDROGÉOLOGIE À UN PROBLÈME D'APPRENTISSAGE**

Il existe quatre problèmes classiques d'apprentissage automatique : l'apprentissage supervisé, l'apprentissage non supervisé, l'apprentissage semi-supervisé et l'apprentissage par renforcement.

#### **1.2.2.1 APPRENTISSAGE SUPERVISÉ**

L'apprentissage supervisé est un problème d'apprentissage automatique qui vise à simuler une variable  $y$  à partir d'une ou de plusieurs autres variables  $x$ . Dans ce type de problème, un algorithme d'apprentissage automatique est entraîné à déterminer un modèle mathématique qui simule avec justesse les valeurs de  $y$  à partir des valeurs de  $x$ , en lui montrant un échantillon suffisant de couples de valeurs  $(x_i, y_i)$ . Ce type de problème est envisagé lorsque le jeu de données disponible est étiqueté. Les étiquettes supervisent l'apprentissage de l'algorithme. Il existe deux types de problèmes d'apprentissage supervisé, selon que la variable à simuler est continue ou discrète. Lorsque la variable à simuler est continue, l'apprentissage supervisé est défini comme un problème

de régression, alors qu'il est défini comme un problème de classification lorsque la variable à simuler est discrète.

### **1.2.2.2 APPRENTISSAGE NON SUPERVISÉ**

L'apprentissage non supervisé est utilisé lorsque le jeu de données ne contient pas d'étiquettes ou de catégories préalablement définies. Ce type d'approche est utile lorsque l'objectif est de découvrir des structures ou des patterns significatifs au sein d'un large ensemble de données, ou de produire une représentation synthétique du jeu de données qui facilite sa compréhension. Le partitionnement et la réduction de dimensionnalité sont deux problèmes typiques d'apprentissage non supervisé. En considérant un jeu de N données non étiquetées  $\{x_i\}_{i=1,\dots,N}$  avec  $x_i$  une donnée de dimension  $D$ , le partitionnement est un problème d'apprentissage non supervisé qui permet de regrouper ce jeu de données en K parties ou clusters ( $K < N$ ) de telle sorte que les données d'un même cluster partagent des caractéristiques similaires et que les données de deux clusters distincts présentent une dissimilarité suffisante. L'objectif de la réduction de dimensionnalité est de projeter le jeu de données de son espace initial de dimension  $D$  dans un espace de dimension inférieur. L'analyse en composantes principales (ACP) est un exemple de technique de réduction de dimensionnalité.

### **1.2.2.3 APPRENTISSAGE SEMI-SUPERVISÉ**

Il peut arriver que le jeu de données ne soit que partiellement étiqueté. Si l'effort requis pour compléter l'étiquetage du jeu de données semble considérable, à la fois en termes de temps et de ressources financières, ou s'il est tout simplement impossible d'effectuer une telle action d'étiquetage, l'apprentissage semi-supervisé peut alors être envisagé. L'apprentissage semi-supervisé permet à un algorithme d'apprendre à estimer les valeurs d'une variable à partir d'un jeu de données partiellement étiquetées, les données étiquetées servant à contraindre l'algorithme dans son

apprentissage. Un exemple concret pourrait être de pouvoir construire des séries de niveaux piézométriques en des points d'un aquifère où il n'y a pas de piézomètres, en utilisant les observations des niveaux d'eau de quelques piézomètres et des données climatiques.

#### **1.2.2.4 APPRENTISSAGE PAR RENFORCEMENT**

Dans l'apprentissage par renforcement, l'algorithme est soumis à un environnement dynamique dans lequel toute action ou séquence d'actions qu'il effectue est soit récompensée, soit punie, et l'objectif est qu'il soit capable de définir une stratégie lui permettant de maximiser ses récompenses. Dans ce type d'apprentissage, les données sont typiquement générées par les interactions de l'algorithme avec l'environnement (Suzuki 2011). L'apprentissage par renforcement peut donc servir à former des algorithmes capables de prendre des décisions en matière de gestion des ressources en eau (Bhattacharya et al. 2003; Bowes et al. 2022).

#### **1.2.3 CHOISIR UN ALGORITHME D'APPRENTISSAGE**

Après les données, le deuxième pilier sur lequel repose l'apprentissage automatique est l'algorithme d'apprentissage (Azencott 2022) qui peut être défini comme un modèle ou une procédure mathématique que l'on calibre sur des données pour résoudre un problème spécifique. Un même algorithme d'apprentissage peut être utilisé pour résoudre un ou plusieurs problèmes d'apprentissage automatique. Cependant, le choix de l'algorithme spécifique permettant de résoudre efficacement un problème n'obéit à aucune règle ni à aucun principe. En effet, un algorithme qui fonctionne bien pour un problème peut ne pas convenir à un autre (Wolpert and Macready 1997). Par conséquent, une palette d'algorithmes est généralement présélectionnée par rapport au problème à résoudre et soumise aux données afin d'identifier et d'isoler les algorithmes qui produisent les modèles les moins complexes et les plus performants. Plusieurs études, dont Tao et al. (2022), Haggerty et al. (2023)

et Fukami et al. (2020) proposent une analyse comparative de certains algorithmes d'apprentissage et pourraient être utiles pour la présélection des algorithmes.

La gamme d'algorithmes sélectionnés représente ce que l'on appelle l'espace des hypothèses (Azencott 2022). Cela signifie que dans un problème d'apprentissage, nous partons du principe que le modèle à découvrir à partir des données se situe nécessairement dans l'espace d'hypothèses choisi. Ainsi, plus l'espace d'hypothèses est grand, plus la probabilité de trouver le modèle qui décrit le mieux les données est élevée, mais les coûts de calcul nécessaires pour trouver ce modèle augmentent proportionnellement. Un espace des hypothèses peut être formé d'algorithmes paramétriques, d'algorithmes non paramétrique ou d'une combinaison de ces deux types d'algorithmes.

#### **1.2.3.1 ALGORITHMES PARAMÉTRIQUES D'APPRENTISSAGE**

Un algorithme paramétrique d'apprentissage est un modèle mathématique avec un nombre fini de paramètres et une forme analytique connue. Son apprentissage a pour but d'ajuster les paramètres du modèle qu'il décrit, à l'aide de données relatives au problème à résoudre. Il existe de nombreux algorithmes paramétriques d'apprentissage, notamment la régression linéaire, la régression logistique, les réseaux bayésiens et les réseaux neuronaux artificiels. Certaines études, comme Singh et al. (2016) ou Osisanwo et al. (2017), traitent des forces et des faiblesses de ces algorithmes.

#### **1.2.3.2 ALGORITHMES NON-PARAMÉTRIQUES D'APPRENTISSAGE**

Un algorithme d'apprentissage non paramétrique ne fait aucune hypothèse sur la forme du modèle, mais utilise les données pour déduire les règles auxquelles elles obéissent. Ces algorithmes

ont un plus grand degré de liberté que les algorithmes paramétriques, mais leur complexité peut augmenter de façon exponentielle avec la quantité de données disponibles. Les arbres de décision, les forêts aléatoires, les machines à vecteurs de support et la méthode des k plus proches voisins sont des exemples d'algorithmes non-paramétriques. Les forces et les faiblesses de certains de ces algorithmes sont énumérées dans Singh et al. (2016).

#### **1.2.4 ENTRAINER, ÉVALUER, SÉLECTIONNER UN MODÈLE**

Entraîner un algorithme d'apprentissage automatique est un problème d'optimisation dans lequel le but est d'optimiser (minimiser ou maximiser) une fonction objective. Par exemple, dans un problème d'apprentissage supervisé utilisant un algorithme paramétrique, l'apprentissage peut consister à ajuster convenablement les valeurs des paramètres du modèle afin de minimiser l'écart moyen entre les observations et les sorties du modèle. L'écart moyen représente ici la fonction objective (ou fonction de coût dans ce cas précis).

Pour entraîner un algorithme d'apprentissage automatique, la procédure traditionnelle consiste à subdiviser l'ensemble de données en trois sous-ensembles indépendants – un jeu d'entraînement, un jeu de validation et un jeu de test. Il n'y a pas de règles sur les proportions à choisir pour ces jeux de données, mais il est courant de voir dans la littérature des subdivisions du type 70%-10%-20% par rapport au jeu de données initial.

Le jeu d'apprentissage est utilisé pour optimiser la fonction objective définie, tandis que le jeu de validation est utilisé pour vérifier si, au cours de l'apprentissage, le modèle ou les règles apprises par l'algorithme maintiennent une fonction objective optimale. Le jeu de données de validation est donc utilisé pour sélectionner le modèle optimal, c'est-à-dire un modèle qui n'a ni sur-appris ni sous-appris. Le sur-apprentissage fait référence à un modèle qui performe très bien sur le

jeu de données d'entraînement mais très mal sur le jeu de données de validation, tandis que le sous-apprentissage désigne un modèle qui performe mal à la fois sur le jeu de données d'entraînement et sur le jeu de données de validation. Enfin, le jeu de test est utilisé pour évaluer la capacité de généralisation du modèle appris. La généralisation est un concept dont la définition n'est pas consensuelle, puisqu'elle se réfère tantôt à la capacité d'interpolation du modèle, tantôt à sa capacité d'extrapolation. Dans cette thèse, nous considérerons la seconde définition. Ainsi, la généralisation fait référence à la capacité d'un modèle à faire des prédictions correctes sur des données statistiquement différentes de celles utilisées pour son entraînement et sa validation. Après la sélection d'un modèle optimal, celui-ci peut être déployé en vue d'une utilisation opérationnelle.

## 1.3 PROBLÈME DE RÉGRESSION ET RÉSEAUX DE NEURONES ARTIFICIELS

### 1.3.1 PROBLÈME DE RÉGRESSION

La régression est un problème d'apprentissage supervisé qui traite de variables continues. Une définition générale de la régression a été donnée dans la Section 1.2.2.1. Dans cette section, une définition formelle de la régression dans le cas spécifique des algorithmes paramétriques, dont les réseaux neuronaux artificiels font partie, est proposée.

#### 1.3.1.1 DÉFINITION

Considérons un jeu de données d'entraînement étiquetées  $\{(x_i, y_i)\}_{i=1,\dots,N}$  avec  $(x_i, y_i) \in \Gamma^n \times \Gamma^m \subset \mathbb{R}^{n+m}$ ,  $x_i$  la i-ème instance de la variable  $x$  de dimension  $n$  associée à la i-ème instance  $y_i$  de la variable  $y$  de dimension  $m$ . Supposons qu'il existe un algorithme paramétrique  $\phi$  de paramètre  $\theta$  qui est tel que pour tout couple de valeur  $(x_i, y_i)$ ,  $y_i = \phi(x_i, \theta) + \varepsilon_i$ , où  $\varepsilon_i$  est un terme d'erreur. Considérons également la fonction de coût  $L$  et le risque empirique  $R$  associé à cette

fonction de coût sur les  $N$  instances (exemples). Le risque empirique  $R$  est définie par l'équation (1.1).

$$R(\theta) = \frac{1}{N} \sum_{i=1 \dots N} L(y_i, \phi(x_i, \theta)) \quad (1.1)$$

La régression est un problème d'optimisation dont le but est de trouver la valeur optimale  $\theta_s$  qui permet de minimiser le risque  $R$  sur le jeu d'entraînement comme défini par l'équation (1.2).

$$\theta_s = \arg \min_{\theta} \{R(\theta)\} \quad (1.2)$$

La recherche de l'optimum  $\theta_s$  qui minimise le risque empirique est effectuée à l'aide d'un algorithme d'optimisation.

### 1.3.1.2 ALGORITHME D'OPTIMISATION

Il existe un large éventail d'algorithmes d'optimisation, regroupés en deux catégories : les algorithmes d'optimisation précise et les algorithmes d'optimisation approximative (Zhang et al. 2022). Les algorithmes d'optimisation précise effectuent une recherche presque complète dans l'espace des valeurs des paramètres  $\theta$ , ce qui les rend coûteux en termes de capacité et de temps de calcul. A l'inverse, les algorithmes d'optimisation approximative effectuent une recherche dans un sous-espace de l'espace des valeurs de  $\theta$ , ce qui leur permet de trouver une solution avec des coûts et un temps de calcul raisonnables, mais il n'y a pas de garantie que la solution obtenue soit un minimum global. Le minimum global représente la plus petite valeur (minimum) que le risque empirique peut prendre dans l'espace des valeurs de  $\theta$ , tandis que le minimum local représente une valeur dans l'ensemble des valeurs minimales que le risque empirique peut prendre dans l'espace des valeurs de  $\theta$ . Dans un problème de minimisation, l'on recherche idéalement un minimum global.

Les algorithmes d'optimisation approximative sont divisés en deux classes : les algorithmes heuristiques et les algorithmes méta-heuristiques. Les algorithmes d'optimisation précise peuvent être subdivisés en plusieurs sous-algorithmes, tels que la descente de gradient, le gradient stochastique, la descente de gradient par mini-lot et l'algorithme d'estimation adaptative des moments (ou Adaptive Moment Estimation – Adam en anglais) (Kingma and Ba 2014; Singarimbun et al. 2019). Les algorithmes d'optimisation utilisés dans cette thèse sont des algorithmes d'optimisation précise. Une brève description des algorithmes d'optimisation précise précédés est présentée. Adam est l'algorithme utilisé tout au long de cette thèse.

#### 1.3.1.2.1 ALGORITHME DE DESCENTE DE GRADIENT

Notons  $x = (x_1, \dots, x_N)$ , le tenseur regroupant  $N$  instances  $x_i \in \Gamma^n$  associé au tenseur  $y = (y_1, \dots, y_N)$  de  $N$  instances  $y_i \in \Gamma^m$ . L'algorithme de descente de gradient est un algorithme itératif qui peut être décrit comme suit :

- **Étape 1 :** initialisation du paramètre  $\theta$  à optimiser. Dans cette étape, une valeur initiale  $\theta_0$  aléatoire est affectée au paramètre  $\theta$ . Il existe différentes stratégies d'initialisation que l'on peut consulter dans Sousa (2016) ou Narkhede et al. (2022).
- **Étape 2 :** estimation des valeurs cibles par l'algorithme. Le tenseur  $x$  et la valeur  $\theta_0$  permettent à l'algorithme d'apprentissage de produire une première estimation  $\hat{y} = (\hat{y}_1, \dots, \hat{y}_N)$  des valeurs de la variable cible :  $\hat{y} = \phi(x, \theta_0)$ .

- **Étape 3 :** calcul du gradient du risque empirique et mise à jour de  $\theta$ . A partir de l'estimation  $\hat{y}$ , l'on peut calculer le gradient  $\nabla R$  du risque empirique  $R$  sur le jeu de donnée d'entraînement  $\Gamma^n \times \Gamma^m$  (Équation (1.3)).

$$\nabla R(\theta) = \frac{1}{N} \sum_{i=1 \dots N} \nabla L(y_i, \phi(x_i, \theta)) \quad (1.3)$$

Comme l'on cherche à minimiser le risque empirique, la nouvelle valeur  $\theta_j$  du paramètre  $\theta$  est donnée par l'équation (1.4).

$$\theta_j = \theta_{j-1} - \eta \nabla R(\theta_{j-1}) \quad (1.4)$$

avec  $\theta_j$  représentant la valeur du paramètre  $\theta$  à la  $j$ -ème itération ( $j \geq 1$ ) et  $\eta$  une constante positive appelée taux d'apprentissage. Le taux d'apprentissage représente la vitesse à laquelle la recherche de l'optimum est effectuée. Une valeur trop grande de  $\eta$  peut entraîner une stagnation ou une oscillation de l'optimisation, tandis qu'une valeur trop petite augmente le temps nécessaire pour atteindre un optimum.

- **Étape 4 :** à partir de la nouvelle valeur  $\theta_j$  de  $\theta$ , on exécute les étapes 2 et 3  $K$  fois ou jusqu'à ce que le risque empirique  $R$  soit inférieur ou égal à un critère objectif  $\xi > 0$  prédéfini. On considère alors qu'à la fin de l'étape 4, la valeur obtenue de  $\theta = \theta_s$ .

### 1.3.1.2.2 ALGORITHME DU GRADIENT STOCHASTIQUE

L'algorithme du gradient stochastique suit les mêmes étapes que celles de la descente de gradient. La principale différence réside à l'étape 3 (Équation (1.3)). Dans la descente de gradient, le risque empirique est calculé en utilisant tout le jeu d'entraînement. Cela rend la minimisation du risque beaucoup plus difficile. Pour surmonter ce problème, l'algorithme du gradient stochastique

sélectionne aléatoirement une instance  $(x_i, y_i)$  à chaque itération et approxime le risque empirique par le coût associé à cette instance (Équation (1.5)).

$$\nabla R(\theta_{j-1}) = \nabla L(y_i, \phi(x_i, \theta_{j-1})) \quad (1.5)$$

### 1.3.1.2.3 ALGORITHME DE DESCENTE DE GRADIENT PAR MINI-LOT

La descente de gradient par mini-lot est une solution intermédiaire entre la descente de gradient, qui présente l'inconvénient de rendre difficile la convergence du risque empirique, et le gradient stochastique, qui facilite la convergence du risque mais peut être beaucoup plus gourmand en ressources. Dans cet algorithme, le gradient du risque empirique n'est ni calculé à partir du jeu de données entier, ni approximé à partir d'une instance  $(x_i, y_i)$  sélectionnée aléatoirement, mais plutôt approximé à partir d'un échantillonnage aléatoire d'un sous-jeu de données contenant  $M_k \leq N$  instances. Ce gradient est donné par l'équation (1.6).

$$\nabla R_k(\theta_{j-1}) = \frac{1}{M_k} \sum_{i=1 \dots M_k} \nabla L(y_i, \phi(x_i, \theta_{j-1})) \quad (1.6)$$

où  $R_k$  est le risque empirique associé au k-ème sous-jeu de données aléatoires pris dans le jeu d'entraînement.

### 1.3.1.2.4 ESTIMATION ADAPTATIVE DES MOMENTS (ADAM)

Adam est une extension de la descente de gradient par mini-lot dans laquelle la mise à jour du paramètre  $\theta$  est effectuée en tenant compte de l'historique de gradients du risque empirique afin d'accélérer la convergence, comme le décrivent les équations (1.7) à (1.9) (Zhang et al. 2021).

$$\theta_j = \theta_{j-1} - \eta \frac{\frac{v_j}{1 - \beta_1^j}}{\sqrt{\frac{s_j}{1 - \beta_2^j} + \epsilon}} \quad (1.7)$$

$$v_j = \beta_1 \cdot v_{j-1} + (1 - \beta_1) \cdot \nabla R_k(\theta_{j-1}) \quad (1.8)$$

$$s_j = \beta_2 \cdot s_{j-1} + (1 - \beta_2) \cdot (\nabla R_k(\theta_{j-1}))^2 \quad (1.9)$$

où  $\beta_1$  et  $\beta_2$  sont des constantes comprises entre 0 et 1.  $\epsilon$  est une constante positive très proche de zéro qui assure la stabilité numérique de l'algorithme sans nuire à sa justesse. Adam nécessite de faibles coûts de calcul et moins de mémoire d'exécution (Ogundokun et al. 2022), c'est pourquoi il a été choisi pour l'apprentissage dans le cadre de cette thèse.

### 1.3.2 RÉSEAUX DE NEURONES ARTIFICIELS

Les réseaux neuronaux artificiels sont une famille d'algorithmes d'apprentissage automatique dont la construction s'inspire de la manière dont les neurones biologiques se transmettent des signaux. Un réseau de neurones artificiels se compose d'une pile de blocs unitaires interconnectés appelés neurones artificiels. Ces neurones artificiels sont organisés en couches d'entrée, en couches cachées et en couches de sortie afin de faciliter la formalisation mathématique des réseaux neuronaux artificiels. La couche d'entrée est constituée des données d'entrée et la couche de sortie produit le résultat final. Entre ces deux couches, il y a une boîte noire composée d'une ou plusieurs couches dites cachées, dont le rôle est d'analyser les données d'entrée afin de produire une sortie qui se rapproche des données cibles (étiquettes). Plus il y a de couches cachées, plus le modèle résultant de l'apprentissage est complexe. Les neurones artificiels pouvant être interconnectés de différentes manières, il est possible de construire une multitude de topologies différentes de réseaux neuronaux artificiels. Toutefois, ces topologies sont regroupées en deux catégories : la topologie acyclique et la topologie cyclique ou récurrente (Krenker et al. 2011).

### 1.3.2.1 RÉSEAUX DE NEURONES ACYCLIQUES

Dans un réseau neuronal acyclique, les données se propagent dans une seule direction, de la couche d'entrée à la couche de sortie. Il existe un important spectre de réseaux acycliques, dont le perceptron multicouche et les réseaux de neurones convolutifs.

#### 1.3.2.1.1 PERCEPTRON MULTICOUCHE

Le perceptron multicouche est un type de réseau de neurones acyclique constitué d'une couche d'entrée, d'une ou plusieurs couches dites cachées et d'une couche de sortie, toutes empilées les unes après les autres. Le nombre de neurones dans la couche d'entrée et le nombre de neurones dans la couche de sortie sont fixés respectivement par le nombre de variables d'entrée et de sortie. Le nombre  $K$  de couches cachées ainsi que le nombre de neurones contenu dans chaque couche cachée sont appelés hyperparamètres du perceptron multicouche. Ces hyperparamètres peuvent être ajustés manuellement ou déterminés par un algorithme d'optimisation méta-heuristique, par exemple. La connexion entre deux couches successives du perceptron multicouche est décrite à l'aide d'un couple de paramètres  $(W^j, b^j)$  et d'une fonction  $F^j$  dite d'activation.  $W^j$  (matrice) est appelé poids ou noyau de la connexion entre les couches  $j - 1$  et  $j$  et  $b^j$  est appelé le biais de la connexion. Si l'on désigne par  $x^j$  l'entrée de la couche  $j$  et par  $y^j$  la sortie de cette couche, la relation entre l'entrée et la sortie est décrite par l'Équation (1.10).

$$y^j = F^j \left( x^j \cdot (W^j)^T + b^j \right) \quad (1.10)$$

Pour  $j = 1$ ,  $x^j = x$  (variables d'entrée) et pour  $j = K + 1$ ,  $y^j = y$  (variables de sortie). Il existe différentes fonctions d'activation, dont les plus couramment utilisées sont la fonction linéaire, la fonction sigmoïde, la fonction tangente hyperbolique et la fonction « redresseur ». En règle générale,

on applique une fonction d'activation linéaire à la couche de sortie. Il est également possible d'avoir une seule fonction d'activation pour toutes les couches cachées.

Un perceptron multicouche est entraîné au moyen d'un algorithme d'optimisation (exemple, Adam). À chaque itération du problème d'optimisation, les données d'entrée transmises à la couche d'entrée sont transformées puis transférées à la première couche cachée selon l'Équation (1.10). Les données reçues par la première couche cachée sont à leur tour transmises de la même manière que précédemment à la couche cachée suivante. La procédure est répétée jusqu'à la couche de sortie. Les résultats de la couche de sortie et les étiquettes associées sont ensuite utilisés pour calculer le gradient du risque empirique. Ce dernier est alors utilisé pour ajuster les valeurs de l'ensemble des noyaux  $W^j$  et des biais  $b^j$  de manière appropriée. La **Figure 2** illustre la topologie d'un perceptron multicouche et son apprentissage.

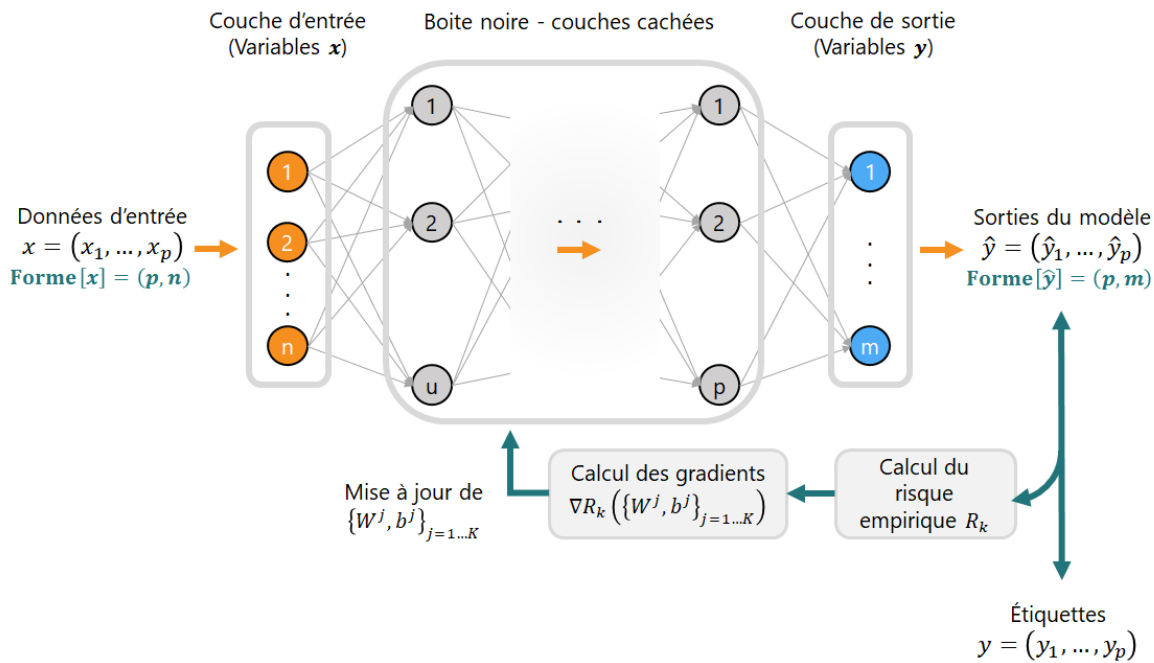


**Figure 2** Topologie du perceptron multicouche et procédure d'apprentissage. Les données d'entrée et de sortie sont bidimensionnelles : la forme des données d'entrée est  $(p, n)$  et celle des données de sortie est  $(p, m)$ , où  $p$  est le nombre d'exemples,  $n$  est le nombre de variables d'entrée et  $m$  est le nombre de variables de sortie.

Il est à noter que lorsque chaque neurone dans une couche est connecté à tous les neurones de la couche précédente et de la couche suivante, cette couche est qualifiée de couche dense. Un perceptron multicouche est donc un empilement de couches denses. Cette définition est importante pour mieux comprendre les réseaux neuronaux convolutifs.

### 1.3.2.1.2 RÉSEAUX DE NEURONES CONVOLUTIFS

Contrairement aux perceptrons multicouches, qui se composent uniquement d'un empilement de couches denses, les réseaux de neurones convolutifs ont une structure composée d'une combinaison de différentes couches organisées, dans les cas les plus simples, comme suit : couche de convolution, couche de mutualisation, couche d'aplatissement et couches denses. La

**Figure 3** illustre la topologie d'un réseau de neurones convolutifs.

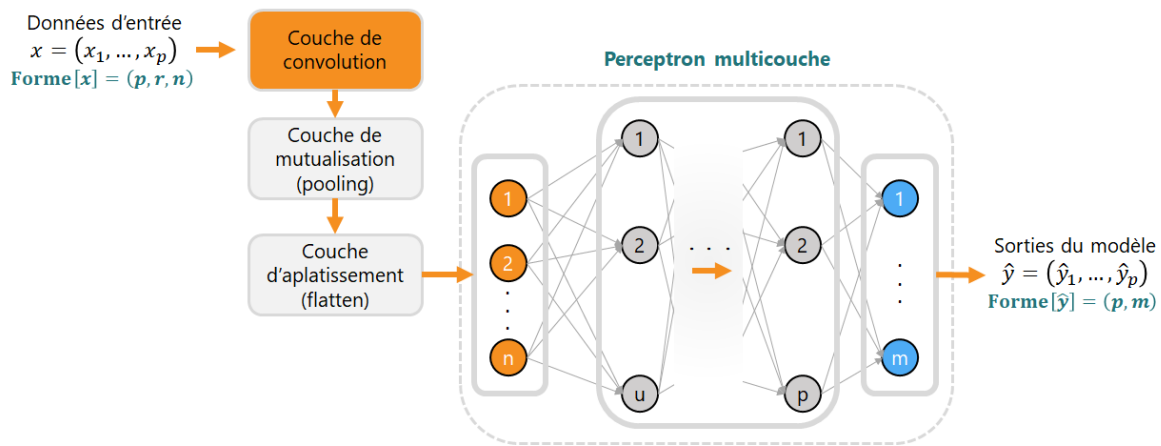


**Figure 3** Topologie d'un réseau de neurones convolutifs simple.  $p$  est le nombre d'exemples,  $r$  est la longueur de la séquence de données et  $n$  est le nombre de variables d'entrée.  $m$  représente le nombre de variables de sortie.

- **Couche de convolution :** La couche de convolution reçoit des données tridimensionnelles  $x$  de la forme  $(p, r, n)$ , effectue une opération de convolution (\*) entre l'entrée et un noyau (ou poids ou filtre)  $W^j$ , ajoute un biais  $b^j$ , transforme le

résultat de la convolution via une fonction d'activation  $F^j$  avant de le transmettre à la couche suivante (Équation (1.11)). Les données  $y^j$  transmises par la couche de convolution à la couche suivante restent des données tridimensionnelles de la forme  $(p, l, h)$  avec  $l \leq r$  et  $h \leq n$ .

$$y^j = F^j(\text{rot}_{180^\circ}(W^j) * x^j + b^j) \quad (1.11)$$

- **Couche de mutualisation (ou pooling)** : cette couche réduit la dimensionnalité des données qu'elle reçoit en n'en récupérant que les informations les plus pertinentes, transformant les données reçues, de la forme  $(p, l, h)$ , en données de la forme  $(p, c, h)$  avec  $c \leq l$ .
- **Couche d'aplatissement (ou flatten)** : Cette couche transforme les données reçues de la couche de mutualisation en données bidimensionnelles  $(p \times c \times h, 1)$  afin qu'elles puissent être utilisées par les couches denses.

### 1.3.2.2 RÉSEAUX DE NEURONES RÉCURRENTS

Dans un réseau de neurones artificiels cyclique ou récurrent, les données se propagent de la couche d'entrée à la couche de sortie, mais au cours de ce trajet, une rétroaction peut se produire entre une couche et la précédente ou au sein de la même couche. Grâce à cette rétroaction, les réseaux neuronaux récurrents disposent d'une mémoire qui leur permet de produire des résultats basés sur des données actuelles et passées. Cette mémoire les rend particulièrement adaptés au traitement de données séquentielles comme les séries temporelles de niveaux d'eau.

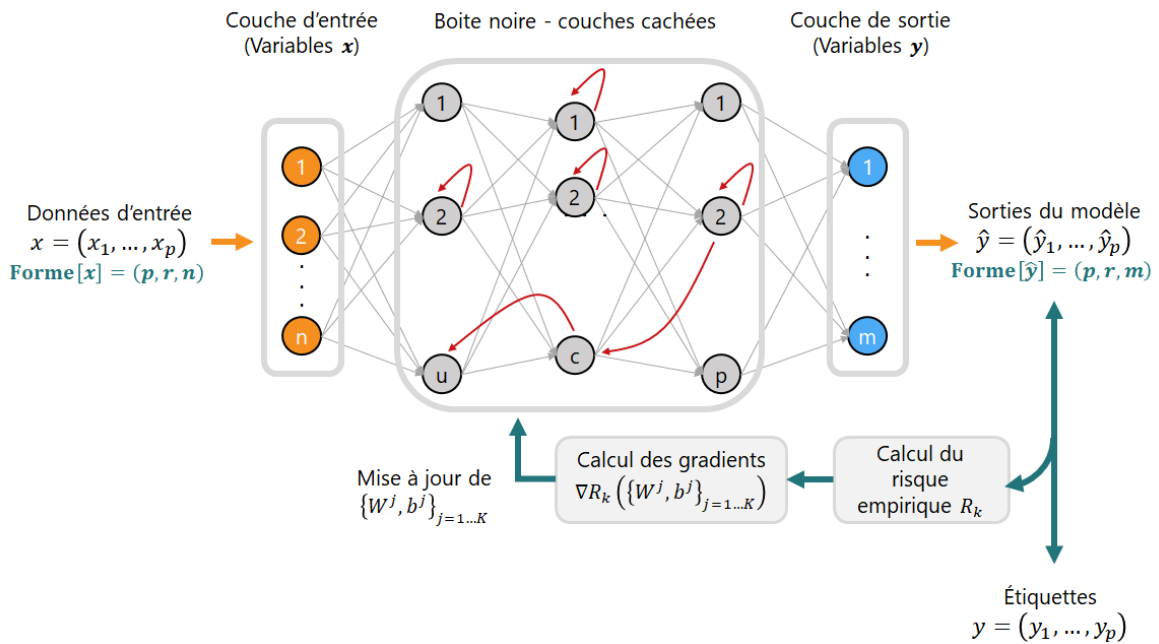


**Figure 4** Exemple de topologie d'un réseau de neurones cyclique

La **Figure 4** est une illustration simpliste des connexions possibles entre les neurones d'un réseau de neurones cyclique. Par ailleurs, il existe une large gamme de réseaux cycliques, tels que les LSTM (Long Short-Term Memory) ou les GRU (Gated Recurrent Unit).

## RÉFÉRENCES

- Azencott, C.-A. 2022. Introduction au Machine Learning-2e éd. Dunod.
- Bhattacharya, B., Lobbrecht, A., and Solomatine, D. 2003. Neural networks and reinforcement learning in control of water systems. *Journal of Water Resources Planning and Management*, **129**: 458-465.
- Bishop, C.M., and Nasrabadi, N.M. 2006. Pattern recognition and machine learning. No. 4. Springer.
- Bowes, B.D., Wang, C., Ercan, M.B., Culver, T.B., Beling, P.A., and Goodall, J.L. 2022. Reinforcement learning-based real-time control of coastal urban stormwater systems to mitigate flooding and improve water quality. *Environmental Science: Water Research & Technology*, **8**: 2065-2086.
- Colom, R., Karama, S., Jung, R.E., and Haier, R.J. 2010. Human intelligence and brain networks. *Dialogues in Clinical Neuroscience*, **12**: 489-501. doi:10.31887/DCNS.2010.12.4/rcolom.
- Fukami, K., Fukagata, K., and Taira, K. 2020. Assessment of supervised machine learning methods for fluid flows. *Theoretical and Computational Fluid Dynamics*, **34**: 497-519. doi:10.1007/s00162-020-00518-y.
- Gupta, R., Srivastava, D., Sahu, M., Tiwari, S., Ambasta, R.K., and Kumar, P. 2021. Artificial intelligence to deep learning: machine intelligence approach for drug discovery. *Molecular Diversity*, **25**: 1315-1360. doi:10.1007/s11030-021-10217-3.
- Haggerty, R., Sun, J., Yu, H., and Li, Y. 2023. Application of machine learning in groundwater quality modeling - A comprehensive review. *Water Research*, **233**: 119745. doi:<https://doi.org/10.1016/j.watres.2023.119745>.
- Hashimoto, D.A., Rosman, G., Rus, D., and Meireles, O.R. 2018. Artificial intelligence in surgery: promises and perils. *Annals of surgery*, **268**: 70.
- Hirschberg, J., and Manning, C.D. 2015. Advances in natural language processing. *Science*, **349**: 261-266. doi:doi:10.1126/science.aaa8685.
- IBM. 2023. What is computer vision? Available from <https://www.ibm.com/topics/computer-vision2023>.

- Khanzode, K.C.A., and Sarode, R.D. 2020. Advantages and disadvantages of artificial intelligence and machine learning: A literature review. International Journal of Library & Information Science (IJLIS), **9**: 3.
- Kingma, D.P., and Ba, J. 2014. Adam: A method for stochastic optimization. arXiv preprint arXiv:1412.6980.
- Krenker, A., Bešter, J., and Kos, A. 2011. Introduction to the artificial neural networks. Artificial Neural Networks: Methodological Advances and Biomedical Applications. InTech: 1-18.
- Narkhede, M.V., Bartakke, P.P., and Sutaone, M.S. 2022. A review on weight initialization strategies for neural networks. Artificial Intelligence Review, **55**: 291-322. doi:10.1007/s10462-021-10033-z.
- Ogundokun, R.O., Maskeliunas, R., Misra, S., and Damaševičius, R. Improved CNN based on batch normalization and adam optimizer. *In* International Conference on Computational Science and Its Applications. 2022. Springer, pp. 593-604.
- Ongsulee, P. Artificial intelligence, machine learning and deep learning. *In* 2017 15th international conference on ICT and knowledge engineering (ICT&KE). 2017. IEEE, pp. 1-6.
- Osisanwo, F., Akinsola, J., Awodele, O., Hinmikaiye, J., Olakanmi, O., and Akinjobi, J. 2017. Supervised machine learning algorithms: classification and comparison. International Journal of Computer Trends and Technology (IJCTT), **48**: 128-138.
- Singarimbun, R.N., Nababan, E.B., and Sitompul, O.S. Adaptive Moment Estimation To Minimize Square Error In Backpropagation Algorithm. *In* 2019 International Conference of Computer Science and Information Technology (ICoSNIKOM). 28-29 Nov. 2019 2019, pp. 1-7.
- Singh, A., Thakur, N., and Sharma, A. A review of supervised machine learning algorithms. *In* 2016 3rd international conference on computing for sustainable global development (INDIACoM). 2016. Ieee, pp. 1310-1315.
- Sousa, C.A.R.d. An overview on weight initialization methods for feedforward neural networks. *In* 2016 International Joint Conference on Neural Networks (IJCNN). 24-29 July 2016 2016, pp. 52-59.

- Suzuki, K. 2011. Artificial neural networks: methodological advances and biomedical applications. BoD–Books on Demand.
- Tao, H., Hameed, M.M., Marhoon, H.A., Zounemat-Kermani, M., Heddam, S., Kim, S., Sulaiman, S.O., Tan, M.L., Sa'adi, Z., Mehr, A.D., Allawi, M.F., Abba, S.I., Zain, J.M., Falah, M.W., Jamei, M., Bokde, N.D., Bayatvarkeshi, M., Al-Mukhtar, M., Bhagat, S.K., Tiyasha, T., Khedher, K.M., Al-Ansari, N., Shahid, S., and Yaseen, Z.M. 2022. Groundwater level prediction using machine learning models: A comprehensive review. *Neurocomputing*, **489**: 271-308. doi:<https://doi.org/10.1016/j.neucom.2022.03.014>.
- Wolpert, D.H., and Macready, W.G. 1997. No free lunch theorems for optimization. *IEEE transactions on evolutionary computation*, **1**: 67-82.
- Zhang, A., Lipton, Z.C., Li, M., and Smola, A.J. 2021. Dive into deep learning. arXiv preprint arXiv:2106.11342.
- Zhang, W., Gu, X., Tang, L., Yin, Y., Liu, D., and Zhang, Y. 2022. Application of machine learning, deep learning and optimization algorithms in geoengineering and geoscience: Comprehensive review and future challenge. *Gondwana Research*, **109**: 1-17. doi:<https://doi.org/10.1016/j.gr.2022.03.015>.

## CHAPITRE 2

### THEORY-GUIDED MACHINE LEARNING APPLIED TO HYDROGEOLOGY: STATE OF THE ART, OPPORTUNITIES AND FUTURE CHALLENGES – A REVIEW

Pour confirmer ou infirmer l'hypothèse de recherche, il est nécessaire d'évaluer comment les modèles d'apprentissage automatique guidé par la théorie (TgML) se comparent aux modèles traditionnels en termes de performance, de capacité à obéir à la physique qui régit l'écoulement des eaux souterraines et de coûts de calcul requis pour l'entraînement ou la calibration dans le cadre de problèmes d'écoulement distribués et localisés. Cette revue de la littérature a permis d'identifier les principales méthodes de développement de modèles TgML pour les problèmes d'écoulement distribué et localisé, méthodes qui ont été employées pour atteindre les deux objectifs de la thèse.

Adoubi Vincent De Paul Adombi<sup>a\*</sup>, Romain Chesnaux<sup>a</sup>, Marie-Amélie Boucher<sup>b</sup>

- a. Research Group R2Eau, Centre d'études sur les ressources minérales, Université du Québec à Chicoutimi, 555 boulevard de l'Université, Chicoutimi, Québec G7H 2B1, Canada.

Email : [adombi.vincentdepaul@gmail.com](mailto:adombi.vincentdepaul@gmail.com)

- b. Department of Civil Engineering, Université de Sherbrooke, 2500 boulevard de l'Université, Sherbrooke, Québec J1R 2R2, Canada

Reçu le 17 mai 2021 - Accepté le 30 août 2021 - Publié le 20 septembre 2021 dans la revue Hydrogeology Journal. DOI : <https://doi.org/10.1007/s10040-021-02403-2>

## 2.1 ABSTRACT

Thanks to recent technological advances, hydrogeologists now have access to large amounts of data acquired in real time. Processing these data using traditional modelling tools is difficult and poses a number of challenges especially for tasks such as extracting useful features, uncertainty quantification or identifying links between various variables. Artificial Intelligence, and more specifically its subset Machine Learning, may represent a way of the future in hydrogeological research and applications. Unfortunately, several aspects of machine learning methods hamper its adoption as a complementary tool for hydrogeologists, namely the black-box nature of most models, an often-limited generalization ability, a hypothetical convergence, and uncertain transferability. Recently, an entirely novel paradigm in the field of machine learning has been identified: theory-guided machine learning, in which the models integrate some specific theoretical knowledge, laws or principles of the field of study. This review article set out to examine three theory-guided methods in their ability to overcome the limitations of machine learning for hydrogeological research and applications. These methods are, respectively, Theory-Guided Constrained Optimization (TGCO), Theory-Guided Refinement of Outputs (TGRO) and Theory-Guided Architecture (TGA). The analyses led to the following conclusions: the opacity of ML models can be reduced by any of the three theory-guided ML methods; convergence and generalizability can be enhanced by TGCO, TGA, or a combination of at least two of the theory-guided ML methods; no study conducted to date has made it possible to deduce the effectiveness of these methods on the transferability of ML models.

**Keywords** Theory-guided machine learning · Groundwater · Machine learning limitations · Statistical modelling

## 2.2 INTRODUCTION

Hydrogeological research and practices have evolved over the years with the challenges facing the world. Today, hydrogeology strives to find solutions to problems such as the sustainable supply of drinking water, geothermal energy production, environmental protection and the fight against climate change and its effects on groundwater. To provide a solution to these problems, Hydrogeologists systematically resort to modelling. To model simple hydrogeological problems, simplified models are usually used. For example, John and Das (2020) used a piezometric contour map to identify risk zone areas of declining piezometric levels, while Chesnaux et al. (2018) proposed analytical solutions obtained through idealized hypotheses, using groundwater travel time in Dupuit-Forchheimer aquifers, for assessing recharge. To address more complex problems, numerical models are employed to derive an approximate solution by iteratively solving a discrete form of the equation that governs the hydrogeological phenomenon under study (Feng et al. 2011; Raazia and Dar 2021).

Thanks to recent technological advances for data collection such as the Internet of Things (Su et al. 2020), hydrogeologists now have access to large amounts of data acquired in real time. Processing such amounts of data poses a challenge to traditional modelling tools for tasks such as extracting useful features, uncertainty quantification or identifying links between various variables (Tahmasebi et al. 2020). As a result, over the past two decades, the field of hydrogeology has viewed Machine Learning (ML) with increasing interest as a new complementary modelling paradigm. As a research subfield of Artificial Intelligence, the goal of ML is to design and implement parametric and non-parametric methods that are used to generate models to solve a specific problem. Besides semi-supervised learning and reinforcement learning, ML methods can be classified into two categories: supervised and unsupervised learning methods (Ayodele 2010).

In supervised learning, the goal is to allow the computer to learn to relate input and output variables using a set of data samples containing the data relating to the input variables and those associated with the output variable. For parametric methods for example, supervised learning consists in automatically adjusting the parameters of the ML method while minimizing a cost function which measures the gap between the outputs of the model and the corresponding true values. The adjustment stage is the first step in the model generation process by supervised learning. This adjustment stage is generally followed by a cross-validation stage which makes it possible to select the model with the best performance and finally, a test stage whose objective is to produce an unbiased evaluation of the model previously selected. Implementing different stages requires splitting the data into three subsets: a training set, a cross-validation set and a test set. Some popular examples of supervised learning methods are linear regression and artificial neural networks.

In unsupervised learning, the computer learns to identify hidden patterns in the data without any outside help. In particular, the computer learns to extract classes or groups of individuals having common characteristics. Principal component analysis is a well-known example of an unsupervised learning method.

In hydrogeology, supervised and unsupervised ML, including deep learning, have been used to address various issues such as the evaluation of groundwater quality (Khalil et al. 2005; Mohamed et al. 2019; Park et al. 2016; Wang et al. 2016), groundwater potential (Arabameri et al. 2019; Bahareh et al. 2019; Moghaddam et al. 2020; Naghibi et al. 2017), aquifer parameters (Tayfur et al. 2014; Tutmez et al. 2006), groundwater vulnerability (Afshar et al. 2007; Sajedi-Hosseini et al. 2018), water balance and recharge of aquifers (Gorgij et al. 2017; Pradhan et al. 2019) and groundwater level (Barzegar et al. 2017a; Chang et al. 2016; Sahoo and Jha 2013; Tapoglou et al. 2014). For example, Tapoglou et al. (2014) used an artificial neural network, trained using an optimisation method called particle swarm, to generate a model to forecast groundwater levels on day  $k$  under climate change scenarios for a unique well. Rainfall at two meteorological stations, temperature and hydraulic head on day  $k-1$  were selected as input variables. To project the effects of climate scenarios, the

meteorological time series were generated by a weather condition generator, the LARS-WG 5. The results indicated that the generated model is very accurate in representing the groundwater level dynamics and only the most severe climate change scenario results in a subsidence of groundwater levels. Chen et al. (2020b) performed a comparative study among ML and numerical models for simulating groundwater dynamics. Artificial neural networks and support vector machines have been used as ML methods, with time series of pumping rate, recharge rate, streamflow rate as input variables. The results have shown that in terms of accuracy, ML models produce better results the majority of time.

Despite the growing interest in ML in hydrogeology and the very high level of accuracy it can offer, at least four factors still hamper the adoption of ML models as an effective complementary tool to traditional models such as numerical models. The first limiting factor is that most ML models have a black-box nature (Rudin 2019). Black-box models establish a relationship between some inputs and outputs of a system, without any knowledge of the laws that govern its functioning or the causal relationships existing between the related variables. Unlike the parameters of hydrogeological variables such as hydraulic conductivity, storativity, parameters of ML black-box models have no physical significance (Zhang 2010). Therefore, the use of ML black-box models does not allow hydrogeologists to explain or justify model outputs, whether it be to gain understanding of the modelled phenomenon or to attain confidence levels sufficient for supporting high-stakes decision-making. Groundwater exploitation activities most often present major issues related to the water supply in regard to populations or their health risks. An erroneous forecast made by a black-box model can therefore have significant socio-economic consequences.

The second limiting factor is that, even if ML models applied to hydrogeology offer an adequate level of simulation accuracy, the same is not always the case for their generalization ability. Several studies have pointed out that ML models are generally subject to poor generalization ability (Adamowski and Chan 2011; Ch and Mathur 2012; Huang et al. 2019). The generalization ability is

poor when the model provides fair simulations but struggles to make predictions for data that it did not encounter during training (Urolagin et al. 2011) . Formally, the generalization ability can be represented as the ratio between the prediction error and the training error (Chen et al. 2020b). When the ratio is higher than 1, the model is said to poorly generalize. A poor generalization ability may be due either to the use of a training dataset that is too small, less representative or that contains too much noise, or it may be due to the trade-off that is made between the desired accuracy and the assumptions on the complexity of the problem to be solved (Ying 2019). Fundamentally, ML models with relatively low generalization ability cannot be used with confidence to study the future behaviour of a hydrogeological system with respect to a given phenomenon.

The third limiting factor is that, ML models may not converge (Zobeiry et al. 2020b). ML models being analogous to a classical discretization scheme used to solve a problem involving differential equations (Bar-Sinai et al. 2019) as is the case for the modelling of groundwater flow, the convergence of ML models is governed by two components namely physical consistency and stability (Arnold 2015). Consistency is a quantity which evaluates to what extent the outputs of ML models satisfy the theory and more specifically, in the context of groundwater modelling, the differential equation governing water dynamics. The physical consistency is evaluated by calculating the average residue of the PDE governing the functioning of the system. The more the mean residual tends towards zero, the more consistent the model. As for stability, it describes the robustness of ML models facing a minor disruption applied to the data (Shaham et al. 2018). Stability can be evaluated by calculating the relative error, given by the ratio between the error associated with the disrupted solution (outputs of the model) and that associated with the disrupted data (e.g., inputs of the model). The model is stable if the relative error is bounded. A ML model converges if it is both consistent and stable. Convergence is essential to provide reliable prediction (Bakshi et al. 2016).

Finally, the fourth limiting factor is that ML models are not automatically extensible to adapt to the occurrence of a new event in the modelled system. The ability of a ML model to adapt to new

tasks is generally referred to as transferability. This can be illustrated by taking the example of an unconfined aquifer whose groundwater levels are influenced only by precipitation and temperature and for which a ML model must be implemented. Intuitively, precipitation and temperature will be chosen as the model input to represent the groundwater levels. Suppose that shortly after implementing the model, a pumping well is installed in the aquifer. It is very likely that the model is not able to represent the influence of the well on the groundwater levels. To handle this new event, a new model must be built. In other words, a ML model that was built based on a certain hydrogeological configuration cannot be used for a different configuration. In various studies such as Sahoo and Jha (2013), Shiri et al. (2013) and Sahoo et al. (2017b), perhaps due to a lack of data, ML is used to relate complex hydrogeological variables such as hydraulic head or contaminant concentration with a set of input variables chosen without necessarily considering domain knowledge and theory. To some extent, these studies limit the modelled problem to a representation of reality that does not represent its true complexity. Therefore, the model transferability is reduced by default.

To alleviate some of the limiting factors of ML in the physical sciences, various authors have proposed different methods. To solve poor generalization ability problems, some authors propose to add a data processing operation aimed at reducing noise (Clark and Niblett 1989; Pazzani and Brunk 1991). Others propose to either acquire more data or manipulate the existing data to generate some new data (Sun et al. 2014; Yip and Gerstein 2009). Still others propose to limit the effect of non-relevant input variables by means of regularization methods (Srivastava et al. 2014; Warde-Farley et al. 2013) or to use validation data to prevent a poor generalization ability (Brodeur et al. 2020). To mitigate the black-box nature of some ML models, methods of a subfield of artificial intelligence, eXplainable Artificial Intelligence (XAI), have been used by several authors such as Nguyen et al. (2020b) and Nguyen et al. (2020c) in the field of hydrogeology or Kavvas et al. (2020) in the field of genetics. XAI aims to design and implement methods that make it possible to understand what is happening in the black box.

Recently, a new paradigm of ML has started to emerge in geosciences. Theory-guided machine learning (Karpatne et al. 2017), sometimes also referred to as Physics-informed machine learning (Raissi et al. 2019), consists of integrating theoretical knowledge into the learning process of ML models. The learning process is made to include, for example, the advection-dispersion equation, the diffusion equation or the applicable physical constraints, so that the ML model not only learns the patterns contained in the data but is also given the knowledge allowing it to avoid violating the known theory about the phenomenon studied. This approach seems likely to present the combined advantages of ML models and numerical models. These include rapid model implementation, e.g. in few days (Chen et al. 2020b), high simulation accuracy, modelling at any scale easily, low computational costs for ML and a better understanding of hydrogeological processes, good generalization ability and a possible transferability under certain conditions for numerical models. Theory-guided machine learning models have shown promising results in various scientific disciplines (Liu et al. 2013; Piccione et al. 2020; Zobeiry et al. 2020a). However, in hydrogeology, the application of Theory-guided machine learning is quite new. Consequently, few studies exist.

The purpose of this article is to review mainly the existing hydrogeological literature on the topic of Theory-guided Machine Learning as well as that of other scientific domain and assess the extent to which Theory-guided Machine Learning can help overcome the stated limiting factors of ML in hydrogeological research and applications. As a reminder, the limiting factors concern the black-box nature of most ML models, an often-limited generalization ability, hypothetical convergence, and uncertain transferability. In view of the current literature, no review on the topic still exists in hydrogeology. This paper is organized as follows: **Section 2.3** describes the state of the art of the methods of Theory-guided machine learning used in hydrogeology, including an analysis of the literature to highlight the ability of Theory-guided methods to overcome or not the limiting factors mentioned above. **Section 2.4** identifies and discusses some of the remaining challenges, as well as future avenues.

## **2.3 THEORY-GUIDED MACHINE LEARNING VS MACHINE LEARNING LIMITING FACTORS IN HYDROGEOLOGY**

Although theory-guided machine learning has been used as a paradigm in the physical sciences for a long time, only recently has a taxonomy of its characteristics been proposed by Karpatne et al. (2017). Theory-guided machine learning consists in incorporating theoretical knowledge, such as governing equations, prior domain knowledge or causal relations into the learning process of ML models. The use of theory-guided learning is supposed to allow the model to agree with both observations and theory. In the existing hydrogeological literature on theory-guided machine learning, there are three approaches for integrating fundamental knowledge of hydrogeology into the models. The first, designated as Theory-Guided Constrained Optimization, consists in integrating the theory into the cost function (Tartakovsky et al. 2020; Wang et al. 2020b; Xu et al. 2020). The second, called Theory-Guided Refinement of Outputs, consists in postprocessing the outputs of the model to make them conform to the theory as accurately as possible (Chen et al. 2020c; Hautier et al. 2010; Khandelwal et al. 2015). The third, designated as Theory-Guided Architecture, consists in using what is known theoretically about the phenomenon under study to design the architecture of the ML model (Daw et al. 2020; Tartakovsky et al. 2020; Udrescu and Tegmark 2020) . In the following section, these three approaches are presented and their ability to overcome the limiting factors of ML models is analysed. It is important to note that other approaches of Theory-guided ML exist in the literature and are well described from a general point of view by various other review articles such as that of Karpatne et al. (2017) or that of Willard et al. (2020).

### **2.3.1 THEORY-GUIDED CONSTRAINED OPTIMIZATION**

To introduce the basic idea behind Theory-Guided Constrained Optimisation (TGCO), consider a 2D subsurface flow in saturated homogeneous and isotropic porous medium as in Wang et al. (2020b). This subsurface flow satisfies the following governing equation (Equation (2.1)):

$$K \left( \frac{\partial^2 h}{\partial x^2} + \frac{\partial^2 h}{\partial y^2} \right) = S_s \frac{\partial h}{\partial t} \quad (2.1)$$

Where  $h$  is the hydraulic head (m);  $K$  is the hydraulic conductivity (m/s);  $S_s$  is the specific yield (1/m);  $x, y$  are the horizontal space variables (m);  $t$  is the time (s). The initial condition can be expressed as follows (Equation (2.2)):

$$h(t_{IC}) = h_{IC} \quad (2.2)$$

The Dirichlet and Neumann boundary conditions can be expressed respectively as follows (Equations (2.3) and (2.4)):

$$h(x_D, y_D) = h_D \quad (2.3)$$

$$K \frac{\partial h}{\partial n} = q \quad (2.4)$$

Where  $h_{IC}$ , represents the initial hydraulic head (m),  $h_D$ , the specified hydraulic head (Dirichlet boundary condition) (m), and  $q$ , the constant flux related to Neumann boundary condition (m/s).  $t_{IC}$  is the initial time (s) and  $x_D, y_D$  are the spatial coordinates of the points located on the Dirichlet boundary (m). Also, denote by  $\hat{h}$  the hydraulic head simulated by the ML model to train (m), and the observed value by  $h$  (m). Generally, a standard cost function for a ML model is defined as follows (Equation (2.5)):

$$\mathcal{L}_{std} = \frac{1}{2} (\hat{h} - h)^2 \quad (2.5)$$

Since the training consists in adjusting the ML model parameters using the cost function as a guide, the adjusted parameters of the ML model that will have led to a low value of the cost function will be closer to the optimal values. However, nothing guarantees that the simulation will not violate the governing equation. Thus, in TGCO, it is considered important to re-constrain the hydraulic head

simulations by adding other terms in the cost function representing the residual of the governing equation and the residual of initial, Dirichlet and Neuman boundary conditions defined respectively as follows (Equations (2.6) to (2.9)):

$$\mathcal{R}_{eq} = K \left( \frac{\partial^2 \hat{h}}{\partial x^2} + \frac{\partial^2 \hat{h}}{\partial y^2} \right) - S_s \frac{\partial \hat{h}}{\partial t} \quad (2.6)$$

$$\mathcal{R}_{IC} = \hat{h} - h_{IC} \quad (2.7)$$

$$\mathcal{R}_D = \hat{h} - h_D \quad (2.8)$$

$$\mathcal{R}_N = K \frac{\partial \hat{h}}{\partial n} - q \quad (2.9)$$

To compute the residual  $\mathcal{R}_{eq}$  of the governing equation and the residual  $\mathcal{R}_N$  of the Neumann boundary condition, Wang et al. (2020b) applied the chain rule through automatic differentiation, but the residuals can also be approximated by discretization methods such as finite element method or finite difference method as in Chen et al. (2020c). Finally, the cost function according to the TGCO method can be defined as follows (Equation (2.10)):

$$\mathcal{L} = \lambda_1 \mathcal{L}_{std} + \lambda_2 \mathcal{R}_{eq}^2 + \lambda_3 \mathcal{R}_{IC}^2 + \lambda_4 \mathcal{R}_D^2 + \lambda_5 \mathcal{R}_N^2 \quad (2.10)$$

where  $\lambda_{i=1\dots 5}$  is a coefficient making it possible to weight the importance of the corresponding term in the cost function. Other constraints can be added according to additional knowledges or observations regarding the aquifer. For example, it could have been observed that the hydraulic head at a point of interest never falls below a certain value. So, it could be useful to impose this constraint during the model training. **Figure 5** locates the part of the ML process modified by the TGCO method, that is, the cost function. Such an intervention is meant to allow the generated ML model to correspond as accurately as possible to the theory.

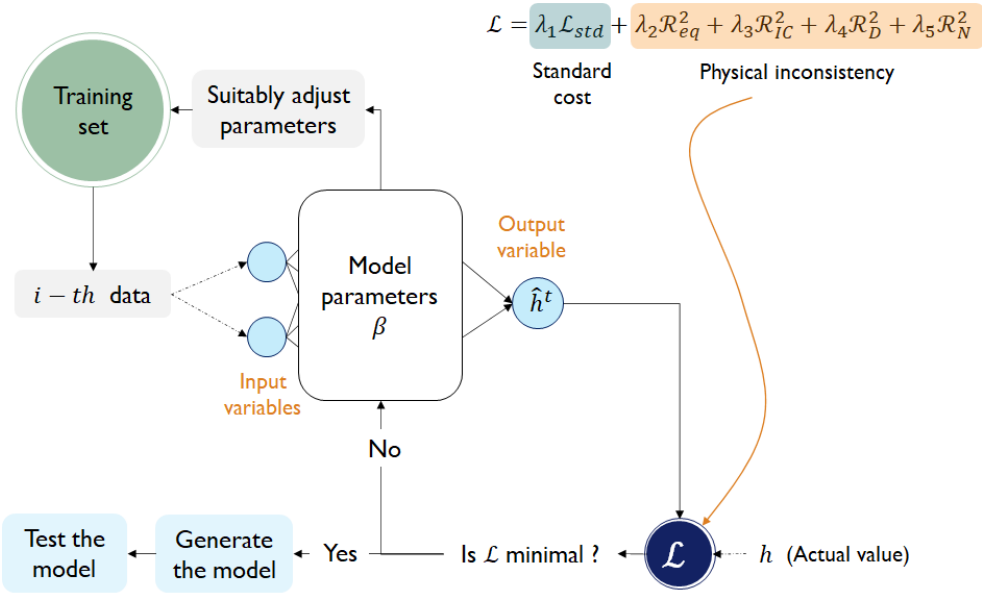


**Figure 5** Part of the ML process modified by the TGCO method, that is, at the level of cost function (solid blue circle)

The TGCO method is one of the most developed methods in the field of physical sciences in general and in hydrogeology in particular for tasks such as solving partial differential equations (Karimpouli and Tahmasebi 2020; Meng et al. 2020), building surrogate models and uncertainty quantification (Wang et al. 2021a), inverse modelling (Kadeethum et al. 2020; Kahana et al. 2020; Sun 2018), or data generation (Zobeiry and Humfeld 2021). Karimpouli and Tahmasebi (2020) compared the performance of two ML methods to solve a time-dependent 1D seismic wave equation, namely a Gaussian process and a TGCO neural network. The results showed that the TGCO neural network is more accurate for velocity (P and S waves) and density inversion. Zobeiry and Humfeld (2021) compared the performances of standard neural network and TGCO neural network with feature engineering in modelling the conductive heat transfer. The models built were validated by comparing their results with those of a numerical finite element model (FE). The results showed that although the standard neural network and the TGCO match the FE results in the training zone, only the TGCO with feature engineering can capture the physics of the problem to produce accurate predictions beyond the training stage. This result demonstrates that TGCO models are physically consistent and stable when properly tuned and correctly constructed. Consistent and stable TGCO

models can be used to generate data for other applications, as might be done with a classical numerical model. Kahana et al. (2020) integrated a cost function term associated with the physical consistency of the temporal dynamics of waves to model the inverse problem of identifying the location of an underwater obstacle from acoustic measurements using a deep learning framework. The results showed that the use of TGCO led to a better accuracy and robustness of the model relative to its generalization. Meng et al. (2020) developed a parareal TGCO neural network by decomposing a long-time problem into many independent short-time problems supervised by an inexpensive solver designed to provide approximate predictions of the solution at discrete times, while initiating many fine TGCO neural networks simultaneously to correct the solution iteratively. The goal of this approach is to allow a significant acceleration of the resolution of partial differential equations (PDEs) on large spatio-temporal domains provided that the solver is fast and can provide reasonable predictions. Applied to solve the Burgers equation and a two-dimensional nonlinear diffusion-reaction equation, the results demonstrated that a parareal TGCO neural network model converges in a couple of iterations with significant speed-ups proportional to the number of time-subdomains employed. Kadeethum et al. (2020) proposed to study the influence of batch size on the TGCO neural network accuracy to approximate the parameters of PDEs in the context of inverse modelling. Applying this study to Biot's equation, they showed that training with small batch sizes provides better approximations of physical parameters than using large batches but at the expense of longer training time.

In hydrogeology, Wang et al. (2020b) used the TGCO method to simulate the dynamics of groundwater levels in different hydrogeological configurations ranging from the simplest to more complex configurations including external variables such as pumping rate and noise in the data or even outliers. The results in Wang et al. (2020b) indicate that, with low noise data, the theory-guided model prediction errors are reduced by a factor of 4 to 11 compared to the model trained in the standard way. The TGCO method is therefore likely to improve the model's performance. Despite using data containing up to 20% noise, the predictions of the theory-guided model are hardly affected by noise. ML models generated using the TGCO method seem to be robust despite more or less

minimal changes in the data. Xu et al. (2020) used a so-called weak form of the governing equation of groundwater flow to reduce computational cost and to capture local discontinuities. The results show an improvement of the model accuracy as well as its robustness in the presence of noise compared to a strong form of the governing equation as used by Wang et al. (2020b). Guo et al. (2020) demonstrated that under certain conditions, the model trained using the TGCO method could converge. Wang et al. (2021) used a TGCO fully connected neural network surrogate model coupled with the Monte Carlo method (MC) for uncertainty quantification for dynamic subsurface flow. The results showed that the TGCO neural network based surrogate can significantly improve the efficiency of uncertainty quantification tasks compared to the simulation-based implementation. Indeed, for any stochastic input sample, the output can be easily obtained from the surrogate TGCO neural network without having to solve the partial differential equation an umpteenth time. Therefore, the TGCO neural network surrogate can speed up the uncertainty quantification tasks.

These studies lead to conclude that the TGCO method improves the convergence of ML models and their ability to generalize. Theoretical models make it possible to represent, understand and explain the functioning of a phenomenon. Therefore, incorporating theory into the training process help to reduce the opacity of ML models to some extent. The cost function, in which the theory is integrated, plays a role only during the training stage. The appropriate choice of model inputs and a better design of the model architecture are therefore necessary to ensure that the model has the capacity to adapt to the occurrence of new events in the system under study. Finally, the use of the TGCO method for solving PDEs may not be fruitful in some real-life applications, in particular when the parameters of PDEs are uncertain or even unknown. Indeed, the resolution of PDEs for the study of the dynamics of a system requires a calibration of the parameters of these PDEs which cannot be possible if the search space of these parameters is unknown. The use of the TGCO method must be well supervised. In particular, the TGCO method must serve primarily to ensure the physical consistency of ML models in contexts where the physical parameters of PDEs are available.

### 2.3.2 THEORY-GUIDED ARCHITECTURE

Theory-Guided Architecture (TGA) consists in using the architectural properties of ML methods to integrate the properties and the laws of physics to ensure that the resulting models are consistent with the physics related to the problem being treated. The TGA method implicitly leads to reducing the opacity of ML models and promoting their interpretation and the understanding of their functioning. The TGA method can be used for inverse modelling (Tartakovsky et al. 2020), uncertainty quantification (Daw et al. 2020) or even the discovery of symbolic governing equations (Udrescu and Tegmark 2020). The applicable theory can be integrated into the architecture of ML models in several ways, namely the explicit incorporation of physically relevant variables, the decomposition of a problem into theoretically related sub-problems or the implementation of basic physical principles common to several dynamic physical systems such as invariance or monotonicity (Karpatne et al. 2017; Willard et al. 2020). For example, Muralidhar et al. (2020) proposed a convolutional neural network model using the TGA method for modelling the drag forces acting on each particle in a Computational Fluid Dynamics-Discrete Element Method. The drag force on a particle can be easily determined by knowing two intermediate variables namely the pressure field and the velocity field around the surface of the particle. Knowing that the pressure field directly affects the pressure component of the drag force, and the velocity field directly affects the shear component of the drag force, they built their model architecture to express physically meaningful intermediate variables such as the pressure field, velocity field, pressure component, and shear component in the neural pathway from the input features to the drag force. In short, this architecture is a succession of layers of neural networks linked together according to the understanding provided by the theory applicable to the problem being studied. The model was compared to several ML models and the results showed that the model achieved a significant performance improvement of 8.46% on average. A similar method was used in hydrogeology by Tartakovsky et al. (2020). Their study consisted in solving an inverse problem: determining the hydraulic conductivity at any point of the field of study by assuming access to either the observations of the hydraulic conductivity and the hydraulic head or only to the observations of the hydraulic head. Since the hydraulic conductivity can depend on the hydraulic

head (e.g., to determine groundwater flow in an unsaturated zone), the authors proposed to model the hydraulic conductivity by adopting an architecture in the form of a two-step process: on the one hand, a model that learns the hydraulic conductivity, and on the other hand, another model which uses the simulations of the previous model to ensure that these simulations better represent the observations of the hydraulic head. Daw et al. (2020) proposed a Long Short-Term Memory model (LSTM), a Deep Learning neural network, using the TGA method in the context of lake temperature modelling. The architecture admits three components, the first of which makes it possible to extract temporal features from the input data. These features were used in the second component to generate an intermediate variable, that is, the density whose monotonicity is ensured (the density of water increases with depth). The third component uses the densities from the second component as well as the input data to predict the lake's temperature. The resulting model, associated with the Monte Carlo approach, is used to quantify the uncertainty. The results demonstrated the effectiveness of the approach in ensuring better generalization as well as physical consistency.

It is possible to implement physically consistent ML models by building their architecture in such a way as to integrate the properties of invariance and symmetry (Oberlack 2002; Willard et al. 2020). Wang et al. (2020c) proposed deep learning models to model physical dynamics by incorporating symmetries into the prediction model. The idea is that the integration of a certain symmetry in the architecture of the model can increase the likelihood of conserving the associated quantity, therefore rendering the prediction of the model more physically accurate. The results showed that the generalization ability of their proposed models was greatly improved. Ling et al. (2016) proposed a TGA neural network which embedded Galilean invariance in order to learn a model for the Reynolds stress anisotropy tensor. The results demonstrated that the TGA neural network made it possible to improve prediction accuracy compared with a standard neural network architecture. Udrescu and Tegmark (2020) combined a neural network with some physics-inspired techniques to help find a symbolic expression that matches the data of an unknown function. They built the architecture of neural networks in such a way that the resulting models were able to discover a hidden simplicity such as symmetry or data separability, which allows more difficult problems to be broken

down recursively into simpler problems with fewer variables. Applied to 100 equations from the Feynman Lectures on Physics, the proposed algorithm was able to uncover them all, improving the peak success rate from 15 to 90% of existing methods.

Studies that have used the TGA method have shown that this method reduces the opacity of ML models. Indeed, the TGA method makes it possible to materialize the physical relationships between input and output variables or to forcibly integrate the laws of conservation into the structure of ML models. This has the advantage of improving the physical consistency of the resulting models and of promoting their convergence. It may further be stated that appropriate construction of the architecture of the model can promote its transferability to other hydrogeological configurations. However, there are currently no studies supporting this latter hypothesis. **Figure 6** illustrates a theory-guided design of architecture by means of decomposition of a problem into theoretically related sub-problems in modelling groundwater flow.

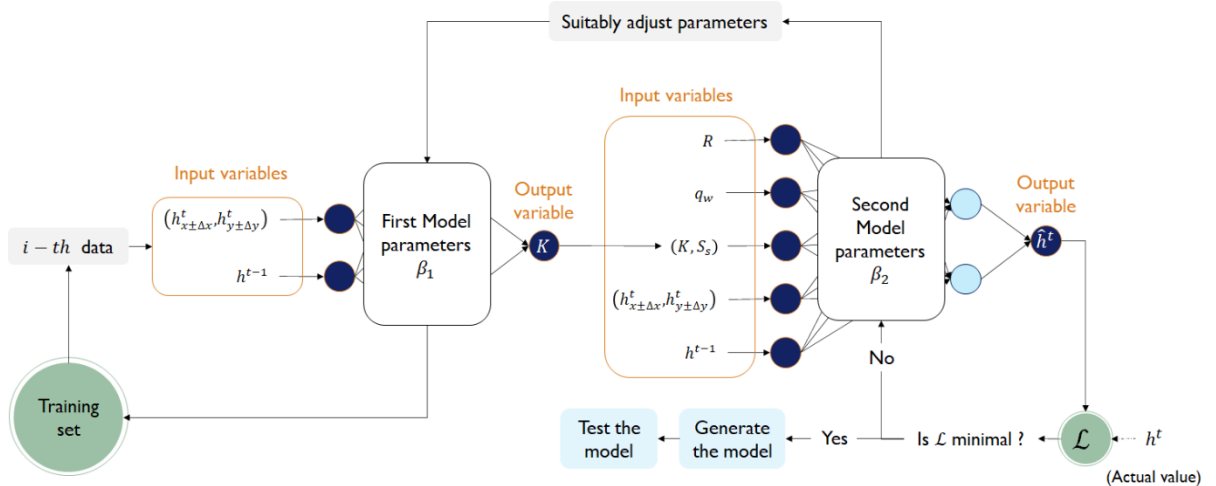


**Figure 6** Example of theory-guided design of architecture by means of decomposition of a problem into theoretically related sub-problems in modelling groundwater flow.  $R$ ,  $q_w$ ,  $K$ ,  $S_s$ ,  $(h_{x\pm\Delta x}^t, h_{y\pm\Delta y}^t)$ ,  $h^{t-1}$ ,  $h^t$ ,  $\hat{h}^t$  represent respectively the recharge rate, pumping rate, hydraulic conductivity, storativity, hydraulic head in the neighbourhood of the point of interest, previous, current, and estimated hydraulic head at the point of interest.

### 2.3.3 THEORY-GUIDED REFINEMENT OF OUTPUTS

The principle of Theory-Guided Refinement of Outputs (TGRO) is to apply a transformation to the outputs of the ML models so that these outputs are consistent with governing equations. In the hydrogeological literature, this method has mainly been used by Chen et al. (2020c). To understand how the TGRO method works, the example employed by Chen et al. (2020c) will be shown here. The example consists in describing a 2D subsurface flow in a saturated porous medium without source or sink terms, whose governing equation is given as (Equation (2.11)):

$$S_s \frac{\partial h}{\partial t} = \frac{\partial}{\partial x} \left( K(x, y) \frac{\partial h}{\partial x} \right) + \frac{\partial}{\partial y} \left( K(x, y) \frac{\partial h}{\partial y} \right) \quad (2.11)$$

The TGRO method consists in applying a transformation function  $\phi$  to the hydraulic head  $\hat{h}$  simulated by the ML model to provide a new value  $\hat{h}_r$  intended to be much closer to observed value  $h$  and to not violate the governing equation. Function  $\phi$  approximates the governing equation while considering the initial and boundary conditions. All the means making it possible to approximate the governing equation and to bring  $\hat{h}$  as close as possible to the observed value can be used. Chen et al. (2020c) proposed to use a projection method. First, they discretize Equation (2.11) by means of a second order centre difference scheme along the  $x$  and  $y$  dimensions and a first-order backward Euler scheme along the  $t$  dimension:

$$\begin{aligned}
0 = -S_s \frac{h^t - h^{t-\Delta t}}{\Delta t} \\
+ \left( \frac{K_{x-\frac{\Delta x}{2}}}{\Delta x^2} h_{x-\Delta x}^t + \frac{K_{x+\frac{\Delta x}{2}}}{\Delta x^2} h_{x+\Delta x}^t - \frac{K_{x-\frac{\Delta x}{2}} + K_{x+\frac{\Delta x}{2}}}{\Delta x^2} h^t \right) \\
+ \left( \frac{K_{y-\frac{\Delta y}{2}}}{\Delta y^2} h_{y-\Delta y}^t + \frac{K_{y+\frac{\Delta y}{2}}}{\Delta y^2} h_{y+\Delta y}^t - \frac{K_{y-\frac{\Delta y}{2}} + K_{y+\frac{\Delta y}{2}}}{\Delta y^2} h^t \right)
\end{aligned} \tag{2.12}$$

Second, they rearrange Equation (2.12) for projection purposes, as follows (Equation (2.13)):

$$\begin{aligned}
0 = \frac{S_s}{\Delta t} h^{t-\Delta t} + \left( -\frac{S_s}{\Delta t} - \frac{K_{x-\Delta x/2} + K_{x+\Delta x/2}}{\Delta x^2} - \frac{K_{y-\Delta y/2} + K_{y+\Delta y/2}}{\Delta y^2} \right) h^t \\
+ \frac{K_{x-\Delta x/2}}{\Delta x^2} h_{x-\Delta x}^t + \frac{K_{x+\Delta x/2}}{\Delta x^2} h_{x+\Delta x}^t + \frac{K_{y-\Delta y/2}}{\Delta y^2} h_{y-\Delta y}^t \\
+ \frac{K_{y+\Delta y/2}}{\Delta y^2} h_{y+\Delta y}^t
\end{aligned} \tag{2.13}$$

Third, a matrix decomposition that divides the discretized equation into a prediction matrix  $\hat{\mathbf{H}}$  and a constraint matrix  $\mathbf{C}$  is realised. The prediction matrix collects all the hydraulic head variables of Equation (2.13) and the constraint matrix gathers all the other parameters. In other words, Equation (2.13) is equal to the product of matrix  $\hat{\mathbf{H}}$  by matrix  $\mathbf{C}$  (Equations (2.14) and (2.15)).

$$\hat{\mathbf{H}} = [\hat{h}^{t-\Delta t}, \hat{h}^t, \hat{h}_{x-\Delta x}^t, \hat{h}_{x+\Delta x}^t, \hat{h}_{y-\Delta y}^t, \hat{h}_{y+\Delta y}^t]^T \tag{2.14}$$

$$\mathbf{C} = \left[ \frac{S_s}{\Delta t}, -\frac{S_s}{\Delta t} - \frac{K_{x-\frac{\Delta x}{2}} + K_{x+\frac{\Delta x}{2}}}{\Delta x^2} - \frac{K_{y-\frac{\Delta y}{2}} + K_{y+\frac{\Delta y}{2}}}{\Delta y^2}, \frac{K_{x-\frac{\Delta x}{2}}}{\Delta x^2}, \frac{K_{x+\frac{\Delta x}{2}}}{\Delta x^2}, \frac{K_{y-\frac{\Delta y}{2}}}{\Delta y^2}, \frac{K_{y+\frac{\Delta y}{2}}}{\Delta y^2} \right] \tag{2.15}$$

$\hat{\mathbf{H}}$  and  $\mathbf{C}$  are a collection in matrix form of the realizations of Equation (2.13) at each of the points located in the vicinity of the point of interest according to the collocation point method that the authors used in their study. From there, the prediction matrix is projected onto the hyperplane determined by the constraint matrix. This results in a new matrix called the projected prediction matrix which collects the values of the hydraulic head at the point of interest and at the adjacent points; these values are

believed to be closer to the observed value. The projected prediction matrix is expressed as follows (Equation (2.16)):

$$\hat{\mathbf{H}}_r = \phi(\hat{\mathbf{H}}) = (\mathbf{I} - \hat{\mathbf{H}}^T(\hat{\mathbf{H}}\hat{\mathbf{H}}^T)^{-1}\hat{\mathbf{H}})\mathbf{C} \quad (2.16)$$

where  $\mathbf{I}$  is the identity matrix,  $\mathbf{C}\hat{\mathbf{H}}_r = \mathbf{0}$  and (Equation 4.12),

$$\hat{\mathbf{H}}_r = [\hat{h}_r^{t-\Delta t}, \hat{h}_r^t, \hat{h}_{r,x-\Delta x}^t, \hat{h}_{r,x+\Delta x}^t, \hat{h}_{r,y-\Delta y}^t, \hat{h}_{r,y+\Delta y}^t]^T \quad (2.17)$$

If the point of interest is a boundary point, it is sufficient to impose values of hydraulic conductivity or hydraulic head corresponding to the boundary condition. For example, for a no-flow boundary point, a zero value of hydraulic conductivity would be appropriate. With the TGRO method, the cost function can remain equal to the standard cost function  $L_{std}$  as presented in Section 2.3.1, or the standard cost function can be combined with the cost related to the violation of the physics of groundwater flow.

**Figure 7** illustrates the TGRO method.

Beyond hydrogeology, the TGRO method has been applied for the mapping of water bodies or the discovery of new materials. For example, Khandelwal et al. (2015) proposed a new method for refining post classification labels in the context of water body mapping. The goal was to use relevant information such as elevation to re-classify classifications that are theoretically inconsistent. The methodology consisted of producing a first map of the extension of a water body from a remote sensing image and to constrain this map with the elevation data to produce a physically consistent map. Hautier et al. (2010) used a combination of machine learning techniques and high throughput ab initio computations to find new compounds and their crystal structures. From a training database of materials of known structure and properties, they were able to train a model capable of finding materials whose properties and structure were previously unknown. To eliminate theoretically inconsistent materials, model outputs were refined using expensive ab initio calculations. This study made it possible to discover 209 new compounds with a limited calculation budget.

The TGCO and TGRO methods are basically equivalent, except that TGCO incorporates the theory into the cost function, whereas the TGRO method post-processes the model outputs to conform as accurately as possible to the theory. Because of this equivalence, the conclusions drawn from the analysis of studies using TGCO can very likely be transposed to studies using the TGRO method. However, a very small number of studies have been published on the topic, so this cannot be confirmed with certainty. One advantage offered by TGRO is that the post-processing operator (e.g.: the transformation function for systems described by partial differential equations) remains present even after the training stage and, therefore, it may always be possible to adapt the model when a new event occurs. Again, a limited number of studies have been published on this topic and at this time, it is not possible to confirm or refute the transferability of ML models generated via the TGRO method.

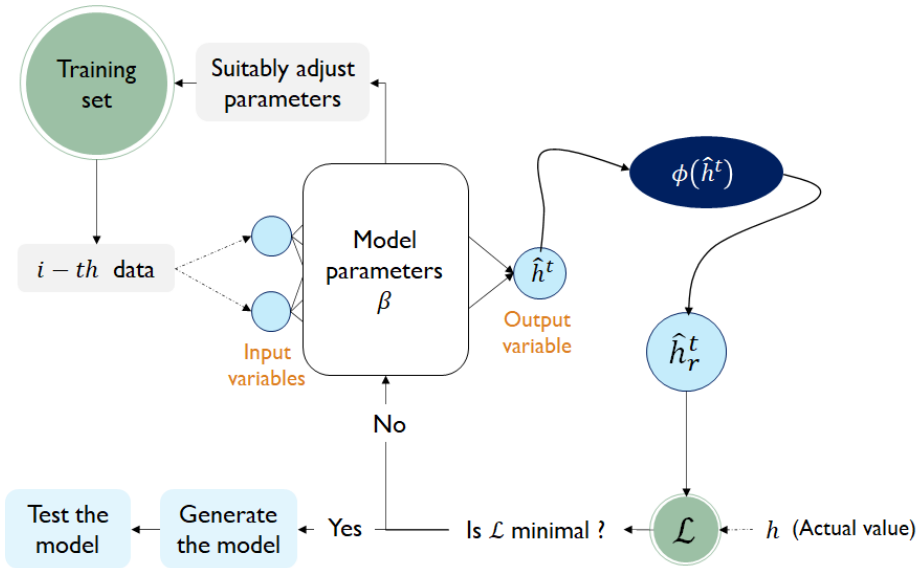


**Figure 7** Part of the ML process modified by the TGRO method, that is, at the level of model outputs (solid blue oval circle)

**Table 1** shows some situations in which each of the theory-guided ML methods presented in this study can be applied. **Table 2** presents a summary of the discussions concerning the ability of theory-guided ML methods to overcome the mentioned limitations of ML for hydrogeological

applications. Question marks indicate a lack of available factual evidence to support the theory-guided method's ability to overcome the identified limitations.

**Table 1** Some situations in which the theory-guided ML methods presented in this study may be applied. A dash indicates the absence of a supporting published study.

Tasks	TGCO	TGA	TGRO
Uncertainty quantification	✓	✓	-
PDE resolution	✓	-	-
Discovery of symbolic governing equation	-	✓	-
Data generation	✓	-	-
Prediction improvement	✓	✓	✓
Inverse modelling	✓	✓	-
Surrogate modelling	✓	-	-

**Table 2** Comparison of efficiency of the different methods of theory-guided machine learning with respect to ML limiting factors. Question marks indicate an absence of available factual evidence.

Methods	Mitigation of black-box nature	Improvement of generalization ability	Improvement of convergence	Transferability
TGCO	✓	✓	✓	?
TGA	✓	✓	✓	?
TGRO	✓	?	?	?
TGRO + TGCO	✓	✓	✓	?
TGCO + TGA	✓	✓	✓	?
TGRO + TGA	✓	✓	✓	?
TGCO + TGRO + TGA	✓	✓	✓	?

The TGCO method, by itself or combined with one of the two other methods makes it possible to reduce the opacity of ML models, to improve their generalization ability and to promote their convergence. However, there is no evidence supporting the transferability of ML models. The TGA

method, by itself or combined with at least one of the two others also makes it possible to overcome all the limitations of ML models, with the exception of transferability for which there are no supporting studies. Finally, concerning the TGRO method, the only certainty is its ability to reduce the black-box nature of ML models.

## 2.4 CHALLENGES OF THEORY-GUIDED MACHINE LEARNING METHODS

Theory-guided machine learning has been identified as a promising paradigm that may make it possible to give ML models the ability to agree with hydrogeological knowledge. The purpose of this article was to assess to what extent theory-guided methods would be able to overcome the various limitations of ML, namely the black-box nature of most models, an often-limited generalization ability, a hypothetical convergence, and uncertain transferability. Three approaches were evaluated as to their capability of satisfying this objective, at least in part. These methods are Theory-Guided Constrained Optimization (TGCO), Theory-Guided Refinement of Outputs (TGRO) and Theory-Guided Architecture (TGA). **Table 2** presents a comparison of the different methods of theory-guided machine learning commonly used in hydrogeology with respect to their ability to overcome ML limiting factors. The table indicates that the opacity of ML models can be reduced by any of the three theory-guided ML methods presented. Convergence and generalizability can be enhanced by TGCO, TGA, or a combination of at least two of the three theory-guided ML methods. To date, there is no study making it possible to deduce the effectiveness of these methods on the transferability of ML models. The first challenge would be to conduct more studies to fill the remaining knowledge gaps on the effectiveness of the presented methods to overcome ML limitations for hydrogeological applications.

In most of the studies analysed in this review, the application of theory-guided methods was performed on idealized configurations. Although these methods are convincing from a theoretical point of view, it is not possible to assess to what extent their use can be generalized in practical

applications. It would therefore be interesting to be able to show or prove the transferability of these methods to real hydrogeological applications.

There does exist a way to quantify the generalization ability and the convergence of ML models. For example, the generalization ability can be defined as the ratio of the mean squared error between the model results and the observations during the test and training stages. When this ratio is close to 1, it is possible to conclude that the model shows a good generalization ability. However, it is not yet possible to measure the degree of attenuation of the black-box nature of ML models as well as the degree of improvement of their transferability in regression tasks through theory-guided methods. This remains an open research subject which could lead to the formulation of related metrics. The notion of mitigating the black box-nature of ML models is subjective in that it depends on the audience questioning the model (e.g., hydrogeologist, stakeholders, ...). The first step in defining a metric to assess the degree of attenuation of the black box nature of theory-guided models would be to provide a mathematical definition, which currently does not exist. To assess the transferability of theory-guided models to new hydrogeological configurations for a given aquifer, it would be interesting to evaluate how well the occurrence of an entirely new event in that aquifer is considered by these models. This could involve evaluating the performance of the model both in the absence of, and in the presence of, the new event. Stable performances would probably indicate a model well suited to new events. In other words, the metric used to assess the generalization ability could be adapted to assess the model's transferability. It should have the merit of being tested. Also, it could be interesting to adapt the metric implemented by Nguyen et al. (2020a), the Log Expected Empirical Prediction (LEEP), to measure the transferability of classifiers, to regression contexts.

In the TGRO method, model outputs need to be transformed to guarantee physical consistency. The transformation function used to refine model output data must be well constructed. But in what manner? This also remains an open research field and a great challenge for hydrogeologists. Possible ways of constructing transformation functions that can be explored are the

use of Laplace transforms on the equations governing groundwater flows or an adaptation of the collocation point method.

Finally, given the increasing availability of globally accessible data and satellite data, it would be interesting to conduct studies as well as large-scale comparison campaigns to better document the application of theory-guided machine learning in hydrogeology and obtain more general conclusions.

## 2.5 CONCLUSION

In this article, three theory-guided machine learning methods that have been used in hydrogeology are assessed for their ability to address four identified ML limiting factors in hydrogeological research and applications, namely the black-box nature of most models, an often-limited generalization ability, a hypothetical convergence, and uncertain transferability. The three methods are Theory-Guided Constrained Optimization (TGCO), Theory-Guided Refinement of Outputs (TGRO) and Theory-Guided Architecture (TGA). The analysis of these three methods through the hydrogeological literature led to the following conclusions: the opacity of ML models can be reduced by any of the three theory-guided ML methods presented; convergence and the generalizability can be enhanced by TGCO, TGA, or a combination of at least two of the three theory-guided ML methods; to date, there is no study making it possible to deduce the effectiveness of these methods on the transferability of ML models. It was concluded that more studies are needed to fill the remaining knowledge gaps regarding the effectiveness of Theory-guided ML methods in overcoming the limitations of ML. Also, given that Theory-guided ML methods have only been applied to idealized configurations and systems, it would be useful to carry out additional studies on real configurations in order to assess to what extent these methods can be generalized. There is a need for methods allowing the development of transformation functions that are consistent with theory to achieve full use of the TGRO method in hydrogeology. This review also identifies the need to define metrics to

quantify the extent to which the black-box nature as well as the transferability of ML models could be overcome by theory-guided methods. Finally, it is hoped that this article will enable and encourage hydrogeologists to use ML in a way that benefits research and practical applications in hydrogeology.

#### **CRediT authorship contribution statement**

**AVDP Adombi:** Literature review, Writing - Original draft preparation. **Romain Chesnaux:** Supervision, Resources, Reviewing and Editing. **Marie-Amélie Boucher:** Supervision, Reviewing and Editing.

#### **Funding sources**

The authors acknowledge the financial support of the Natural Sciences and Engineering Research Council (NSERC-federal funding) of Canada in the framework of the Individual Discovery Grant Program held by Prof. Romain Chesnaux.

#### **Declaration of Competing Interest**

On behalf of all authors, the corresponding author states that there is no conflict of interest.

## REFERENCES

- Adamowski, J., and Chan, H.F. 2011. A wavelet neural network conjunction model for groundwater level forecasting. Journal of Hydrology, **407**: 28-40. doi:<https://doi.org/10.1016/j.jhydrol.2011.06.013>.
- Afshar, A., Mariño, M.A., Ebtehaj, M., and Moosavi, J. 2007. Rule-Based Fuzzy System for Assessing Groundwater Vulnerability. Journal of Environmental Engineering, **133**: 532-540. doi:[https://doi.org/10.1061/\(ASCE\)0733-9372\(2007\)133:5\(532\)](https://doi.org/10.1061/(ASCE)0733-9372(2007)133:5(532)).
- Arabameri, A., Roy, J., Saha, S., Blaschke, T., Ghorbanzadeh, O., and Tien Bui, D. 2019. Application of Probabilistic and Machine Learning Models for Groundwater Potentiability Mapping in Damghan Sedimentary Plain, Iran. Remote Sensing, **11**. doi:<https://doi.org/10.3390/rs11243015>.
- Arnold, D.N. 2015. Stability, consistency, and convergence of numerical discretizations. Encyclopedia of Applied and Computational Mathematics: 1358-1364. doi:[https://doi.org/10.1007/978-3-540-70529-1\\_407](https://doi.org/10.1007/978-3-540-70529-1_407).
- Ayodele, T.O. 2010. Types of machine learning algorithms. New advances in machine learning, **3**: 19-48. doi:<https://doi.org/10.5772/9385>.
- Bahareh, K., Husam, A.H.A.-N., Biswajeet, P., Vahideh, S., Alfian Abdul, H., Naonori, U., and Seyed Amir, N. 2019. Optimized Conditioning Factors Using Machine Learning Techniques for Groundwater Potential Mapping [online]. Water **11** [cited].
- Bakshi, S., de Lange, E., van der Graaf, P., Danhof, M., and Peletier, L. 2016. Understanding the Behavior of Systems Pharmacology Models Using Mathematical Analysis of Differential Equations: Prolactin Modeling as a Case Study. CPT: Pharmacometrics & Systems Pharmacology, **5**: 339-351. doi:<https://doi.org/10.1002/psp4.12098>.
- Bar-Sinai, Y., Hoyer, S., Hickey, J., and Brenner, M.P. 2019. Learning data-driven discretizations for partial differential equations. Proceedings of the National Academy of Sciences, **116**: 15344-15349. doi:<https://doi.org/10.1073/pnas.1814058116>.

- Barzegar, R., Fijani, E., Asghari Moghaddam, A., and Tziritis, E. 2017a. Forecasting of groundwater level fluctuations using ensemble hybrid multi-wavelet neural network-based models. *Science of the Total Environment*, **599**. doi:<https://doi.org/10.1016/j.scitotenv.2017.04.189>.
- Brodeur, Z.P., Herman, J.D., and Steinschneider, S. 2020. Bootstrap Aggregation and Cross-Validation Methods to Reduce Overfitting in Reservoir Control Policy Search. *Water Resources Research*, **56**: e2020WR027184. doi:<https://doi.org/10.1029/2020WR027184>.
- Ch, S., and Mathur, S. 2012. Groundwater level forecasting using SVM-PSO. *International Journal of Hydrology Science and Technology*, **2**: 202-218.
- Chang, F.J., Huang, C.W., Chang, L.C., and Kao, I.F. 2016. Prediction of monthly regional groundwater levels through hybrid soft-computing techniques. *Journal of Hydrology*, **541**: 965-976. doi:<https://doi.org/10.1016/j.jhydrol.2016.08.006>.
- Chen, C., He, W., Zhou, H., Xue, Y., and Zhu, M. 2020b. A comparative study among machine learning and numerical models for simulating groundwater dynamics in the Heihe River Basin, northwestern China. *Scientific reports*, **10**: 3904. doi:<https://doi.org/10.1038/s41598-020-60698-9>.
- Chen, Y., Huang, D., Zhang, D., Zeng, J., Wang, N., Zhang, H., and Yan, J. 2020c. Theory-guided hard constraint projection (HCP): a knowledge-based data-driven scientific machine learning method. *arXiv preprint arxiv-2012.06148*.
- Chesnaux, R., Santoni, S., Garel, E., and Huneau, F. 2018. An Analytical Method for Assessing Recharge Using Groundwater Travel Time in Dupuit-Forchheimer Aquifers. *Groundwater*, **56**: 986-992. doi:<https://doi.org/10.1111/gwat.12794>.
- Clark, P., and Niblett, T. 1989. The CN2 induction algorithm. *Machine learning*, **3**: 261-283. doi:<https://doi.org/10.1023/A:1022641700528>.
- Daw, A., Thomas, R.Q., Carey, C.C., Read, J.S., Appling, A.P., and Karpatne, A. Physics-guided architecture (pga) of neural networks for quantifying uncertainty in lake temperature modeling. *In Proceedings of the 2020 siam international conference on data mining*. 2020. SIAM, pp. 532-540.

- Feng, S., Huo, Z., Kang, S., Tang, Z., and Wang, F. 2011. Groundwater simulation using a numerical model under different water resources management scenarios in an arid region of China. ENVIRONMENTAL EARTH SCIENCES, **62**: 961-971. doi:<https://doi.org/10.1007/s12665-010-0581-8>.
- Gorgij, A.D., Moghaddam, A.A., and Kisi, O. 2017. Groundwater budget forecasting, using hybrid wavelet-ANN-GP modelling: A case study of Azarshahr Plain, East Azerbaijan, Iran. Hydrology Research, **48**: 455-467. doi:<https://doi.org/10.2166/nh.2016.202>.
- Hautier, G., Fischer, C.C., Jain, A., Mueller, T., and Ceder, G. 2010. Finding nature's missing ternary oxide compounds using machine learning and density functional theory. Chemistry of Materials, **22**: 3762-3767. doi:<https://doi.org/10.1021/cm100795d>.
- Huang, X., Gao, L., Crosbie, R.S., Zhang, N., Fu, G., and Doble, R. 2019. Groundwater recharge prediction using linear regression, multi-layer perception network, and deep learning. Water, **11**: 1879. doi:<https://doi.org/10.3390/w11091879>.
- John, B., and Das, S. 2020. Identification of risk zone area of declining piezometric level in the urbanized regions around the City of Kolkata based on ground investigation and GIS techniques. Groundwater for Sustainable Development, **11**: 100354. doi:<https://doi.org/10.1016/j.gsd.2020.100354>.
- Kadeethum, T., Jørgensen, T.M., and Nick, H.M. 2020. Physics-informed Neural Networks for Solving Inverse Problems of Nonlinear Biot's Equations: Batch Training. arXiv preprint arXiv:2005.09638.
- Kahana, A., Turkel, E., Dekel, S., and Givoli, D. 2020. Obstacle segmentation based on the wave equation and deep learning. Journal of Computational Physics, **413**: 109458. doi:<https://doi.org/10.1016/j.jcp.2020.109458>.
- Karimpouli, S., and Tahmasebi, P. 2020. Physics informed machine learning: Seismic wave equation. Geoscience Frontiers, **11**: 1993-2001. doi:<https://doi.org/10.1016/j.gsfs.2020.07.007>.
- Karpatne, A., Atluri, G., Faghmous, J.H., Steinbach, M., Banerjee, A., Ganguly, A., Shekhar, S., Samatova, N., and Kumar, V. 2017. Theory-Guided Data Science: A New Paradigm for

- Scientific Discovery from Data. IEEE Transactions on Knowledge and Data Engineering, **29**: 2318-2331. doi:<https://doi.org/10.1109/TKDE.2017.2720168>.
- Kavvas, E.S., Yang, L., Monk, J.M., Heckmann, D., and Palsson, B.O. 2020. A biochemically-interpretable machine learning classifier for microbial GWAS. Nature communications, **11**: 1-11. doi:<https://doi.org/10.1038/s41467-020-16310-9>.
- Khalil, A., Almasri, M.N., McKee, M., and Kaluarachchi, J.J. 2005. Applicability of statistical learning algorithms in groundwater quality modeling. Water Resources Research, **41**. doi:<https://doi.org/10.1029/2004WR003608>.
- Khandelwal, A., Mithal, V., and Kumar, V. Post Classification Label Refinement Using Implicit Ordering Constraint Among Data Instances. In 2015 IEEE International Conference on Data Mining. 14-17 Nov. 2015 2015, pp. 799-804.
- Ling, J., Kurzawski, A., and Templeton, J. 2016. Reynolds averaged turbulence modelling using deep neural networks with embedded invariance. Journal of Fluid Mechanics, **807**: 155-166. doi:<https://doi.org/10.1017/jfm.2016.615>[Opens].
- Liu, J., Wang, K., Ma, S., and Huang, J. 2013. Accounting for Linkage Disequilibrium in Genome-Wide Association Studies: A Penalized Regression Method. Statistics and its interface, **6**: 99-115. doi:<https://doi.org/10.4310/SII.2013.v6.n1.a10>.
- Meng, X., Li, Z., Zhang, D., and Karniadakis, G.E. 2020. PPINN: Parareal physics-informed neural network for time-dependent PDEs. Computer Methods in Applied Mechanics and Engineering, **370**: 113250. doi:<https://doi.org/10.1016/j.cma.2020.113250>.
- Moghaddam, D.D., Rahmati, O., Panahi, M., Tiefenbacher, J., Darabi, H., Haghizadeh, A., Haghghi, A.T., Nalivan, O.A., and Tien Bui, D. 2020. The effect of sample size on different machine learning models for groundwater potential mapping in mountain bedrock aquifers. Catena, **187**. doi:<https://doi.org/10.1016/j.catena.2019.104421>.
- Mohamed, A., Dan, L., Kai, S., Mohamed, M., Aldaw, E., and Elubid, B. 2019. Hydrochemical Analysis and Fuzzy Logic Method for Evaluation of Groundwater Quality in the North Chengdu Plain, China. International Journal of Environmental Research and Public Health, **16**: 302. doi:<https://doi.org/10.3390/ijerph16030302>.

- Muralidhar, N., Bu, J., Cao, Z., He, L., Ramakrishnan, N., Tafti, D., and Karpatne, A. PhyNet: Physics Guided Neural Networks for Particle Drag Force Prediction in Assembly. *In* Proceedings of the 2020 SIAM International Conference on Data Mining. 2020. SIAM, pp. 559-567.
- Naghibi, S.A., Ahmadi, K., and Daneshi, A. 2017. Application of Support Vector Machine, Random Forest, and Genetic Algorithm Optimized Random Forest Models in Groundwater Potential Mapping. Water Resources Management : An International Journal - Published for the European Water Resources Association (EWRA), **31**: 2761-2775.  
doi:<https://doi.org/10.1007/s11269-017-1660-3>.
- Nguyen, C., Hassner, T., Seeger, M., and Archambeau, C. Leep: A new measure to evaluate transferability of learned representations. *In* International Conference on Machine Learning. 2020a. PMLR, pp. 7294-7305.
- Nguyen, P.T., Ha, D.H., Jaafari, A., Nguyen, H.D., Van Phong, T., Al-Ansari, N., Prakash, I., Le, H.V., and Pham, B.T. 2020b. Groundwater Potential Mapping Combining Artificial Neural Network and Real AdaBoost Ensemble Technique: The DakNong Province Case-study, Vietnam. International Journal of Environmental Research and Public Health, **17**: 2473.  
doi:<https://doi.org/10.3390/ijerph17072473>.
- Nguyen, P.T., Ha, D.H., Nguyen, H.D., Van Phong, T., Trinh, P.T., Al-Ansari, N., Le, H.V., Pham, B.T., Ho, L.S., and Prakash, I. 2020c. Improvement of credal decision trees using ensemble frameworks for groundwater potential modeling. Sustainability, **12**: 2622.  
doi:<https://doi.org/10.3390/su12072622>.
- Oberlack, M. 2002. Symmetries and invariant solutions of turbulent flows and their implications for turbulence modelling. *In* Theories of Turbulence. Springer. pp. 301-366.
- Park, Y., Ligaray, M., Kim, Y.M., Kim, J.H., Cho, K.H., and Sthiannopkao, S. 2016. Development of enhanced groundwater arsenic prediction model using machine learning approaches in Southeast Asian countries. Desalination and Water Treatment, **57**: 12227-12236.  
doi:<https://doi.org/10.1080/19443994.2015.1049411>.

- Pazzani, M.J., and Brunk, C.A. 1991. Detecting and correcting errors in rule-based expert systems: an integration of empirical and explanation-based learning. *Knowledge Acquisition*, **3**: 157-173. doi:[https://doi.org/10.1016/1042-8143\(91\)90003-6](https://doi.org/10.1016/1042-8143(91)90003-6).
- Piccione, A., Berkery, J., Sabbagh, S., and Andreopoulos, Y. 2020. Physics-guided machine learning approaches to predict the ideal stability properties of fusion plasmas. *Nuclear Fusion*, **60**. doi:<https://doi.org/10.1088/1741-4326/ab7597>.
- Pradhan, S., Kumar, S., Kumar, Y., and Sharma, H.C. 2019. Assessment of groundwater utilization status and prediction of water table depth using different heuristic models in an Indian interbasin. *Soft Computing : A Fusion of Foundations, Methodologies and Applications*, **23**: 10261-10285. doi:<https://doi.org/10.1007/s00500-018-3580-4>.
- Raazia, S., and Dar, A.Q. 2021. A numerical model of groundwater flow in Karewa-Alluvium aquifers of NW Indian Himalayan Region. *Modeling Earth Systems and Environment*: 1-12. doi:<https://doi.org/10.1007/s40808-021-01126-3>.
- Raissi, M., Perdikaris, P., and Karniadakis, G.E. 2019. Physics-informed neural networks: A deep learning framework for solving forward and inverse problems involving nonlinear partial differential equations. *Journal of Computational Physics*, **378**: 686-707. doi:<https://doi.org/10.1016/j.jcp.2018.10.045>.
- Rudin, C. 2019. Stop explaining black box machine learning models for high stakes decisions and use interpretable models instead. *Nature Machine Intelligence*, **1**: 206-215. doi:<https://doi.org/10.1038/s42256-019-0048-x>.
- Sahoo, S., and Jha, M.K. 2013. Groundwater-level prediction using multiple linear regression and artificial neural network techniques: a comparative assessment. *Hydrogeology Journal*, **21**. doi:<https://doi.org/10.1007/s10040-013-1029-5>.
- Sahoo, S., Russo, T., Elliott, J., and Foster, I. 2017b. Machine learning algorithms for modeling groundwater level changes in agricultural regions of the US. *Water Resources Research*, **53**: 3878-3895.
- Sajedi-Hosseini, F., Malekian, A., Choubin, B., Rahmati, O., Cipullo, S., Coulon, F., and Pradhan, B. 2018. A novel machine learning-based approach for the risk assessment of nitrate

- groundwater contamination. *Science of the Total Environment*, **644**: 954-962. doi:<https://doi.org/10.1016/j.scitotenv.2018.07.054>.
- Shaham, U., Yamada, Y., and Negahban, S. 2018. Understanding adversarial training: Increasing local stability of supervised models through robust optimization. *Neurocomputing*, **307**: 195-204. doi:<https://doi.org/10.1016/j.neucom.2018.04.027>.
- Shiri, J., Kisi, O., Yoon, H., Lee, K.-K., and Nazemi, A.H. 2013. Predicting groundwater level fluctuations with meteorological effect implications—A comparative study among soft computing techniques. *Computers & Geosciences*, **56**: 32-44. doi:<http://dx.doi.org/10.1016/j.cageo.2013.01.007>.
- Srivastava, N., Hinton, G., Krizhevsky, A., Sutskever, I., and Salakhutdinov, R. 2014. Dropout: a simple way to prevent neural networks from overfitting. *The journal of machine learning research*, **15**: 1929-1958.
- Su, Y.-S., Ni, C.-F., Li, W.-C., Lee, I.-H., and Lin, C.-P. 2020. Applying deep learning algorithms to enhance simulations of large-scale groundwater flow in IoTs. *APPLIED SOFT COMPUTING*, **92**: 106298. doi:<https://doi.org/10.1016/j.asoc.2020.106298>.
- Sun, A.Y. 2018. Discovering state-parameter mappings in subsurface models using generative adversarial networks. *Geophysical Research Letters*, **45**: 11,137-111,146. doi: <https://doi.org/10.1029/2018GL080404>.
- Sun, Y., Wang, X., and Tang, X. Deep learning face representation from predicting 10,000 classes. *In Proceedings of the IEEE conference on computer vision and pattern recognition*. 2014, pp. 1891-1898.
- Tahmasebi, P., Kamrava, S., Bai, T., and Sahimi, M. 2020. Machine learning in geo- and environmental sciences: From small to large scale. *Advances in Water Resources*, **142**: 103619. doi:<https://doi.org/10.1016/j.advwatres.2020.103619>.
- Tapoglou, E., Trichakis, I.C., Dokou, Z., Nikolos, I.K., and Karatzas, G.P. 2014. Groundwater-level forecasting under climate change scenarios using an artificial neural network trained with particle swarm optimization. *Hydrological sciences journal = Journal des sciences hydrologiques.*, **59**: 1225-1239. doi:<http://dx.doi.org/10.1080/02626667.2013.838005>.

- Tartakovsky, A.M., Marrero, C.O., Perdikaris, P., Tartakovsky, G.D., and Barajas-Solano, D. 2020. Physics-Informed Deep Neural Networks for Learning Parameters and Constitutive Relationships in Subsurface Flow Problems. *Water Resources Research*, **56**: e2019WR026731. doi:<https://doi.org/10.1029/2019WR026731>.
- Tayfur, G., Nadiri, A.A., and Moghaddam, A.A. 2014. Supervised Intelligent Committee Machine Method for Hydraulic Conductivity Estimation. *Water Resources Management*, **28**: 1173-1184. doi:10.1007/s11269-014-0553-y.
- Tutmez, B., Hatipoglu, Z., and Kaymak, U. 2006. Modelling electrical conductivity of groundwater using an adaptive neuro-fuzzy inference system. *Computers and Geosciences*, **32**: 421-433. doi:<https://doi.org/10.1016/j.cageo.2005.07.003>.
- Udrescu, S.-M., and Tegmark, M. 2020. AI Feynman: A physics-inspired method for symbolic regression. *Science Advances*, **6**: eaay2631. doi:<https://doi.org/10.1126/sciadv.aay2631>.
- Urolagin, S., kv, P., and Reddy, N.V.S. 2011. Generalization Capability of Artificial Neural Network Incorporated with Pruning Method.
- Wang, B., Oldham, C., and Hipsey, M.R. 2016. Comparison of Machine Learning Techniques and Variables for Groundwater Dissolved Organic Nitrogen Prediction in an Urban Area. *Procedia Engineering*, **154**: 1176-1184. doi:<https://doi.org/10.1016/j.proeng.2016.07.527>.
- Wang, N., Chang, H., and Zhang, D. 2021a. Efficient uncertainty quantification for dynamic subsurface flow with surrogate by Theory-guided Neural Network. *Computer Methods in Applied Mechanics and Engineering*, **373**: 113492. doi:<https://doi.org/10.1016/j.cma.2020.113492>.
- Wang, N., Zhang, D., Chang, H., and Li, H. 2020b. Deep learning of subsurface flow via theory-guided neural network. *Journal of Hydrology*, **584**: 124700. doi:<https://doi.org/10.1016/j.jhydrol.2020.124700>.
- Wang, R., Walters, R., and Yu, R. 2020c. Incorporating symmetry into deep dynamics models for improved generalization. *arXiv preprint arXiv:2002.03061*.
- Warde-Farley, D., Goodfellow, I.J., Courville, A., and Bengio, Y. 2013. An empirical analysis of dropout in piecewise linear networks. *arXiv preprint arXiv:1312.6197*.

- Willard, J., Jia, X., Xu, S., Steinbach, M., and Kumar, V. 2020. Integrating physics-based modeling with machine learning: A survey. arXiv preprint arXiv:2003.04919.
- Xu, R., Zhang, D., Rong, M., and Wang, N. 2020. Weak Form Theory-guided Neural Network (TgNN-wf) for Deep Learning of Subsurface Single and Two-phase Flow.
- Ying, X. An overview of overfitting and its solutions. In *Journal of Physics: Conference Series*. 2019. IOP Publishing. Vol. 1168, p. 022022.
- Yip, K.Y., and Gerstein, M. 2009. Training set expansion: an approach to improving the reconstruction of biological networks from limited and uneven reliable interactions. *Bioinformatics*, **25**: 243-250. doi:<https://doi.org/10.1093/bioinformatics/btn602>.
- Zhang, P. 2010. Industrial control system simulation routines. pp. 781-810.
- Zobeiry, N., and Humfeld, K.D. 2021. A physics-informed machine learning approach for solving heat transfer equation in advanced manufacturing and engineering applications. *Engineering Applications of Artificial Intelligence*, **101**: 104232. doi:<https://doi.org/10.1016/j.engappai.2021.104232>.
- Zobeiry, N., Reiner, J., and Vaziri, R. 2020a. Theory-guided machine learning for damage characterization of composites. *Composite Structures*, **246**. doi:<https://doi.org/10.1016/j.compstruct.2020.112407>.
- Zobeiry, N., Stewart, A., and Poursartip, A. Applications of Machine Learning for Process Modeling of Composites In SAMPE Virtual Conference. 2020b.

## CHAPITRE 3

### COMPARING NUMERICAL MODELLING, TRADITIONAL MACHINE LEARNING AND THEORY-GUIDED MACHINE LEARNING IN INVERSE MODELING OF GROUNDWATER DYNAMICS: A FIRST STUDY CASE APPLICATION

Ce chapitre aborde le premier objectif de la recherche, qui est de tester l'hypothèse de recherche en comparant un modèle TgML avec des modèles traditionnels dans un contexte de modélisation distribuée de l'écoulement des eaux souterraines. L'aquifère de Saint-Honoré dans la région du Saguenay-Lac-Saint-Jean au Québec, Canada a servi de laboratoire d'étude. Plus spécifiquement, l'étude menée consistait à répondre à la question suivante : dans une tâche de simulation distribuée de l'écoulement des eaux souterraines, comment un modèle TgML, notamment un perceptron multicouche guidé par la théorie (TgMLP), se compare-t-il à un modèle numérique (NumMod) et un perceptron multicouche conventionnel (MLP) ? Les modèles ont été comparés en termes de (a) performance, (b) de capacité à capturer la dynamique de l'écoulement (équation EDP de diffusivité) et (c) de coûts de calculs requis pour leur entraînement / calibration. Le modèle TgMLP a été construit selon la méthode d'optimisation sous contrainte. L'étude visait également à comprendre l'impact qu'a une transgression de l'EDP par le modèle TgMLP sur la justesse des résultats. Les résultats ont montré que le modèle TgMLP démontre la meilleure justesse et surpassé de loin les modèles numériques et MLP traditionnels, que le modèle MLP est un bon interpolateur mais est incapable d'extrapoler, et que seuls les modèles numériques et TgMLP sont fiables parce qu'ils sont les seuls capables de capturer la dynamique spatio-temporelle de l'écoulement des eaux souterraines et de représenter la direction dominante de l'écoulement dans l'aquifère. L'analyse des couts requis pour entraîner / calibrer les différents modèles montre qu'en l'absence d'un accélérateur de calculs, la calibration du TgMLP réquerirait 10 fois de temps comparé à celui du modèle numérique et 48 fois celui du MLP mais avec un accélérateur de calcul, ces ratios descendent à 1.66 et 8 respectivement. Il a été également constaté que le modèle TgMLP ne réussit à approcher la solution de l'EDP que dans 70 % des cas. La mauvaise approximation dans 30 % des endroits

pourrait être due à un effet de non-respect de l'EDP au niveau des sources/puits ou des conditions de Neumann.

En somme, pour la modélisation distribuée, l'hypothèse sur laquelle repose le TgML est vérifiée dans une certaine mesure, si ce n'est que l'apprentissage de ces modèles requiert plus de temps par rapport à l'entraînement/calibration des modèles traditionnels.

Adoubi Vincent De Paul Adombi<sup>a</sup>, Romain Chesnaux<sup>a</sup>, Marie-Amélie Boucher<sup>b</sup>

- a. Research Group R2Eau, Centre d'études sur les ressources minérales, Université du Québec à Chicoutimi, 555 boulevard de l'Université, Chicoutimi, Québec G7H 2B1, Canada.  
Email : [adombi.vincentdepaul@gmail.com](mailto:adombi.vincentdepaul@gmail.com)
- b. Department of Civil Engineering, Université de Sherbrooke, 2500 boulevard de l'Université, Sherbrooke, Québec J1R 2R2, Canada

Reçu le 01 juin 2022 - Accepté le 26 septembre 2022 - Publié le 04 novembre 2022 dans la revue Journal of Hydrology. DOI : <https://doi.org/10.1016/j.jhydrol.2022.128600>

### 3.1 ABSTRACT

This study proposes to test the hypothesis that theory-guided machine learning model can be effectively applied to model the behavior of a real aquifer. For this purpose, a theory-guided multilayer perceptron model (TgMLP) for real aquifers was developed to simulate groundwater flow dynamics. A comparison of the performance of the TgMLP with that of a numerical model (NumMod) and a traditional multilayer perceptron model (MLP) was performed. The ability of these three models to capture the spatiotemporal dynamics of groundwater was evaluated, the degree of PDE violation of the TgMLP model was also assessed, and the applicability of these three models in a real-world setting was discussed. The Saint-Honoré unconfined aquifer (Quebec, Canada), which has been

extensively monitored over the last few years, was used as an experimental laboratory for this study. Historical groundwater levels, recharge, precipitation, mean temperature and streamflow data were used to calibrate/train/validate and test the models. The results show that the performance of the TgMLP far exceeds that of the numerical and traditional MLP models, that the MLP model is a good interpolator but is unable to extrapolate, and that only the numerical and TgMLP models are able to capture the spatiotemporal dynamics of groundwater flow and represent the dominant flow direction in the aquifer. It was found that the TgMLP model better approximates the solution of the PDE at 70% of the locations. These results support the hypothesis that TgMLP is effective in modeling the spatiotemporal dynamics of groundwater in a real aquifer even if improvements are needed. Although the TgMLP model is capable of representing groundwater flow dynamics to some degree, its implementation requires much higher computational costs than a numerical model; however, these can be reduced with the use of a GPU to speed up the calculations.

**Keywords:** Theory-guided machine learning · Numerical modelling · Groundwater flow · Statistical modelling · Optimization

### 3.2 INTRODUCTION

Studying the workings of groundwater systems involves a number of traditional tools and techniques to determine the nature of the terrain through which groundwater flows and the physical properties that control this flow. Such characterization also requires determining how these systems are supplied, where they discharge, their physical boundaries and their interaction with neighboring hydrogeologic systems. All this information can be used to formulate a so-called conceptual model of a hydrogeological system. The conceptual model can be defined as the set of assumptions made to describe the understanding of a groundwater system (Enemark et al. 2019).

Based on the conceptual model, a numerical model can be constructed to simulate and eventually predict how the hydrogeological system functions when it undergoes disturbances. The numerical model is a tool commonly used in hydrogeology; its purpose is to solve a discrete form of the equations that describe the groundwater flow under the assumptions that constitute the conceptual model. Feng et al. (2011), for example, developed a FEFLOW numerical groundwater model to simulate regional flow variations under different water management scenarios. The results of their study showed a continuous decline in groundwater levels over time under the management conditions prevailing at the time of the study. Vu et al. (2021b) used an integrated method of overlaying a modified version of the DRASTIC index and a MODFLOW numerical model to predict the vulnerability and sustainability of groundwater under various climatic conditions and anthropogenic activities. The results of their study showed that variations in future climate conditions exerted little influence on the variations in vulnerability of the studied basin but based on the analysis of sustainability indicators, the groundwater resource system was in a critical condition of high vulnerability.

Although numerical models are an effective tool for studying groundwater systems, the assumptions on which they are built are a major source of structural uncertainty and can affect the accuracy of the model. To address the issue of uncertainty and model accuracy, the multi-model approach, which consists in developing plausible alternative conceptual models and evaluating them through numerical modelling, is one of the traditional possible solutions (Enemark et al. 2019). However, the multi-model approach can be time consuming, which limits its practical use.

Since the popularization of artificial intelligence in the 1980's (Barr et al. 1981), machine learning (ML), a branch of artificial intelligence, is increasingly used in various scientific fields. Machine Learning relies on a sufficient set of data to approximate any non-linear function between some input and output variables.

In hydrogeology, ML algorithms are used with a good level of satisfaction to perform specific modeling tasks such as mapping the spatial distribution of groundwater salinity (Mosavi et al. 2021; Sahour et al. 2020; Tran et al. 2021), uncertainty quantification (Gadd et al. 2019; Lykkegaard et al. 2021; Song et al. 2020), improving the accuracy of groundwater level prediction (Banadkooki et al. 2020; Cai et al. 2021), groundwater potential mapping (Kalantar et al. 2019; Kumar et al. 2021; Lee et al. 2020) or determination of physical parameters of aquifers (Hou et al. 2021; Tayfur et al. 2014). For example, Banadkooki et al. (2020) investigated the impact of different input variables on the accuracy of groundwater level prediction of hybrid machine learning models. The algorithms used were neural network with radial basis function-whale algorithm, multilayer perception, and genetic programming. Precipitation, mean temperatures and their time-shifted equivalents combined in various ways were used as inputs. The results show that the algorithm that generates the best performing model depends on the combinations of input variables used. Tayfur et al. (2014) used Sugeno fuzzy logic, Mamdani fuzzy logic, multilayer perceptron neural network, neuro-fuzzy algorithms, and an ensemble algorithm that combines the predictions of the previous algorithms to determine the best model for hydraulic conductivity estimation for a heterogeneous aquifer in their study using hydrogeological and geoelectric data. It was found that the best model was the one generated by the ensemble aggregation algorithm.

Machine learning algorithms, in their traditional form, are effective tools for learning any non-linear relationship between a set of inputs and a set of outputs with a high level of accuracy and a relatively short computation time. However, machine learning algorithms generally have poor explanatory power and therefore are not as useful as physics-based modelling to improve our understanding of the physical phenomena. In many contexts, this black-box aspect limits the operational applicability of traditional machine learning techniques.

Recently, Raissi et al. (2019) popularized a new paradigm by incorporating, during training, certain constraints related to the physics governing the phenomenon under study so that the algorithm

not only learns from the data but also refrains from deviating too far from the known governing laws of physics. This paradigm is commonly referred to as theory-guided machine learning (Adombi et al. 2021; Esterhuizen et al. 2020; Karpatne et al. 2017; Wagner and Rondinelli 2016). Wang et al. (2020b) compared the predictive performance of a deep neural network (DNN) model against that of a theory-guided DNN (TgDNN) model. To do this, they used simple, idealized two-dimensional hydrogeological configurations for spatio-temporal modelling of groundwater levels. Using time series of groundwater levels synthetically generated by a numerical model as reference data, the results showed that the TgDNN model achieves much better predictability, reliability, and generalization than the DNN models. Tartakovsky et al. (2020) used a theory-guided deep neural network to estimate hydraulic conductivity in saturated and unsaturated flows governed by Darcy's law in idealized synthetic hydrogeological settings. The results show that the model is well suited for hydraulic conductivity estimation.

Unlike traditional machine learning, to our knowledge, theory-guided machine learning has never been applied to a real-world hydrogeological setting. In such a setting, aquifer geometry can affect groundwater flow, the spatial distribution of observation wells is sparse, hydrodynamic properties are known only at a few points within the study area, and many uncertainties are pervasive - such as partial knowledge of the geology. Studies in idealized synthetic hydrogeological settings have shown some interest in applying theory-guided machine learning, but do not document its effectiveness and limitations in real-world applications. Considering the inherent difficulties in assessing aquifer systems and the necessity of representing these "invisible" systems by conceptual models, theory-guided machine learning could be a useful tool to be integrated in the toolbox of hydrogeologists to assess these systems with a higher degree of confidence.

This study proposes to test the hypothesis that a theory-guided machine learning model can be effectively applied for inverse modeling of the groundwater dynamics of a real aquifer. To verify this hypothesis, we built and used a theory-guided machine learning model to simulate groundwater

dynamics and compare it both to observations and to other commonly used tools such as numerical modelling and traditional machine learning. Our starting hypothesis is based on the fact that theory-guided machine learning considers the actual behavior of an aquifer and not solely on its hydrogeological properties, which are assessed by hydrogeologists with a generally high degree of uncertainty and poor confidence. We posit that this approach could be effective in a real-world case study.

In this study, the inverse modeling of the spatiotemporal dynamics of groundwater in a real aquifer is investigated and compared using three methods: a numerical model (NumMod), a multilayer perceptron (MLP) and a theory-guided multilayer perceptron (TgMLP). The Saint-Honoré aquifer (Quebec, Canada) constitutes a good experimental laboratory for this study because of the significant extent of knowledge previously acquired at this site (e.g., Boumaiza 2008; Boumaiza et al. 2020; Boumaiza et al. 2021; Labrecque et al. 2019; Parent and Occhietti 2007; Tremblay 2005). This unconfined granular aquifer has been equipped with a sufficient number of piezometers that are continuously monitored, and has been well characterized over time in terms of geology, hydrodynamic properties and hydraulic limits.

In this study, the temporal extrapolation ability of the different models is not investigated; this study is therefore limited to the following objectives:

- Compare the performance of NumMod, TgMLP and MLP for the inverse modeling of GWL dynamics;
- Evaluate the ability of the three models to capture the spatiotemporal dynamics of GWL;
- Evaluate the effect of partial differential equation (PDE) violation by the TgMLP model;
- Discuss the applicability of the three models in a real-world setting.

### 3.3 STUDY AREA AND DATA

#### 3.3.1 STUDY AREA

The Saint-Honoré aquifer belongs to the Saguenay Lac Saint Jean (SLSJ) region of Quebec, Canada (**Figure 8**).

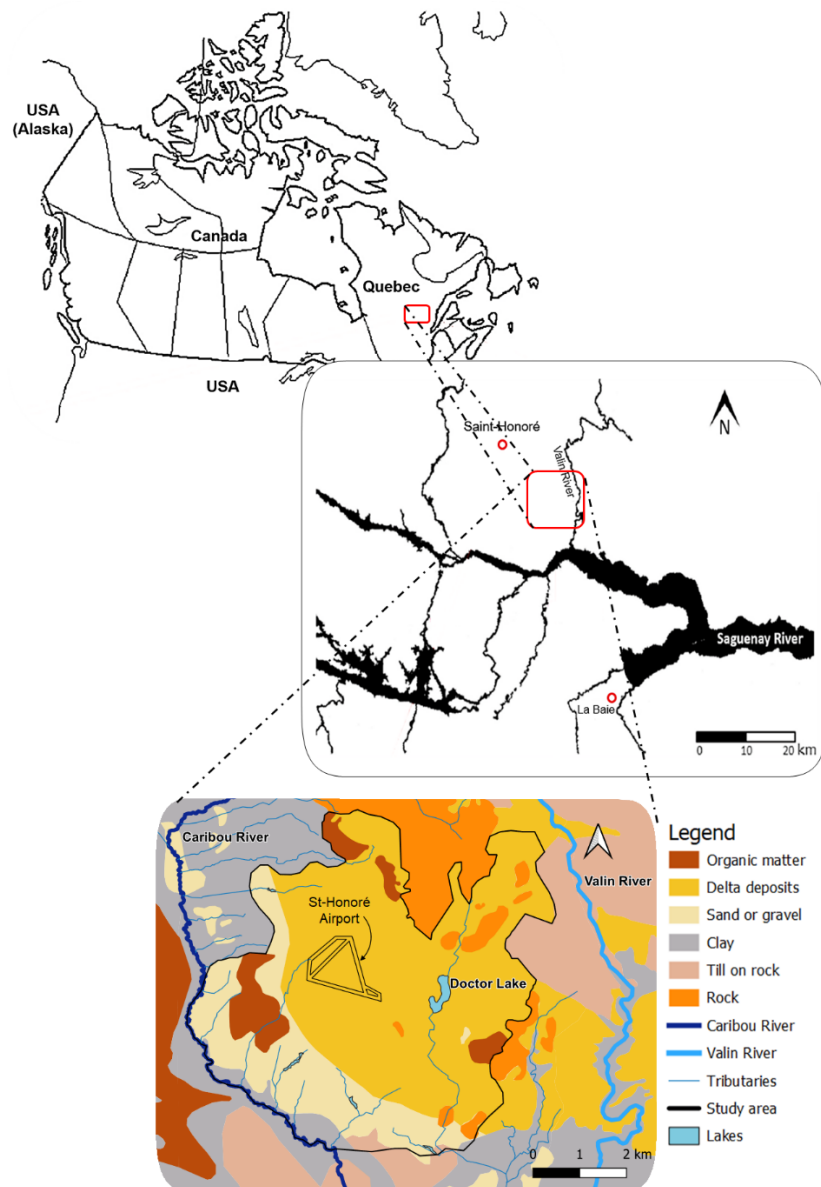


**Figure 8** Geographic location of the study area, geological outcrops consisting of deltaic sediments, sands and gravels, clays, tills, rocks and location of the Valin River, Caribou River and tributaries of interest. Created in part from figures in Boumaiza et al. (2021).

The portion of the aquifer considered as the study area is located near the Saint-Honoré airport, between the Caribou River (ungauged) to the west and the Valin River (gauged) to the east, and covers approximately 36.7 km<sup>2</sup>. In addition to pumping wells, streams constitute the discharge sites of the aquifer while the primary source of recharge of the aquifer is precipitation (Tremblay 2005). Precipitation is estimated to average 930 mm per year (Boumaiza et al. 2021). During most of a given year, three directions of groundwater flow are observed (southwestward, northwestward, and westward), but the southwestward flow is dominant (Tremblay 2005).,

The development of the Saint-Honoré unconfined aquifer can be traced back to the last glacial event in the SLSJ area between 85,000 and 7,000 years ago, when the overlying glacier retreated to form a discontinuous and heterogeneous layer of geologic materials including glaciolacustrine and glaciofluvial deposits and till (Parent and Occhietti 2007). A marine invasion subsequently occurred, causing the deposition of fine clay-like sediments. A marine regression then followed, and these sediments were covered by deltaic granular sediments that constitute the Saint-Honoré aquifer (Boumaiza et al. 2021). The granular sediments are up to 50 m thick in the study area and consist mainly of sands and silts. In some parts of the study area, the granular sediments are directly underlain by Precambrian crystalline bedrock belonging to the Canadian Shield, and in other parts they are underlain by clays or till. The northern boundary of the study area is marked by an outcrop of Precambrian bedrock, the western boundary by an outcrop of a clay layer with the presence of the Caribou River a little further south. All along the eastern boundary, outcrops of the bedrock or till layers are found. The portion of the Saint-Honoré aquifer considered in this study has been represented in Tremblay (2005) as a succession of four stratigraphic units, each composed of several hydrogeologic layers that are homogeneous and isotropic in their hydrodynamic properties. **Figure 9** illustrates the layout of the stratigraphic units (S. Units) and their hydrogeological layers, and also locates the wells and the monitored piezometers.

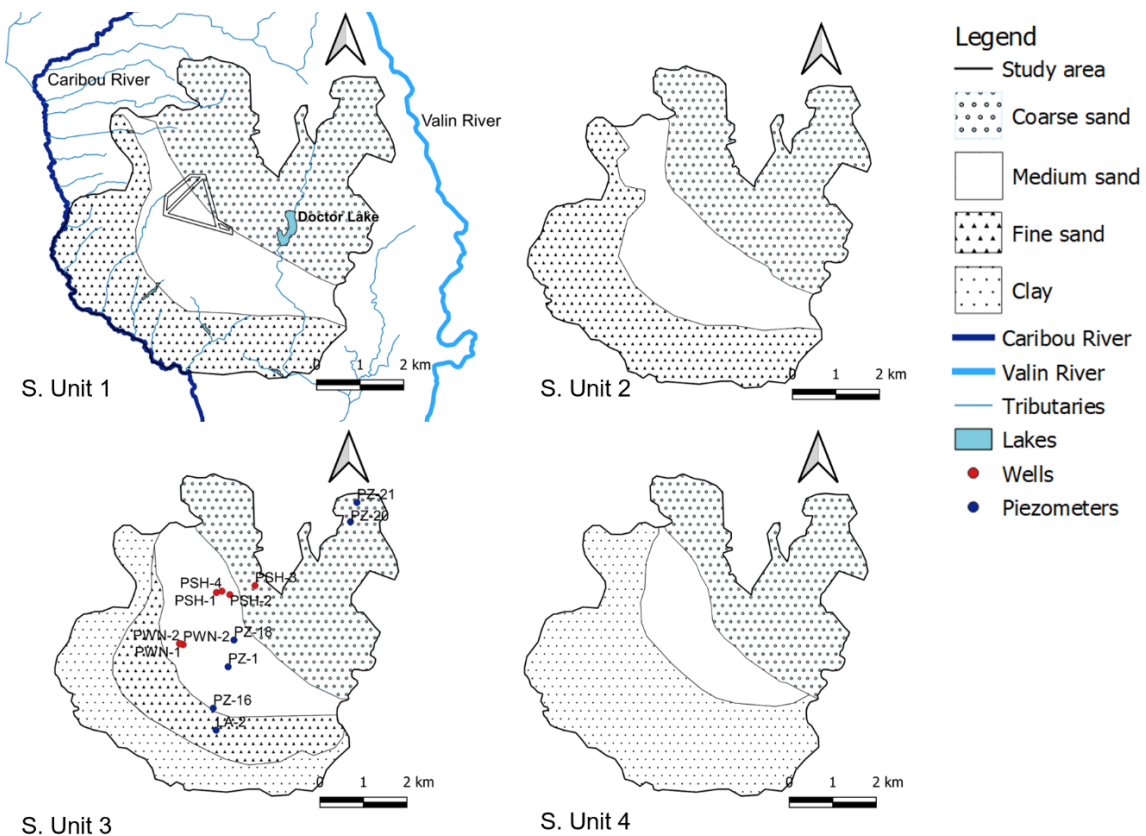


**Figure 9** Stratigraphic units, from the most superficial (S. Unit 1) to the deepest (S. Unit 4), each composed of a combination of at least three of the hydrogeological layers of coarse, medium and fine sands and clays. Location of the six monitored piezometers and seven pumping wells.

### 3.3.2 DATA

The models in this study were developed using hydrogeological, hydrological and meteorological variables. The data, including the processed input data and raw and processed results, algorithms, numerical model, and software used for numerical modeling are available on Mendeley Data [reserved doi:10.17632/87fkztgbh.2]. Specifically, the data used are daily GWL at the six continuously monitored piezometers, daily precipitation and mean temperature, daily recharge rate, monthly pumping rates at the seven wells in the aquifer, and stream flow measurements taken between 2001 and 2004 by Tremblay (2005).

The groundwater levels data were measured automatically between 09/11/2016 and 30/11/2017 at 15-minute time steps and then processed into daily time series. Daily precipitation and mean temperature were provided in the form of  $0.1^\circ \times 0.1^\circ$  weather grids by the “Info-climat” service of Quebec’s Ministère de l’Environnement et de la Lutte contre les Changements Climatiques (MELCC). Since the study area was intersected by six weather grids, a spatial average of precipitation and that of the mean temperature were calculated. Pumping rate data were obtained through direct communication with the institutions in charge of their management (Niobec Mine and Municipality of Saint-Honoré). Monthly pumping rates were also transformed into daily data. For the numerical and TgMLP models, the topographic surface and bedrock elevations were retrieved from the *Programme d’Acquisition des Connaissances sur les Eaux Souterraines* (PACES) database of the MELCC. The sequence of stratigraphic units used in this paper is based primarily on the interpretation of the stratigraphy proposed by Tremblay (2005). The hydrodynamic property ranges of the hydrogeological layers of the stratigraphic units were compiled from the data in Tremblay (2005) but also from the PACES database. The ranges of values for hydrodynamic properties are shown in **Table 3**. The daily recharge series was inferred by the Water Table Fluctuation (WTF) method over the period 09/11/2016 to 30/12/2017 at piezometer Pz-18, data produced by Labrecque et al. (2019). The recharge time series at Pz-18 is considered to be representative of recharge dynamics over the entire aquifer.

**Table 3** Range of values of physical properties of hydrogeological layers.

	Hydraulic Conductivity ( $\times 10^{-4}$ ) [m/s]	Hydraulic Conductivity ( $\times 10^{-4}$ ) [m/s]	
Hydrogeological layer	Range	Reference value	Storage coefficient (effective porosity) [-]
Coarse sand	[1.1 – 70]	45	0.27
Medium sand	[1.1 – 70]	6.0	0.28
Fine sand	[1.1 – 70]	0.75	0.23
Clay	$[1.0 \cdot 10^{-7} – 4.7 \cdot 10^{-5}]$	$2.0 \cdot 10^{-7}$	0.03

### 3.4 METHODS AND MODELS

In groundwater dynamics modeling, the inverse problem is resolved in two steps. The first step is to identify the model that most appropriately describes the groundwater flow in the aquifer under study. This involves, for example, determining the governing equations, boundary conditions or heterogeneities in the aquifer. This leads to the establishment of a conceptual model. The second step is then to estimate or calibrate the model parameters such as hydrodynamic parameters, recharge and boundary conditions in order to reproduce field observations such as groundwater levels as closely as possible.

Because the Saint-Honoré aquifer has been extensively characterized, we assume that the conceptual model already established for this aquifer (see Tremblay (2005)) and summarized in **Section 3.4.1** and **Figure 10** has a high degree of representativity. Therefore, the inverse problem of the numerical model will be to calibrate the hydrodynamic parameters of the aquifer. For the TgMLP model, the hydrodynamic parameters calibrated by the numerical model will be provided as prior knowledge and the inverse problem will then consist in estimating the neural network parameters. Finally, for the MLP, the inverse problem will also be to calibrate the neural network parameters.

#### 3.4.1 NUMERICAL MODEL

The numerical groundwater flow simulation model was built using the free version of the MARTHE software developed by the French Geological Survey (Thiéry 1990). The free version of MARTHE can be downloaded at <https://www.brgm.fr/fr/logiciel/marthe-logiciel-modelisation-ecoulements-souterrains>. MARTHE solves a 3D form of the groundwater equation of continuity using the finite volume method, with initial and boundary conditions. More details on the equations and

approximation methods can be found in Thiéry (1990). The finite volume method consists in approximating the groundwater equation by discretizing the groundwater flow system into finite volumes and the simulation time into discrete time steps. At each time step, the input data (recharge and pumping rates) is considered invariant.

MARTHE is able to couple groundwater flow with stream exchanges through a water balance equation that considers exchanges between groundwater and streams, runoff, source/sink terms and possibly a storage term. It is also possible to model the interaction between saturated and unsaturated zones. Given the strong non-linearity of the coupling with the unsaturated zone, MARTHE exploits the notion of "pseudo vadose zone". The "pseudo vadose zone" is used to simulate the water flows in the unsaturated zone without having to provide retention and permeability laws. The details of the "pseudo vadose zone" concept are given in Thiéry (1990).

The MARTHE model built in this paper is a 3D groundwater flow model coupled with groundwater-stream exchanges and a pseudo vadose zone. The study area was discretized along both the x, y and z axes and the time dimension t. In the horizontal plane, the mesh is square with side  $\Delta x = \Delta y = 100$  m. The vertical mesh consists of four model layers representing the stratigraphic units of the Saint-Honoré aquifer. The vertical mesh is made so that at each point the stratigraphic units have approximately the same thickness. The vertical mesh was created based on the surface and bedrock elevation maps of the Saint-Honoré aquifer. Time was discretized into a finite number of daily intervals corresponding to the available GWL time series, i.e., 387 daily time steps. The lateral hydraulic boundaries of the aquifer were chosen to coincide with the natural boundaries (see **Section 3.3.1**). Thus, everywhere on the lateral boundary of the aquifer, except at the border of the Caribou River, a no-flow boundary was defined as it corresponds either to a clay barrier or to the outcrop of the Precambrian bedrock or till. The Caribou River and its tributaries in the study area are defined as Cauchy boundaries. Doctor Lake is considered a constant groundwater level boundary. Wells are represented as flow-imposed boundaries. The upper aquifer boundary is considered a flux-imposed

boundary, with the flux corresponding to the recharge rate. Finally, the aquifer lower boundary is considered a no-flow boundary. This is because the aquifer is underlain by bedrock which is considered impermeable. **Figure 10** presents the synthesis of the conceptual model of the aquifer.

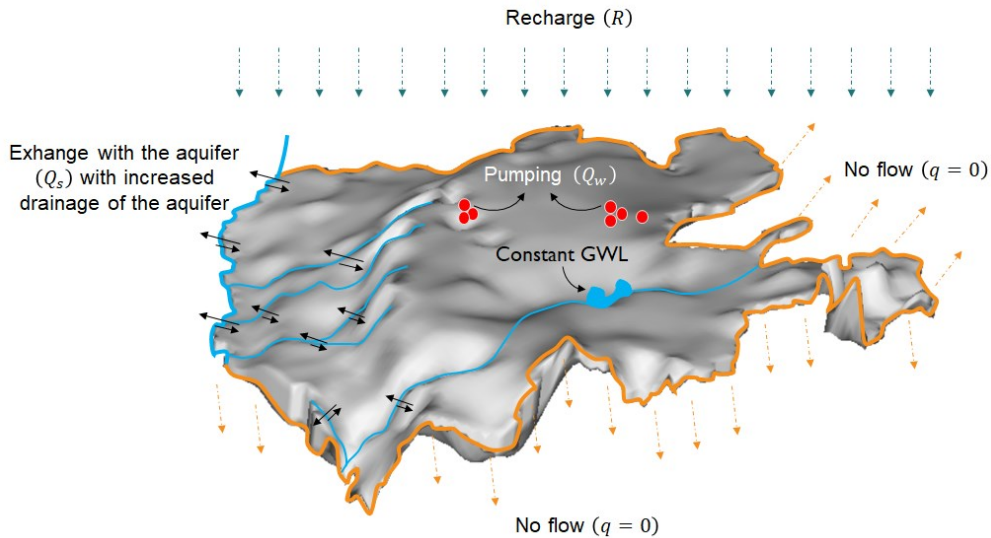


**Figure 10** Synthesis of the conceptual model used for the Saint-Honoré aquifer.

A steady-state calibration performed on 09/11/2016 allowed an initial adjustment of the hydraulic conductivity of the different hydrogeological layers of the model. The physical properties of the streams (hydraulic conductivity and bed thickness) were also calibrated in order to ensure that the stream flows remained within the range of values of the discontinuous flows measured over the period 2001-2004. Indeed, due to the absence of flow measurements in the Caribou River over the period investigated in this study, it was assumed that the average stream flows measured over the period 2001-2004 are not significantly different from those that would have been measured over the period of investigation, i.e. from 09/11/2016 to 30/11/2017.

Next, a transient calibration was performed using the groundwater level time series from four of the available piezometers in the study area as a calibration quality criterion to adjust the storage coefficient values and improve the hydraulic conductivity calibration. These piezometers are LA-2,

Pz-16, Pz-1, Pz-20 (see **Figure 9**); they were selected to ensure approximately one piezometer per hydrogeological layer. The initial groundwater levels used for transient calibration were those obtained after steady-state calibration. The final model selected is the one for which not only the values of the storage coefficient and hydraulic conductivity remain within the ranges of values specific to the Saint-Honoré aquifer (see **Table 3**) but also for which the simulated groundwater level series follow the same dynamics and present an acceptable accuracy compared to the observations. The other two piezometers are used for testing. These are the piezometers Pz-18 and Pz-21 (see **Figure 9**).

Initially, the calibration of the numerical model was performed automatically using the optimization algorithms integrated into the MARTHE software and the ranges of values in **Table 3**. However, the values of the calibrated hydrodynamic parameters and their spatial distribution were not in agreement with the hydrogeology of the terrain. This is why we then opted for a manual calibration. The simulated groundwater levels following this manual calibration are very close to those of the automatic calibration but provide a better agreement with the hydrogeology of the terrain. Furthermore, the values of the manual calibration parameters and their spatial distribution support those of previous numerical modeling studies performed in the study area (e.g., Tremblay 2005). In addition, the pumping tests, a field experiment whose purpose is to evaluate the physical properties of the medium with a certain level of uncertainty, support the results of the manual calibration. Field data remain a reference even if they are measured in a punctual way and with a certain level of uncertainty.

### 3.4.2 MACHINE LEARNING MODELS

#### 3.4.2.1 MULTILAYER PERCEPTRON

The multilayer perceptron (MLP) is an algorithmic structure belonging to the family of feedforward artificial neural networks, considered as universal approximators of any continuous function (Cybenko 1989; Hornik 1991). An MLP is composed of an input layer, an output layer and one or more hidden layers. The number of hidden layers defines the depth of the network. Beyond one hidden layer, the network can be qualified as “deep”. Each layer is made of a given number of neurons. Neurons in two given contiguous layers of the MLP are fully interconnected. and each of the connections is represented by the parameter  $\theta = (W, b)$ , where  $W$  and  $b$  are the weight and bias parameters, respectively. Data from a given layer is aggregated using weights and biases before being transformed by a nonlinear activation function, and then passed on to the next layer. One by one, the input data undergoes transformations through the hidden layers until it reaches the output layer. To ensure that each input variable is given equal weight, they are normalized between -1 and 1. This reduces the effect of the differences in magnitude between the range of different input variables on the model approximation. Using a back-propagation algorithm, data transmitted from the input layer to the output layer is analyzed to iteratively adjust the network parameters until the outputs minimize a predefined cost function.

The process of transmitting data from the input layer to the output layer, followed by backpropagation, is repeated on small batches of data over a number of iterations, called epochs or until certain values of the selected stopping criteria are met. It is important to note that an epoch is composed of a certain number of sub-iterations, defined in particular by the number of batches of data to be used per sub-iteration.

The mean square error between the observed outputs and the outputs simulated by the MLP model is often used as a cost function ( $L_{obs}(\theta)$ ) to constrain its learning. The update of the neural network parameters by the backpropagation algorithm is done according to Equation (3.1).

$$\theta_i = \theta_{i-1} - \lambda \cdot \nabla L_{obs}(\theta) \quad (3.1)$$

where  $\theta_{i-1}$  and  $\theta_i$  represent respectively the previous and the updated value of  $\theta$ ;  $\lambda$  is a hyperparameter of the network to be defined and is called the learning rate;  $\nabla L_{obs}(\theta)$  is the gradient of the cost function  $L_{obs}$  with respect to  $\theta$ . In contrast to the numerical model, the spatial and temporal simulation of groundwater dynamics with the MLP is two-dimensional. **Figure 11a** illustrates the MLP architecture and summarizes the learning process.

### 3.4.2.2 THEORY-GUIDED MULTILAYER PERCEPTRON

The TgMLP is a MLP whose learning is constrained not only by the observed data but also by the theory governing the phenomenon under study. In this study, the equation governing the groundwater flow as well as the boundary and initial conditions are used as additional constraints to the  $L_{obs}$  cost function (MSE) used for the traditional MLP. As with the MLP, the spatiotemporal simulation of groundwater dynamics with TgMLP is two-dimensional and only the flow in the saturated zone is considered. The general partial differential equation (PDE) describing such a system is given by Equation (3.2).

$$S_{aq} \frac{\partial \varphi}{\partial t} = \frac{\partial}{\partial x} \left( T_x \frac{\partial \varphi}{\partial x} \right) + \frac{\partial}{\partial y} \left( T_y \frac{\partial \varphi}{\partial y} \right) + Q, \quad (x, y) \in \Omega, \quad t > 0 \quad (3.2)$$

where  $T_x$  and  $T_y$ , are the transmissivity values ( $m^2/d$ ) along the  $x$  and  $y$  coordinate axes ( $m$ );  $\varphi$  is the groundwater level ( $m$ );  $Q$  represents the water source and/or sink term ( $m/d$ ) with  $Q < 0$  for

flow out of the groundwater system, and  $Q > 0$  for flow into the system;  $S_{aq}$  denotes the storage coefficient (–);  $t$  is time ( $d$ );  $\Omega$  denotes the internal aquifer domain.

Transmissivity is given by the product of hydraulic conductivity and saturated water thickness. For an unconfined aquifer, the saturated water thickness can be defined as the difference between the GWL and the aquifer bottom elevation. Thus, Equation (3.2) is rewritten as Equation (3.3).

$$S_{aq} \frac{\partial \varphi}{\partial t} = \frac{\partial}{\partial x} \left( K_x (\varphi - z_b) \frac{\partial \varphi}{\partial x} \right) + \frac{\partial}{\partial y} \left( K_y (\varphi - z_b) \frac{\partial \varphi}{\partial y} \right) + Q, \quad (x, y) \in \Omega, \quad (3.3)$$

$$t > 0$$

where  $K_x$  and  $K_y$  are the hydraulic conductivity ( $m/d$ ) along the  $x$  and  $y$  coordinate axes;  $Z_b$  represents the aquifer bottom elevation ( $m$ ). Because the TgMLP model is a 2D model, we chose stratigraphic unit 3 as representative of the current knowledge available about the aquifer. As mentioned in **Section 3.3.1**, the stratigraphic units are considered as a succession of homogeneous and isotropic hydrogeological layers. Therefore, the hydraulic conductivities are independent of the  $(x, y)$  coordinates for a given hydrogeological layer. In addition, according to the conceptual model summarized in **Figure 10**, the aquifer is composed of Cauchy boundaries represented by the rivers, a Dirichlet boundary represented by Doctor Lake, imposed flow boundaries represented by recharge and pumping, and finally a zero-flow boundary represented by the edges of the aquifer other than the Caribou River. Thus, the final PDE that represents the aquifer according to the conceptual model defined earlier is given by Equations (3.4) to (3.7).

$$S_{aq} \frac{\partial \varphi}{\partial t} = K \left( \frac{\partial}{\partial x} \left( (\varphi - z_b) \frac{\partial \varphi}{\partial x} \right) + \frac{\partial}{\partial y} \left( (\varphi - z_b) \frac{\partial \varphi}{\partial y} \right) \right) + R + \delta_w \frac{Q_w}{\Delta x^2} \quad (3.4)$$

$$+ \delta_s q_s, \quad (x, y) \in \Omega, \quad t > 0$$

$$\varphi(t, x, y) = \varphi_{ini}(t, x, y), \quad (x, y) \in \Omega \cup \partial\Omega_D \cup \partial\Omega_N, \quad t = 0 \quad (3.5)$$

$$\varphi(t, x, y) = \varphi_{dir}(t, x, y), \quad (x, y) \in \partial\Omega_D, \quad t \geq 0 \quad (3.6)$$

$$\frac{\partial \varphi}{\partial n}(t, x, y) = 0, \quad (x, y) \in \partial\Omega_N, \quad t > 0 \quad (3.7)$$

where  $\varphi_{ini}$  and  $\varphi_{dir}$  are, respectively, the GWLs at the initial time and the GWLs imposed as the Dirichlet condition;  $q_S$  is the exchange flux between the sections of rivers and the aquifer ;  $\Omega$ ,  $\partial\Omega_D$  and  $\partial\Omega_N$  denote the internal aquifer domain, Dirichlet and Neuman boundary condition domains of the study area;  $n$  is the direction normal to the Neumann boundary domain;  $\Delta x$  is the distance between two points in the  $x$  or  $y$  direction.  $\delta_w$  and  $\delta_s$  are equal to 1 if the point where the equation is applied is, respectively, a well or a section of river. Otherwise,  $\delta_w$  and  $\delta_s$  are equal to 0.

The training is performed by forcing the TgMLP model not only to fit the GWLs observations but also to approximate the solution of the PDE defined by Equation (3.8). To achieve this, the training consists in minimizing the difference between the observed and simulated GWLs as well as the residuals of equations (3.4) to (3.7). Thus, the total cost function to be minimized is given by Equation (3.8).

$$L_{TOT} = L_{obs} + L_{ini} + L_{dir} + L_{neu} + L_{pde} \quad (3.8)$$

where  $L_{pde}$ ,  $L_{ini}$ ,  $L_{dir}$  and  $L_{neu}$  are the cost functions related to the residual of the Equations (3.4) to (3.7) respectively.

To evaluate the derivatives in Equations (3.4 to (3.7, one can use the automatic differentiation (AD) method (Wang et al. 2020b) or traditional methods such as the finite difference method (FDM) (e.g., Tartakovsky et al. 2020; Wang et al. 2021b). The FDM was considered in this study because of the advantage of computational cost and the weak nonlinearity of Equation (3.4 which reduces the

approximation error. FDM is 1.411 to 1.562 times faster than AD. Using a GPU for computational acceleration, this difference appears to be minor, as it corresponds to a gain of 31 to 42 minutes in this study. On the other hand, without the use of a GPU, the time difference would increase, corresponding to more than 3.1 to 4.2 hours. In addition, the applicability of the TgMLP model in a real-world setting, discussed here, includes the issue of computational time. This is also one of the reasons why the least time-consuming derivation method (FDM) was presented in this study. In problems with very strong nonlinearity or involving PDE of an order greater than or equal to 3, it would be more advantageous to use automatic differentiation, which provides an exact derivative. Consider the TgMLP model represented by Equation (3.9).

$$\varphi_{sim} = \text{TgMLP}(t, x, y, \theta) \quad (3.9)$$

Each term of the total cost function, obtained by the FDM with the introduction of dummy points at the boundaries of the study domain for the Neumann condition, is defined in Equations (3.10) to (3.14).

$$L_{dir} = \frac{1}{M_{dir} M_B} \sum_{i=1}^{M_{dir}} \sum_{j=1}^{M_B} (\varphi_{sim}^{ij} - \varphi_{ini}^{ij})^2 \quad (3.10)$$

$$L_{ini} = \frac{1}{M_{ini}} \sum_{i=1}^{M_{ini}} (\varphi_{sim}^{ij} - \varphi_{ini}^{ij})^2 \quad (3.11)$$

$$L_{neu} = \frac{1}{M_{neuX} M_B} \sum_{i=1}^{M_{neuX}} \sum_{j=1}^{M_B} \left( \frac{\varphi_{sim}^{E,ij} - \varphi_{sim}^{W,ij}}{2\Delta x} \right)^2 + \frac{1}{M_{neuY} M_B} \sum_{i=1}^{M_{neuY}} \sum_{j=1}^{M_B} \left( \frac{\varphi_{sim}^{N,ij} - \varphi_{sim}^{S,ij}}{2\Delta x} \right)^2 \quad (3.12)$$

$$L_{pde} = \frac{1}{M_{PDE} M_B} \sum_{i=1}^{M_{PDE}} \sum_{j=1}^{M_B} (f_{PDE}^{ij})^2 \quad (3.13)$$

with

$$f_{PDE} = \frac{S_{aq}^P}{\Delta t} (\varphi_{sim}^{t,P} - \varphi_{sim}^{t-\Delta t,P}) - \frac{K^P (\varphi_{sim}^{t,P} - z_b^P)}{\Delta x^2} (\varphi_{sim}^{t,E} + \varphi_{sim}^{t,W} - 4\varphi_{sim}^{t,P} + \varphi_{sim}^{t,N} + \varphi_{sim}^{t,S}) \\ - R^{t,P} - \delta_w \frac{Q_w^{t,P}}{\Delta x^2} - \delta_s \frac{K_s^P}{e_s} (\varphi_{ref}^{t,P} - \varphi_{sim}^{t,P}) \quad (3.14)$$

where  $\varphi_{sim}^{t,P}$ ,  $\varphi_{sim}^{t,E}$ ,  $\varphi_{sim}^{t,W}$ ,  $\varphi_{sim}^{t,N}$ ,  $\varphi_{sim}^{t,S}$  represents the GWL at location P and the GWL of its eastern (E), western (W), northern (N), southern (S) neighbors respectively, at time  $t$ ;  $\Delta x$  is the width of the square mesh;  $\Delta t$  is the length of a time step;  $S_{aq}^P$  and  $K^P$  are the storage coefficient and the hydraulic conductivity at P, respectively;  $Z_b^P$  is the aquifer bottom elevation at P;  $K_s^P$  is the hydraulic conductivity of the bed of the stream section and  $\varphi_{ref}^{t,P}$  is the elevation of the water level in the stream at P;  $Q_w^{t,P}$  is the pumping rate;  $R^{t,P}$  is the recharge rate;  $M_{dir}$ ,  $M_{ini}$ ,  $M_{neuX} + M_{neuY}$ ,  $M_{PDE}$  are respectively the number of locations sampled to evaluate the cost functions related to the Dirichlet condition  $L_{dir}$  (Doctor lake,  $\partial\Omega_D$ ), the initial condition  $L_{ini}$  (entire domain,  $\Omega \cup \partial\Omega_D \cup \partial\Omega_N$ ), the no-flow boundary condition  $L_{neu}$  (external boundaries of the study area except the Caribou River,  $\partial\Omega_N$ ) and the governing equation  $L_{pde}$  (internal domain,  $\Omega$ );  $M_B$  is the number of time steps (batch size) used for a given training epoch. **Figure 11b** illustrates the TgMLP architecture and summarizes the learning process. The methodology used for numerical model calibration, training and validation of machine learning models and their testing is summarized in **Figure 12**.

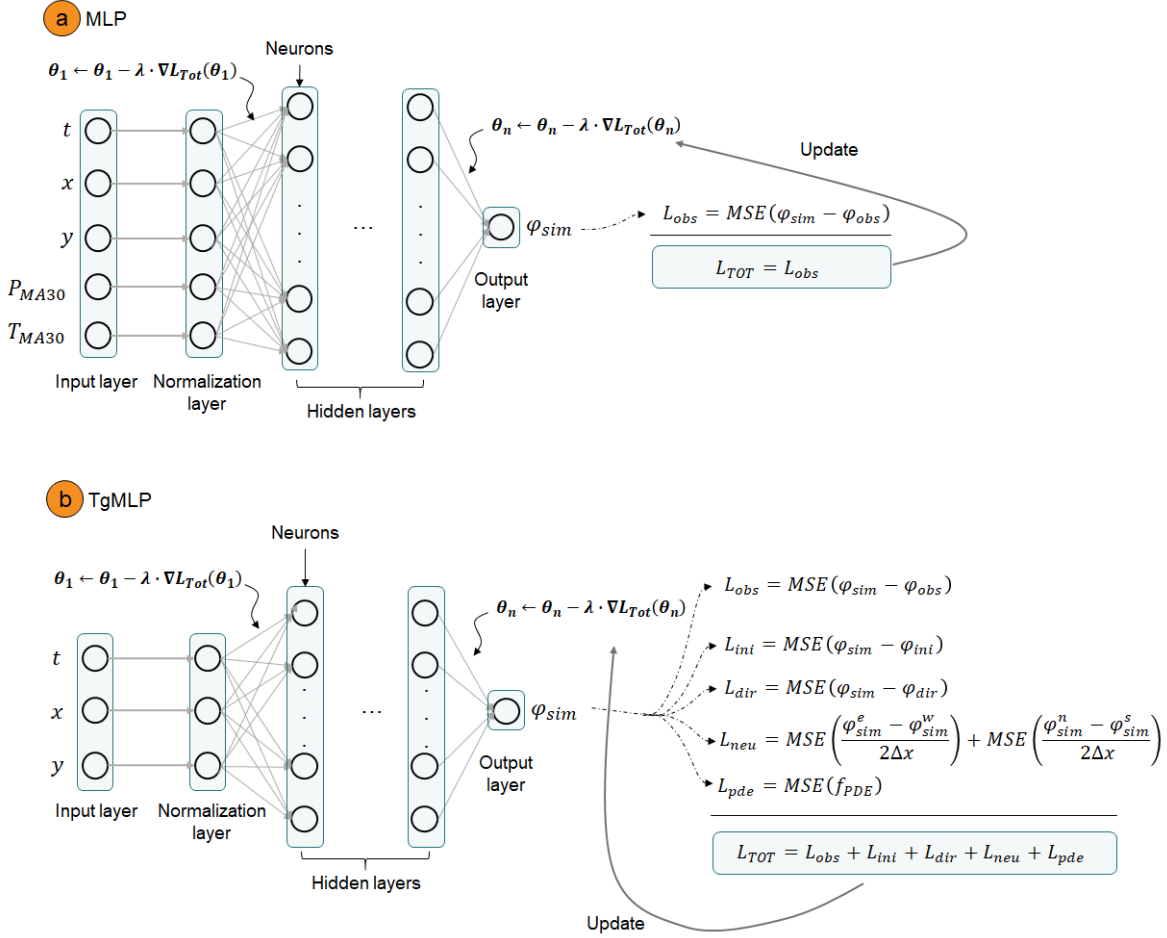


**Figure 11** The architecture of the (a) MLP and (b) TgMLP models and the corresponding learning process. The  $\theta$  parameters of the neural networks need to be optimized;  $\lambda$  is the learning rate and  $\nabla L_{TOT}(\theta)$  is the gradient of the cost function  $L_{TOT}$ .  $t$ ,  $x$ ,  $y$  represent time and spatial coordinates respectively;  $P_{MA30}$  and  $T_{MA30}$  are the 30-day moving average of precipitation and mean temperature respectively;  $\varphi_{sim}$  is the groundwater level simulated.

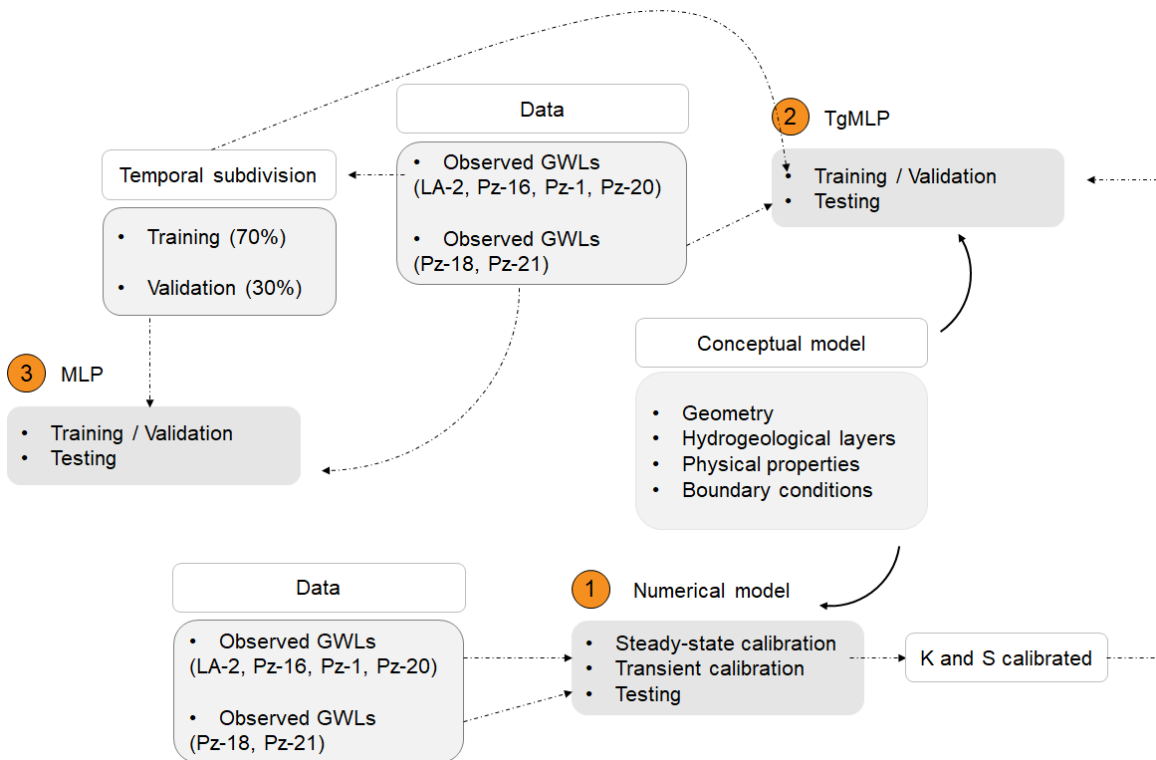


**Figure 12** Summary of the methodology used for numerical model calibration, training and validation of machine learning models and their testing.

### 3.4.2.3 CONDITION FOR STOPPING THE TRAINING

The training of ML models consists in adjusting their parameters in order to make the cost function tend towards a minimum value considered satisfactory to stop the training. In this study, to follow the evolution of the training, two metrics were used for the MLP and a third metric was added for the TgMLP. The first metric is the root mean square error between the observed and simulated GWLs (RMSE). The second is the interpolation capacity (IC) and the third is the mean residual of the PDE (MRP). The IC is defined by Equation (3.15).

$$IC = \frac{RMSE \text{ [validation data]}}{RMSE \text{ [training data]}} \quad (3.15)$$

The perfect model is the one with  $RMSE = 0$ ,  $IC = 1$  and  $MRP = 0$ . In this study, training is stopped when  $RMSE \leq a$ ,  $IC = 1 \pm b$ , and  $MRP \leq c$ . The fixed values of  $a$ ,  $b$ , and  $c$  are presented in **Section 3.4.2.4**.

#### 3.4.2.4 ARCHITECTURE DEVELOPMENT

The ML models were developed in Python with the TensorFlow library and run in the “*Google Colab Pro*” environment with computational acceleration using a Tesla P100-PCIE-16GB GPU. The number of neurons in the input and output layers is known and depends on the number of dimensions of the input and output data. In this study, time  $t$ , spatial coordinates  $x$  and  $y$ , the moving average of precipitation  $P_{MA30}$  and mean temperature  $T_{MA30}$  (30-day window) are the inputs of the MLP model, i.e., five neurons, whereas only  $t$ ,  $x$ , and  $y$  are the inputs of the TgMLP model, i.e., three neurons. Groundwater levels are the only output variable, i.e., one neuron for both models.

The choice of the variables  $t$ ,  $x$ ,  $y$  makes it possible to consider the spatial and temporal character of the problem studied for the MLP and TgMLP models. Moreover, these variables are useful to evaluate the physics-related cost functions (Equations (3.12) and (3.13)) during the training of TgMLP. Since recharge is incorporated directly into the total cost function, it was not considered useful to include it as an input variable for TgMLP. The reason for choosing the moving average of precipitation and that of the mean temperature as MLP input variables is that GWL dynamics in the Saint-Honoré aquifer are determined in part by precipitation and evapotranspiration. The latter is partly related to temperature. To facilitate the training of the MLP, it is advisable to choose variables that are independent but correlated with the output variable. After several tests, it was found that the

30-day moving average of precipitation and mean temperature showed the highest correlation with groundwater elevations in all piezometers in the study area. **Table 4** summarizes the cross-correlation results.

**Table 4** Cross-correlation coefficients between groundwater levels at the six piezometers of the study area and the 30-day moving averages of precipitation and mean temperature.

	LA-2	Pz-16	Pz-1	Pz-18	Pz-20	Pz-21
$P_{MA30}$	61.9%	85.8%	82.7%	82.9%	38.5%	46.4%
$T_{MA30}$	60.8%	86.3%	88.3%	86.7%	37.4%	48.6%

The hyperbolic tangent activation function was applied to the hidden layer neurons, while the linear function was applied to the output layer neurons. The number of hidden layers and the number of their neurons were determined by a trial and error procedure. The procedure starts with one hidden layer at the beginning and increases up to 10 hidden layers with a step of 1 at each trial. For a given trial, the number of neurons varies with steps of 5 starting from 10 neurons to a maximum of 50 neurons.

For each trial representing a given number of hidden layers and neurons, the MLP is trained to minimize the mean square error between observations and simulated values. This means that only points where piezometric observations exist were used for training/validation, i.e., in four piezometers chosen so that there is approximately one piezometer per hydrogeological layer. These piezometers are the same as those used for the calibration of the numerical model. The other two piezometers (of a total of six) were used for the test stage. For each of the training/validation piezometers, a temporal sampling was performed. In particular, the duration of the simulation, defined by the length of the GWL time series of the piezometers, was discretized and then randomly sampled at 70% for training.

The remaining 30% was used to evaluate the interpolation capacity IC of the model at each training epoch in the validation stage.

Training TgMLP consists in optimizing its parameters by minimizing the total cost function (Equation (3.8)). To evaluate the physics-related cost functions in Equation (3.8), spatial sampling of locations was performed in the different hydrogeologic layers of stratigraphic unit 3, using the spatial points generated by the numerical model discretization. Then, for each of the locations, the same time sampling as performed for the MLP was applied. The piezometers used for numerical model calibration or MLP model training/validation are the same as those used for TgMLP model training/validation. The same applies to the test piezometers. The values of the hydrodynamic parameters of the aquifer and the physical properties of the stream bed used in the TgMLP method are those obtained after the calibration step of the numerical model. Unlike for the numerical model, streams and wells are considered as source/sink terms and are directly incorporated into the governing equation (see Equation (3.4)). The initial groundwater levels used for TgMLP training/validation are those observed at the 6 piezometers at date zero (09/11/2016).

The Adam optimization algorithm was used to appropriately adjust the values of the weight and bias parameters for the MLP and TgMLP. The goal is to build machine learning models that are as parsimonious as possible while showing good interpolation ability. Thus, the stopping criterion for MLP learning is to achieve a IC equal to  $1 \pm 2\%$  and a RMSE in the training stage lower than 0.05 m. The MLP model that meets these two criteria with the lowest-density structure is selected as the final model. The stopping criterion for TgMLP training is not only to achieve a IC equal to  $1 \pm 2\%$  and an RMSE in the training stage lower than 0.05 m, but also, to present a residual of the PDE lower than 0.0125 m/d, a value justified by the desired degree of physical consistency for TgMLP models. This value corresponds to a physical inconsistency of approximately 0.05 m. The TgMLP model that meets all these criteria and presents the lowest-density structure is selected as the final model. The learning rate and batch size used are respectively  $5 \times 10^{-4}$  and 2 for both MLP and TgMLP.

### 3.4.3 PERFORMANCE ASSESSMENT METRICS

The performance of the different models was evaluated using the Nash-Sutcliffe Efficiency (NSE) and the percentage of normalized RMSE (hereafter called NRMSE). NRMSE is defined by Equation (3.16).

$$NRMSE = 100 \times \frac{RMSE}{\varphi_{obs}^{max} - \varphi_{obs}^{min}} \quad (3.16)$$

with  $\varphi_{obs}^{max}$  and  $\varphi_{obs}^{min}$  the minimum and maximum values of the time series of the observations (m).

NSE is used to evaluate the simulation ability of a model. A perfect model is one whose simulation ability is 1. The NRMSE quantifies the accuracy of a model with values ranging from 0 to infinity. A model with perfect accuracy will have a value of NRMSE equal to 0%, while values further increasing from 0% will indicate decreasing model accuracy.

## 3.5 RESULTS

The results of the calibration/training/validation are presented in **Section 3.5.1**. The results obtained with the test data set are presented in **Section 3.5.2**. NRMSE and NSE values were used to evaluate the performance of the models, both in the calibration/training-validation stage and the test stage. A comparison of the spatial distribution of the GWL field is performed between the different models to evaluate their ability to capture the groundwater flow dynamics in **Section 3.5.3**. Finally, the degree of PDE violation by the TgMLP model is examined in **Section 3.5.4**.

### 3.5.1 MODEL CALIBRATION / TRAINING - VALIDATION

The numerical model was calibrated using daily data from 09/11/2016 to 30/11/2017 drawn from the four piezometers mentioned in **Section 3.4.1** and, to a lesser extent, stream flow measured at specific timepoints over the period 2001-2004. The final numerical model was chosen so that the simulation would match the observed GWLs as closely as possible. The determination of the MLP and TgMLP architectures was performed as described in **Section 3.4.2.4**.

For the implementation of the MLP and TgMLP models, the observed GWLs of the four piezometers were randomly subdivided according to the temporal component into a training set and a validation set. The MLP model that best satisfies all stopping criteria is composed of 3 hidden layers of 25 neurons each (results not shown). As for the TgMLP model, it is composed of 7 hidden layers of 40 neurons (results not shown). **Figure 13** shows the convergence of cost functions for the two selected architectures during training as a function of epochs for the MLP and TgMLP models. **Figure 14** shows the comparison between observed GWLs and GWLs simulated by the different models in the four piezometers and **Figure 15** summarizes the results for the performance criteria in the calibration/training-validation stage.

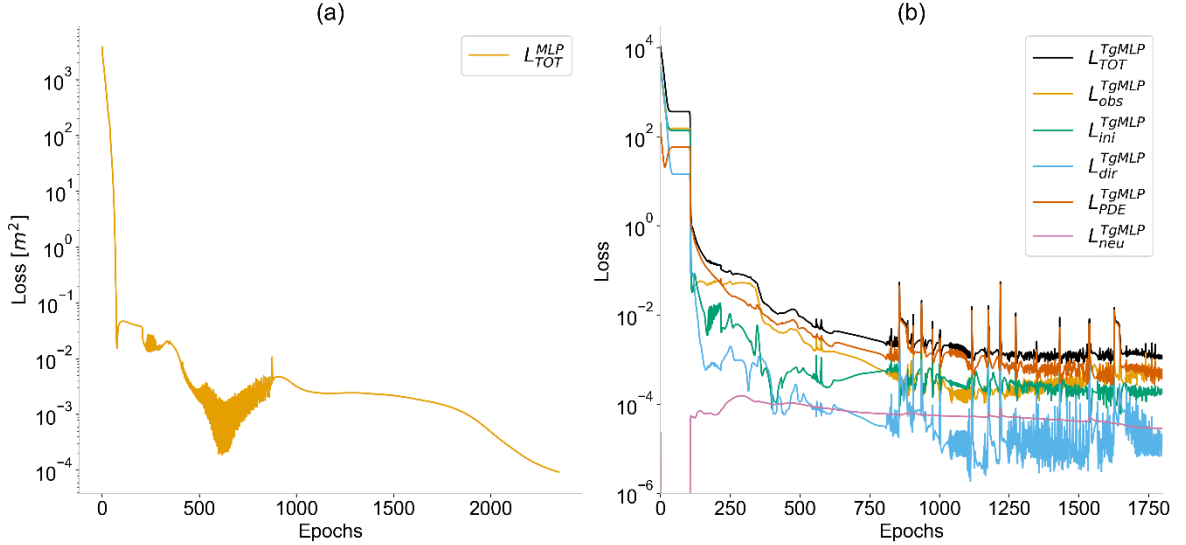


**Figure 13** (a) Convergence of total cost functions during learning as a function of epochs for the MLP model and (b) convergence of the components of the TgMLP total cost function.

For all piezometers, we observe that the NRMSE values (**Figure 15a**) decrease from the numerical model to the TgMLP model and the NSE values increase from the numerical model to the TgMLP model (**Figure 15b**). NRMSE values for TgMLP are less than 4%, for all piezometers, nearly 4 times less than the lowest NRMSE value from the numerical model. The NRMSE values for MLP range from just over 11% to nearly 2%. As for the NSE value, it is very close to 1 for the TgMLP model. The NSE is greater than 0.7 for all piezometers for the MLP model, while its value is very mixed for the numerical model. All this means that the accuracy and simulation ability of the TgMLP model are higher than those of the MLP model, which in turn are higher than those of the numerical model.

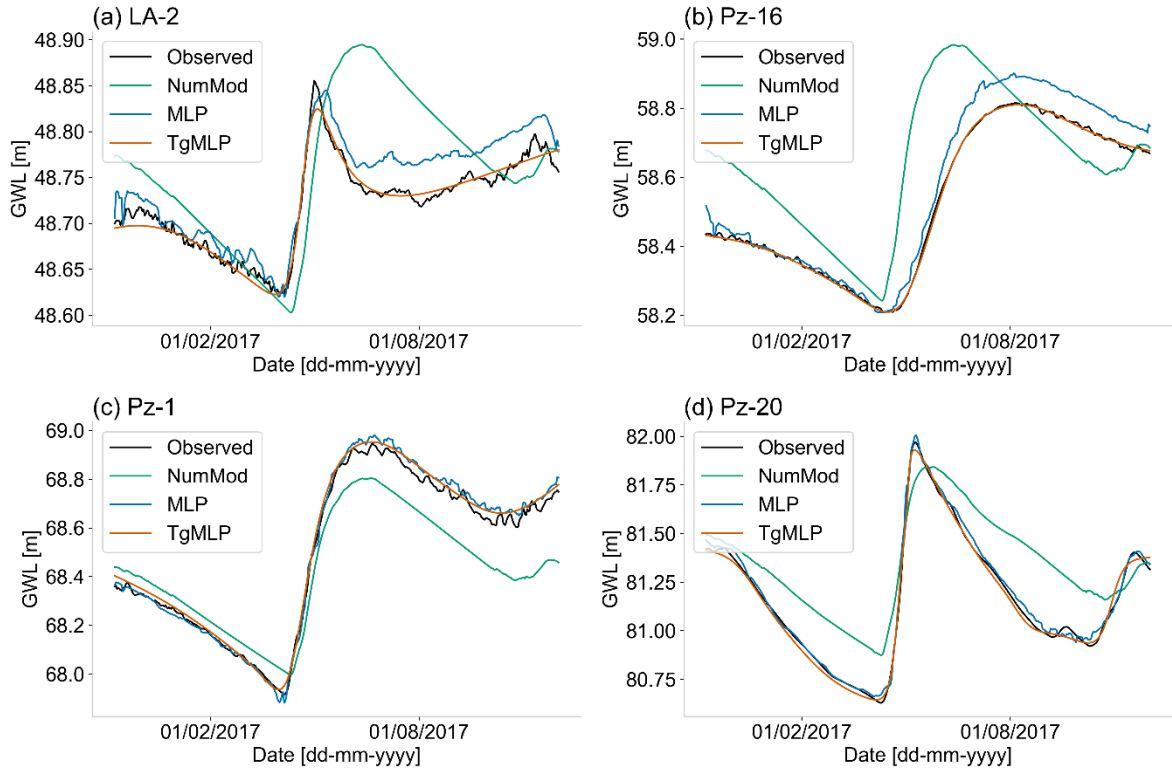


**Figure 14** Comparison of observed groundwater levels in the four calibration/training piezometers ((a) LA-2, (b) Pz-16, (c) Pz-1 and (d) Pz-20) against groundwater levels simulated by the different models.

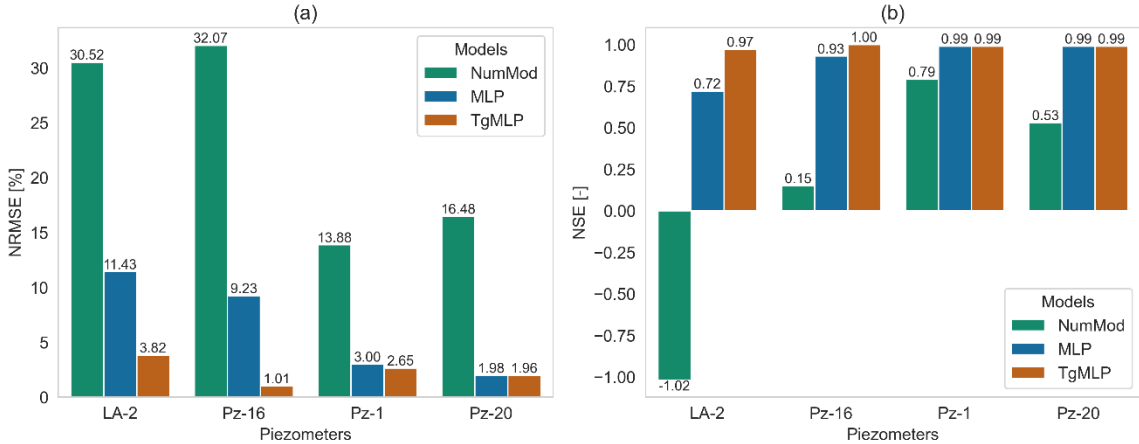


**Figure 15** Comparison of performance criteria ((a) percentage of normalized RMSE (b) Nash-Sutcliffe Efficiency) during the calibration/training stage.

Referring to the LA-2 and Pz-16 piezometers, it can be observed that the NRMSE values of the numerical model are all above 30% and the NSE values are close to 0 or negative. All this clearly

indicates that the numerical model has a low accuracy and its simulation ability is at most equal to the average groundwater level observed in these piezometers. The poor simulation ability of the numerical model for LA-2 and Pz-16 can also be explained visually by the time lag seen between the observed and simulated series (**Figure 14**). The time lag of the simulated series compared to those observed at the LA-2 and Pz-16 piezometers may be due to several factors. The first factor is the diffusivity of the aquifer in the vicinity of the two piezometers. An increase in diffusivity in the vicinity of LA-2 and a decrease in diffusivity in the vicinity of Pz-16 could improve the fit of the simulations to observations. This would probably require a review of the initial conceptual model by introducing heterogeneity around the two piezometers. The second factor is related to the thickness of the pseudo vadose zone which, if reduced around LA-2 and increased around Pz-16, could also improve the fit. The third factor may correspond to phenomena not considered in the conceptual model that would influence GWLs around the piezometers such as private wells and various small lakes around LA-2 (**Figure 9**). As mentioned above, the investigation of all these factors requires proposing an alternative conceptual model based on the acquisition of new data; these are currently not available but may be interesting for future studies.

At Pz-1 and Pz-20, the NSE values (**Figure 15b**) greater than 0.5 show that the numerical model demonstrates a certain simulation ability for both piezometers. However, the simulation ability of the numerical model remains low compared to those of the MLP and TgMLP models for which the NSE value tends to approach 1.

In summary, for the calibration/training-validation stage, it can be concluded that the TgMLP model is much more accurate than the MLP model, and that both are much more accurate than the numerical model. The simulation ability of the TgMLP model and the MLP model are very high, with the TgMLP being superior. In addition, the simulation ability of the TgMLP and MLP models is far superior to that of the numerical model, which has an average simulation ability.

### 3.5.2 MODEL TESTING

Testing of the different models was performed using the GWLs time series at the two remaining piezometers, i.e., Pz-18 and Pz-21. **Figure 16** shows the comparison between the GWLs at test stage. **Figure 17** summarizes the performance criteria values of the different models.

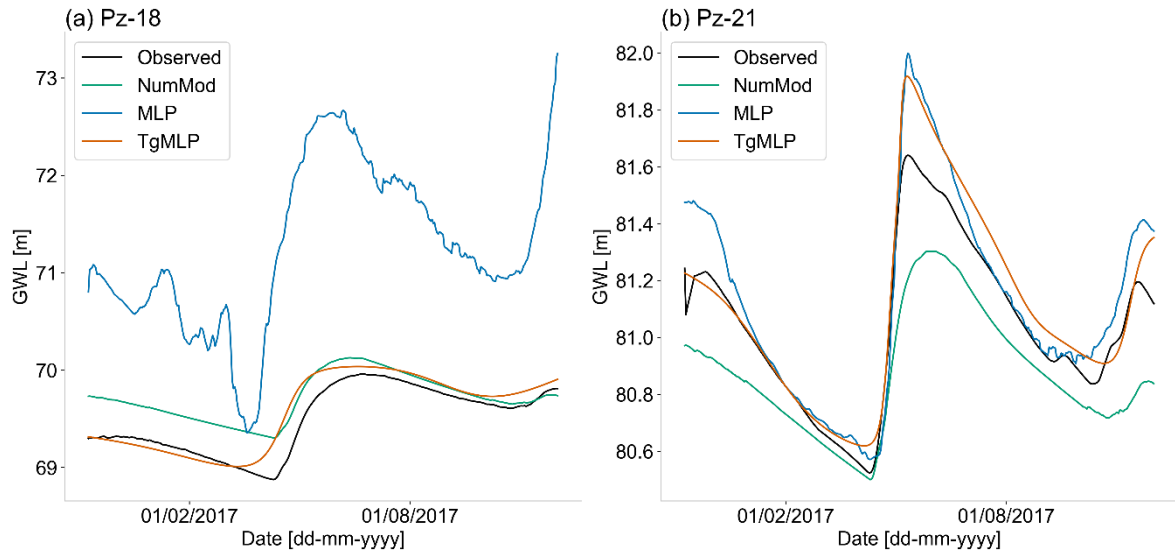


**Figure 16** Comparison of observed and simulated groundwater levels in the two test piezometers ((a) Pz-18 and (b) Pz-21) by the different models.

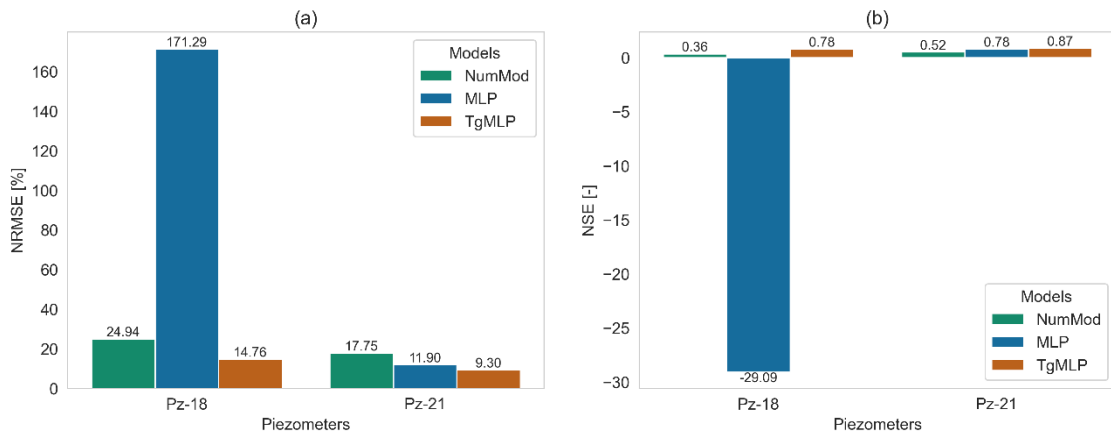


**Figure 17** Comparison of performance criteria ((a) percentage of normalized RMSE (b) Nash-Sutcliffe Efficiency) during the test stage.

At Piezometer Pz-18, the value of NRMSE (**Figure 16a**) of the MLP model, which exceeds 100% and reaches almost 7 times that of the numerical model and more than 11 times that of the TgMLP model expresses the fact that the accuracy of the numerical and TgMLP models is much better than that of the MLP. The NSE value (**Figure 16b**), which is well below 0, shows that the MLP has a low simulation ability compared to both the numerical and TgMLP models, for which the NSE value is greater than 0.3. The NSE of the TgMLP is twice as high as that of the numerical model, showing that its simulation ability is much higher than that of the numerical model. Although the NSE value of the numerical model is low, it expresses an acceptable simulation ability.

At Piezometer Pz-21, all models have good accuracy and simulation ability, with the TgMLP model being superior to the MLP model, which is also superior to the numerical model in terms of NRMSE (**Figure 16a**) and NSE (**Figure 16b**) values. However, the better accuracy and simulation ability of the MLP model compared to the numerical model is not surprising since the Pz-21 (test) and Pz-20 (training) piezometers are close of each other with a very similar piezometric signature and it is certainly the spatial interpolation ability of the MLP that has been brought into play in this case.

In summary, the performance of the TgMLP model in the test stage, which also expresses its extrapolation ability, exceeds that of the numerical model. Similarly, the performance of the numerical model is superior to that of the MLP.

### 3.5.3 CAPTURE OF GROUNDWATER DYNAMICS BY THE MODELS

The numerical model is purely physics-based and has acceptable simulation ability. It is designed to capture the groundwater flow dynamics within the accuracy limit of the conceptual model. Thus, the examination of the ability of ML models to capture groundwater flow dynamics is evaluated with respect to the numerical model. **Figure 18** and **Figure 19** show the results for two different dates as illustration while **Figure 20** provides more detail on the differences between the ML models, with respect to the numerical model, in capturing groundwater dynamics.

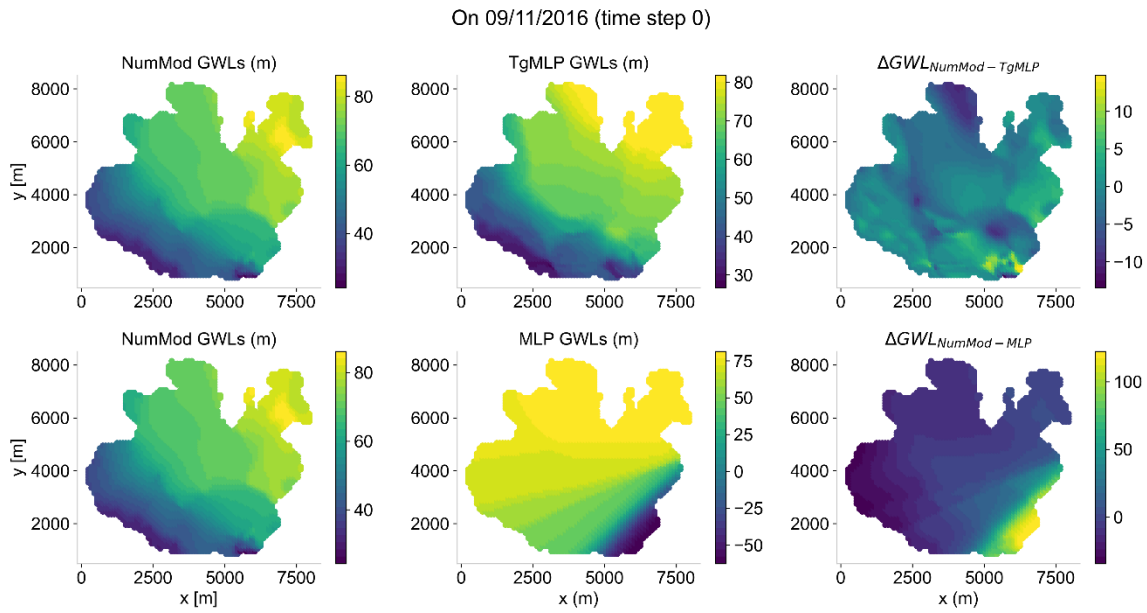


**Figure 18** Comparison of groundwater level fields over the entire study area between the numerical model (NumMod) and the TgMLP model and between the NumMod and the MLP model on 09/11/2016.

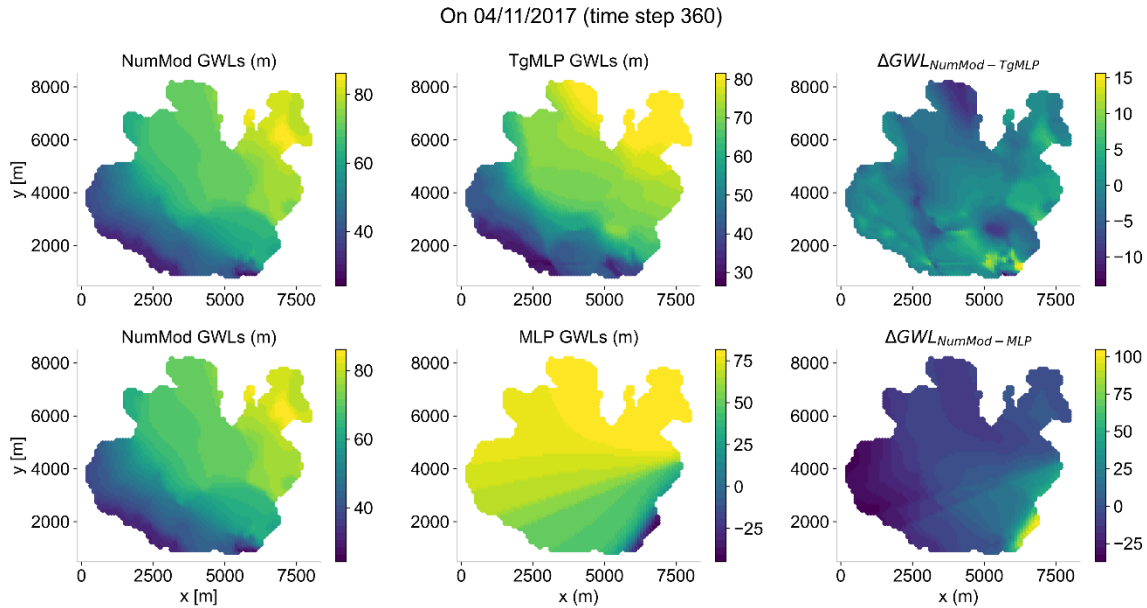


**Figure 19** Comparison of groundwater level fields over the entire study area between the numerical model (NumMod) and the TgMLP model and between the NumMod and the MLP model on 04/11/2017.

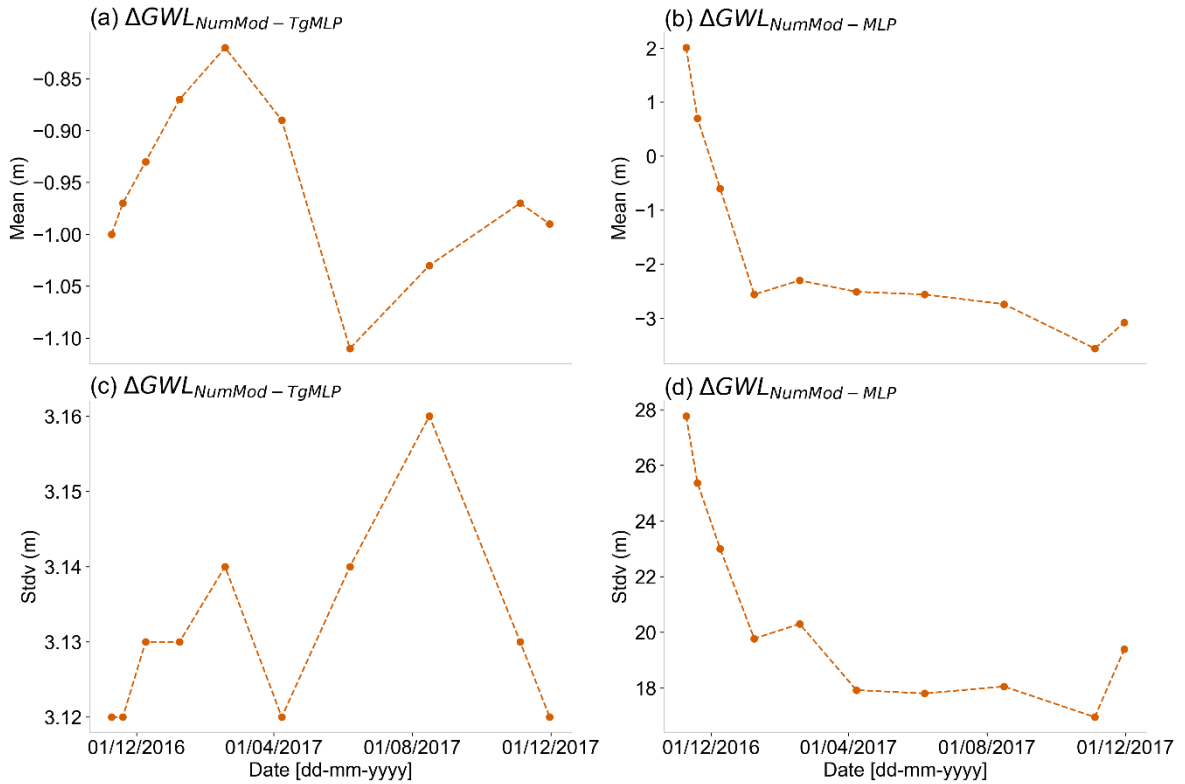


**Figure 20** Temporal evolution of the mean and standard deviation calculated on the differences of GWL simulated over the entire aquifer between the numerical model (NumMod) and the TgMLP model (a and c respectively) and between the NumMod and the MLP model (b and d respectively).

It can be seen both visually and statistically that the TgMLP model is the closest to the numerical model. Moreover, from one date to another, the statistics of the differences remain constant for the TgMLP model in contrast to the MLP model. On average, the difference between the numerical and TgMLP simulations is -1 m with a standard deviation of 3.14 m. In addition, the dominant flow direction of the GWL field simulated by the TgMLP model is toward the southwest and agrees with the conceptual aquifer model, since the southwestward flow is dominant (Tremblay 2005). In contrast, the flow direction proposed by the MLP model is toward the southeast, which is the opposite direction to that proposed by the conceptual model. **Figure 21** shows the GWL field simulated by the TgMLP model over a great number of time points, to illustrate the spatial consistency of this field with the conceptual model.

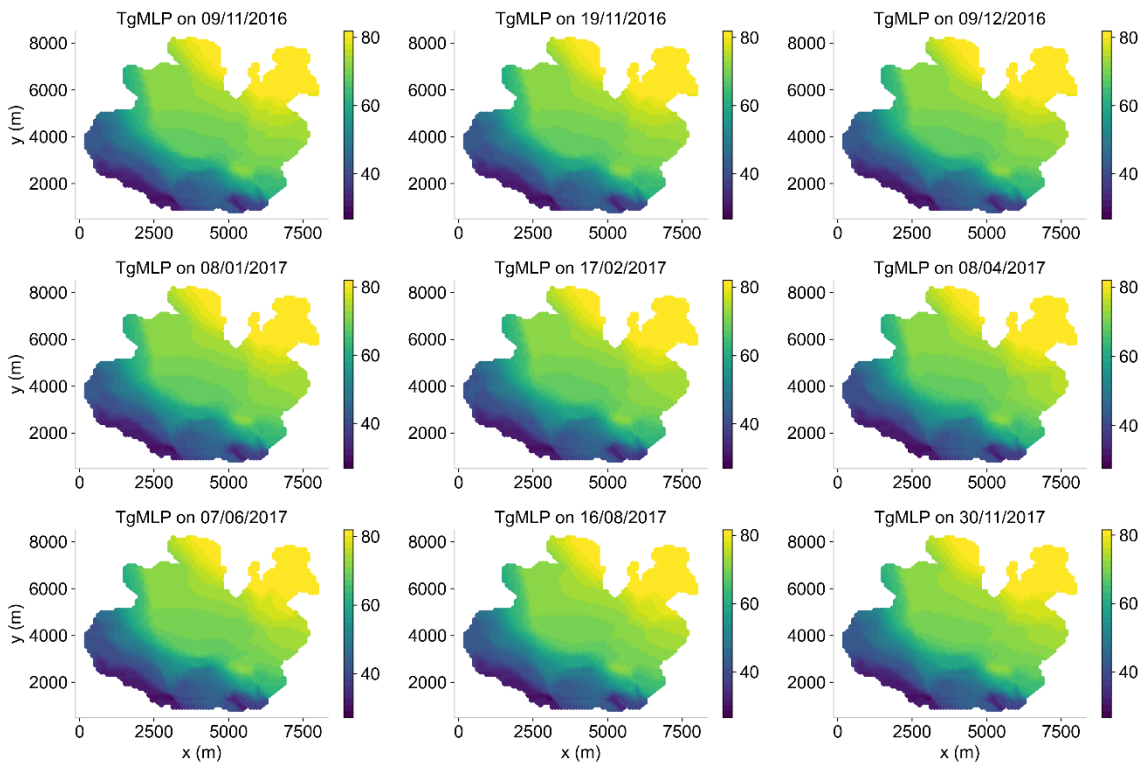


**Figure 21** Illustration of the spatial consistency of the GWL fields simulated by the TgMLP model with the conceptual model over time.

These results mean that only the numerical model and the TgMLP model are capable of capturing the spatial and temporal dynamics of groundwater levels. Also, these results mean that the numerical model and the TgMLP model represent two "parallel" versions of the modeled aquifer system.

### 3.5.4 EFFECTS OF PDE VIOLATION BY THE TGMLP MODEL

A TgMLP model that perfectly approximates the PDE is a model that provides a zero-physical inconsistency. In reality, it is not possible to reach the zero limit. For this reason, we set a physical inconsistency limit of 0.0125 m/d. This means that the TgMLP violates the PDE on a number of

locations. To assess the degree of PDE violation by TgMLP, we plotted the distribution of the PDE residual given the GWLs simulated by TgMLP at different dates, and we displayed the proportion of points where the PDE residual is below the threshold of 0.0125 m/day (**Figure 22**).

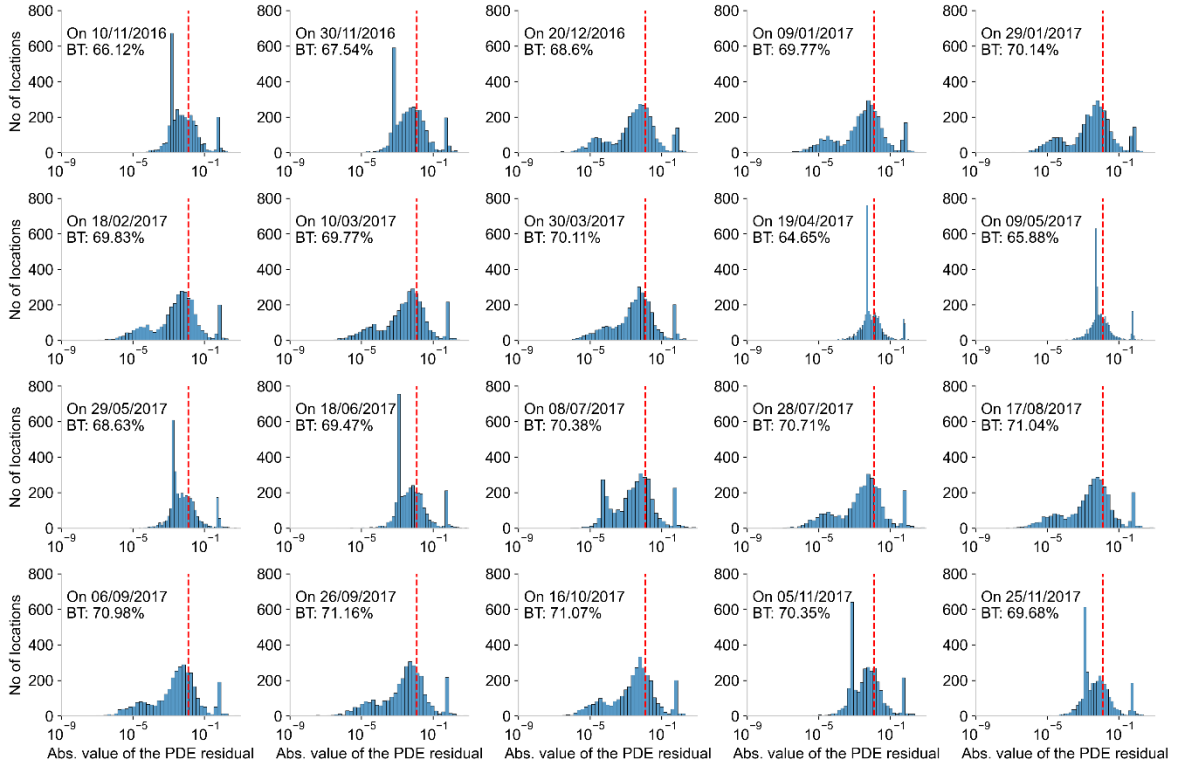


**Figure 22** Distribution of the PDE residual given the GWL simulated by TgMLP at different dates. The red dotted line represents the physical inconsistency threshold set during TgMLP training. And at the top left of each figure is displayed the proportion of points where the residual is below the threshold (BT).

**Figure 22** shows that the TgMLP model correctly approximates the solution to the PDE, depending on the threshold set, at a rate of about 70% from one date to another. The TgMLP model fails to correctly approximate the PDE nearly 30% of the time. **Figure 23** shows the set of unobserved locations where the effects of PDE violation were examined for illustration and **Figure 24** shows the GWLs simulated and the absolute mean value of the PDE residual at these locations.

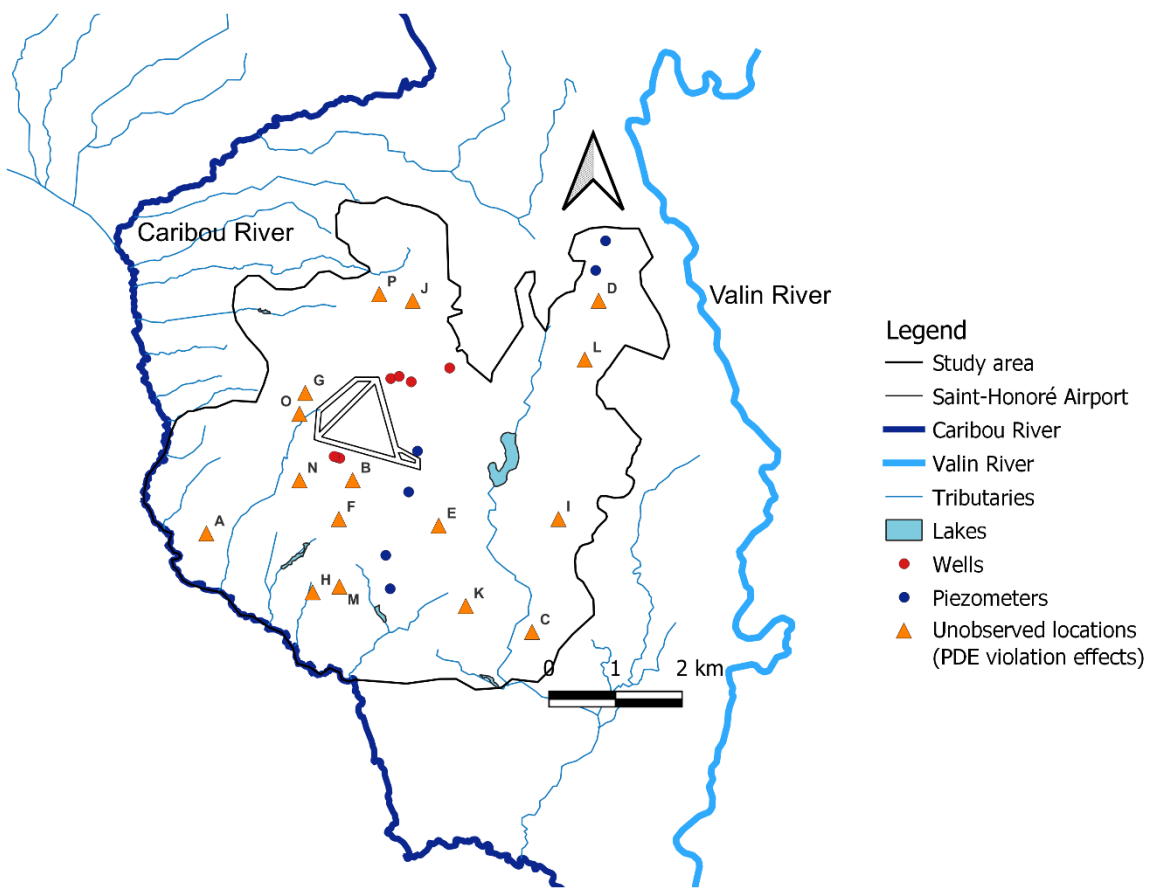


**Figure 23** The unobserved locations where the effects of PDE violation was examined

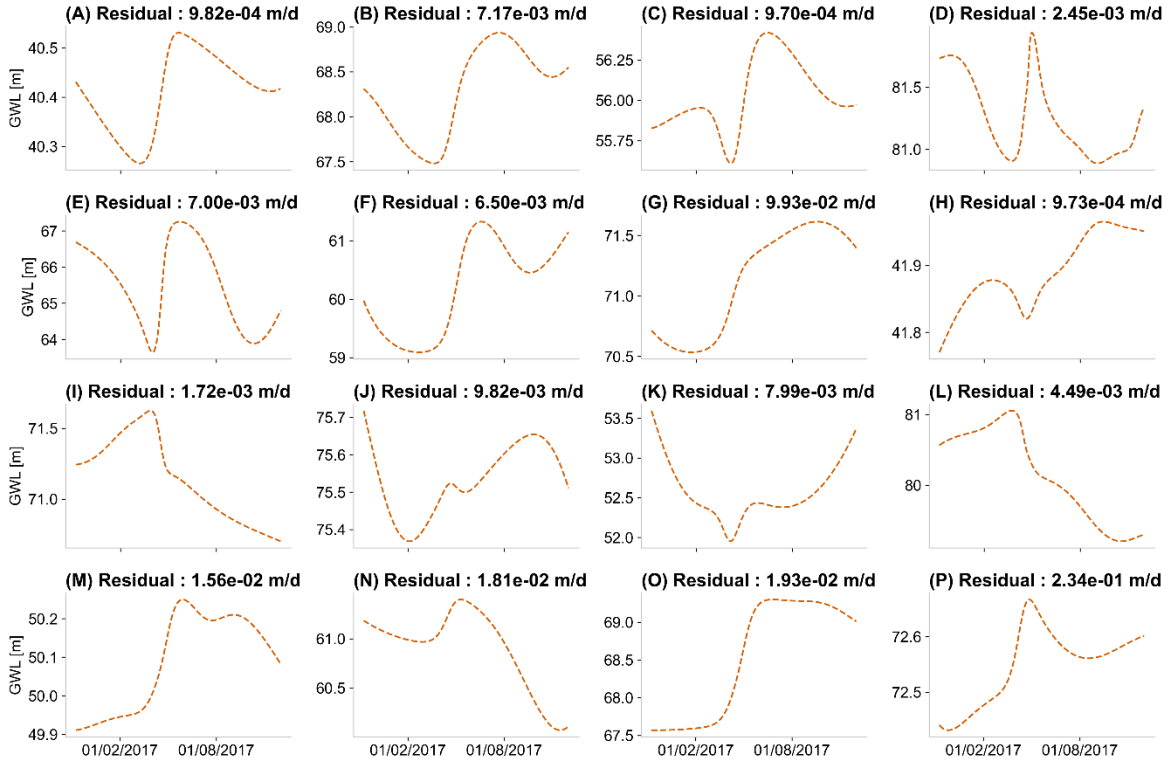


**Figure 24** Illustration of GWLs at unobserved locations for different values of the absolute mean of the PDE residual. The threshold below which the PDE residual was considered acceptable to stop the training is 0.0125 m/d.

At locations A through F, the PDE residual is below threshold and the same piezometric signatures as the observation piezometers are obtained. For locations H to L where the PDE residual is below the threshold or for location G and locations M to P where the PDE residual is above the threshold, the piezometer signatures do not match the observed piezometers. In **Section 3.5.3**, it was shown that from date to date, the TgMLP model produced GWL fields that were spatially consistent with the conceptual model. The fact that there are locations where the PDE is not violated, but which have particular piezometric signatures, could mean that these signatures are the result of a strong influence of the source/sink terms or Neumann conditions near which they are located. Similarly, at locations where the PDE is violated, the shape of the piezometric signatures may be explained by a poor model constraint on the source/sink terms and Neumann conditions, thus propagating the effect of the PDE violation to other locations in the aquifer. This remains a hypothesis

to be explored and it would be interesting to test this hypothesis in a future investigation. For such a study, it would probably be more interesting to separate each source/sink term into its own equation to better constrain the TgMLP model. The particular piezometric signature found could also be due to the fact that the boundary conditions of the conceptual model are incomplete, forcing the model to display an undesired behavior. It would probably be worthwhile for future investigations to consider the identification of the boundary conditions and the identification of the sink terms for the rivers as part of the inverse problem. Indeed, despite the level of confidence that one may develop concerning a conceptual model, such a model will always remain an approximation of reality and will maintain a certain degree of uncertainty that must be taken into account in the modeling process.

### **3.6 DISCUSSION**

The study conducted in this paper aimed to test the hypothesis that theory-guided machine learning can be effectively applied to model groundwater dynamics in a real aquifer. The methodology used was to conceptualize and build a theory-guided multilayer perceptron (TgMLP) model suitable for real porous aquifers; use it to simulate groundwater dynamics; and compare it to observations, a numerical model (NumMod) and a multilayer perceptron model (MLP), with emphasis on applicability to practical hydrogeology.

The analysis of the results shows that the performance of the TgMLP model outperforms the MLP model, which in turn outperforms the numerical model in the calibration/training stage. However, in the test stage, the MLP model is unable to extrapolate based on data that it has never encountered before, unlike the numerical and TgMLP models. Therefore, the reliability of the numerical and TgMLP models is higher than that of the MLP model. Also, in the test stage, the performance of the TgMLP is superior to that of the numerical model. In addition, the lack of physical constraints in the MLP training resulted in the systematic inability of the MLP to capture groundwater flow dynamics, unlike the numerical and TgMLP models. The superior performance of the TgMLP model over the numerical

model at observation points is probably due to the fact that the TgMLP model was built to learn the physics of groundwater flow in the aquifer and to provide optimal fidelity to observations. Constraining learning from physics and data probably allows the TgMLP model to benefit from the advantages of both numerical models and traditional multilayer perceptron models, which justifies its high performance at these observation points. These results confirm the basic hypothesis of this study. However, it was found that the TgMLP model approximates the PDE solution with only 70% of success. The poor approximation in 30% of the locations could be due to an effect of PDE violation at the sources/sinks or in the vicinity of the Neumann conditions. Thus, an improvement in the approximation of the PDE solution could be achieved by separating the PDE cost function into sub-cost functions corresponding to the different source/sink terms or by considering the source/sink terms and boundary conditions as part of the inverse problem. This is a hypothesis that remains to be explored.

It is also interesting to note that, because during training the main unknown parameters that determine the accuracy of the model and its physical consistency are the weight-bias  $\theta$ -parameter of the neural network, the TgMLP paradigm opens up a new way to give physical meaning to  $\theta$  and thus reduce the black-box nature that is usually attributed to artificial neural networks. The study of the physical meaning of the  $\theta$ -parameters is beyond the scope of this study, but it would be interesting for future works to address this issue, especially in the context of the new branch of artificial intelligence called eXplainable Artificial Intelligence (XAI). XAI aims to design and implement methods to understand what is going on in the black box (Adombi et al. 2021).

The use of physics to constrain learning may in certain ways, limits some of the traditional advantages of machine learning algorithms such as MLP. One of the main characteristics of the MLP is its ability to model any nonlinear relationship between inputs and outputs, but this can come at the cost of creating a black box model. Machine learning lends itself well to large-scale and hydrogeological applications where spatial data remain scarce and expensive and can be replaced

by easy-to-access data such as satellite data. Thus, using physics to constrain learning is to reconsider machine learning problems as boundary problems. Therefore, TgMLP can only be applied to terrains for which at least partial information on boundary conditions exist (Karniadakis et al. 2021) and for which physical properties have been estimated, as in the process of setting up numerical models.

Another point concerns the computational costs required to implement TgMLP models. Indeed, the optimization process requires a very large number of iterations to converge towards an acceptable solution. In the present case, at least 1800 epochs of 135 iterations per epoch were required, i.e. 243 000 iterations in total to reach a result satisfying the stopping criteria. Without computation acceleration using a GPU that performed the computations at a speed of about one epoch per 2.5 seconds, or 75 minutes, the computations would have required about 450 minutes with an Intel(R) Core (TM) i7-10510U processor, 1.80 GHz 2.30 GHz, 16 GB RAM. Even though, unlike MLP, the number of possible solutions/models that TgMLP can produce is drastically reduced (four possible patterns in the present study), obtaining the one pattern for which the stopping criteria are all met may not be achieved on the first try. The 450 minutes that would have been required for the TgMLP training without GPU correspond to 10.2 times the time required for a simulation with the MARTHE numerical model over the entire study period. For the MLP model, the training took only 9.4 minutes. This corresponds to 2351 epochs of 135 iterations per epoch, or 317 385 iterations in total.

### 3.7 CONCLUSION

In this paper, a theory-guided multilayer perceptron model (TgMLP) was developed to test its effectiveness in simulating groundwater flow dynamics in a real-world setting. The performance of the TgMLP was compared against that of a numerical model (NumMod) and a traditional multilayer perceptron model (MLP). In addition, the ability of these three models to capture the spatiotemporal dynamics of groundwater was evaluated. The degree of PDE violation of the TgMLP model was also

assessed. Finally, the applicability of these three models in a real-world setting was discussed. The Saint-Honoré unconfined aquifer (Quebec, Canada) was used as an experimental laboratory for this study because of the extent of the knowledge and data acquired on this aquifer. Historical groundwater levels, recharge, precipitation, mean temperature and qualitatively streamflow data were used to calibrate/train/validate and test the models.

The results show that the TgMLP demonstrates the best performance and far outperforms the traditional numerical and MLP models, that the MLP model is a good interpolator but is unable to extrapolate, and that only the numerical and TgMLP models are reliable because they are the only ones able to capture the spatiotemporal dynamics of groundwater flow and represent the dominant flow direction in the aquifer. However, it was found that the TgMLP model successfully approximates the PDE solution only 70% of the time. The poor approximation in 30% of the locations could be due to an effect of PDE violation at the sources/sinks or at the Neumann conditions. Treating each source/sink term as an independent term of the total cost function should be explored to assess how much this improves the approximation of the PDE solution. It may also be interesting to consider the source/sink terms and boundary conditions as part of the inverse problem.

Beyond that, the TgML paradigm opens a new way to make physical sense of the parameters of artificial neural networks and thus reduce the black box nature that has usually been attributed to artificial neural network models. Also, the computational cost of TgMLP training is high, but can be reduced using GPU acceleration. The results of this study may be useful to practitioners and researchers in selecting a model for their hydrogeological investigations.

### **CRediT authorship contribution statement**

**AVDP Adombi:** Conceptualization, Methodology, Data curation, Software, Visualization, Validation, Writing- Original draft preparation, Investigation. **Romain Chesnaux:** Conceptualization, Supervision, Resources, Reviewing and Editing. **Marie-Amélie Boucher:** Conceptualization, Supervision, Reviewing and Editing.

### **Acknowledgements**

The authors would like to thank Niobec Mine and the municipality of Saint-Honoré for providing data on pumping rates for wells in the study area.

### **Funding sources**

The authors acknowledge the financial support of the Natural Sciences and Engineering Research Council (NSERC-federal funding) of Canada in the framework of the Individual Discovery Grant Program held by Prof. Romain Chesnaux. The financial support of Fondation de l'Université du Québec à Chicoutimi (FUQAC), Rio Tinto through its Excellence Scholarships program and Fonds de Recherche du Québec - Nature et Technologie (FRQNT-provincial funding) are also acknowledged.

### **Declaration of Competing Interest**

On behalf of all authors, the corresponding author states that there is no conflict of interest.

## REFERENCES

- Adombi, A.V.D.P., Chesnaux, R., and Boucher, M.-A. 2021. Review: Theory-guided machine learning applied to hydrogeology—state of the art, opportunities and future challenges. *Hydrogeology Journal*, **29**: 2671-2683. doi:<https://doi.org/10.1007/s10040-021-02403-2>.
- Banadkooki, F.B., Ehteram, M., Ahmed, A.N., Teo, F.Y., Fai, C.M., Afan, H.A., Sapitang, M., and El-Shafie, A. 2020. Enhancement of groundwater-level prediction using an integrated machine learning model optimized by whale algorithm. *Natural resources research*, **29**: 3233-3252. doi:<https://doi.org/10.1007/s11053-020-09634-2>.
- Barr, A., Feigenbaum, E.A., and Cohen, P.R. 1981. *The handbook of artificial intelligence*. William Kaufmann Inc., Los Altos, CA.
- Boumaiza, L. 2008. Caractérisation hydrogéologique des hydrofaciès dans le paléodelta de la rivière Valin au Saguenay [Hydrogeological characterization of hydrofacies in the Valin River Paleodelta in Saguenay]. Applied Sciences, Université du Québec à Chicoutimi.
- Boumaiza, L., Chesnaux, R., Walter, J., and Stumpp, C. 2020. Assessing groundwater recharge and transpiration in a humid northern region dominated by snowmelt using vadose-zone depth profiles. *Hydrogeology Journal*, **28**: 2315-2329.
- Boumaiza, L., Chesnaux, R., Walter, J., and Meghnefi, F. 2021. Assessing response times of an alluvial aquifer experiencing seasonally variable meteorological inputs. *Groundwater for Sustainable Development*, **14**: 100647. doi:<https://doi.org/10.1016/j.gsd.2021.100647>.
- Cai, H., Shi, H., Liu, S., and Babovic, V. 2021. Impacts of regional characteristics on improving the accuracy of groundwater level prediction using machine learning: The case of central eastern continental United States. *Journal of Hydrology: Regional Studies*, **37**: 100930.
- Cybenko, G.V. 1989. Approximation by superpositions of a sigmoidal function. *Mathematics of Control, Signals and Systems*, **2**: 303-314.
- Enemark, T., Peeters, L.J.M., Mallants, D., and Batelaan, O. 2019. Hydrogeological conceptual model building and testing: A review. *Journal of Hydrology*, **569**: 310-329. doi:<https://doi.org/10.1016/j.jhydrol.2018.12.007>.

- Esterhuizen, J.A., Goldsmith, B.R., and Linic, S. 2020. Theory-guided machine learning finds geometric structure-property relationships for chemisorption on subsurface alloys. *Chem*, **6**: 3100-3117. doi:<https://doi.org/10.1016/j.chempr.2020.09.001>.
- Feng, S., Huo, Z., Kang, S., Tang, Z., and Wang, F. 2011. Groundwater simulation using a numerical model under different water resources management scenarios in an arid region of China. *ENVIRONMENTAL EARTH SCIENCES*, **62**: 961-971. doi:<https://doi.org/10.1007/s12665-010-0581-8>.
- Gadd, C., Xing, W., Nezhad, M.M., and Shah, A. 2019. A surrogate modelling approach based on nonlinear dimension reduction for uncertainty quantification in groundwater flow models. *Transport in porous media*, **126**: 39-77.
- Hornik, K. 1991. Approximation capabilities of multilayer feedforward networks. *Neural Networks*, **4**: 251-257. doi:[https://doi.org/10.1016/0893-6080\(91\)90009-T](https://doi.org/10.1016/0893-6080(91)90009-T).
- Hou, Z., Lao, W., Wang, Y., and Lu, W. 2021. Homotopy-based hyper-heuristic searching approach for reciprocal feedback inversion of groundwater contamination source and aquifer parameters. *Applied Soft Computing*, **104**: 107191. doi:<https://doi.org/10.1016/j.asoc.2021.107191>.
- Kalantar, B., Al-Najjar, H.A., Pradhan, B., Saeidi, V., Halin, A.A., Ueda, N., and Naghibi, S.A. 2019. Optimized conditioning factors using machine learning techniques for groundwater potential mapping. *Water*, **11**: 1909.
- Karniadakis, G.E., Kevrekidis, I.G., Lu, L., Perdikaris, P., Wang, S., and Yang, L. 2021. Physics-informed machine learning. *Nature Reviews Physics*, **3**: 422-440. doi:<https://doi.org/10.1038/s42254-021-00314-5>.
- Karpatne, A., Atluri, G., Faghmous, J.H., Steinbach, M., Banerjee, A., Ganguly, A., Shekhar, S., Samatova, N., and Kumar, V. 2017. Theory-Guided Data Science: A New Paradigm for Scientific Discovery from Data. *IEEE Transactions on Knowledge and Data Engineering*, **29**: 2318-2331. doi:<https://doi.org/10.1109/TKDE.2017.2720168>.

- Kumar, R., Dwivedi, S.B., and Gaur, S. 2021. A comparative study of machine learning and Fuzzy-AHP technique to groundwater potential mapping in the data-scarce region. *Computers & Geosciences*, **155**: 104855.
- Labrecque, G., Chesnaux, R., and Boucher, M.A. 2019. Water-table fluctuation method for assessing aquifer recharge: application to Canadian aquifers and comparison with other methods. *Hydrogeology Journal*, **28**: 521-533.
- Lee, S., Hyun, Y., Lee, S., and Lee, M.-J. 2020. Groundwater potential mapping using remote sensing and GIS-based machine learning techniques. *Remote Sensing*, **12**: 1200.
- Lykkegaard, M.B., Dodwell, T.J., and Moxey, D. 2021. Accelerating uncertainty quantification of groundwater flow modelling using a deep neural network proxy. *Computer Methods in Applied Mechanics and Engineering*, **383**: 113895.
- Mosavi, A., Sajedi Hosseini, F., Choubin, B., Taromideh, F., Ghodsi, M., Nazari, B., and Dineva, A.A. 2021. Susceptibility mapping of groundwater salinity using machine learning models. *Environmental Science and Pollution Research*, **28**: 10804-10817. doi:10.1007/s11356-020-11319-5.
- Parent, M., and Occhietti, S. 2007. Late Wisconsinan Deglaciation and Champlain Sea Invasion in the St. Lawrence Valley, Québec. *Geographie Physique Et Quaternaire*, **42**: 215-246.
- Raissi, M., Perdikaris, P., and Karniadakis, G.E. 2019. Physics-informed neural networks: A deep learning framework for solving forward and inverse problems involving nonlinear partial differential equations. *Journal of Computational physics*, **378**: 686-707. doi:<https://doi.org/10.1016/j.jcp.2018.10.045>.
- Sahour, H., Gholami, V., and Vazifedan, M. 2020. A comparative analysis of statistical and machine learning techniques for mapping the spatial distribution of groundwater salinity in a coastal aquifer. *Journal of Hydrology*, **591**: 125321. doi:<https://doi.org/10.1016/j.jhydrol.2020.125321>.
- Song, T., Ding, W., Liu, H., Wu, J., Zhou, H., and Chu, J. 2020. Uncertainty quantification in machine learning modeling for multi-step time series forecasting: Example of recurrent neural networks in discharge simulations. *Water*, **12**: 912.

- Tartakovsky, A.M., Marrero, C.O., Perdikaris, P., Tartakovsky, G.D., and Barajas-Solano, D. 2020. Physics-Informed Deep Neural Networks for Learning Parameters and Constitutive Relationships in Subsurface Flow Problems. *Water Resources Research*, **56**: e2019WR026731. doi:<https://doi.org/10.1029/2019WR026731>.
- Tayfur, G., Nadiri, A.A., and Moghaddam, A.A. 2014. Supervised Intelligent Committee Machine Method for Hydraulic Conductivity Estimation. *Water Resources Management*, **28**: 1173-1184. doi:10.1007/s11269-014-0553-y.
- Thiéry, D. 1990. Logiciel MARTHE. Modélisation d'Aquifère par un maillage Rectangulaire en régime Transitoire pour le calcul hydrodynamique des écoulements, version, **4**.
- Tran, D.A., Tsujimura, M., Ha, N.T., Nguyen, V.T., Binh, D.V., Dang, T.D., Doan, Q.-V., Bui, D.T., Anh Ngoc, T., Phu, L.V., Thuc, P.T.B., and Pham, T.D. 2021. Evaluating the predictive power of different machine learning algorithms for groundwater salinity prediction of multi-layer coastal aquifers in the Mekong Delta, Vietnam. *Ecological Indicators*, **127**: 107790. doi:<https://doi.org/10.1016/j.ecolind.2021.107790>.
- Tremblay, P. 2005. Étude hydrogéologique de l'aquifère de Saint-Honoré avec emphase sur son bilan hydrique [Hydrogeologic analysis of Saint-Honoré aquifer with emphasis on its water budget]. Applied Sciences, Université du Québec à Chicoutimi.
- Vu, T.-D., Ni, C.-F., Li, W.-C., Truong, M.-H., and Hsu, S.M. 2021b. Predictions of groundwater vulnerability and sustainability by an integrated index-overlay method and physical-based numerical model. *Journal of Hydrology*, **596**. doi:10.1016/j.jhydrol.2021.126082.
- Wagner, N., and Rondinelli, J.M. 2016. Theory-guided machine learning in materials science. *Frontiers in Materials*: 28. doi:<https://doi.org/10.3389/fmats.2016.00028>.
- Wang, N., Chang, H., and Zhang, D. 2021b. Theory-guided Auto-Encoder for surrogate construction and inverse modeling. *Computer Methods in Applied Mechanics and Engineering*, **385**: 114037. doi:<https://doi.org/10.1016/j.cma.2021.114037>.
- Wang, N., Zhang, D., Chang, H., and Li, H. 2020b. Deep learning of subsurface flow via theory-guided neural network. *Journal of Hydrology*, **584**: 124700. doi:<https://doi.org/10.1016/j.jhydrol.2020.124700>.



## CHAPITRE 4

### A CAUSAL PHYSICS-INFORMED DEEP LEARNING FORMULATION FOR GROUNDWATER FLOW MODELING AND CLIMATE CHANGE EFFECTS ANALYSIS

Ce chapitre aborde le second objectif de la recherche, qui est de tester l'hypothèse de recherche en comparant un modèle TgML avec des modèles traditionnels dans un contexte de modélisation localisée de l'écoulement des eaux souterraines. Le réseau de suivi piézométrique du Ministère de l'Environnement du Québec (MELCCFP) a été utilisé comme laboratoire d'étude. Les modèles TgML actuels pour la modélisation localisée utilisent la formulation de Jiang et al. (2020) qualifiée de traditionnelle dans cette thèse. Cette dernière consiste à intégrer des équations de bilan hydrique issues de modèles conceptuels hydrologiques (tels que le modèle HBV) dans l'architecture des réseaux de neurones artificiels. HBV est l'abréviation de *Hydrologiska Byråns Vattenbalansavdelning*. Dans cette thèse, il est montré que les modèles basés sur la formulation de Jiang et al. (2020) ont une grande susceptibilité à transgresser certains principes de la physique tels que le principe de causalité. Une nouvelle formulation a été donc élaborée pour assurer que les modèles TgML obéissent au principe de causalité. Cette nouvelle formulation exige que les noyaux des couches de neurones soient contraints à des valeurs positives, tout comme la dérivée de leur fonction d'activation. Ces deux conditions sont désignées ici par le terme CRC (Causal Relationship Constraints). Ainsi, l'étude menée dans ce chapitre consistait à répondre à la question suivante : dans une tâche de simulation localisée de l'écoulement des eaux souterraines, comment des modèles TgML avec les contraintes CRC (H-Lin et H-HB), se comparent-ils à un modèle TgML de Jiang et al. (2020) (H-HBVo) et un modèle conventionnel d'apprentissage automatique (1D-CNN) ? Les modèles ont été comparés en termes de (a) performance, (b) de capacité à obéir au principe de causalité et (c) de coûts de calculs en phase d'entraînement et de projection. La différence entre les modèles H-Lin et H-HBV réside dans le modèle conceptuel hydrologique qu'ils intègrent. Le premier

intègre un modèle hydrologique linéaire simple tandis que le second intègre le modèle HBV. Les résultats ont montré que le modèle traditionnel d'apprentissage est légèrement plus performant que les modèles basés sur la formulation proposée, et que ces derniers obtiennent ensemble des résultats légèrement meilleurs que le modèle basé sur la formulation traditionnelle. Il a également été montré que les modèles basés sur la formulation proposée (H-Lin et H-HBV) sont ceux qui présentent des propriétés de causalité satisfaisantes, mais surtout que l'intégration des connaissances du domaine (modèle conceptuel hydrologique) n'est pas suffisante pour obtenir des modèles causaux et donc interprétables dans le cadre de la méthode de l'architecture guidé par la théorie. Il convient toutefois de noter qu'en fonction de la complexité du modèle hydrologique à intégrer dans l'architecture du réseau neuronal, les coûts de calcul associés à l'entraînement peuvent être relativement élevés. En plus de l'étude comparative réalisée, une étude préliminaire de l'impact du changement climatique sur l'évolution des niveaux d'eau souterraine a été conduite sur le réseau de suivi piézométrique du Québec, à l'aide du modèle H-HBV. Les scenarios climatiques RCP4.5, RCP8.5, SSP2-4.5 et SSP5-8.5 ont été utilisés. Les résultats ont montré qu'indépendamment du scenario, une augmentation modérée des niveaux piézométriques est prévue sur la période 2011-2090.

En somme, pour la modélisation localisée, l'hypothèse sur laquelle repose le TgML est valide grâce à la nouvelle formulation proposée dans cette thèse, à ceci près qu'elle peut nécessiter plus de temps pour l'apprentissage de tels modèles.

Adoubi Vincent De Paul Adombi<sup>a</sup>, Romain Chesnaux<sup>a</sup>, Marie-Amélie Boucher<sup>b</sup>, Marco Braun<sup>c</sup>, Juliette Lavoie<sup>c</sup>

a. Research Group R2Eau, Centre d'études sur les ressources minérales, Université du Québec à Chicoutimi, 555 boulevard de l'Université, Chicoutimi, Québec G7H 2B1, Canada.

Email : [adombi.vincentdepaul@gmail.com](mailto:adombi.vincentdepaul@gmail.com)

b. Department of Civil Engineering, Université de Sherbrooke, 2500 boulevard de l'Université, Sherbrooke, Québec J1R 2R2, Canada

Reçu le 02 novembre 2023 - Accepté avec correction le 05 février 2024 dans la revue Journal of Hydrology.

#### 4.1 ABSTRACT

In this study, we propose and test a formulation for building causal physics-informed hybrid models over traditional physics-informed hybrid models (H-HBVo) and a convolutional neural network (1D-CNN) in groundwater level (GWL) modeling. Two types of models are built based on our formulation and named H-HBV and H-Lin, because they integrate two different hydrological models. The comparison is made in terms of performance and ability to learn cause-and-effect relationships between inputs and outputs. The novelty of this study lies in the CRC (Causal Relationship Constraints) conditions, derived from a mathematical development, that are imposed on the layers of the physics-informed hybrid model to force it to learn causal relationships. The results showed that the 1D-CNN algorithm performed slightly better than the hybrid algorithms, and that the H-Lin and H-HBV algorithms together achieved slightly better results than the traditional hybrid algorithm, H-HBVo. It is also obtained that the algorithms subjected to our formulations (H-Lin and H-HBV) are the ones with satisfactory causality properties and that the integration of domain knowledge is not sufficient to obtain causal and interpretable models within the framework of hybrid algorithms. Subsequently, an analysis of the effect of climate change is carried out for Quebec (Canada) using H-HBV models. The results show that the RCP and SSP scenarios give fairly similar results, i.e. an increase in GWL between 2011 and 2090 with median amplitudes varying between +5.6 and +7.0 cm. In some cases, the amplitude of increase can exceed between +14.0 and +23 cm, and even reach between +35.0 and +70 cm. The results of the climate change analysis are consistent with changes in vertical inflow and potential evapotranspiration, the input variables, for the different climate scenarios, confirming the robustness of our formulation.

**Keywords:** Physics-informed neural networks · Causality · Interpretability · Machine learning · Climate change · Groundwater modeling

## 4.2 INTRODUCTION

Recent economic development and agricultural innovation, as well as long-term effects of climate change, are exerting increasing pressure on groundwater resources. In some regions, groundwater levels are decreasing, which could have notable consequences such as water scarcity, deterioration of water quality, or ecosystem degradation (Bui et al. 2012; Hoque et al. 2007; Konikow and Kendy 2005; Wada et al. 2010). The sustainable management of groundwater resources is becoming increasingly important (Lijzen et al. 2014; Luo et al. 2020); this requires a better characterization of the resource in terms of quality and quantity as well as an examination of the effects of different anthropogenic and climatic scenarios on the evolution of groundwater resources.

Characterization of groundwater resources is generally done through modeling. In hydrogeology, physics-based models remain the traditional tool for modeling groundwater flow, as they allow for improved understanding and prediction of processes at certain spatio-temporal scales (Maxwell et al. 2015). For example, Hussain et al. (2022) used WASH123D, a physics-based numerical model, to assess the response of groundwater levels to rainfall and determine the recharge potential of shallow aquifers in four districts in southern Taiwan. They found that the rise in groundwater level is linearly dependent on the amount of rainfall per event and they estimated annual recharge rates between 244 and 1472 mm/year, corresponding to 12–43% of rainfall. Sulis et al. (2010) compared two physics-based numerical models for simulating surface water and groundwater interactions. These two models use different approaches for coupling the land surface and subsurface. The first one uses an explicit exchange term solved by applying the continuity principles and the second one considers a special treatment of atmospheric boundary conditions. According to their results, the two models are in agreement despite using different approaches. While physics-based

models have been applied successfully for groundwater modeling in various studies, they remain complex, computationally prohibitive, require very large amounts of data, and are difficult to apply at large scales (Clark et al. 2015; Faticchi et al. 2016; Yoon et al. 2011). Sun et al. (2016) points out that due to the inevitable simplifying assumptions in the development of physics-based models, they can sometimes produce inaccurate results.

In recent years, the academic hydrogeology community has become increasingly involved in the development of data-driven models as complementary modeling tools for groundwater flow modeling (Adombi et al. 2021; Asher et al. 2015). The successful development and application of various types of machine learning algorithms have been reported in the literature for groundwater flow simulation (Banadkooki et al. 2020; Pham et al. 2022; Sahoo et al. 2017b; Wei et al. 2022). Deep learning algorithms, such as recurrent neural networks (RNN) and convolutional neural networks (CNN), are gaining ground due to their very high performance when it comes to processing sequential data or extracting useful features from complex data (Bowes et al. 2019; Jeong et al. 2020; Kochhar et al. 2022; Secci et al. 2023; Wunsch et al. 2021). For example, Kochhar et al. (2022) used a Long Short-Term Memory (LSTM), an improved version of RNN, as well as a deep multilayer perceptron (MLP) and a Seasonal Autoregressive Integrated Moving Average (SARIMA) for modeling, predicting, and forecasting pre-monsoon and post-monsoon groundwater levels in Punjab, India. The authors determined that the deep learning models outperformed the SARIMA model, and that the MLP gave the best representation of variability for pre-monsoon data and the LSTM for post-monsoon data. Wunsch et al. (2022) calibrated convolutional neural network models at 118 well-distributed sites in Germany to assess groundwater level evolution under different representative concentration scenarios (RCP). According to their results, groundwater level in Germany could decrease until 2100 due only to climate change. Machine learning algorithms in general and deep learning in particular offer significant advantages compared to physics-based models, especially when it comes to obtaining accurate and efficient models, while maintaining very high performance, even when computing resources are limited (Cai et al. 2022; Reichstein et al. 2019). Despite these advantages, machine learning algorithms have not yet moved beyond the academic sphere to reach an operational

use. This is mostly due to their opaque nature, that does not allow for an understanding of the underlying physics of groundwater flow. In addition, machine learning algorithms, including deep learning, tend to produce generally inconsistent physical results and may demonstrate poor generalization capabilities compared to physics-based models (Chen et al. 2020a; Karpatne et al. 2017). It seems clear that neither physics-based models nor machine learning approaches can solve current groundwater flow problems on their own with a high degree of efficiency.

Recently, researchers have begun to explore the “continuum between physics-based models and machine-learning models, bringing scientific knowledge and data together in a synergistic way” (Slater et al. 2023; Vadyala et al. 2022). This new paradigm, called physics-informed machine learning (Karniadakis et al. 2021; Raissi et al. 2019) or theory-guided machine learning (Esterhuizen et al. 2020; Karpatne et al. 2017; Wagner and Rondinelli 2016), consists in integrating domain knowledge into the learning process of machine-learning algorithms. Domain knowledge can be integrated in several ways, including three in particular. A first approach is to modify the cost function to force the model to satisfy the principles and laws of physics related to the domain (Secci et al. 2024; Tartakovsky et al. 2020; Wang et al. 2021b; Wang et al. 2020b; Xu et al. 2021). This first approach is particularly suitable for distributed modeling problems. A second approach is to post-process the outputs of the trained models to force them to respect the underlying physics (e.g., Chen et al. 2021; Khandelwal et al. 2015). A third approach, suitable for lumped modeling problems, consists in incorporating intermediate variables with physical meaning or mass balance equations into the internal structure of the machine learning algorithm (Cai et al. 2022; Jiang et al. 2020). Here, the focus is on this third approach, which typically uses recurrent neural networks (RNNs) and their “memory” properties as analogs for groundwater reservoirs to solve ordinary differential equations (ODEs) in order to simulate groundwater levels. For example, Cai et al. (2022) developed a hybrid physics-informed machine-learning model combining a pure physics-informed RNN and a CNN for groundwater level modeling and compared its performance with the pure physics-informed RNN as well as with two deep-learning (DL) models, namely a CNN and a Gated Recurrent Unit (GRU). In this application of the models to 91 catchments in the middle-eastern continental United States

(CONUS), the hybrid model outperforms pure DL models in terms of predictive accuracy, generality, and robustness. However, pure physics-informed RNNs generally perform poorly, thus highlighting the need for hybridization. In the hydrogeological literature, with the exception of Cai et al. (2022), there are no other studies using physics-informed hybrid algorithms for lumped modeling of groundwater levels. In addition, to the best of our knowledge, no study, either in or outside the hydrogeological literature, has addressed the issue of evaluating the ability of physics-informed hybrid algorithms to learn causal relationships between forcing drivers and groundwater responses. The principle of causality, in addition to high performance, is mandatory for simulation and forecasting / prediction. The objectives of this study are as follows:

- Demonstrate that traditional formulation of physics-informed hybrid models, as proposed by Jiang et al. (2020) or Cai et al. (2022), does not necessarily lead to models complying with the principle of causality;
- Propose a new formulation of physics-informed hybrid models, derived from a mathematical development, that satisfies the principle of causality;
- Test and compare the performance of the proposed formulation of physics-informed hybrid models against a pure CNN model and a traditional physics-informed hybrid model in terms of accuracy and causality;
- Apply a physics-informed hybrid model based on our formulation to study the effect of climate change on GWL in the province of Quebec, Canada. In this last part, future projections are made using two climate simulation ensembles from phase 5 and 6 of the Coupled Model Intercomparison Project (CMIP) (Bock et al. 2020; Meehl et al. 2000).

For the sake of readability, the term "physics-informed hybrid model" will be replaced by "hybrid model" in what follows. The novelty of this study lies in the CRC (Causal Relationship Constraints, see **Section 4.4.1.4**) conditions that we imposed on the layers of the hybrid model to force it to learn causal relationships and consequently, to compel it to "correctly rationalize". The new

formulation proposed is original in that it shows that if CRC conditions are not applied, hybrid models based on the formulations proposed by Jiang et al. (2020) or Cai et al. (2022) are not guaranteed to learn causal relationships, these being essential if a model is to be used for forecasting/projection.

## 4.3 STUDY AREA AND DATA

### 4.3.1 STUDY AREA

The study area covers approximately 612,000 km<sup>2</sup> and lies between 45° – 51°N and 60° – 80°W, encompassing most of southern Quebec, Canada (**Figure 25**). The territory is marked by a cold and humid continental climate with an average temperature of 2°C with wide variations between the different regions within that zone, falling below average in the extreme west and increasing to 3°C towards the center-north and the extreme east and up to 7°C towards the south (MELCCFP 2023b). Temperature differences between the warm and cold seasons also vary greatly, with temperatures reaching an average of 17°C in July, while in January the average is about -15°C. Solid and liquid precipitation totals an average of 1,000 millimeters per year, of which nearly 75% is rain, with significant snowfall generally occurring between December and March (MELCCFP 2023b). Several important geological domains in Quebec are covered in the area, including the Superior and Grenville Provinces, the St. Lawrence Platform and the Appalachian Province (Larocque et al. 2018; Rivera 2014). The deposition of unconsolidated sediment and the formation of proglacial lakes following marine invasions during the last glaciation/deglaciation cycle had a decisive impact on the geology and hydrogeology of the current aquifer systems in the study area (Larocque et al. 2018). For example, in the western part of the study area, there is a clay belt composed of numerous esker and moraine aquifers (Rey et al. 2018) whereas toward the south, the main aquifer is located in the fractured sedimentary basement and is covered by till, sand and clay (Gagné et al. 2018). In the vicinity of the center-north, a multilayered aquifer system can be noted, composed of glaciofluvial sediments covered by a marine clay-silt aquitard, deltaic and shore deposits and finally fractured rock aquifers

(Walter et al. 2018). In terms of land use, with the exception of residential and urban areas, the study area is mainly covered by forest, followed by agricultural and agroforestry areas.

In the study area, groundwater supplies 25% of the population over 90% of the inhabited territory. Although 10% of Quebec's territory is covered by freshwater, with tens of thousands of rivers and more than three million bodies of water, groundwater is often the only economically exploitable source because of its generally good quality and its proximity to the place of consumption. This is why a sound management of this resource and its adequate protection is a major issue for the Quebec Ministry of Environment (MELCCFP 2023a), resulting in the establishment of a groundwater monitoring network.

#### **4.3.2 DATA AND PROCESSING**

The models in this study are developed using daily groundwater level time series from the Quebec groundwater monitoring network, daily historical climate data (precipitation and temperature) and data from CMIP5 and CMIP6 for the study of the effect of climate change on groundwater level development. Details of each type of data are given in the following sections, and their processing is briefly explained.

##### **4.3.2.1 GROUNDWATER LEVEL TIME SERIES**

The groundwater monitoring network of the Quebec Ministry of Environment was developed to monitor the changes in groundwater levels and temperatures in the context of climate change (MELCCFP 2023c). Although some observation wells were active as early as 1968, most of the network has been developed since 2008 and comprises 263 observation wells to date. Each well is equipped with a hydrostatic pressure sensor and a temperature sensor. Some wells have a second

pressure sensor placed on the surface of the water to correct the groundwater level according to changes in atmospheric pressure. These sensors are connected to a data logger. The data is synthesized in the form of daily time series. While there are a large number of observation wells, data from most of them are inadequate for this study, either because the record is too short (i.e. less than 10 years) or because there is a very large proportion of missing data. In this study, only wells with less than 2% missing data, in place during at least 10 years and coinciding with the period 2011 - 2021 were selected. In fact, this period provides the greatest number of observation wells with usable data.

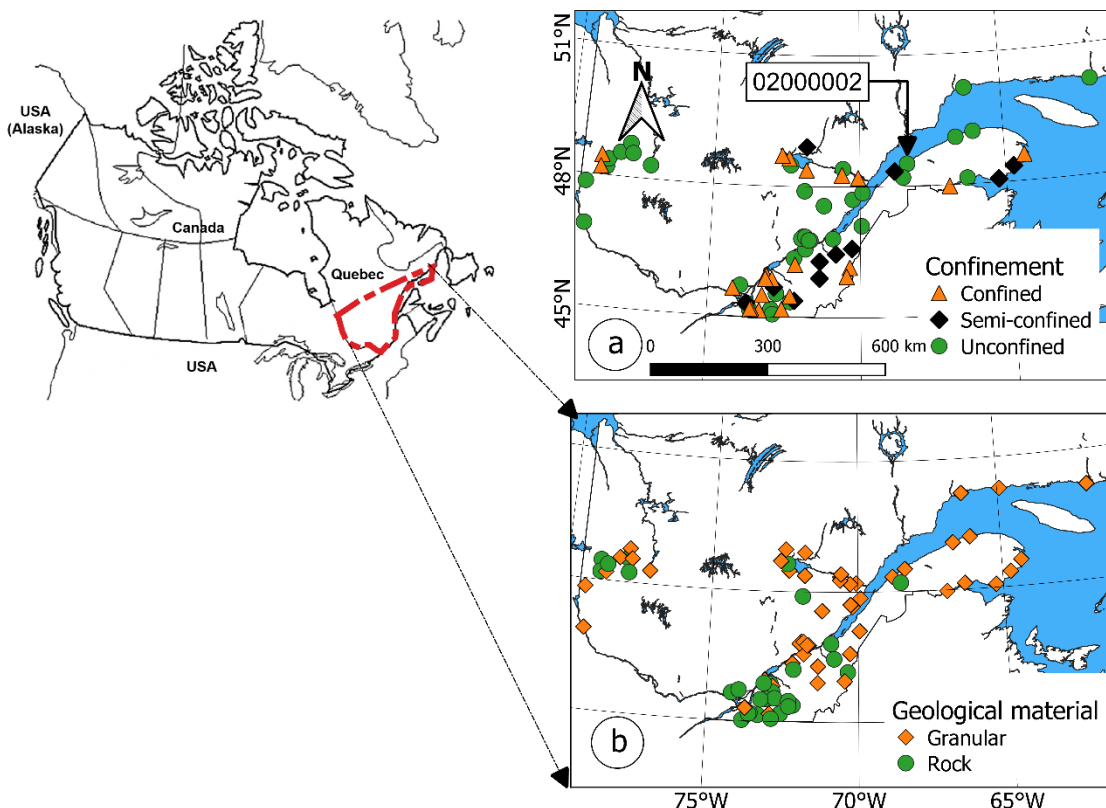


**Figure 25** Location of the study area and the observation wells from the Quebec groundwater monitoring network, (a) the state of confinement of the aquifers observed by each well and (b) the geological nature of these aquifers.

The location of the selected observation wells (70 wells) is shown in **Figure 25**. For wells with missing data, extrapolation is performed using data from wells with which they are sufficiently

correlated. The wells are located in different types of aquifers at an average depth of approximately 12 m, but can be as deep as 43 m (**Figure 25a**): 37 wells are located in unconfined aquifers, 11 in semi-confined aquifers and 22 in confined aquifers. 64% of the observation wells are in a granular context, while the remaining 36% are in rock (**Figure 25b**). The above classification of observation wells on aquifer confinement state, based on well stratigraphy, is associated with uncertainties. Firstly, observation wells monitor a certain thickness of the aquifer, not a specific point, so classification based on well stratigraphy is not always accurate. Secondly, most of the 70 wells selected do not have a pressure transducer to define the well's barometric response function (BRF) and to determine its confinement state. Following quality control, some observation wells may demonstrate a particular behavior that is not representative of the surrounding aquifers. For example, some wells have a water level that oscillates between unconsolidated deposits and bedrock; this can generate an atypical signal, i.e. a variable response to precipitation depending on whether the initial level is low to be in bedrock or high to be in unconsolidated deposits. Thirdly, some wells may be poorly developed/clogged, producing a signal that represents the state of the well and not its environment. Given the uncertainties associated with the confinement state of aquifers, we have chosen a conceptual hydrological model (the "physical" part of the hybrid algorithms) which accounts for these limitations. This conceptual model, which represents the functioning of the groundwater system as a succession of communicating reservoirs, implicitly introduces an intermediate layer between the aquifer reservoir and the overlying reservoir. This intermediate layer can be interpreted as a layer of variable permeability, depending on whether the aquifer is confined, semi-confined or unconfined. This way, the uncertainties associated with the confinement state of the aquifer are considered (see **Section 4.4.1**).

To improve GWL data quality and build the most efficient models possible, a two-stage data processing approach is implemented for multi-input/multi-output modeling. First, the observation wells are clustered according to their hydrodynamic behavior. This clustering is performed using the time series clustering (TSC) method, itself based on the k-means method. The first step is to separate the observation wells according to the aquifer's initial state of confinement, i.e. three groups: unconfined,

semi-confined and confined. Then, for each of these groups, the TSC method is applied to generate clusters of wells based on hydrodynamic behavior. The observation wells in a given cluster react similarly to exogenous factors such as climate variables, which may suggest that the associated aquifers have similar hydrodynamic properties (diffusivity). The clustering approach, presented in greater detail in **Fig. S1** of the Supplementary Material 1 (Adombi 2023f), allowed for the generation of 6 clusters. In what follows, modelling will be carried out for each cluster, rather than by aquifer confinement conditions, because the aquifers associated with the observation wells in each cluster react identically, meaning that they have comparable diffusivities, but also because the chosen hydrological conceptual model chosen (**Section 4.4.1**) enables the recharge process in aquifers, regardless of their confinement state, to be described consistently. As the wells in a given cluster are not grouped together geographically, the centroid well in each cluster is not considered representative of all cluster members, given that climatic variability can be very significant from one location to another. Second, GWL time series for all wells of the monitoring network are corrected using the reference hydrograph method developed in Lehr and Lischeid (2020).

#### 4.3.2.2 HISTORICAL CLIMATIC DATA

Daily historical data (from climate stations) near the observation wells are retrieved. Climatic data, namely precipitation and temperature, are obtained from the Environment and Climate Change Canada database (ECCC 2022). ECCC collects data using a variety of methods and sources, including automatic weather observation stations, and ensures quality control. Precipitation and temperature are used to calculate daily vertical inflow and potential evapotranspiration. To calculate potential evapotranspiration, the simple and efficient model proposed by Oudin et al. (2005) is used. This model uses minimum and maximum temperatures as input and outputs the potential evapotranspiration. The calculation of vertical inflow is performed using the CemaNeige snow accumulation and melt model described in Valéry (2010) and Valéry et al. (2014). In this study, vertical inflow, refers to the amount of water originating from snowmelt and rainfall. The CemaNeige model receives as input precipitation as well as minimum, mean and maximum temperatures and provides

the vertical inflow as the only output. CemaNeige is a simple degree-day model that has two parameters that must be calibrated jointly with those of a hydrological model, against streamflow data. The calibrated average of these parameters over the analyzed watersheds in Quebec is used in this study (see Valéry et al. 2014).

#### 4.3.2.3 CLIMATE SCENARIO DATA

Climate data for this study were sourced from CMIP5 and CMIP6 climate model simulation ensembles, i.e. phases 5 and 6 of the Coordinated Model Intercomparison Project (CMIP) (Eyring et al. 2016; Taylor et al. 2012). CMIP5 ensemble data corresponds to Representative Concentration Pathway scenarios RCP4.5 and RCP8.5 (van Vuuren et al. 2011) and CMIP6 simulations follow Shared Socioeconomic Pathway SSP2-4.5 and SSP5-8.5 (Riahi et al. 2017). Simulations from both CMIP ensembles were bias corrected by the Ouranos Consortium. CMIP5 and CMIP6 data were post-processed as part of the "Thématische évolution du climat du projet de soutien à info-cru" projects (Rondeau-Genesse and Braun 2020). For each RCP/SSP, the climate models used in this study are presented in **Table S1** of the Supplementary Material **1**. CMIP5 simulation data for 1971 – 2000 were post-processed with NRCan gridded reference data from the periods 1971 – 2002, skipping 1995 and 1996 due to known interpolation artefacts. The post-processing methods used were detrended quantile mapping (for temperature and precipitation) and parametric extreme value correction (for precipitation) (Rondeau-Genesse and Braun 2020). CMIP6 data were post-processed using the same methods as for CMIP5 data, but the reference data are ERA5-Land over the period 1991-2020. Please refer to Rondeau-Genesse and Braun (2020) for more details on the processing of climate scenario data.

For each observation well in the groundwater monitoring network, CMIP5 and CMIP6 data from the nearest grid cells were retrieved. From each scenario, daily historical data, namely precipitation and temperature, were extracted. Precipitation and temperature are then transformed

into vertical inflow and potential evapotranspiration using the models described in **Section 4.3.2.2**.

Finally, changes in groundwater levels from 2011 to 2090 (i.e. 80 years) due solely to climate change are investigated. Note that CMIP6 were statistically downscaled to grid cells of approximately 10km while CMIP5 data were bias corrected on their native grids of variable resolution of approximately 1-3° (~100-300km). As a result, CMIP6 data are more sensitive to local extremes. The different grid sizes between CMIP5 and CMIP6 are a feature of the available data for this study and open the possibility to evaluate the impact of the spatial resolution of the driving data on model results.

## 4.4 METHODS

### 4.4.1 CONCEPTUAL HYDROLOGIC MODELS, DEEP LEARNING MODELS, TRADITIONAL THEORY-GUIDED DEEP LEARNING MODELS AND THE PROPOSED THEORY-GUIDED DEEP LEARNING MODELS

There are several conceptual bucket-type models describing recharge processes, such as HBV and GR4J models (Knoben et al. 2020). Conceptual models describe the functioning of the aquifer system as a succession of communicating reservoirs. Hereafter, the HBV model is considered because it provides a fairly comprehensive description of the processes that influence recharge and provides explicit equations that can be easily implemented in an RNN architecture. There are several versions of the HBV model in addition to the original version developed by Bergström (1976). In this work, the version implemented by Schellekens (2018), consisting of three routines, namely a snow routine, a soil routine and a groundwater routine, is considered. The snow routine is not implemented here since the input data we will consider later are vertical inflow and potential evapotranspiration. In addition, the greater the number of routines used to build the hybrid models, the greater the computational resources required. This is also one of the reasons why sparser models were built in this study. The groundwater routine of the HBV model consists of an upper and a lower reservoir. These two reservoirs are linked by the percolation variable  $q_p$  defined by Equation (4.1).

$$q_p = K_p \cdot S_u \quad (4.1)$$

where  $K_p$  is the percolation coefficient that controls the amplitude of water flow reaching the lower reservoir (aquifer) and  $S_u$  is the storage of the upper reservoir.  $K_p$  can be interpreted as analogous to the hydraulic conductivity of an intermediate layer between the upper reservoir and the lower reservoir (aquifer). Thus, the value of  $K_p$  varies according to the confinement conditions of the aquifer, being higher for unconfined aquifers and much lower for "confined" aquifers (confined meaning that the permeability contrast between the intermediate layer and the aquifer is significant). Consequently, the HBV model provides a consistent description of the recharge process in aquifers, regardless of their confinement conditions, which is suitable for our study. For more details on the HBV model equations, the reader is invited to refer to Schellekens (2018) or to the Supplementary Material 1 (Adombi 2023f).

In addition to the HBV model, a simpler model is also considered. This second model, which will be referred to hereafter as the linear model, considers that water level variations are only due to the net vertical inflow (Equation (4.2)), i.e. the difference between vertical inflow  $vi$  and potential evapotranspiration  $ep$  corrected by a constant factor  $k_v$ .

$$v_{net} = vi - k_v \cdot ep \quad (4.2)$$

A schematic structure of the considered HBV model is shown in **Fig. S2** of the Supplementary Material 1 (Adombi 2023f).

#### 4.4.1.1 RECURRENT NEURAL NETWORKS

A recurrent neural network (RNN) is a family of neural networks with feedback connections specifically designed to learn sequential or time-varying patterns (Fausett 2006; Medsker and Jain 2001). RNNs differ from traditional artificial neural networks by their recurrent neurons (or cells), which give them a memory property. This memory, represented by a hidden state, stores past information

and can be compared to the functioning of a water reservoir. The current hidden state  $S_t$  depends on the previous state  $S_{t-\Delta t}$  and is used to predict the current output  $y_t$ . Depending on how the recurrent neurons are designed, different types of RNNs can be distinguished, such as simple or traditional RNN and LSTM (or GRU). More formally, the traditional version of an RNN is described by the two-step function given by Equations (4.3) and (4.4) (Cai et al. 2022).

$$S_t = \sigma_s(W_s^T \cdot x_t + U_s^T \cdot S_{t-\Delta t} + b_s) \quad (4.3)$$

$$y_t = \sigma_y(W_y^T \cdot S_t + b_y) \quad (4.4)$$

where  $\sigma$  is an activation function;  $W$  and  $U$ , the weight parameters;  $b$ , the bias;  $t$ , the time variable;  $y$ , the output of the RNN;  $T$ , the transpose operation; subscripts  $s$  and  $y$  are associated with the state  $S_t$  and the output  $y$  of the RNN respectively. A schematic structure of a simple traditional RNN is shown in **Fig. S3** of the Supplementary material 1 (Adombi 2023f) and more details on RNN can be found in Lukoševičius and Jaeger (2009) or De Mulder et al. (2015).

#### 4.4.1.2 CONVOLUTIONAL NEURAL NETWORK

Convolutional neural networks (CNNs), originally proposed by LeCun et al. (1989), are feed-forward neural networks with a basic architecture consisting of a convolution layer followed by a pooling layer, eventually a dropout layer that acts as a regularizer and a succession of fully connected (dense) layers. Traditionally used for image recognition and classification tasks, 2D CNNs consist of many hidden layers with a very large number of parameters to optimize (Kiranyaz et al. 2021). They have the ability to learn complex relationships, but their success depends on the availability of a massive amount of data. In groundwater applications, where data are typically one-dimensional and sparse, 2D CNN models are not viable (Kiranyaz et al. 2021). To circumvent this limitation, 1D-CNN has recently been proposed and is gaining popularity for groundwater flow simulation (e.g., Wunsch et al. 2021; Wunsch et al. 2022). A schematic structure of the 1D-CNN architecture used in this study is shown in **Fig. S4** of the Supplementary Material 1 (Adombi 2023f).

#### 4.4.1.3 TRADITIONAL HYDBRID MODEL

The architecture of a traditional hybrid model consists of two blocks. The first block is a theory-guided layer in which “physical” equations such as those of a conceptual bucket-type model are embedded. The theory-guided layer transforms the input data into intermediate output data with physical meaning. One or more intermediate variables are then passed to the second block, which is a 1D-CNN. The theory-guided layer is used to provide the model with physical interpretability and the 1D-CNN handles processes that are not represented by the theory-guided layer (Jiang et al. 2020).

Using the HBV model, the theory-guided layer is represented by an RNN where the two-step function is replaced by the ODEs (Schellekens 2018) expressing the principle of mass conservation. Thus, the extent to which the theory-guided layer perceives long-term memory depends on the integrated hydrological model. It's worth noting that the ODEs of hydrological models such as HBV inherently have long-term memory, thus circumventing the gradient vanishing and explosion problems (Cai et al. 2022). For more details on how a hydrological model is incorporated into the RNN layer, please refer to Cai et al. (2022). The theory-guided layer is also used to simulate physical variables such as actual evaporation or percolation. In the theory-guided layer, three types of hidden state variables are incorporated that represent soil moisture storage  $S_m$ , quick groundwater storage  $S_u$  (upper reservoir) and slow groundwater storage  $S_g$  (lower reservoir), respectively. Using the linear model (**Section 4.4.1**), the theory-guided layer is a perceptron where the kernel (weight) represents the correction factor  $k_v$  of potential evapotranspiration (Equation (4.2)). No activation function or bias is applied to this perceptron. A schematic structure of the traditional hybrid algorithm used in this study is shown in **Fig. S5** of the Supplementary Material 1 (Adombi 2023f).

#### 4.4.1.4 THE PROPOSED CAUSAL HYBRID MODEL

In the traditional hybrid model, because the theory-guided layer is wrapped by mass balance equations, the cause-and-effect relationship is satisfied between the input (i.e., vertical inflow  $vi$  and potential evapotranspiration  $ep$ ) and output (i.e., a given physical output  $y$ ) variables of this layer. However, by coupling the theory-guided layer to a traditional CNN, the cause-and-effect relationship is no longer necessarily assured, and this is even more true when the CNN receives  $N$ -dimensional inputs ( $N > 1$ ).

Consider  $y = (y_1, \dots, y_N)$  as an  $N$ -dimensional output of the theory-guided layer where  $y$  may correspond, for example, to the percolation for  $N$  groundwater observation wells and  $c = (c_1, \dots, c_M)$ , the output of the 1D-CNN convolutional layer. A given component  $c_l$  of the convolutional layer output  $c$  is the weighted sum of all inputs  $y_{l-j}$ , plus a bias  $b_l$ , passed to an activation function  $\sigma$  (Equation (4.5)).

$$c_l = \sigma \left( b_l + \sum_j W_j \cdot y_{l-j} \right) \quad (4.5)$$

Let  $\alpha = b_l + \sum_j W_j \cdot y_{l-j}$ . Changes in  $c_l$  with respect to  $vi$  and  $ep$  are given by Equations (4.6) and (4.7) respectively.

$$\frac{\partial c_l}{\partial vi} = \frac{\partial c_l}{\partial \alpha} \frac{\partial \alpha}{\partial vi} = \sigma'(\alpha) \sum_j W_j \cdot \frac{\partial y_{l-j}}{\partial vi} \quad (4.6)$$

$$\frac{\partial c_l}{\partial ep} = \frac{\partial c_l}{\partial \alpha} \frac{\partial \alpha}{\partial ep} = \sigma'(\alpha) \sum_j W_j \cdot \frac{\partial y_{l-j}}{\partial ep} \quad (4.7)$$

where  $W_j$  is the weight (or Kernel) and takes its values in  $\mathbb{R}$  and  $\sigma'$  is the derivative of the activation function  $\sigma$ . Since  $y_j$  satisfies a causal relationship with  $vi$  and  $ep$ ,  $y_{l-j}$  increases with  $vi$  and vice

versa, while  $y_{l-j}$  increases with decreasing  $ep$  and vice versa. If one considers the special case of a linear activation function,  $\sigma'(\alpha)$  is equal to unity. Therefore, to ensure that the convolutional layer preserves the causal relationships acquired by the theory-guided layer, it is imperative that  $\frac{\partial c_l}{\partial v_i}$  (resp.  $\frac{\partial c_l}{\partial e_p}$ ) keeps the sign of  $\frac{\partial y_{l-j}}{\partial v_i}$  (resp.  $\frac{\partial y_{l-j}}{\partial e_p}$ ). This is possible if  $W_j > 0$ . So, as a general rule, for any activation function, whether linear or non-linear, the following two conditions, which we call “CRC (Causal Relationship Constraints) conditions”, must be imposed (Equation (4.8)):

$$CRC = (W_j > 0 \text{ and } \sigma'(\alpha) > 0, \forall j) \quad (4.8)$$

Similarly, it can be shown that in order to maintain the causal relationship for dense layers of the CNN, it is necessary that the kernels and derivative of the activation functions are strictly positive. If the CRC conditions are not met, any model based on traditional formulation of hybrid model (see Cai et al. 2022; Jiang et al. 2020) has a greater probability of transgressing the principle of causality, which could render it unusable for simulation or projection.

The CRC conditions also implies specific properties for the activation function, namely that its derivative must be strictly positive or, in the ideal case, but not necessarily, that its derivative must be a monotonically increasing and positive function. Most derivatives of traditional activation functions, such as the hyperbolic tangent, the sigmoid or linear functions, satisfy the positivity property. A schematic structure of the proposed formulation of hybrid models is shown in **Figure 26**.

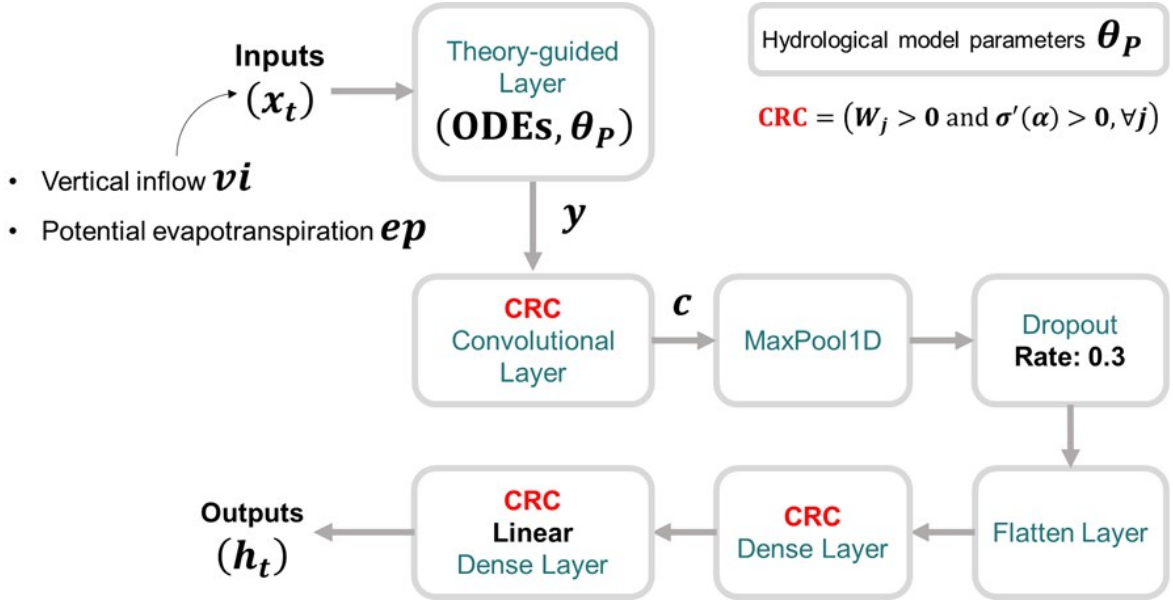


**Figure 26** A schematic structure of the proposed formulation of hybrid algorithms. CRC stands for causal relationship constraints;  $W_j$  is the  $j - th$  component of the kernel (or weight) of a layer and  $\sigma'$  is the derivative of the  $\sigma$ activation function.

#### 4.4.2 MODEL DEVELOPMENT

#### 4.5 RESULTS

The 70 observation wells in Quebec's groundwater monitoring network are divided into 6 clusters according to their hydrodynamic behavior. The observation wells in a given cluster react in the same way to exogenous drivers such as vertical inflow and potential evapotranspiration. For each cluster, four models are calibrated/validated using daily vertical inflow, potential evapotranspiration from ECCC climate station data and GWL for the period 21/03/2011 to 04/04/2019 (80% of data) and tested using data from 05/04/2019 to 07/04/2021 (20% of data). The four models are respectively a 1D-CNN, a traditional hybrid model wrapping the HBV model (H-HBVo), and two hybrid models based on our formulation and wrapping the conceptual linear model (H-Lin) and the HBV model (H-HBV) respectively. The models are compared on the basis of their performance and their ability to learn cause-and-effect relationships between inputs and outputs. The results for the testing data set are presented in **Section 4.5.1**. Thereafter, hybrid models based on our formulation are used to assess the effect of climate change on GWL development over the period 2011 - 2090 and using the CMIP5

(RCP4.5 and RCP8.5) and CMIP6 (SSP2-4.5 and SSP5-8.5) scenarios. Trends and trend magnitudes are calculated using the trend free pre-whitening Mann-Kendall (TFPW-MK) test (Yue et al. 2002b). The results of the climate change analysis are presented in **Section 4.5.2**.

#### 4.5.1 COMPARISON OF MODEL RESULTS

In what follows, the models developed are compared according to three distinct criteria: performance, ability to satisfy the principle of causality and the computational costs required during the training and projection stages respectively.

##### 4.5.1.1 PERFORMANCE

Performance of the 15-member ensembles, each associated with one of the four algorithms (1D-CNN, H-HBVo, H-Lin, H-HBV), for all observation wells in each of the 6 clusters C1 to C6 are shown in **Figure 27**. For all four algorithms, the percentage bias (PBIAS) hovers around 0 with values below 5% in absolute terms, regardless of the cluster. As PBIAS is a measure of the average tendency of simulated values to be larger or smaller than observed values, it can be deduced that, on average, simulations tend to be very close to observations, regardless of the algorithm.

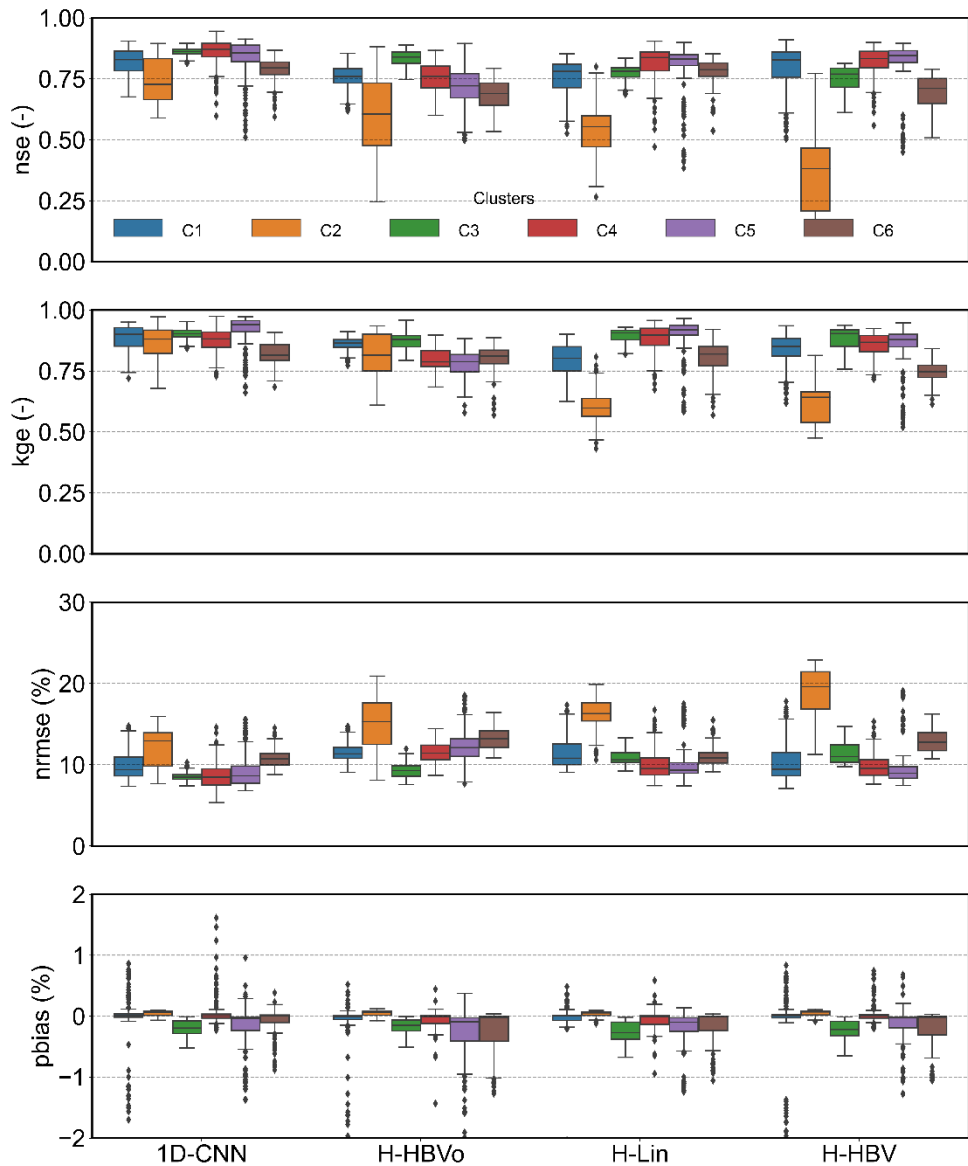


**Figure 27** Performance of 15-member ensembles, each associated with one of the four algorithms (1D-CNN, H-HBVo, H-Lin and H-HBV), for all observation wells in each of the 6 clusters. Clusters C1 to C6 each contain 24, 6, 7, 11, 13 and 9 observation wells respectively.

It can be noted that the values of NRMSE are on average fairly close to 12% for all algorithms and all clusters, with a median ranging from 8% to 13%. The exception is cluster 2, where the highest NRMSE values are recorded, with a median ranging from 13% to almost 20%. NRMSE values of 12% on average mean that the dispersion of simulation quality represents 12% of the GWL time series

amplitude, and is therefore an acceptable value. For cluster 2, in addition to the highest NRMSE values observed, there is a strict increase in NRMSE between the 1D-CNN model and the H-HBV model, from around 13% to around 20%. This tends to indicate that, in some cases, the more the algorithm is constrained, the more its performance decreases. For all clusters except cluster 2, all algorithms show NSE and KGE values overall above 0.5 and 0.7 respectively, indicating sufficiently high predictive power. For cluster 2, the 1D-CNN and H-HBVo algorithms exhibit NSE and KGE values globally above 0.5 and 0.7, respectively, while the H-Lin and H-HBV models show values globally below the acceptability criteria. H-Lin and H-HBV are algorithms with strong constraints (CRC), which tends to indicate that the flexibility of these two algorithms is reduced compared to 1D-CNN and H-HBVo. It's also clear that 1D-CNN performs slightly better than H-Lin, which performs marginally better than H-HBV, which in turn performs relatively better than H-HBVo as regards to NSE and KGE values. In fact, for all but cluster 2, median NSE and KGE values are between 0.8 and 0.87 and between 0.82 and 0.94, respectively, for 1D-CNN, from 0.69 to 0.84 and 0.79 to 0.88 for H-HBVo, from 0.78 to 0.84 and 0.8 to 0.92 for H-Lin and from 0.71 to 0.85 and 0.75 to 0.9 for H-HBV.

Overall, the 1D-CNN algorithm performed slightly better than the hybrid algorithms. The hybrid algorithms based on our formulation (H-Lin and H-HBV) together achieved slightly better results than the traditional hybrid algorithm (H-HBVo) for all clusters, with the exception of cluster 2, where H-HBVo performed better. A comparison of the GWLs observed and simulated using the four algorithms is shown in **Figure 28**, with observation well 02000002 (for location, see **Figure 25**) as an illustration.

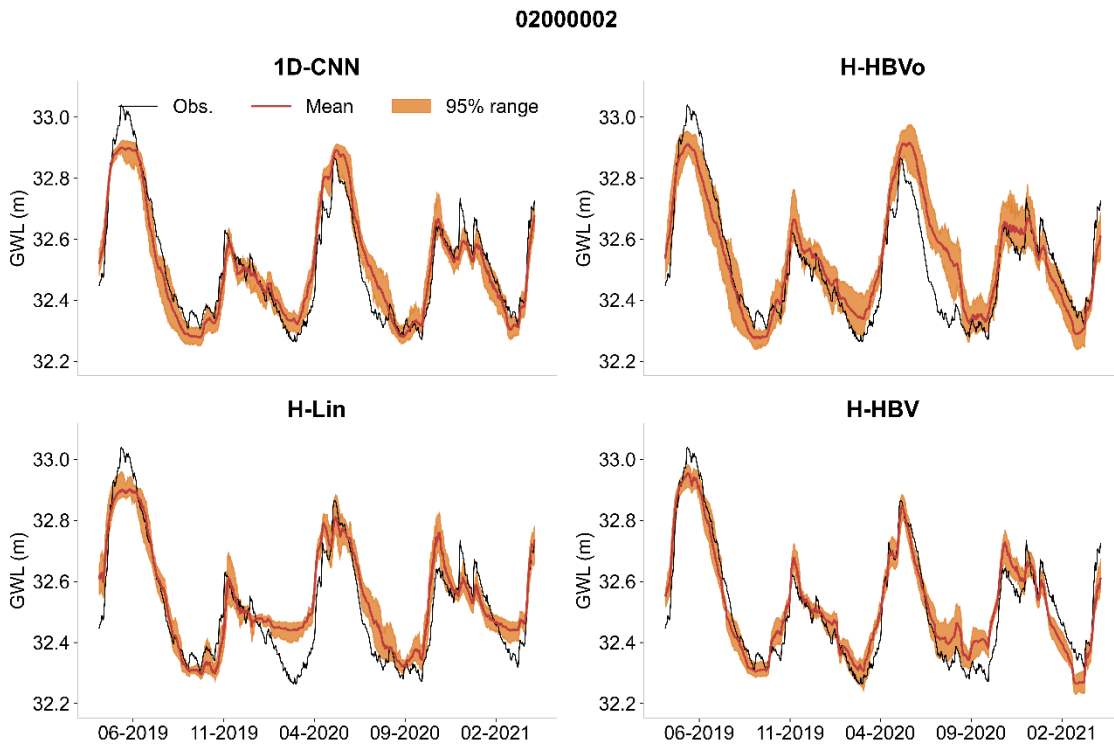


**Figure 28** Groundwater levels observed and simulated by the four models, namely 1D-CNN, H-HBVo, H-Lin and H-HBV at observation well 02000002 during the testing stage. Further illustrations are provided in the Supplementary Material 2 (Adombi 2023e).

Analysis of **Figure 28** shows that the simulations of the four algorithms fit the observations fairly well, with a slight inaccuracy for the H-Lin algorithm during the second half of winter 2019-2020. More importantly, 1D-CNN and H-HBVo show greater variation in the simulations than H-Lin and H-HBV, which are clearly under-dispersed (results not shown). This tends to show that imposing strong constraints on algorithm parameters reduces the range of values that these parameters can take, thus forcing a reduction in the variability of the resulting ensemble and, in turn, leading to less consideration of the uncertainties that may be associated with the modeling process.

#### 4.5.1.2 ABILITY TO LEARN CAUSAL RELATIONSHIPS

Beyond performance, trust in a model necessarily relies on its ability to learn causal relationships between input and output variables. To examine the ability of the four algorithms studied to satisfy the principle of causality, the SHAP value is considered.

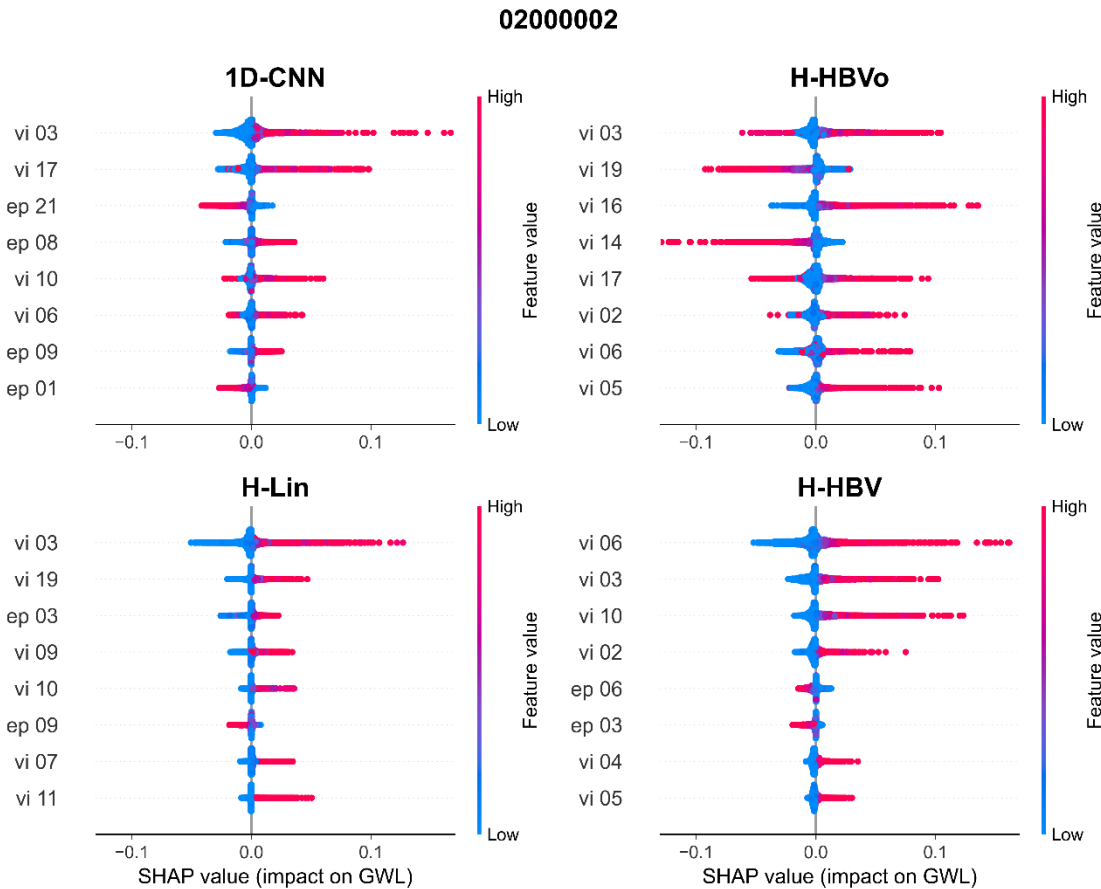


**Figure 29** Impact of vertical inflow (vi) and potential evapotranspiration (ep) on groundwater levels using the SHAP summary plot for the four algorithms studied. Only the first 8 most decisive variables are shown. The number associated with each variable represents an observation well number in the cluster to which well 02000002 belongs.

In particular, Shapley value allows for a graphical examination of the impact of the input variables on the output variable. Observation well 02000002 is used for illustration purposes (**Figure 29**). It should be noted that the conclusions drawn from the analysis of the results for the well

02000002 can be generalized to all other observation wells. Further illustrations are provided in the Supplementary Material 3 (Adombi 2023g).

The 1D-CNN SHAP summary plot shows that the first three input variables (vi03, vi17, ep21) and the last one (ep01) have physically consistent impacts on GWL. For these variables, an increase in vertical inflow leads to an increase in GWL ( $\text{SHAP} > 0$ ) and vice versa ( $\text{SHAP} < 0$ ), and an increase in potential evapotranspiration leads to a decrease ( $\text{SHAP} < 0$ ) in GWL and vice versa ( $\text{SHAP} > 0$ ). However, for the other four variables, their impact on GWL is not physically consistent. For example, some increases in variable vi10 (vertical inflow) lead to a decrease in GWL, while increases in variable ep09 (potential evapotranspiration) result in an increase in GWL. The impact of variables such as vi10 or ep09 on GWL changes is not consistent with what is known consensually about groundwater flow dynamics. This means that, overall, the 1D-CNN algorithm does not satisfy the principle of causality. A similar conclusion can be drawn from the analysis of the hybrid algorithm H-HBVo. For the H-Lin algorithm, all variables have a physically consistent impact on GWL, with the exception of ep03 (potential evapotranspiration). Finally, for the H-HBV algorithm, all variables show a monotonic relationship with GWL, indicating that this algorithm is the one with the best causality property. It can also be noted that for H-HBV, the most important decision variables for GWL development are vertical inflows. Indeed, on the basis of illustrative case 02000002, but also for the majority of observation wells (see **Supplementary Material 3**, Adombi (2023g)), at least the first two most significant variables are vertical inflows, which is not surprising given that the study area has a cold, humid climate.

From the above, it can be deduced that the algorithms that have been subjected to the constraints presented in **Section 4.4.1.4** are those that exhibit satisfactory causality properties, but above all that the integration of domain knowledge is not sufficient to obtain causal and therefore interpretable models within the framework of hybrid algorithms, i.e., coupling a theory-guided block and a traditional machine-learning block. Among the above algorithms, the H-Lin algorithm may

represent a good compromise between H-HBV and the 1D-CNN and H-HBVo algorithms. Indeed, its architecture is clearer and simpler than that of H-HBV, enabling it to be run at similar costs to 1D-CNN (**Figure 30**), while presenting satisfactory causality properties with, however, some artifacts. In the following, only the H-HBV algorithm will be used, as it gives satisfactory results and fully respects the causality properties.

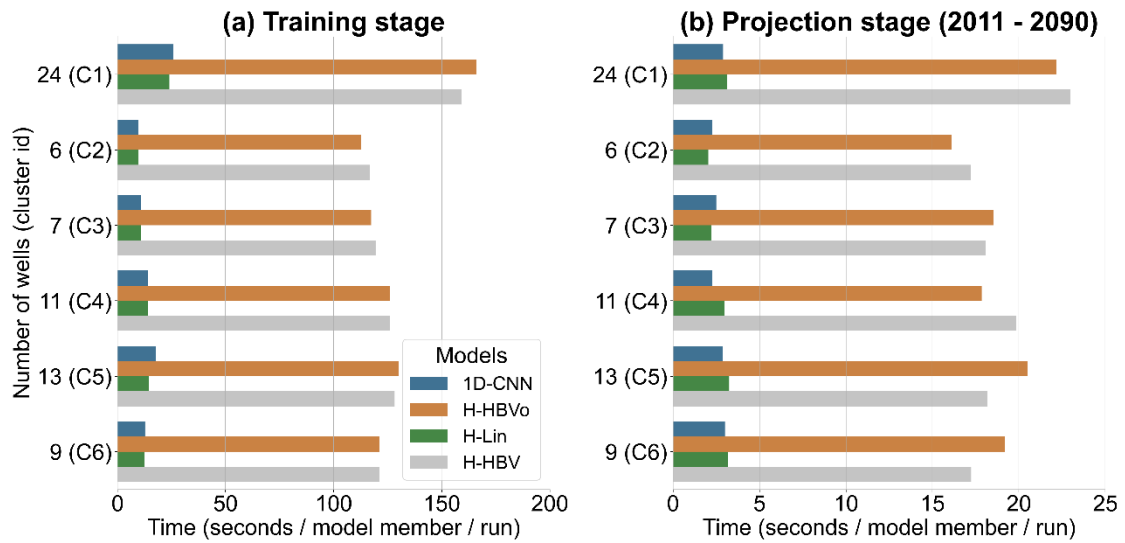


**Figure 30** Computation time (CPU) required for a single model member per run in (a) the training stage and (b) the projection stage.

Each algorithm is trained over K epochs (60 in this study), during which M small parts of the training data (called batches) are fed to the algorithm. At the end of an epoch, a gradient descent algorithm is used to update the algorithm's parameters (weights and biases). Thus, in training mode, the training time is dependent on the time required for  $M * K$  data passes through the algorithm and the time associated with K uses of the gradient descent algorithm. In inference mode (projection), all projection data are fed into the algorithm at once, producing the output without any gradient calculation. This essentially explains the difference in computation time between the training and projection stages.

#### 4.5.2 CLIMATE CHANGE EFFECT ANALYSIS

In this section, for each of the clusters, the H-HBV algorithm was trained 15 times to build up a 15-member ensemble. The choice of the H-HBV algorithm is motivated by its ability to fully satisfy the principle of causality. The ensembles were then used to assess the effects of climate change on GWL development in Quebec, Canada. As the H-HBV model showed poor performance for cluster 2, containing 6 observation wells, this cluster is excluded from the analysis, which is therefore carried out using all 64 observation wells out of a total of 70. Data from the RCP4.5 and RCP8.5 scenarios for the CMIP5 climate ensemble, and from the SSP2-4.5 and SSP5-8.5 scenarios for CMIP6, are considered. Be reminded that our CMIP6 data has a higher spatial resolution than our CMIP5 data. After training the models with observed climate data obtained from the climate stations closest to the observation wells, CMIP5 and CMIP6 data are used to feed the models in order to project GWLs between 2011 and 2090. After running the H-HBV model to produce annual time series of GWLs, trends in GWL are calculated using the TFPW-MK method. TFPW-MK is used here because it eliminates the negative effect of data autocorrelation on MK test performance, thus satisfying the independence condition required by this MK test (for more details, see Yue et al., 2002). **Figure 31** summarizes the changes in vertical inflow and potential evapotranspiration over the 80 years period from 2011 to 2090, according to the different CMIP 5 and 6 scenarios.

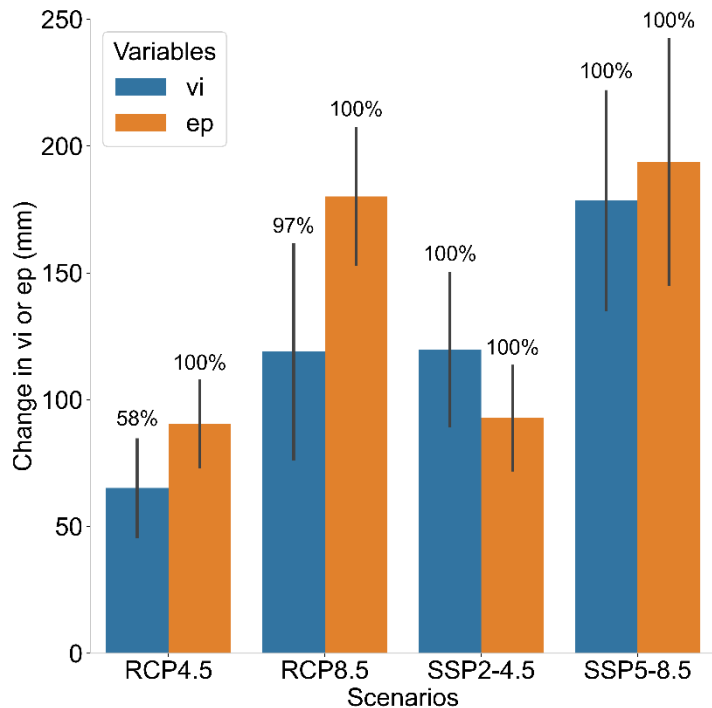


**Figure 31** Mean change and associated standard deviation in vertical inflow and potential evapotranspiration based on trends from 2011 to 2090 over the entire study area. Trends were calculated using the TFPW-MK method, and the percentage of significant trends is indicated.

For all scenarios, there is a simultaneous increase in vertical inflow and potential evapotranspiration for the period 2011 – 2090. The magnitude of the increase in vertical inflow is generally lower than or roughly equal to that of potential evapotranspiration, with the exception of scenario SSP2-4.5, for which the increase in vertical inflow is greater than that of potential evapotranspiration. However, given that vertical inflows are the most important drivers for almost all ensemble members using the H-HBV model for projection, it is possible that an increase in GWL will be observed for all scenarios, with potential evapotranspiration acting as a mitigating factor for this potential increase.

In what follows, only the results of the RCP8.5 and SSP5-8.5 scenarios are presented, as the same conclusions are drawn regarding the direction of groundwater level evolution whatever the

climate scenario. Graphs showing the results of the other two scenarios (RCP4.5 and SSP2-4.5) are presented in **Appendix I**.

Changes in GWL over the period 2011 - 2090 are shown in **Figure 32** for RCP scenarios and in **Figure 33** for SSP scenarios. For RCP8.5 (**Figure 32**), a general increase in GWL is observed, with a median amplitude of +5.6 cm for almost all observation wells, with a significant trend percentage of at most 90%. For 25% of the wells showing an increase in GWL, the amplitude of the increase is greater than +8 cm, and exceeds +14 cm for some wells, even reaching +35 cm in exceptional cases. These few wells with relatively substantial GWL increases (~ +35 cm) are located in the northeastern part of the study area, near the St. Lawrence River. However, for some wells located mainly to the south of the study area, 25% of the calculated trends (first quartile) show a decline in the 97.5% annual GWL percentile of up to -10 cm.

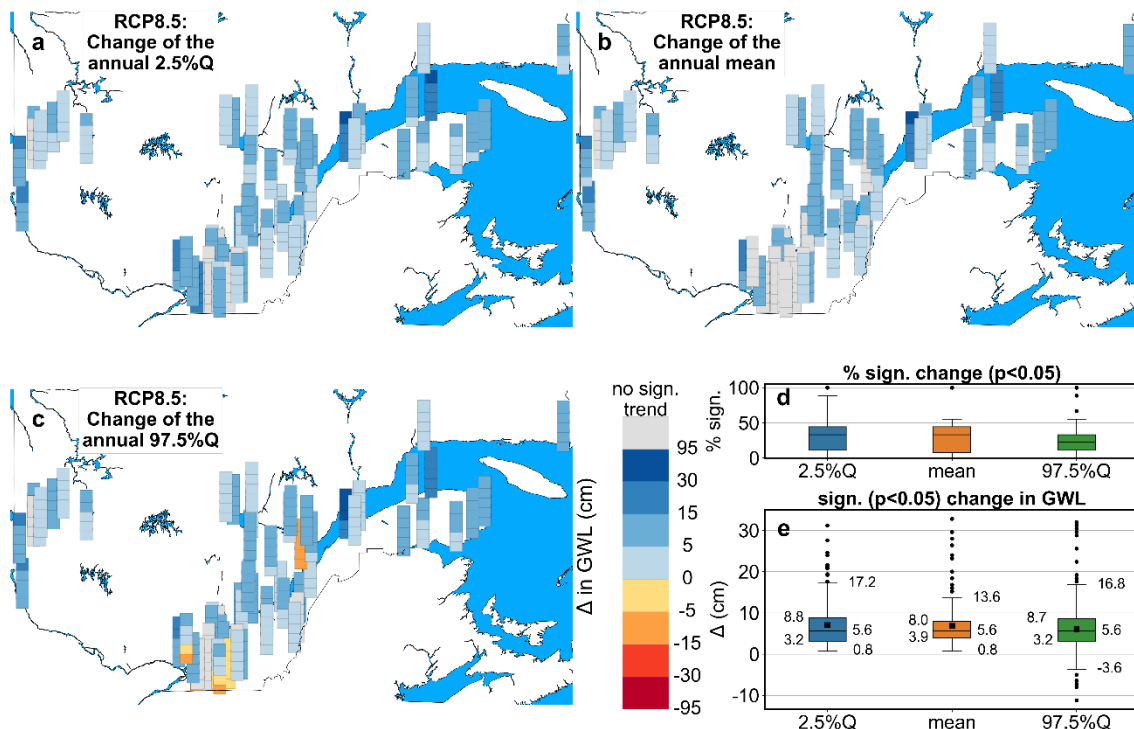


**Figure 32** Change in groundwater levels over the period 2011 - 2090 for each well, for all 15-member H-HBV ensembles, for all RCP8.5 scenario simulations, based on trend analysis with the TFPW-MK method on projected GWLs: **a** 2.5% percentile, **b** mean and **c** 97.5% percentile. Each observation well is represented by a band which is a boxplot providing from bottom to top the

minimum GWL change value, the 25% percentile value, the median, the 75% percentile and the maximum value. **d** Boxplots of the percentage of significant trends and (e) boxplots of significant changes in GWL for **a - c**. Note that the adoption of the 2.5% and 97.5% percentiles allows 95% of the uncertainties associated with the climate data and machine learning models used to be covered.

Finally, for SSP5-8.5 (**Figure 33**), a general increase in GWL is also observed, with a median amplitude of +7.0 cm for almost all observation wells, with a significant trend percentage of at most 100%. For 25% of wells showing an increase in GWL, the amplitude of the increase is greater than +11 cm, and exceeds +21.6 cm for some wells, even reaching +70 cm in exceptional cases. These results on GWL development over the period 2011 - 2090 are consistent with the changes observed in vertical inflows and potential evapotranspiration over the same period, and with the fact that vertical inflows are the most important decision variables in the developed models.

In summary, it can be seen that the RCP and SSP scenarios lead to more or less the same results, i.e. an increasing trend in groundwater levels over the period 2011 - 2090, with median amplitudes varying between +5.6 and +7.0 cm. The physical significance of changes in GWL depends on several factors, such as the geological nature of the aquifer (granular, fractured rock, ...), its hydrodynamic properties and its degree of confinement. For a fractured crystalline rock aquifer, amplitudes of several tens of meters are possible, whereas a granular aquifer can only have an amplitude of a few centimeters, due to storage coefficients. In this study, 69% of wells were in semi-confined or unconfined aquifers and 64% in granular contexts. A median amplitude of 5.6 to 7.0 cm remains low but physically significant. Similarly, for 25% of wells, the amplitudes of increase in GWL vary between +8.0 and +11.0 cm, can exceed between +14.0 and +23 cm, and can even reach between +35.0 and +70 cm in exceptional cases.

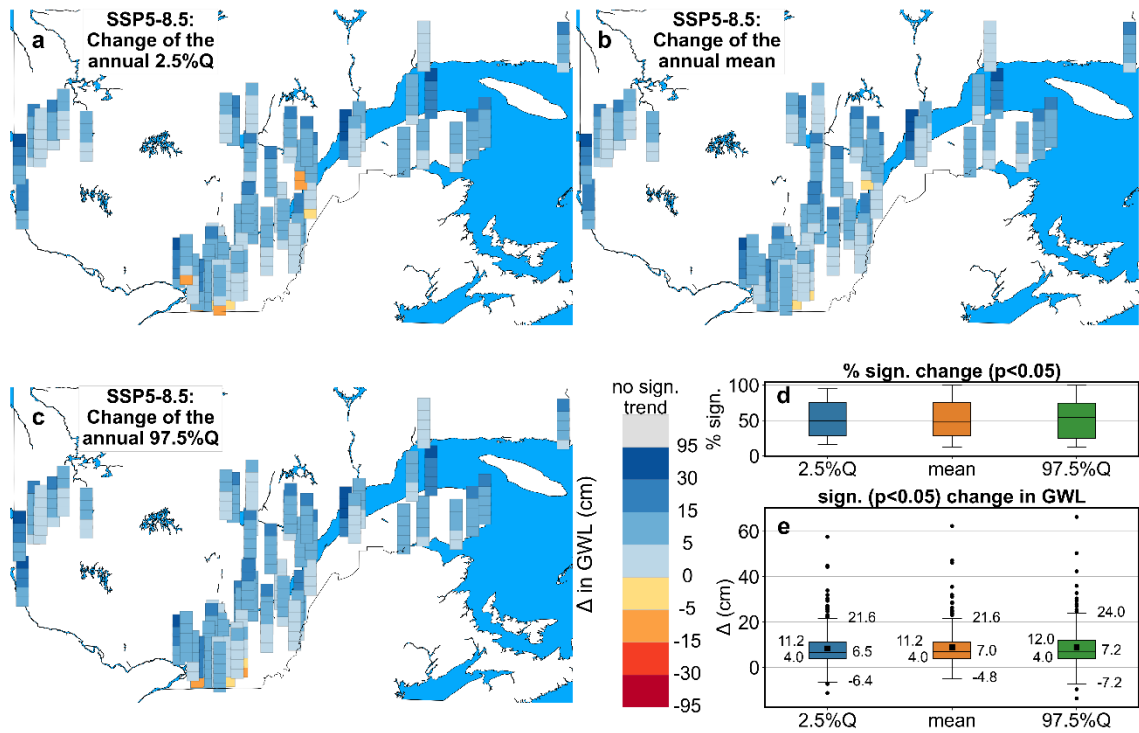


**Figure 33** Change in groundwater levels over the period 2011 - 2090 for each well, for all 15-member H-HBV ensembles, for all SSP5-8.5 scenario simulations, based on trend analysis with the TFPW-MK method: **a** 2.5% percentile, **b** mean and **c** 97.5% percentile. **d** Boxplots of the percentage of significant trends and (e) boxplots of significant changes in GWL for **a - c**.

## 4.6 DISCUSSION

### 4.6.1 GENERAL DISCUSSION OF THE STUDY RESULTS

This study has shown that imposing specific constraints on neural network layer kernels, namely the non-negativity constraint and the choice of a positive-derivative activation function, is a necessary condition for a hybrid model to satisfy the causality relationships between inputs and outputs. These constraints are necessary in the context of multi-input / multi-output hybrid modeling. For single-output modeling, it's not impossible for the principle of causality to be satisfied, but it's a matter of serendipity, as the learning process has to be repeated until a model that satisfies this causal relationship is obtained, as in Wunsch et al. (2022). With the formulation proposed in this study, the principle of causality is consistently satisfied, although there may be a few artifacts that are

probably due to numerical errors. Besides, it should be noted that the proposed formulation imposes a strong constraint on kernels and activation functions, to the extent that in some situations, even if the principle of causality is upheld, predictive performance may be poor. This is particularly valid for cluster 2 in this study. It may be necessary to propose a formulation with weak constraints, along the lines of what has been done by Xu et al. (2021) in the context of hybrid models for distributed modeling. Overall, the proposed formulation has produced satisfactory results in terms of performance and adequacy of the principle of causality, and can be used successfully for multi-input / multi-output and single-output modeling.

Given that machine learning models are often criticized for their mitigated ability to generalize on data that is statistically different from that used for training (Chen et al. 2020a), developing models that are able to “rationalize correctly” due to their causal properties is one way of dealing with generalization concerns, particularly when these models are intended to be used for forecasting/projection.

The proposed formulation, used to project GWL under different climate scenarios, proved highly effective, since the development of GWL is highly consistent not only with the principle of causality and importance of the input variables in determining model results, but also with the changes in the input variables, namely vertical inflow and potential evapotranspiration. It is also found that the ensemble methodology used to analyze the effects of climate change, involving the causal hybrid models (H-HBV), resulted in H-HBV ensembles that are under-dispersed (results not shown), i.e. they are unable to represent all possible types of uncertainty that would have enabled the model simulations to fully encompass GWL observations. This was to be expected, since the members of the ensembles differ only in the values of their parameters, i.e. only the uncertainty of these parameters has been considered. Under-dispersion is a very common challenge in ensemble simulations and forecasting (Sylvain et al. 2021). In order to correct the under-dispersion of ensembles so that the predictive distribution has sufficient coverage probability, post-processing methods, such as quantile regression forest (QRF) (Nguyen et al. 2015; Taillardat et al. 2016), may

be applied. Future studies could examine the effects of applying the QRF method to the H-HBV ensembles in this study on GWL projections. This is beyond the scope of the present study.

Finally, this study showed that the RCP4.5 and RCP8.5 scenario of CMIP5, as well as the SSP2-4.5 and SSP5-8.5 scenarios of CMIP6, predict a general increase in GWL with median amplitudes varying between +5.6 and +7.0 cm over the period 2011 - 2090. However, in some cases, the amplitude of the increase can exceed between +14.0 and +23 cm, and can even reach between +35.0 and +70 cm. These results also show that the difference in grid size between CMIP5 (low resolution) and CMIP6 (high resolution) had no significant impact on GWL evolution, since comparable GWL projections were obtained. The comparable results obtained between CMIP5 and CMIP6 could be partly explained by the modeling approach adopted in this study, i.e., the multi-input/multi-output modeling approach, which could attenuate the sensitivity of CMIP6 to the effects of local variations. Finally, the results of the GWL projection obtained are consistent with the trends observed in vertical inflows and potential evapotranspiration, as well as with the fact that vertical inflows are the most important decision variables in the developed models.

#### **4.6.2 PREVIOUS STUDIES ON THE EFFECTS OF CLIMATE CHANGE ON GWL DEVELOPMENT IN NORTH AMERICA**

It is important to note that most previous studies examine the impact of climate change on GWL development indirectly through recharge (Negm et al. 2021), in contrast to our study where the impact is assessed directly on groundwater levels. Furthermore, changes in recharge in previous studies are generally expressed in relative terms (%), whereas in our study, changes are assessed in absolute terms. Consequently, the comparison is made here with greater emphasis on the direction of development, even if quantities are presented.

Meixner et al. (2016) reviewed existing studies on the potential impact of climate change on groundwater recharge in eight representative aquifers west of the 100th parallel in the United States. It emerges that in the southern aquifers, an average 10-20% decline in total recharge is estimated, but with a wide margin of uncertainty that includes no change, while the northern aquifers as a whole should see little change or slight increases in total recharge.

Larocque et al. (2019) reviewed 22 studies summarizing the state of knowledge on the possible impacts of climate change on groundwater dynamics in Eastern Canada, including provinces such as Ontario and Quebec. In Ontario, studies have been carried out only in the southwest, mainly on the Grand River watershed aquifer (6800 km<sup>2</sup>), using various hydrological modeling approaches and projections spread over periods ranging from 20 to 60 years, with the earliest projection horizon starting in 2020 (Larocque et al. 2019). Jyrkama and Sykes (2007) predicted an increase in future groundwater recharge from +10% to +53%. Brouwers (2007) forecasts an increase of +0.36 mm (urban area, 2040-2060) to +4.12 mm (agricultural land, 2060-2080) in monthly recharge. Colautti (2010) anticipated changes of -0.55 m to +1.25 m in GWL. Motiee and McBean (2017) predicted changes of +7% to +12% in recharge. In Quebec, studies have been carried out on the Rivière des Anglais area (690 km<sup>2</sup>, Montérégie region) and the Lanoraie peatland complex (364 km<sup>2</sup>), using various hydrological modeling approaches and projections spread over periods ranging from 24 to 32 years, with the earliest projection horizon starting in 2010 and the latest in 2071 (Larocque et al. 2019). Sulis et al. (2011) estimated a +16% change in total recharge due to climate change in the Rivière des Anglais, while Sulis et al. (2012) projected in the same area a -15% to -4% change in total recharge. Bourgault et al. (2013) projected a 0% to -50% change in total recharge in the Lanoraie peatland complex.

Overall, most of these studies show an increase in recharge (Brouwers 2007; Jyrkama and Sykes 2007; Meixner et al. 2016; Motiee and McBean 2017; Sulis et al. 2011), in line with the results of our study. However, in some cases, a decrease in recharge or a mixed trend is expected (Bourgault

et al. 2013; Colautti 2010; Sulis et al. 2012). As Larocque et al. (2019) points out, the variability in projections may be due to the use of different climate models, emissions scenarios, data processing methods, future time horizons and hydrological modeling approaches. It should be noted, however, that the increase in GWL in our study occurs at a relatively low median amplitude compared with the duration of the study (80 years).

#### 4.7 CONCLUSION

In this study, we have proposed a physics-informed hybrid model formulation to satisfy the principle of causality that is essential to increase confidence in a model. The proposed formulation was then used to develop a first type of hybrid model called H-HBV, which encompasses the hydrological conceptual model HBV, and a second type of hybrid model, which encompasses a simple linear conceptual model (H-Lin). These two types of model were then compared against a purely data-driven 1D-CNN model and a hybrid model (H-HBVo) that ignored our formulation, in terms of performance and ability to learn cause-and-effect relationships in a multi-input/multi-output modeling approach. The results showed that the 1D-CNN algorithm performs slightly better than the hybrid algorithms, and that the H-Lin and H-HBV algorithms together achieved slightly better results than the traditional hybrid algorithm (H-HBVo). It was also shown that the algorithms subjected to our formulations (H-Lin and H-HBV) are the ones with satisfactory causality properties, but above all that the integration of domain knowledge is not sufficient to obtain causal and therefore interpretable models within the framework of hybrid algorithms.

Subsequently, 15-member ensembles using the H-HBV algorithm were used to project the impact of climate change on GWL development over the period 2011 - 2090 in Quebec (Canada) according to bias corrected CMIP5 simulations driven by RCP 4.5 and RCP 8.5 scenarios and bias corrected CMIP6 simulations driven by SSP2-4.5 and SSP5-8.5. The results showed that the RCP4.5 and RCP8.5 scenarios (CMIP5), as well as the SSP2-4.5 and SSP5-8.5 scenarios (CMIP6), predict

a general increase in GWL with median amplitudes varying between +5.6 and +7.0 cm over the period 2011 - 2090. In some cases, the amplitude of the increase can exceed between +14.0 and +23 cm, and can even reach between +35.0 and +70 cm. These results are consistent with the trend in vertical inflow and potential evapotranspiration for the different climate scenarios, as well as with the fact that vertical inflow is the most important decision variable in the models developed, confirming the robustness of the formulation we propose. Also, the proposed formulation can be successfully applied to multi-input/multi-output or single-output modeling tasks, and can also be generalized to various geoscientific fields and the physical sciences in general. Finally, over time, new data from the Quebec Ministry of Environment's monitoring network may be collected, enabling the results obtained in this study to be updated.

#### **CRediT authorship contribution statement**

**AVDP Adombi:** Conceptualization, Methodology, Data curation, Software, Investigation, Formal analysis, Visualization, Validation, Writing - Original draft preparation. **Romain Chesnaux:** Conceptualization, Supervision, Resources, Reviewing and Editing. **Marie-Amélie Boucher:** Conceptualization, Supervision, Reviewing and Editing. **Marco Braun:** Conceptualization, Review and Editing, Data Curation. **Juliette Lavoie:** Conceptualization, Data Curation.

#### **Funding sources**

The authors acknowledge the financial support of the Natural Science and Engineering Research Council (NSERC-federal funding) of Canada in the framework of the Individual Discovery Grant Program held by Prof. Romain Chesnaux. The financial support of Fondation de l'Université du Québec à Chicoutimi (FUQAC), Rio Tinto Graduate Scholarships Program, as well as Fonds de Recherche du Québec - Nature et Technologie (FRQNT-provincial funding) are also acknowledged.

### **Competing Interests**

The authors declare that they have no known competing financial interests or personal relationships that could have appeared to influence the work reported in this paper.

### **Data and code availability**

Time series of groundwater level observations can be retrieved in (MELCCFP 2023c). Climate simulations can be requested from Ouranos. Codes is available at Adombi (2023d). Please note that the code for the theory-guided layer is inspired by that of (Jiang et al. 2020).

### **Acknowledgements**

The authors would like to thank the Quebec Ministry of Environment for the data provided. The authors are also grateful to the Ouranos Consortium (and Rondeau-Genesse Gabriel of Ouranos) for providing downscaled and bias-corrected climate scenarios and acknowledge the model output data from the World Climate Research Programme's Coupled Modelling Intercomparison Project Phases 5 and 6 (CMIP5, CMIP6), as well as the gridded observation data made available by Natural Resources Canada's (NRCan) and the ERA5-Land reanalysis data made available by the Copernicus Climate Change and Atmosphere Monitoring Services.

## REFERENCES

- Adombi, A.V.D.P. 2023d. Code: Proposal of a causal theory-guided Deep Learning formulation for groundwater flow modeling. Zenodo. doi:<https://doi.org/10.5281/zenodo.8155740>.
- Adombi, A.V.D.P. 2023e. Supplementary Material 2. Available from [https://github.com/avadombi/SupplementaryMaterial/blob/main/Article4/Supplementary\\_Material\\_2.docx](https://github.com/avadombi/SupplementaryMaterial/blob/main/Article4/Supplementary_Material_2.docx).
- Adombi, A.V.D.P. 2023f. Supplementary Material 1. Available from [https://github.com/avadombi/SupplementaryMaterial/blob/main/Article4/Supplementary\\_Material\\_1.docx](https://github.com/avadombi/SupplementaryMaterial/blob/main/Article4/Supplementary_Material_1.docx).
- Adombi, A.V.D.P. 2023g. Supplementary Material 3. Available from [https://github.com/avadombi/SupplementaryMaterial/blob/main/Article4/Supplementary\\_Material\\_3.docx](https://github.com/avadombi/SupplementaryMaterial/blob/main/Article4/Supplementary_Material_3.docx).
- Adombi, A.V.D.P., Chesnaux, R., and Boucher, M.-A. 2021. Review: Theory-guided machine learning applied to hydrogeology—state of the art, opportunities and future challenges. *Hydrogeology Journal*, **29**: 2671-2683. doi:<https://doi.org/10.1007/s10040-021-02403-2>.
- Asher, M.J., Croke, B.F.W., Jakeman, A.J., and Peeters, L.J.M. 2015. A review of surrogate models and their application to groundwater modeling. *Water Resources Research*, **51**: 5957-5973. doi:<https://doi.org/10.1002/2015WR016967>.
- Banadkooki, F.B., Ehteram, M., Ahmed, A.N., Teo, F.Y., Fai, C.M., Afan, H.A., Sapitang, M., and El-Shafie, A. 2020. Enhancement of groundwater-level prediction using an integrated machine learning model optimized by whale algorithm. *Natural resources research*, **29**: 3233-3252. doi:<https://doi.org/10.1007/s11053-020-09634-2>.
- Bergström, S. 1976. Development and application of a conceptual runoff model for Scandinavian catchments.
- Bock, L., Lauer, A., Schlund, M., Barreiro, M., Bellouin, N., Jones, C., Meehl, G.A., Predoi, V., Roberts, M.J., and Eyring, V. 2020. Quantifying Progress Across Different CMIP Phases With the

ESMValTool. Journal of Geophysical Research: Atmospheres, **125**: e2019JD032321.

doi:<https://doi.org/10.1029/2019JD032321>.

Bourgault, M.A., Larocque, M., and Roy, M. 2013. Simulation of aquifer-peatland-river interactions under climate change. Hydrology Research, **45**: 425-440.  
doi:<https://doi.org/10.2166/nh.2013.228>.

Bowes, B.D., Sadler, J.M., Morsy, M.M., Behl, M., and Goodall, J.L. 2019. Forecasting Groundwater Table in a Flood Prone Coastal City with Long Short-term Memory and Recurrent Neural Networks. Water, **11**: 1098. doi:<https://doi.org/10.3390/w11051098>.

Brouwers, M.H. 2007. A case study for assessing the hydrologic impacts of climate change at the watershed scale. University of Waterloo, Ontario.

Bui, D.D., Kawamura, A., Tong, T.N., Amaguchi, H., and Nakagawa, N. 2012. Spatio-temporal analysis of recent groundwater-level trends in the Red River Delta, Vietnam. Hydrogeology Journal, **20**: 1635-1650. doi:<https://doi.org/10.1007/s10040-012-0889-4>.

Cai, H., Liu, S., Shi, H., Zhou, Z., Jiang, S., and Babovic, V. 2022. Toward improved lumped groundwater level predictions at catchment scale: Mutual integration of water balance mechanism and deep learning method. Journal of Hydrology, **613**: 128495.  
doi:<https://doi.org/10.1016/j.jhydrol.2022.128495>.

Chen, C., He, W., Zhou, H., Xue, Y., and Zhu, M. 2020a. A comparative study among machine learning and numerical models for simulating groundwater dynamics in the Heihe River Basin, northwestern China. Scientific reports, **10**: 1-13. doi:<https://doi.org/10.1038/s41598-020-60698-9>.

Chen, Y., Huang, D., Zhang, D., Zeng, J., Wang, N., Zhang, H., and Yan, J. 2021. Theory-guided hard constraint projection (HCP): A knowledge-based data-driven scientific machine learning method. Journal of Computational Physics, **445**: 110624.  
doi:<https://doi.org/10.1016/j.jcp.2021.110624>.

Clark, M.P., Fan, Y., Lawrence, D.M., Adam, J.C., Bolster, D., Gochis, D.J., Hooper, R.P., Kumar, M., Leung, L.R., Mackay, D.S., Maxwell, R.M., Shen, C., Swenson, S.C., and Zeng, X. 2015.

- Improving the representation of hydrologic processes in Earth System Models. *Water Resources Research*, **51**: 5929-5956. doi:<https://doi.org/10.1002/2015WR017096>.
- Colautti, D. 2010. Modelling the Effects of Climate Change on the Surface and Subsurface Hydrology of the Grand River Watershed. University of Waterloo, Ontario.
- De Mulder, W., Bethard, S., and Moens, M.-F. 2015. A survey on the application of recurrent neural networks to statistical language modeling. *Computer Speech & Language*, **30**: 61-98. doi:<https://doi.org/10.1016/j.csl.2014.09.005>.
- ECCC. 2022. Environment and Climate Change Canada.
- Esterhuizen, J.A., Goldsmith, B.R., and Linic, S. 2020. Theory-guided machine learning finds geometric structure-property relationships for chemisorption on subsurface alloys. *Chem*, **6**: 3100-3117. doi:<https://doi.org/10.1016/j.chempr.2020.09.001>.
- Eyring, V., Bony, S., Meehl, G.A., Senior, C.A., Stevens, B., Stouffer, R.J., and Taylor, K.E. 2016. Overview of the Coupled Model Intercomparison Project Phase 6 (CMIP6) experimental design and organization. *Geoscientific Model Development*, **9**: 1937-1958. doi:<https://doi.org/10.5194/gmd-9-1937-2016>.
- Faticchi, S., Vivoni, E.R., Ogden, F.L., Ivanov, V.Y., Mirus, B., Gochis, D., Downer, C.W., Camporese, M., Davison, J.H., Ebel, B., Jones, N., Kim, J., Mascaro, G., Niswonger, R., Restrepo, P., Rigon, R., Shen, C., Sulis, M., and Tarboton, D. 2016. An overview of current applications, challenges, and future trends in distributed process-based models in hydrology. *Journal of Hydrology*, **537**: 45-60. doi:<https://doi.org/10.1016/j.jhydrol.2016.03.026>.
- Fausett, L.V. 2006. Fundamentals of neural networks: architectures, algorithms and applications. Pearson Education India.
- Gagné, S., Larocque, M., Pinti, D.L., Saby, M., Meyzonnat, G., and Méjean, P. 2018. Benefits and limitations of using isotope-derived groundwater travel times and major ion chemistry to validate a regional groundwater flow model: example from the Centre-du-Québec region, Canada. *Canadian Water Resources Journal / Revue canadienne des ressources hydriques*, **43**: 195-213. doi:<https://doi.org/10.1080/07011784.2017.1394801>.

- Hoque, M.A., Hoque, M.M., and Ahmed, K.M. 2007. Declining groundwater level and aquifer dewatering in Dhaka metropolitan area, Bangladesh: causes and quantification. *Hydrogeology Journal*, **15**: 1523-1534. doi:<https://doi.org/10.1007/s10040-007-0226-5>.
- Hussain, F., Wu, R.-S., and Shih, D.-S. 2022. Water table response to rainfall and groundwater simulation using physics-based numerical model: WASH123D. *Journal of Hydrology: Regional Studies*, **39**: 100988. doi:<https://doi.org/10.1016/j.ejrh.2022.100988>.
- Jeong, J., Park, E., Chen, H., Kim, K.-Y., Shik Han, W., and Suk, H. 2020. Estimation of groundwater level based on the robust training of recurrent neural networks using corrupted data. *Journal of Hydrology*, **582**: 124512. doi:<https://doi.org/10.1016/j.jhydrol.2019.124512>.
- Jiang, S., Zheng, Y., and Solomatine, D. 2020. Improving AI System Awareness of Geoscience Knowledge: Symbiotic Integration of Physical Approaches and Deep Learning. *Geophysical Research Letters*, **47**: e2020GL088229. doi:<https://doi.org/10.1029/2020GL088229>.
- Jyrkama, M.I., and Sykes, J.F. 2007. The impact of climate change on spatially varying groundwater recharge in the grand river watershed (Ontario). *Journal of Hydrology*, **338**: 237-250. doi:<https://doi.org/10.1016/j.jhydrol.2007.02.036>.
- Karniadakis, G.E., Kevrekidis, I.G., Lu, L., Perdikaris, P., Wang, S., and Yang, L. 2021. Physics-informed machine learning. *Nature Reviews Physics*, **3**: 422-440. doi:<https://doi.org/10.1038/s42254-021-00314-5>.
- Karpatne, A., Atluri, G., Faghmous, J.H., Steinbach, M., Banerjee, A., Ganguly, A., Shekhar, S., Samatova, N., and Kumar, V. 2017. Theory-Guided Data Science: A New Paradigm for Scientific Discovery from Data. *IEEE Transactions on Knowledge and Data Engineering*, **29**: 2318-2331. doi:<https://doi.org/10.1109/TKDE.2017.2720168>.
- Khandelwal, A., Mithal, V., and Kumar, V. Post Classification Label Refinement Using Implicit Ordering Constraint Among Data Instances. In 2015 IEEE International Conference on Data Mining. 14-17 Nov. 2015 2015, pp. 799-804.
- Kiranyaz, S., Avci, O., Abdeljaber, O., Ince, T., Gabbouj, M., and Inman, D.J. 2021. 1D convolutional neural networks and applications: A survey. *Mechanical Systems and Signal Processing*, **151**: 107398. doi:<https://doi.org/10.1016/j.ymssp.2020.107398>.

- Knoben, W.J.M., Freer, J.E., and Woods, R.A. 2019. Technical note: Inherent benchmark or not? Comparing Nash–Sutcliffe and Kling–Gupta efficiency scores. *Hydrol. Earth Syst. Sci.*, **23**: 4323-4331. doi:<https://doi.org/10.5194/hess-23-4323-2019>.
- Knoben, W.J.M., Freer, J.E., Peel, M.C., Fowler, K.J.A., and Woods, R.A. 2020. A Brief Analysis of Conceptual Model Structure Uncertainty Using 36 Models and 559 Catchments. *Water Resources Research*, **56**: e2019WR025975. doi:<https://doi.org/10.1029/2019WR025975>.
- Kochhar, A., Singh, H., Sahoo, S., Litoria, P.K., and Pateriya, B. 2022. Prediction and forecast of pre-monsoon and post-monsoon groundwater level: using deep learning and statistical modelling. *Modeling Earth Systems and Environment*, **8**: 2317-2329. doi:<https://doi.org/10.1007/s40808-021-01235-z>.
- Konikow, L.F., and Kendy, E. 2005. Groundwater depletion: A global problem. *Hydrogeology Journal*, **13**: 317-320. doi:<https://doi.org/10.1007/s10040-004-0411-8>.
- Larocque, M., Cloutier, V., Levison, J., and Rosa, E. 2018. Results from the Quebec Groundwater Knowledge Acquisition Program. *Canadian Water Resources Journal / Revue canadienne des ressources hydriques*, **43**: 69-74. doi:<https://doi.org/10.1080/07011784.2018.1472040>.
- Larocque, M., Levison, J., Martin, A., and Chaumont, D. 2019. A review of simulated climate change impacts on groundwater resources in Eastern Canada. *Canadian Water Resources Journal / Revue canadienne des ressources hydriques*, **44**: 22-41. doi:<https://doi.org/10.1080/07011784.2018.1503066>.
- LeCun, Y., Boser, B., Denker, J.S., Henderson, D., Howard, R.E., Hubbard, W., and Jackel, L.D. 1989. Backpropagation applied to handwritten zip code recognition. *Neural computation*, **1**: 541-551. doi:<https://doi.org/10.1162/neco.1989.1.4.541>.
- Lehr, C., and Lischeid, G. 2020. Efficient screening of groundwater head monitoring data for anthropogenic effects and measurement errors. *Hydrol. Earth Syst. Sci.*, **24**: 501-513. doi:<https://hess.copernicus.org/articles/24/501/2020/>.
- Lijzen, J.P.A., Otte, P., and van Dreumel, M. 2014. Towards sustainable management of groundwater: Policy developments in The Netherlands. *Science of the Total Environment*, **485-486**: 804-809. doi:<https://doi.org/10.1016/j.scitotenv.2014.02.081>.

- Liu, Q., Gui, D., Zhang, L., Niu, J., Dai, H., Wei, G., and Hu, B.X. 2022. Simulation of regional groundwater levels in arid regions using interpretable machine learning models. *Science of the Total Environment*, **831**: 154902. doi:<https://doi.org/10.1016/j.scitotenv.2022.154902>.
- Lukoševičius, M., and Jaeger, H. 2009. Reservoir computing approaches to recurrent neural network training. *Computer Science Review*, **3**: 127-149. doi:<https://doi.org/10.1016/j.cosrev.2009.03.005>.
- Lundberg, S.M., and Lee, S.-I. 2017. A unified approach to interpreting model predictions. *Advances in neural information processing systems*, **30**.
- Luo, Q., Yang, Y., Qian, J., Wang, X., Chang, X., Ma, L., Li, F., and Wu, J. 2020. Spring protection and sustainable management of groundwater resources in a spring field. *Journal of Hydrology*, **582**: 124498. doi:<https://doi.org/10.1016/j.jhydrol.2019.124498>.
- Maxwell, R.M., Condon, L.E., and Kollet, S.J. 2015. A high-resolution simulation of groundwater and surface water over most of the continental US with the integrated hydrologic model ParFlow v3. *Geosci. Model Dev.*, **8**: 923-937. doi:<https://doi.org/10.5194/gmd-8-923-2015>.
- Medsker, L.R., and Jain, L. 2001. Recurrent neural networks. *Design and Applications*, **5**: 64-67.
- Meehl, G.A., Boer, G.J., Covey, C., Latif, M., and Stouffer, R.J. 2000. The coupled model intercomparison project (CMIP). *Bulletin of the American Meteorological Society*, **81**: 313-318.
- Meixner, T., Manning, A.H., Stonestrom, D.A., Allen, D.M., Ajami, H., Blasch, K.W., Brookfield, A.E., Castro, C.L., Clark, J.F., Gochis, D.J., Flint, A.L., Neff, K.L., Niraula, R., Rodell, M., Scanlon, B.R., Singha, K., and Walvoord, M.A. 2016. Implications of projected climate change for groundwater recharge in the western United States. *Journal of Hydrology*, **534**: 124-138. doi:<https://doi.org/10.1016/j.jhydrol.2015.12.027>.
- MELCCFP. 2023a. Programme d'acquisition de connaissances sur les eaux souterraines. Available from <http://www.mddelcc.gouv.qc.ca/eau/souterraines/programmes/acquisition-connaissance.htm> [accessed January 2023].
- MELCCFP. 2023b. Normales climatiques 1981-2010. Available from <https://www.environnement.gouv.qc.ca/climat/normales/climat-qc.htm2023>.

MELCCFP. 2023c. Réseau de suivi des eaux souterraines du Québec. Available from <https://www.environnement.gouv.qc.ca/eau/piezo/2023>.

Motiee, H., and McBean, E. 2017. Assessment of Climate Change Impacts on Groundwater Recharge for Different Soil Types-Guelph Region in Grand River Basin, Canada. Ecopersia, **5**: 1731-1744.

Negm, A., Abdurakhimova, P., Hayashi, M., and Rasouli, K. 2021. Effects of climate change on depression-focused groundwater recharge in the Canadian Prairies. Vadose Zone Journal, **20**: e20153. doi:<https://doi.org/10.1002/vzj2.20153>.

Nguyen, T.-T., Huang, J.Z., and Nguyen, T.T. 2015. Two-level quantile regression forests for bias correction in range prediction. Machine Learning, **101**: 325-343. doi:<https://doi.org/10.1007/s10994-014-5452-1>.

Oudin, L., Hervieu, F., Michel, C., Perrin, C., Andréassian, V., Anctil, F., and Loumagne, C. 2005. Which potential evapotranspiration input for a lumped rainfall–runoff model?: Part 2—Towards a simple and efficient potential evapotranspiration model for rainfall–runoff modelling. Journal of Hydrology, **303**: 290-306. doi:<https://doi.org/10.1016/j.jhydrol.2004.08.026>.

Pham, Q.B., Kumar, M., Di Nunno, F., Elbeltagi, A., Granata, F., Islam, A.R.M.T., Talukdar, S., Nguyen, X.C., Ahmed, A.N., and Anh, D.T. 2022. Groundwater level prediction using machine learning algorithms in a drought-prone area. Neural Computing and Applications, **34**: 10751-10773. doi:10.1007/s00521-022-07009-7.

Raissi, M., Perdikaris, P., and Karniadakis, G.E. 2019. Physics-informed neural networks: A deep learning framework for solving forward and inverse problems involving nonlinear partial differential equations. Journal of Computational Physics, **378**: 686-707. doi:<https://doi.org/10.1016/j.jcp.2018.10.045>.

Reichstein, M., Camps-Valls, G., Stevens, B., Jung, M., Denzler, J., Carvalhais, N., and Prabhat. 2019. Deep learning and process understanding for data-driven Earth system science. Nature, **566**: 195-204. doi:<https://doi.org/10.1038/s41586-019-0912-1>.

- Rey, N., Rosa, E., Cloutier, V., and Lefebvre, R. 2018. Using water stable isotopes for tracing surface and groundwater flow systems in the Barlow-Ojibway Clay Belt, Quebec, Canada. Canadian Water Resources Journal / Revue canadienne des ressources hydriques, **43**: 173-194. doi:<https://doi.org/10.1080/07011784.2017.1403960>.
- Riahi, K., van Vuuren, D.P., Kriegler, E., Edmonds, J., O'Neill, B.C., Fujimori, S., Bauer, N., Calvin, K., Dellink, R., Fricko, O., Lutz, W., Popp, A., Cuaresma, J.C., Kc, S., Leimbach, M., Jiang, L., Kram, T., Rao, S., Emmerling, J., Ebi, K., Hasegawa, T., Havlik, P., Humpenöder, F., Da Silva, L.A., Smith, S., Stehfest, E., Bosetti, V., Eom, J., Gernaat, D., Masui, T., Rogelj, J., Strefler, J., Drouet, L., Krey, V., Luderer, G., Harmsen, M., Takahashi, K., Baumstark, L., Doelman, J.C., Kainuma, M., Klimont, Z., Marangoni, G., Lotze-Campen, H., Obersteiner, M., Tabeau, A., and Tavoni, M. 2017. The Shared Socioeconomic Pathways and their energy, land use, and greenhouse gas emissions implications: An overview. Global Environmental Change, **42**: 153-168. doi:<https://doi.org/10.1016/j.gloenvcha.2016.05.009>.
- Rivera, A. 2014. Canada's groundwater resources. Fitzhenry & Whiteside.
- Rondeau-Genesse, G., and Braun, M. 2020. Production des scénarios climatiques pour les projets : Impact des changements climatiques sur les débits au Québec (cQ2) et la thématique Évolution du climat du projet de Soutien à INFO-Crue. Ouranos.
- Sahoo, S., Russo, T., Elliott, J., and Foster, I. 2017b. Machine learning algorithms for modeling groundwater level changes in agricultural regions of the US. Water Resources Research, **53**: 3878-3895.
- Schellekens, J. 2018. wflow Documentation. Detares, Delft.
- Secci, D., A. Godoy, V., and Gómez-Hernández, J.J. 2024. Physics-Informed Neural Networks for solving transient unconfined groundwater flow. Computers & Geosciences, **182**: 105494. doi:<https://doi.org/10.1016/j.cageo.2023.105494>.
- Secci, D., Giovanna Tanda, M., D'Oria, M., and Todaro, V. 2023. Artificial intelligence models to evaluate the impact of climate change on groundwater resources. Journal of Hydrology, **627**: 130359. doi:<https://doi.org/10.1016/j.jhydrol.2023.130359>.

- Slater, L.J., Arnal, L., Boucher, M.-A., Chang, A.Y.-Y., Moulds, S., Murphy, C., Nearing, G., Shalev, G., Shen, C., and Speight, L. 2023. Hybrid forecasting: blending climate predictions with AI models. *Hydrology and Earth System Sciences*, **27**: 1865-1889.
- Sulis, M., Paniconi, C., Rivard, C., Harvey, R., and Chaumont, D. 2011. Assessment of climate change impacts at the catchment scale with a detailed hydrological model of surface-subsurface interactions and comparison with a land surface model [<https://doi.org/10.1029/2010WR009167>]. *Water Resources Research*, **47**. doi:<https://doi.org/10.1029/2010WR009167>.
- Sulis, M., Paniconi, C., Marrocq, M., Huard, D., and Chaumont, D. 2012. Hydrologic response to multimodel climate output using a physically based model of groundwater/surface water interactions [<https://doi.org/10.1029/2012WR012304>]. *Water Resources Research*, **48**. doi:<https://doi.org/10.1029/2012WR012304>.
- Sulis, M., Meyerhoff, S.B., Paniconi, C., Maxwell, R.M., Putti, M., and Kollet, S.J. 2010. A comparison of two physics-based numerical models for simulating surface water–groundwater interactions. *Advances in Water Resources*, **33**: 456-467. doi:<https://doi.org/10.1016/j.advwatres.2010.01.010>.
- Sun, Y., Wendi, D., Kim, D.E., and Liang, S.Y. 2016. Technical note: Application of artificial neural networks in groundwater table forecasting – a case study in a Singapore swamp forest. *Hydrol. Earth Syst. Sci.*, **20**: 1405-1412. doi:10.5194/hess-20-1405-2016.
- Sylvain, J.-D., Anctil, F., and Thiffault, É. 2021. Using bias correction and ensemble modelling for predictive mapping and related uncertainty: A case study in digital soil mapping. *Geoderma*, **403**: 115153. doi:<https://doi.org/10.1016/j.geoderma.2021.115153>.
- Taillardat, M., Mestre, O., Zamo, M., and Naveau, P. 2016. Calibrated Ensemble Forecasts Using Quantile Regression Forests and Ensemble Model Output Statistics. *Monthly Weather Review*, **144**: 2375-2393. doi:<https://doi.org/10.1175/MWR-D-15-0260.1>.
- Tartakovsky, A.M., Marrero, C.O., Perdikaris, P., Tartakovsky, G.D., and Barajas-Solano, D. 2020. Physics-Informed Deep Neural Networks for Learning Parameters and Constitutive

- Relationships in Subsurface Flow Problems. Water Resources Research, **56**: e2019WR026731. doi:<https://doi.org/10.1029/2019WR026731>.
- Taylor, K.E., Stouffer, R.J., and Meehl, G.A. 2012. An Overview of CMIP5 and the Experiment Design. Bulletin of the American Meteorological Society, **93**: 485-498. doi:<https://doi.org/10.1175/BAMS-D-11-00094.1>.
- Vadyala, S.R., Betgeri, S.N., Matthews, J.C., and Matthews, E. 2022. A review of physics-based machine learning in civil engineering. Results in Engineering, **13**: 100316. doi:<https://doi.org/10.1016/j.rineng.2021.100316>.
- Valéry, A. 2010. Modélisation précipitations débit sous influence nivale : Elaboration d'un module neige et évaluation sur 380 bassins versants. Doctorat Hydrobiologie, Institut des Sciences et Industries du Vivant et de l'Environnement AgroParisTech.
- Valéry, A., Andréassian, V., and Perrin, C. 2014. 'As simple as possible but not simpler': What is useful in a temperature-based snow-accounting routine? Part 2 – Sensitivity analysis of the Cermeneige snow accounting routine on 380 catchments. Journal of Hydrology, **517**: 1176-1187. doi:<https://doi.org/10.1016/j.jhydrol.2014.04.058>.
- van Vuuren, D.P., Edmonds, J., Kainuma, M., Riahi, K., Thomson, A., Hibbard, K., Hurtt, G.C., Kram, T., Krey, V., Lamarque, J.-F., Masui, T., Meinshausen, M., Nakicenovic, N., Smith, S.J., and Rose, S.K. 2011. The representative concentration pathways: an overview. Climatic Change, **109**: 5. doi:<https://doi.org/10.1007/s10584-011-0148-z>.
- Wada, Y., van Beek, L.P.H., van Kempen, C.M., Reckman, J.W.T.M., Vasak, S., and Bierkens, M.F.P. 2010. Global depletion of groundwater resources. Geophysical Research Letters, **37**. doi:<https://doi.org/10.1029/2010GL044571>.
- Wagner, N., and Rondinelli, J.M. 2016. Theory-guided machine learning in materials science. Frontiers in Materials: 28. doi:<https://doi.org/10.3389/fmats.2016.00028>.
- Walter, J., Rouleau, A., Chesnaux, R., Lambert, M., and Daigneault, R. 2018. Characterization of general and singular features of major aquifer systems in the Saguenay-Lac-Saint-Jean region. Canadian Water Resources Journal / Revue canadienne des ressources hydriques, **43**: 75-91. doi:<https://doi.org/10.1080/07011784.2018.1433069>.

- Wang, N., Chang, H., and Zhang, D. 2021b. Theory-guided Auto-Encoder for surrogate construction and inverse modeling. *Computer Methods in Applied Mechanics and Engineering*, **385**: 114037. doi:<https://doi.org/10.1016/j.cma.2021.114037>.
- Wang, N., Zhang, D., Chang, H., and Li, H. 2020b. Deep learning of subsurface flow via theory-guided neural network. *Journal of Hydrology*, **584**: 124700. doi:<https://doi.org/10.1016/j.jhydrol.2020.124700>.
- Wang, S., Peng, H., and Liang, S. 2022. Prediction of estuarine water quality using interpretable machine learning approach. *Journal of Hydrology*, **605**: 127320. doi:<https://doi.org/10.1016/j.jhydrol.2021.127320>.
- Wei, A., Chen, Y., Li, D., Zhang, X., Wu, T., and Li, H. 2022. Prediction of groundwater level using the hybrid model combining wavelet transform and machine learning algorithms. *Earth Science Informatics*, **15**: 1951-1962. doi:<https://doi.org/10.1007/s12145-022-00853-0>.
- Wunsch, A., Liesch, T., and Broda, S. 2021. Groundwater level forecasting with artificial neural networks: a comparison of long short-term memory (LSTM), convolutional neural networks (CNNs), and non-linear autoregressive networks with exogenous input (NARX). *Hydrol. Earth Syst. Sci.*, **25**: 1671-1687. doi:<https://doi.org/10.5194/hess-25-1671-2021>.
- Wunsch, A., Liesch, T., and Broda, S. 2022. Deep learning shows declining groundwater levels in Germany until 2100 due to climate change. *Nature Communications*, **13**: 1-13. doi:<https://doi.org/10.1038/s41467-022-28770-2>.
- Xu, R., Zhang, D., Rong, M., and Wang, N. 2021. Weak form theory-guided neural network (TgNN-wf) for deep learning of subsurface single- and two-phase flow. *Journal of Computational Physics*, **436**: 110318. doi:<https://doi.org/10.1016/j.jcp.2021.110318>.
- Yoon, H., Jun, S.-C., Hyun, Y., Bae, G.-O., and Lee, K.-K. 2011. A comparative study of artificial neural networks and support vector machines for predicting groundwater levels in a coastal aquifer. *Journal of Hydrology*, **396**: 128-138. doi:<https://doi.org/10.1016/j.jhydrol.2010.11.002>.
- Yue, S., Pilon, P., Phinney, B., and Cavadias, G. 2002b. The influence of autocorrelation on the ability to detect trend in hydrological series. *Hydrological Processes*, **16**: 1807-1829. doi:<https://doi.org/10.1002/hyp.1095>.

## CHAPITRE 5

### DISCUSSIONS ET PERSPECTIVES DE RECHERCHE

#### **5.1 CONTRIBUTIONS ET IMPLICATIONS DU PROJET DE RECHERCHE**

##### **5.1.1 APPORT DE L'APPRENTISSAGE AUTOMATIQUE GUIDÉ PAR LA THÉORIE A LA MODÉLISATION HYDROGÉOLOGIQUE**

La nécessité de conceptualiser un monde souterrain invisible a conduit les hydrogéologues à aborder les problèmes de l'hydrogéologie par le biais de la modélisation. Cependant, les approches traditionnelles de modélisation présentent diverses limitations dans la résolution des problèmes hydrogéologiques. Récemment, l'apprentissage automatique guidé par la théorie (TgML) est apparue comme un possible moyen de contourner les limites des approches traditionnelles. Le TgML est une nouvelle branche de l'apprentissage automatique qui découle de l'hypothèse qu'en hybridant l'apprentissage automatique et des connaissances scientifiques (e.g., lois de conservation), les modèles résultants pourront bénéficier des forces combinées des approches traditionnelles de modélisation. L'objectif de cette thèse était de tester cette hypothèse sur deux problèmes d'écoulements souterrain : distribué et localisé.

Dans le premier problème d'écoulement distribué, un modèle TgML a été comparé à un modèle basé sur la physique et à un modèle d'apprentissage traditionnel. Le modèle TgML a montré une grande justesse de simulation tout en respectant les mécanismes physiques qui régissent l'écoulement des eaux souterraines. Cependant, il a nécessité des coûts de calcul plus élevés pour l'apprentissage que les autres modèles.

Aussi, il a été démontré dans cette thèse que les modèles TgML traditionnels pour la modélisation localisée étaient incapables de simuler correctement les processus hydrologiques en raison de leur transgression du principe de causalité. L'objectif était donc de développer des modèles TgML qui respectent le principe de causalité et de les comparer avec des modèles TgML traditionnels et des modèles d'apprentissage automatique traditionnels dans un problème d'écoulement localisé. Les nouveaux modèles TgML développés ont montré des performances et des propriétés causales satisfaisantes, alors que les autres modèles ne respectaient pas le principe de causalité. Il en ressort donc que l'intégration des connaissances scientifiques dans l'architecture des modèles d'apprentissage n'est pas suffisante pour obtenir des modèles causaux et donc interprétables. Cette conclusion avait fait, dans un certain sens, l'objet de spéculations par Nearing et al. (2021): « l'idée selon laquelle la compréhension hydrologique est nécessaire pour des prévisions fiables...n'est peut-être pas vraie ». Il est désormais possible de dire que l'intégration des connaissances de la physique dans l'architecture des algorithmes d'apprentissage est nécessaire mais pas suffisante pour des simulations et des prévisions fiables.

Les deux problèmes d'écoulement étudiés dans le cadre de cette thèse permettent de confirmer l'hypothèse principale de recherche selon laquelle l'apprentissage automatique guidé par la théorie peut bénéficier des atouts des approches traditionnelles de modélisation. Cela signifie que lorsque les objectifs de modélisation requièrent des modèles de grande justesse capables de contribuer à la compréhension de la dynamique des écoulements souterrains, l'apprentissage automatique guidé par la théorie peut s'avérer approprié. Cependant, compte tenu des résultats obtenus dans cette thèse, le potentiel de l'apprentissage automatique guidé par la théorie pour la modélisation hydrogéologique est atténué par les coûts de calcul beaucoup plus élevés qu'il requiert par rapport aux approches traditionnelles en phase d'entraînement (calibration). Toutefois, l'un des principaux attraits de l'apprentissage automatique est qu'il est généralement beaucoup moins coûteux en termes de calcul une fois qu'il a été appris (Gelbrecht et al. 2023).

### **5.1.2 ETUDE PRELIMINAIRE DE L'IMPACT DU CHANGEMENT CLIMATIQUE SUR L'EVOLUTION DES NIVEAUX D'EAU SOUTERRAINE AU QUÉBEC**

Dans cette thèse, une étude préliminaire de l'impact seul des variables climatiques – apports verticaux et évapotranspiration potentielle – sur l'évolution des niveaux d'eau souterraine du réseau de suivi piézométrique du Québec en contexte de changement climatique a également été réalisée. Des modèles d'apprentissage automatique, qui intègrent des équations de bilan hydrique dans leur architecture tout en respectant les principes de causalité, ont été développés. Les projections des niveaux d'eau souterraines se sont basées sur les scenarios climatiques RCP4.5 et RCP8.5 du CMIP5 (version 5 du projet d'intercomparaison des modèles couplés) et les scenarios SSP2-4.5 et SSP5-8.5 du CMIP6. Les résultats ont montré qu'indépendamment du scenario climatique considéré, une augmentation des niveaux piézométriques est projetée sur la période 2011-2090 avec des augmentations médianes variant entre +5,6 et +7 cm. Dans certains cas, l'augmentation pourrait dépasser +14 à +23 cm, voire atteindre +35 à +70 cm. Ces résultats préliminaires ne demandent qu'à être infirmés ou confirmés. C'est pourquoi des travaux complémentaires doivent être menés, en s'appuyant sur des bases de données hydrogéologiques qui continueront à s'enrichir au fil du temps et qui permettront de mieux alimenter les modèles développés, qui à leur tour affineront la justesse des résultats que l'on obtiendra.

## **5.2 LIMITES DU PROJET DE RECHERCHE ET RECOMMANDATIONS**

### **5.2.1 MODÉLISATION DISTRIBUÉE ET APPRENTISSAGE AUTOMATIQUE GUIDÉ PAR LA THÉORIE**

Dans les problèmes de modélisation distribuée, l'algorithme d'apprentissage automatique guidé par la théorie est entraîné non seulement à s'ajuster au mieux aux observations, mais aussi à correctement approximer les équations différentielles partielles (EDP) qui régissent l'écoulement. Dans le cadre de ce projet, une évaluation de l'impact d'une mauvaise approximation de l'EDP sur la représentation de l'écoulement a été effectuée. Il a été considéré que l'algorithme produisait une

mauvaise approximation de l'EDP lorsque les valeurs résiduelles de l'EDP étaient supérieures au critère objectif de 0,0125 m/j. L'objectif était alors d'inspecter la signature piézométrique afin de comprendre l'impact qu'a cette mauvaise approximation sur la signature piézométrique. Il a été constaté que la signature piézométrique produite par l'algorithme (ou le modèle) peut ne pas représenter le comportement hydrodynamique attendu, que le résidu de l'EDP dépasse ou non le critère objectif. Trois raisons principales pourraient expliquer ce phénomène. La première est qu'il est probable que les erreurs d'approximation aux limites internes ou externes du modèle conceptuel se soient propagées dans l'ensemble du domaine spatio-temporel modélisé. La deuxième raison peut être due à une influence significative des limites internes du modèle (par exemple, les termes source/puits tels que le pompage ou la recharge) dans l'approximation de l'EDP. La troisième raison pourrait être que le problème de modélisation abordé est un problème limite incomplètement défini, c'est-à-dire qu'une part essentielle de la complexité du système aquifère n'ait pas été prise en compte dans le modèle conceptuel qui le décrit. Pour résoudre ce problème, il est suggéré comme première approche, dans le cadre de recherches futures, de considérer chaque terme de puits/source comme un terme à part entière dans la fonction de coût globale à minimiser : l'objectif est d'améliorer l'approximation du modèle aux points de l'espace concernés et de réduire la propagation des erreurs d'approximation éventuelles dans la performance du modèle. Une deuxième approche consisterait à considérer toutes les variables incertaines du modèle conceptuel (par exemple, les paramètres hydrodynamiques, les conditions aux limites, la recharge, ...) comme faisant partie du problème d'optimisation.

L'un des principaux inconvénients des modèles d'apprentissage automatique guidé par la théorie (TgML) est le coût de calcul très élevé nécessaire pour les entraîner. Il serait utile d'étudier les moyens de réduire ces coûts de calcul sans nuire de manière significative à leurs performances. Puisque l'entraînement des modèles TgML implique l'approximation de l'EDP sur un certain nombre de points spatio-temporels, il pourrait être intéressant d'évaluer l'évolution de la performance du modèle en fonction du nombre de points spatio-temporels considérés pour l'approximation de l'EDP.

L'utilisation de moins de points spatio-temporels que nécessaire permettrait d'améliorer les coûts de calcul.

Si les modèles TgML peuvent offrir des avantages significatifs en termes de performances par rapport aux approches traditionnelles, leur transférabilité reste à démontrer. Par exemple, le modèle TgML pourrait-il être utilisé pour simuler les variations temporelles du niveau d'eau d'un puits dont le débit a été modifié, ou d'un puits nouvellement installé, sans avoir à le recalibrer ? C'est certainement l'une des questions les plus importantes à traiter dans les recherches futures. En effet, cette transférabilité est pleinement acquise avec les modèles numériques, ce qui n'a pas encore été démontré pour l'apprentissage automatique guidé par la théorie. Pour ce faire, il est suggéré de tirer parti du concept d'intégration automatique (par opposition à l'auto-différenciation) pour construire une architecture de réseau neuronal dans laquelle certains neurones peuvent effectuer des opérations d'intégration sur les EDP régissant l'écoulement de l'eau souterraine. Ainsi, le modèle simulera non seulement la dynamique de l'écoulement, mais il sera également adaptable à tout changement des conditions initiales et entièrement transférable.

Dans ce projet de recherche, le TgML n'a été confronté qu'à un problème d'écoulement saturé dans un aquifère non confiné. Quelles sont ses performances dans les problèmes d'écoulement à saturation variable, dans les environnements confinés, dans les systèmes aquifères multicouches, dans les problèmes de couplage écoulement/transport, écoulement/transfert de chaleur, écoulement/transport/transfert de chaleur, dans les problèmes d'écoulement fractionnaire, dans les écoulements en zone fracturée ? Toutes ces questions sont également parmi les plus importantes à explorer dans les recherches futures. La méthodologie à adopter pour répondre à ces questions sera globalement similaire à celle du Chapitre 3.

## 5.2.2 MODÉLISATION LOCALISÉE ET APPRENTISSAGE AUTOMATIQUE GUIDÉ PAR LA THÉORIE

Dans ce projet de recherche, il a été démontré que la formulation traditionnelle de Jiang et al. (2020) pour la mise en œuvre de modèle d'apprentissage automatique guidé par la théorie (TgML) ne permet pas de construire des modèles TgML qui satisfont au principe de causalité. Il a ensuite été proposé une nouvelle formulation qui permet d'y remédier. La nouvelle formulation propose d'imposer des valeurs positives aux noyaux (ou poids) des réseaux de neurones artificiels et de choisir une fonction d'activation dont la dérivée est positive. Cette nouvelle formulation impose une forte contrainte sur les noyaux et les fonctions d'activation, à tel point que dans certaines situations (voir **Figure 27**), même si la propriété de causalité est respectée, les performances de simulation peuvent être médiocres. Comment adoucir les contraintes imposées aux noyaux et fonctions d'activation du réseau neuronal pour gagner en performance de simulation sans perdre la propriété de causalité est une question qui nécessite d'être investiguée dans les recherches futures. À cette fin, deux options peuvent être suggérées. La première option pourrait consister à introduire le concept de noyaux et de fonctions d'activation flous, à l'instar de la logique floue. Si  $W$  est le noyau et  $\sigma'$  la dérivée de la fonction d'activation, au lieu de conserver la propriété causale si  $W > 0$  et  $\sigma' > 0$  ou, au contraire, de la transgresser si  $W < 0$  et  $\sigma' > 0$ , les noyaux  $W_f$  et fonctions d'activation  $\sigma_f$  flous permettront de construire des modèles qui satisfont à un certain degré le principe de causalité. De cette manière, la flexibilité est introduite dans le modèle afin d'en améliorer les performances. Cette approche n'est pas idéale, mais reste un compromis entre un modèle qui transgresse le principe de causalité et un modèle avec des contraintes strictes telles que définies dans cette thèse. La deuxième option pourrait consister à dériver de nouvelles conditions sur  $W$  de sorte que ses valeurs d'une couche à l'autre puissent alterner entre des valeurs positives et négatives. Cela élargit l'espace de définition de la fonction de coût et augmente ainsi les chances d'obtenir un minimum global, ce qui n'est pas toujours le cas avec les conditions dérivées dans cette thèse.

Il est recommandé également de réaliser une étude comparative des performances des modèles TgML basés sur la formulation qui a été proposée, mais incorporant divers modèles hydrologiques tels que GR4J, GSFLOW ou TOPMODEL. Cette étude pourrait être utilisée pour fournir des informations sur la présélection d'un modèle TgML pour des applications pratiques en hydrogéologie. La méthodologie à adopter pour réaliser une telle étude sera globalement similaire à celle du Chapitre 4.

### **5.2.3 ÉTUDE DE L'IMPACT DU CHANGEMENT CLIMATIQUE SUR LA RESSOURCE EN EAU SOUTERRAINE**

Pour évaluer l'impact du changement climatique sur l'évolution des niveaux d'eau dans le réseau de suivi piézométrique du Québec, des ensembles de 15 modèles ont été utilisés. Cependant, il est apparu que ces ensembles étaient sous-dispersés, c'est-à-dire que les simulations sont caractérisées par une variabilité moindre que celle observées dans les données réelles. Autrement dit, les valeurs simulées sont plus regroupées que les observations réelles correspondantes. Il est donc suggéré, pour les recherches futures, d'utiliser des techniques de post-traitement des simulations comme la régression quantile afin que ces dernières soient correctement dispersées. Il est également recommandé d'étudier comment l'impact du changement climatique sur les niveaux d'eau souterraine se reflète dans les différentes saisons hydrologiques et d'un mois à l'autre. Cela peut se faire de la manière suivante : après que le modèle a projeté les niveaux d'eau journaliers futurs, il faut isoler les niveaux d'eau saison après saison (resp. mois après mois) avant d'effectuer une analyse de tendance.

Aussi, l'analyse des effets du changement climatique sur l'évolution des niveaux d'eau souterraine réalisée dans le cadre de ce projet ne tient pas compte des effets anthropiques directs. L'impact de la variabilité climatique à long terme et des diverses combinaisons possibles de pressions anthropiques sur l'évolution des niveaux d'eau souterraine au Québec est une question importante

qu'il serait bon d'étudier à l'avenir. Cela permettrait de compléter les connaissances actuelles sur l'évolution future des ressources en eau souterraine et de soutenir davantage les plans d'action pour la gestion des ressources. La méthodologie à adopter pour réaliser une telle étude sera globalement similaire à celle du Chapitre 4 à la différence qu'il faudra modifier la structure de l'algorithme pour intégrer diverses variables anthropiques. Cela nécessitera également de collecter plus de données, notamment celles relatives aux pressions anthropiques.

### **5.3 AUTOMATIQUE GUIDÉ PAR LA THEORIE EN PRATIQUE**

Bien que l'apprentissage automatique guidé par la théorie (TgML) bénéficie de certains atouts des approches traditionnelles de modélisation, l'obtention de modèles performants reste tributaire d'une quantité et d'une qualité suffisantes de données. Comme pour toutes les applications d'apprentissage automatique, la collecte des données et le contrôle de la qualité jouent un rôle très important dans le développement des modèles d'apprentissage automatique, et les applications en hydrogéologie ne font pas exception à la règle. Les applications hydrogéologiques sont diverses et variées, mais peuvent être regroupées en trois catégories de problèmes. La première concerne les problèmes spatiaux, impliquant la simulation d'une variable spatiale telle que la vulnérabilité des eaux souterraines. La deuxième classe représente les problèmes temporels, impliquant la simulation d'une variable qui évolue dans le temps, comme les niveaux d'eau ou la concentration d'un polluant. Et la troisième classe de problèmes représente les problèmes spatio-temporels, où il s'agit de simuler l'évolution d'une variable qui varie à la fois dans le temps et dans l'espace : c'est aussi le cas des niveaux d'eau souterraine ou de la température. Chacune de ces classes de problèmes utilise des données dont l'acquisition et le traitement ne nécessitent pas les mêmes ressources et les mêmes efforts.

Les problèmes spatiaux utilisent généralement des données satellitaires, géologiques (profil lithologique, diagraphe, classification des sols), hydrogéologiques (propriétés hydrauliques,

profondeur de la surface piézométrique) et quelques fois météorologiques (température, précipitation) (Barzegar et al. 2018; Elzain et al. 2022). Si les données satellitaires et météorologiques sont facilement accessibles, l'accès aux données hydrogéologiques et à certaines données géologiques est limité par le nombre et la répartition spatiale des puits d'observation. S'agissant de problèmes spatiaux, ces données difficiles d'accès peuvent être substituées par les données issues de l'interprétation de données géophysiques. C'est le cas, par exemple, de la profondeur de la surface piézométrique.

Les problèmes temporels concernent des points géographiques où il existe des puits d'observation. Pour résoudre ces problèmes, la longueur et la qualité des séries temporelles des variables explicatives (indépendantes) et expliquées (dépendantes) sont déterminantes. Plus il y a de données, plus grande est la probabilité d'obtenir un modèle d'apprentissage performant. Le traitement de ces données peut impliquer l'imputation des valeurs manquantes, le filtrage des séries temporelles pour réduire le bruit, ou la dérivation de nouvelles données par la décomposition des données d'origine. Le choix des variables explicatives doit être étayé par une expertise hydrogéologique. Par exemple, dans un aquifère peu profond et non confiné, il est très probable que les variations du niveau de la nappe soient corrélées à celles des précipitations. Dans ce cas, les précipitations peuvent être considérées comme des variables explicatives.

Pour les problèmes spatio-temporels, moins il y a de puits d'observation, plus il peut être difficile de développer un modèle d'apprentissage automatique guidé par la théorie. Si des modèles numériques (modèles basés sur la physique) ont déjà été développés pour l'aquifère à étudier, ces modèles numériques peuvent être utilisés pour reconstruire des séries temporelles de niveaux d'eau souterraine afin de compenser le manque de données dû au faible nombre de puits d'observation. Dans ce cas, le modèle d'apprentissage automatique guidé par la théorie doit être développé de manière à traiter les données reconstruites par le modèle numérique comme des données approximatives des observations de terrain.

Pour faciliter l'application de l'apprentissage automatique guidé par la théorie par les praticiens, il peut leur être conseillé de mettre en œuvre des pipelines de données telles que les ETL (Extract, Transform, Load) (Pogiatzis and Samakovitis 2021), qui sont un ensemble de processus interdépendants utilisés pour extraire des données de diverses sources, les transformer en données pertinentes et fiables, et stocker ces données traitées dans des bases de données auxquelles le modélisateur peut accéder pour le développement de modèles. Les pipelines ETL sont utiles car ils permettent un traitement continu des données au fur et à mesure qu'elles sont collectées, ce qui facilite le développement et la mise à jour des modèles d'apprentissage automatique. Actuellement, des efforts considérables sont déployés non seulement pour acquérir et compiler des données hydrogéologiques, mais aussi pour les diffuser à différentes échelles territoriales : de régionale à mondiale. Les pipelines ETL peuvent être un moyen approprié pour les entreprises privées ou les organismes publics de tirer parti de ces bases de données mondiales, tout en les alimentant avec des données acquises localement.

Une fois les pipelines de données mis en place, des pipelines d'apprentissage automatique peuvent également être développés et connectés à ces pipelines de données. Les pipelines d'apprentissage peuvent être utilisés pour automatiser des séquences de tâches qui conduisent à l'implémentation des modèles d'apprentissage. En utilisant des mesures de performance prédéfinies, il est possible de suivre les performances des modèles d'apprentissage dans le temps et au fur et à mesure que de nouvelles données sont ingérées. De cette manière, les modèles d'apprentissage peuvent être mis à jour automatiquement lorsqu'une dégradation des performances est observée dans le temps. Le couplage des pipelines de données avec les pipelines d'apprentissage permet d'obtenir des modèles « dynamiques » dont la justesse peut évoluer avec la croissance et l'apport de nouvelles données. Les pipelines de données et d'apprentissage sont bien développés dans les secteurs du numérique et de l'innovation, dont l'expérience peut grandement aider l'hydrogéologie

pratique. Ces pipelines peuvent être utiles également aux modèles à base physique (par exemple, les modèles numériques).

#### **5.4 BRÈVE OUVERTURE SUR LES AVANTAGES TECHNIQUES DE L'APPRENTISSAGE AUTOMATIQUE GUIDÉ PAR LA THÉORIE PAR RAPPORT A LA MODÉLISATION NUMÉRIQUE**

Les outils actuels de mise en œuvre des algorithmes d'apprentissage automatique intègrent le concept de la *programmation différentiable* (Cuomo et al. 2023; Gelbrecht et al. 2023; Shen et al. 2023). La programmation différentiable permet aux algorithmes de calculer le gradient d'une variable de sortie par rapport à une variable d'entrée, sans utiliser les méthodes numériques traditionnelles telles que les éléments finis, mais plutôt en se basant sur le principe de la dérivation en chaîne. Cette caractéristique confère aux algorithmes d'apprentissage automatique un avantage majeur sur les modèles numériques. En effet, les modèles numériques utilisent des algorithmes complexes de plusieurs milliers de lignes de code pour résoudre les équations directrices par des méthodes numériques traditionnelles, alors qu'avec la programmation différentiable des outils d'apprentissage automatique, cela ne nécessiterait que quelques lignes de code (Gelbrecht et al. 2023). De plus, grâce à la programmation différentiable, les algorithmes d'apprentissage automatique peuvent plus facilement approximer des équations directrices de haute dimension et explorer plus facilement des phénomènes physiques plus complexes, notamment à petite échelle (Cuomo et al. 2023; Rackauckas et al. 2020), ce qui serait très difficile, voire impossible, pour les modèles numériques.

Un autre point important est la *flexibilité* dans le développement des modèles d'apprentissage automatique guidé par la théorie (TgML). Dans le contexte de la modélisation distribuée, contrairement aux modèles numériques qui nécessitent une connaissance approfondie des conditions initiales et limites pour dériver une solution aux équations différentielles partielles (EDP), les modèles TgML autorisent la définition de contraintes dites souples qui peuvent consister, par exemple, à spécifier uniquement l'EDP sans connaissance ou avec une connaissance partielle des

conditions initiales et limites sans qu'il y ait une dégradation notable des performances (Razavi et al. 2022).

## RÉFÉRENCE

- Barzegar, R., Moghaddam, A.A., Deo, R., Fijani, E., and Tziritis, E. 2018. Mapping groundwater contamination risk of multiple aquifers using multi-model ensemble of machine learning algorithms. *Science of the Total Environment*, **621**: 697-712. doi:<https://doi.org/10.1016/j.scitotenv.2017.11.185>.
- Cuomo, S., De Rosa, M., Giampaolo, F., Izzo, S., and Schiano Di Cola, V. 2023. Solving groundwater flow equation using physics-informed neural networks. *Computers & Mathematics with Applications*, **145**: 106-123. doi:<https://doi.org/10.1016/j.camwa.2023.05.036>.
- Elzain, H.E., Chung, S.Y., Senapathi, V., Sekar, S., Lee, S.Y., Roy, P.D., Hassan, A., and Sabarathinam, C. 2022. Comparative study of machine learning models for evaluating groundwater vulnerability to nitrate contamination. *Ecotoxicology and Environmental Safety*, **229**: 113061. doi:<https://doi.org/10.1016/j.ecoenv.2021.113061>.
- Gelbrecht, M., White, A., Bathiany, S., and Boers, N. 2023. Differentiable programming for Earth system modeling. *Geoscientific Model Development*, **16**: 3123-3135.
- Jiang, S., Zheng, Y., and Solomatine, D. 2020. Improving AI System Awareness of Geoscience Knowledge: Symbiotic Integration of Physical Approaches and Deep Learning. *Geophysical Research Letters*, **47**: e2020GL088229. doi:<https://doi.org/10.1029/2020GL088229>.
- Nearing, G.S., Kratzert, F., Sampson, A.K., Pelissier, C.S., Klotz, D., Frame, J.M., Prieto, C., and Gupta, H.V. 2021. What role does hydrological science play in the age of machine learning? *Water Resources Research*, **57**: e2020WR028091.
- Pogiatzis, A., and Samakovitis, G. 2021. An Event-Driven Serverless ETL Pipeline on AWS. *Applied Sciences*, **11**: 191. Available from <https://www.mdpi.com/2076-3417/11/1/191> [accessed].
- Rackauckas, C., Ma, Y., Martensen, J., Warner, C., Zubov, K., Supekar, R., Skinner, D., Ramadhan, A., and Edelman, A. 2020. Universal differential equations for scientific machine learning. *arXiv preprint arXiv:2001.04385*.
- Razavi, S., Hannah, D.M., Elshorbagy, A., Kumar, S., Marshall, L., Solomatine, D.P., Dezfuli, A., Sadegh, M., and Famiglietti, J. 2022. Coevolution of machine learning and process-based

modelling to revolutionize Earth and environmental sciences: A perspective. *Hydrological Processes*, **36**: e14596.

Shen, C., Appling, A.P., Gentine, P., Bandai, T., Gupta, H., Tartakovsky, A., Baity-Jesi, M., Fenicia, F., Kifer, D., and Li, L. 2023. Differentiable modelling to unify machine learning and physical models for geosciences. *Nature Reviews Earth & Environment*: 1-16.

## CONCLUSION

L'apprentissage automatique guidé par la théorie (TgML) est une nouvelle branche de l'apprentissage automatique qui se focalise sur le développement de modèle d'apprentissage capable d'intégrer des connaissances scientifiques. Cette thèse visait à tester l'hypothèse selon laquelle les modèles d'apprentissage automatique guidés par la théorie peuvent bénéficier des forces combinées des approches traditionnelles de modélisation. Pour tester cette hypothèse, la thèse s'est concentrée uniquement sur les problèmes d'écoulements distribués et localisés. Dans le contexte de la modélisation distribuée, le modèle TgML développé présentait la meilleure justesse de simulation en comparaison avec d'un modèle à base physique et un modèle traditionnel d'apprentissage, tout en obéissant à la physique qui régit les écoulements d'eau souterraine. Dans le contexte de la modélisation localisée, la thèse a montré que la manière traditionnelle de construire des modèles TgML ne leur permettait pas de satisfaire au principe de causalité essentielle pour représenter correctement les processus hydrologiques. Une nouvelle approche a ensuite été proposée dans cette thèse pour permettre aux modèles TgML de satisfaire au principe de causalité. Les modèles dérivés à partir de l'approche proposée dans cette thèse présentent des performances plus ou moins similaires à celles des modèles traditionnels d'apprentissage automatique et supérieures à celles des modèles dérivés selon l'approche originale, tout en affichant des propriétés causales satisfaisantes. La confrontation de l'apprentissage automatique guidé par la théorie à ces deux problèmes d'écoulements a permis de confirmer l'hypothèse de recherche selon laquelle l'apprentissage automatique guidé par la théorie peut bénéficier des avantages combinés des approches traditionnelles de modélisation. Toutefois, les modèles TgML ont présenté l'inconvénient d'être couteux en ressources computationnelles. Le projet de recherche a également permis d'effectuer une étude préliminaire de l'impact seul des variables climatiques sur l'évolution des niveaux d'eau souterraine du réseau de suivi piézométrique du Québec (Canada) en contexte de changement climatique. Il en résultait qu'indépendamment du scenario climatique considéré (RCP4.5, RCP8.5, SSP2-4.5 et SSP5-8.5), une augmentation des niveaux piézométriques est prévue sur la période 2011-2090 avec des augmentations médianes variant entre +5,6 et +7 cm. Dans certains cas,

l'augmentation peut dépasser +14 à +23 cm, voire atteindre +35 à +70 cm. Ces résultats sur l'impact du changement climatique ne demandent qu'à être réfutés ou confirmés dans les recherches futures.

## LISTE DE RÉFÉRENCES

- Abbs, D.J. 1999. A numerical modeling study to investigate the assumptions used in the calculation of probable maximum precipitation. *Water Resources Research*, **35**: 785-796. doi:<https://doi.org/10.1029/1998WR900013>.
- Adamowski, J., and Chan, H.F. 2011. A wavelet neural network conjunction model for groundwater level forecasting. *Journal of Hydrology*, **407**: 28-40. doi:<https://doi.org/10.1016/j.jhydrol.2011.06.013>.
- Adombi, A.V.D.P. 2023a. Groundwater Monitoring Network Analysis Tool. doi:<https://doi.org/10.5281/zenodo.7933551>.
- Adombi, A.V.D.P. 2023b. Online Resource 2. Available from [https://github.com/avadombi/SupplementaryMaterial/blob/main/Article3/Supplementary\\_material\\_2.docx](https://github.com/avadombi/SupplementaryMaterial/blob/main/Article3/Supplementary_material_2.docx).
- Adombi, A.V.D.P. 2023c. Online Resource 1. Available from [https://github.com/avadombi/SupplementaryMaterial/blob/main/Article3/Supplementary\\_material\\_1.xlsx](https://github.com/avadombi/SupplementaryMaterial/blob/main/Article3/Supplementary_material_1.xlsx).
- Adombi, A.V.D.P. 2023d. Code: Proposal of a causal theory-guided Deep Learning formulation for groundwater flow modeling. Zenodo. doi:<https://doi.org/10.5281/zenodo.8155740>.
- Adombi, A.V.D.P. 2023e. Supplementary Material 2. Available from [https://github.com/avadombi/SupplementaryMaterial/blob/main/Article4/Supplementary\\_Material\\_2.docx](https://github.com/avadombi/SupplementaryMaterial/blob/main/Article4/Supplementary_Material_2.docx).
- Adombi, A.V.D.P. 2023f. Supplementary Material 1. Available from [https://github.com/avadombi/SupplementaryMaterial/blob/main/Article4/Supplementary\\_Material\\_1.docx](https://github.com/avadombi/SupplementaryMaterial/blob/main/Article4/Supplementary_Material_1.docx).
- Adombi, A.V.D.P. 2023g. Supplementary Material 3. Available from [https://github.com/avadombi/SupplementaryMaterial/blob/main/Article4/Supplementary\\_Material\\_3.docx](https://github.com/avadombi/SupplementaryMaterial/blob/main/Article4/Supplementary_Material_3.docx).

- Adombi, A.V.D.P., Chesnaux, R., and Boucher, M.-A. 2021. Review: Theory-guided machine learning applied to hydrogeology—state of the art, opportunities and future challenges. *Hydrogeology Journal*, **29**: 2671-2683. doi:<https://doi.org/10.1007/s10040-021-02403-2>.
- Afshar, A., Mariño, M.A., Ebtehaj, M., and Moosavi, J. 2007. Rule-Based Fuzzy System for Assessing Groundwater Vulnerability. *Journal of Environmental Engineering*, **133**: 532-540. doi:[https://doi.org/10.1061/\(ASCE\)0733-9372\(2007\)133:5\(532\)](https://doi.org/10.1061/(ASCE)0733-9372(2007)133:5(532)).
- Akakuru, O.C., Akudinobi, B., Opara, A.I., Onyekuru, S.O., and Akakuru, O.U. 2021. Hydrogeochemical facies and pollution status of groundwater resources of Owerri and environs, Southeastern Nigeria. *Environmental monitoring and assessment*, **193**: 623. doi:<https://doi.org/10.1007/s10661-021-09364-9>.
- Al Aamery, N., Adams, E., Fox, J., Husic, A., Zhu, J., Gerlitz, M., Agouridis, C., and Bettel, L. 2021. Numerical model development for investigating hydrologic pathways in shallow fluvikarst. *Journal of Hydrology*, **593**: 125844. doi:<https://doi.org/10.1016/j.jhydrol.2020.125844>.
- Aldrich, C. 2015. Chapter One - Hydrocyclones. In *Progress in Filtration and Separation*. Edited by S. Tarleton. Academic Press, Oxford. pp. 1-24.
- Arabameri, A., Roy, J., Saha, S., Blaschke, T., Ghorbanzadeh, O., and Tien Bui, D. 2019. Application of Probabilistic and Machine Learning Models for Groundwater Potentiality Mapping in Damghan Sedimentary Plain, Iran. Remote Sensing, **11**. doi:<https://doi.org/10.3390/rs11243015>.
- Arnold, D.N. 2015. Stability, consistency, and convergence of numerical discretizations. *Encyclopedia of Applied and Computational Mathematics*: 1358-1364. doi:[https://doi.org/10.1007/978-3-540-70529-1\\_407](https://doi.org/10.1007/978-3-540-70529-1_407).
- Arora, R., Toffolon, M., Tockner, K., and Venohr, M. 2018. Thermal discontinuities along a lowland river: The importance of urban areas and lakes. *Journal of Hydrology*, **564**: 811-823. doi:<https://doi.org/10.1016/j.jhydrol.2018.05.066>.
- Asher, M.J., Croke, B.F.W., Jakeman, A.J., and Peeters, L.J.M. 2015. A review of surrogate models and their application to groundwater modeling. *Water Resources Research*, **51**: 5957-5973. doi:<https://doi.org/10.1002/2015WR016967>.

- Ashoor, B.B., Giwa, A., and Hasan, S.W. 2019. Chapter 5 - Full-Scale Membrane Distillation Systems and Performance Improvement Through Modeling: A Review. *In Current Trends and Future Developments on (Bio-) Membranes*. Edited by A. Basile and E. Curcio and Inamuddin. Elsevier. pp. 105-140.
- Atangana, A. 2018. Chapter 2 - Principle of Groundwater Flow. *In Fractional Operators with Constant and Variable Order with Application to Geo-Hydrology*. Edited by A. Atangana. Academic Press. pp. 15-47.
- Awadh, S.M., Al-Mimar, H., and Yaseen, Z.M. 2021. Groundwater availability and water demand sustainability over the upper mega aquifers of Arabian Peninsula and west region of Iraq. Environment, Development and Sustainability, **23**: 1-21. doi:<https://doi.org/10.1007/s10668-019-00578-z>.
- Ayodele, T.O. 2010. Types of machine learning algorithms. New advances in machine learning, **3**: 19-48. doi:<https://doi.org/10.5772/9385>.
- Azencott, C.-A. 2022. Introduction au Machine Learning-2e éd. Dunod.
- Azodi, C.B., Tang, J., and Shiu, S.-H. 2020. Opening the Black Box: Interpretable Machine Learning for Geneticists. Trends in Genetics, **36**: 442-455. doi:<https://doi.org/10.1016/j.tig.2020.03.005>.
- Bahareh, K., Husam, A.H.A.-N., Biswajeet, P., Vahideh, S., Alfian Abdul, H., Naonori, U., and Seyed Amir, N. 2019. Optimized Conditioning Factors Using Machine Learning Techniques for Groundwater Potential Mapping [online]. Water **11** [cited].
- Bakshi, S., de Lange, E., van der Graaf, P., Danhof, M., and Peletier, L. 2016. Understanding the Behavior of Systems Pharmacology Models Using Mathematical Analysis of Differential Equations: Prolactin Modeling as a Case Study. CPT: Pharmacometrics & Systems Pharmacology, **5**: 339-351. doi:<https://doi.org/10.1002/psp4.12098>.
- Banadkooki, F.B., Ehteram, M., Ahmed, A.N., Teo, F.Y., Fai, C.M., Afan, H.A., Sapitang, M., and El-Shafie, A. 2020. Enhancement of groundwater-level prediction using an integrated machine learning model optimized by whale algorithm. Natural resources research, **29**: 3233-3252. doi:<https://doi.org/10.1007/s11053-020-09634-2>.

- Bar-Sinai, Y., Hoyer, S., Hickey, J., and Brenner, M.P. 2019. Learning data-driven discretizations for partial differential equations. *Proceedings of the National Academy of Sciences*, **116**: 15344-15349. doi:<https://doi.org/10.1073/pnas.1814058116>.
- Barr, A., Feigenbaum, E.A., and Cohen, P.R. 1981. *The handbook of artificial intelligence*. William Kaufmann Inc., Los Altos, CA.
- Barzegar, R., Fijani, E., Asghari Moghaddam, A., and Tziritis, E. 2017a. Forecasting of groundwater level fluctuations using ensemble hybrid multi-wavelet neural network-based models. *Science of the Total Environment*, **599**. doi:<https://doi.org/10.1016/j.scitotenv.2017.04.189>.
- Barzegar, R., Fijani, E., Asghari Moghaddam, A., and Tziritis, E. 2017b. Forecasting of groundwater level fluctuations using ensemble hybrid multi-wavelet neural network-based models. *Science of the Total Environment*, **599-600**: 20-31. doi:<https://doi.org/10.1016/j.scitotenv.2017.04.189>.
- Barzegar, R., Moghaddam, A.A., Deo, R., Fijani, E., and Tziritis, E. 2018. Mapping groundwater contamination risk of multiple aquifers using multi-model ensemble of machine learning algorithms. *Science of the Total Environment*, **621**: 697-712. doi:<https://doi.org/10.1016/j.scitotenv.2017.11.185>.
- Bedi, S., Samal, A., Ray, C., and Snow, D. 2020. Comparative evaluation of machine learning models for groundwater quality assessment. *Environmental monitoring and assessment*, **192**: 776. doi:10.1007/s10661-020-08695-3.
- Bergeron, O. 2016. Guide d'utilisation 2016 - Grilles climatiques quotidiennes du Programme de surveillance du climat du Québec. Ministère du Développement durable, de l'Environnement et de la Lutte contre les changements climatiques, Direction du suivi de l'état de l'environnement version 1.2, Québec.
- Bergström, S. 1976. Development and application of a conceptual runoff model for Scandinavian catchments.
- Bhat, S., Motz, L.H., Pathak, C., and Kuebler, L. 2014. Geostatistics-based groundwater-level monitoring network design and its application to the Upper Floridan aquifer, USA.

Environmental monitoring and assessment, **187**: 4183. doi:<https://doi.org/10.1007/s10661-014-4183-x>.

Bhattacharya, B., Lobbrecht, A., and Solomatine, D. 2003. Neural networks and reinforcement learning in control of water systems. Journal of Water Resources Planning and Management, **129**: 458-465.

Bikše, J., Retike, I., Haaf, E., and Kalvāns, A. 2023. Assessing automated gap imputation of regional scale groundwater level data sets with typical gap patterns. Journal of Hydrology, **620**: 129424. doi:<https://doi.org/10.1016/j.jhydrol.2023.129424>.

Bishop, C.M., and Nasrabadi, N.M. 2006. Pattern recognition and machine learning. No. 4. Springer.  
Bock, L., Lauer, A., Schlund, M., Barreiro, M., Bellouin, N., Jones, C., Meehl, G.A., Predoi, V., Roberts, M.J., and Eyring, V. 2020. Quantifying Progress Across Different CMIP Phases With the ESMValTool. Journal of Geophysical Research: Atmospheres, **125**: e2019JD032321. doi:<https://doi.org/10.1029/2019JD032321>.

Boumaiza, L. 2008. Caractérisation hydrogéologique des hydrofaciès dans le paléodelta de la rivière Valin au Saguenay [Hydrogeological characterization of hydrofacies in the Valin River Paleodelta in Saguenay]. Applied Sciences, Université du Québec à Chicoutimi.

Boumaiza, L., Chesnaux, R., Walter, J., and Stumpp, C. 2020. Assessing groundwater recharge and transpiration in a humid northern region dominated by snowmelt using vadose-zone depth profiles. Hydrogeology Journal, **28**: 2315-2329.

Boumaiza, L., Chesnaux, R., Walter, J., and Meghnefi, F. 2021. Assessing response times of an alluvial aquifer experiencing seasonally variable meteorological inputs. Groundwater for Sustainable Development, **14**: 100647. doi:<https://doi.org/10.1016/j.gsd.2021.100647>.

Bourgault, M.A., Larocque, M., and Roy, M. 2013. Simulation of aquifer-peatland-river interactions under climate change. Hydrology Research, **45**: 425-440. doi:<https://doi.org/10.2166/nh.2013.228>.

Bowes, B.D., Sadler, J.M., Morsy, M.M., Behl, M., and Goodall, J.L. 2019. Forecasting Groundwater Table in a Flood Prone Coastal City with Long Short-term Memory and Recurrent Neural Networks. Water, **11**: 1098. doi:<https://doi.org/10.3390/w11051098>.

- Bowes, B.D., Wang, C., Ercan, M.B., Culver, T.B., Beling, P.A., and Goodall, J.L. 2022. Reinforcement learning-based real-time control of coastal urban stormwater systems to mitigate flooding and improve water quality. *Environmental Science: Water Research & Technology*, **8**: 2065-2086.
- Brodeur, Z.P., Herman, J.D., and Steinschneider, S. 2020. Bootstrap Aggregation and Cross-Validation Methods to Reduce Overfitting in Reservoir Control Policy Search. *Water Resources Research*, **56**: e2020WR027184. doi:<https://doi.org/10.1029/2020WR027184>.
- Brouwers, M.H. 2007. A case study for assessing the hydrologic impacts of climate change at the watershed scale. University of Waterloo, Ontario.
- Brunner, P., Simmons, C.T., Cook, P.G., and Therrien, R. 2010. Modeling Surface Water-Groundwater Interaction with MODFLOW: Some Considerations. *Groundwater*, **48**: 174-180. doi:<https://doi.org/10.1111/j.1745-6584.2009.00644.x>.
- Bui, D.D., Kawamura, A., Tong, T.N., Amaguchi, H., and Nakagawa, N. 2012. Spatio-temporal analysis of recent groundwater-level trends in the Red River Delta, Vietnam. *Hydrogeology Journal*, **20**: 1635-1650. doi:<https://doi.org/10.1007/s10040-012-0889-4>.
- Cai, H., Shi, H., Liu, S., and Babovic, V. 2021. Impacts of regional characteristics on improving the accuracy of groundwater level prediction using machine learning: The case of central eastern continental United States. *Journal of Hydrology: Regional Studies*, **37**: 100930.
- Cai, H., Liu, S., Shi, H., Zhou, Z., Jiang, S., and Babovic, V. 2022. Toward improved lumped groundwater level predictions at catchment scale: Mutual integration of water balance mechanism and deep learning method. *Journal of Hydrology*, **613**: 128495. doi:<https://doi.org/10.1016/j.jhydrol.2022.128495>.
- Ch, S., and Mathur, S. 2012. Groundwater level forecasting using SVM-PSO. *International Journal of Hydrology Science and Technology*, **2**: 202-218.
- Chang, F.J., Huang, C.W., Chang, L.C., and Kao, I.F. 2016. Prediction of monthly regional groundwater levels through hybrid soft-computing techniques. *Journal of Hydrology*, **541**: 965-976. doi:<https://doi.org/10.1016/j.jhydrol.2016.08.006>.

- Chen, C., He, W., Zhou, H., Xue, Y., and Zhu, M. 2020a. A comparative study among machine learning and numerical models for simulating groundwater dynamics in the Heihe River Basin, northwestern China. *Scientific reports*, **10**: 1-13. doi:<https://doi.org/10.1038/s41598-020-60698-9>.
- Chen, C., He, W., Zhou, H., Xue, Y., and Zhu, M. 2020b. A comparative study among machine learning and numerical models for simulating groundwater dynamics in the Heihe River Basin, northwestern China. *Scientific reports*, **10**: 3904. doi:<https://doi.org/10.1038/s41598-020-60698-9>.
- Chen, Y., Xu, Y., Wang, L., and Li, T. 2023. Modeling water flow in unsaturated soils through physics-informed neural network with principled loss function. *Computers and Geotechnics*, **161**: 105546. doi:<https://doi.org/10.1016/j.compgeo.2023.105546>.
- Chen, Y., Huang, D., Zhang, D., Zeng, J., Wang, N., Zhang, H., and Yan, J. 2020c. Theory-guided hard constraint projection (HCP): a knowledge-based data-driven scientific machine learning method. arXiv preprint arxiv-2012.06148.
- Chen, Y., Huang, D., Zhang, D., Zeng, J., Wang, N., Zhang, H., and Yan, J. 2021. Theory-guided hard constraint projection (HCP): A knowledge-based data-driven scientific machine learning method. *Journal of Computational Physics*, **445**: 110624. doi:<https://doi.org/10.1016/j.jcp.2021.110624>.
- Chesnaux, R., Santoni, S., Garel, E., and Huneau, F. 2018. An Analytical Method for Assessing Recharge Using Groundwater Travel Time in Dupuit-Forchheimer Aquifers. *Groundwater*, **56**: 986-992. doi:<https://doi.org/10.1111/gwat.12794>.
- Clark, M.P., Fan, Y., Lawrence, D.M., Adam, J.C., Bolster, D., Gochis, D.J., Hooper, R.P., Kumar, M., Leung, L.R., Mackay, D.S., Maxwell, R.M., Shen, C., Swenson, S.C., and Zeng, X. 2015. Improving the representation of hydrologic processes in Earth System Models. *Water Resources Research*, **51**: 5929-5956. doi:<https://doi.org/10.1002/2015WR017096>.
- Clark, P., and Niblett, T. 1989. The CN2 induction algorithm. *Machine learning*, **3**: 261-283. doi:<https://doi.org/10.1023/A:1022641700528>.

- Colautti, D. 2010. Modelling the Effects of Climate Change on the Surface and Subsurface Hydrology of the Grand River Watershed. University of Waterloo, Ontario.
- CollentEUR, R.A., Bakker, M., Klammler, G., and Birk, S. 2021. Estimation of groundwater recharge from groundwater levels using nonlinear transfer function noise models and comparison to lysimeter data. *Hydrol. Earth Syst. Sci.*, **25**: 2931-2949. doi:<https://hess.copernicus.org/articles/25/2931/2021/>.
- Colom, R., Karama, S., Jung, R.E., and Haier, R.J. 2010. Human intelligence and brain networks. *Dialogues in Clinical Neuroscience*, **12**: 489-501. doi:10.31887/DCNS.2010.12.4/rkolom.
- Coron, L., Thirel, G., Delaigue, O., Perrin, C., and Andréassian, V. 2017. The suite of lumped GR hydrological models in an R package. *Environmental Modelling & Software*, **94**: 166-171. doi:<https://doi.org/10.1016/j.envsoft.2017.05.002>.
- Cugnet, M., Dubarry, M., and Liaw, B.Y. 2009. SECONDARY BATTERIES – LEAD–ACID SYSTEMS | Modeling. In *Encyclopedia of Electrochemical Power Sources*. Edited by J. Garche. Elsevier, Amsterdam. pp. 816-828.
- Cuomo, S., De Rosa, M., Giampaolo, F., Izzo, S., and Schiano Di Cola, V. 2023. Solving groundwater flow equation using physics-informed neural networks. *Computers & Mathematics with Applications*, **145**: 106-123. doi:<https://doi.org/10.1016/j.camwa.2023.05.036>.
- Cybenko, G.V. 1989. Approximation by superpositions of a sigmoidal function. *Mathematics of Control, Signals and Systems*, **2**: 303-314.
- Daw, A., Thomas, R.Q., Carey, C.C., Read, J.S., Appling, A.P., and Karpatne, A. Physics-guided architecture (pga) of neural networks for quantifying uncertainty in lake temperature modeling. In *Proceedings of the 2020 siam international conference on data mining*. 2020. SIAM, pp. 532-540.
- De Mulder, W., Bethard, S., and Moens, M.-F. 2015. A survey on the application of recurrent neural networks to statistical language modeling. *Computer Speech & Language*, **30**: 61-98. doi:<https://doi.org/10.1016/j.csl.2014.09.005>.
- Depina, I., Jain, S., Mar Valsson, S., and Gotovac, H. 2022. Application of physics-informed neural networks to inverse problems in unsaturated groundwater flow. *Georisk: Assessment and*

- Management of Risk for Engineered Systems and Geohazards, **16**: 21-36.  
doi:10.1080/17499518.2021.1971251.
- Devia, G.K., Ganasri, B.P., and Dwarakish, G.S. 2015. A Review on Hydrological Models. *Aquatic Procedia*, **4**: 1001-1007. doi:<https://doi.org/10.1016/j.aqpro.2015.02.126>.
- ECCC. 2022. Environment and Climate Change Canada.
- El Bilali, A., Taleb, A., and Brouziyne, Y. 2021. Groundwater quality forecasting using machine learning algorithms for irrigation purposes. *Agricultural water management*, **245**: 106625. doi:<https://doi.org/10.1016/j.agwat.2020.106625>.
- Elzain, H.E., Chung, S.Y., Senapathi, V., Sekar, S., Lee, S.Y., Roy, P.D., Hassan, A., and Sabarathinam, C. 2022. Comparative study of machine learning models for evaluating groundwater vulnerability to nitrate contamination. *Ecotoxicology and Environmental Safety*, **229**: 113061. doi:<https://doi.org/10.1016/j.ecoenv.2021.113061>.
- Elzain, H.E., Chung, S.Y., Venkatramanan, S., Selvam, S., Ahemd, H.A., Seo, Y.K., Bhuyan, M.S., and Yassin, M.A. 2023. Novel machine learning algorithms to predict the groundwater vulnerability index to nitrate pollution at two levels of modeling. *Chemosphere*, **314**: 137671. doi:<https://doi.org/10.1016/j.chemosphere.2022.137671>.
- Enemark, T., Peeters, L.J.M., Mallants, D., and Batelaan, O. 2019. Hydrogeological conceptual model building and testing: A review. *Journal of Hydrology*, **569**: 310-329. doi:<https://doi.org/10.1016/j.jhydrol.2018.12.007>.
- Environmental Reporting BC. 2019. Long-term Trends in Groundwater Levels in B.C. Available from <https://www.env.gov.bc.ca/soe/indicators/water/groundwater-levels.html2023>.
- Esterhuizen, J.A., Goldsmith, B.R., and Linic, S. 2020. Theory-guided machine learning finds geometric structure-property relationships for chemisorption on subsurface alloys. *Chem*, **6**: 3100-3117. doi:<https://doi.org/10.1016/j.chempr.2020.09.001>.
- Eyring, V., Bony, S., Meehl, G.A., Senior, C.A., Stevens, B., Stouffer, R.J., and Taylor, K.E. 2016. Overview of the Coupled Model Intercomparison Project Phase 6 (CMIP6) experimental design and organization. *Geoscientific Model Development*, **9**: 1937-1958. doi:<https://doi.org/10.5194/gmd-9-1937-2016>.

- Ezugwu, A.E., Ikotun, A.M., Oyelade, O.O., Abualigah, L., Agushaka, J.O., Eke, C.I., and Akinyelu, A.A. 2022. A comprehensive survey of clustering algorithms: State-of-the-art machine learning applications, taxonomy, challenges, and future research prospects. *Engineering Applications of Artificial Intelligence*, **110**: 104743. doi:<https://doi.org/10.1016/j.engappai.2022.104743>.
- Famiglietti, J.S. 2014. The global groundwater crisis. *Nature Climate Change*, **4**: 945-948. doi:<https://doi.org/10.1038/nclimate2425>.
- Farrell, R.P., and Whiteman, M. 2023. The Environment Agency Chalk groundwater level monitoring network in England. Geological Society, London, Special Publications, **517**: 163-182. doi:<https://www.lyellcollection.org/doi/abs/10.1144/SP517-2022-274>.
- Faticchi, S., Vivoni, E.R., Ogden, F.L., Ivanov, V.Y., Mirus, B., Gochis, D., Downer, C.W., Camporese, M., Davison, J.H., Ebel, B., Jones, N., Kim, J., Mascaro, G., Niswonger, R., Restrepo, P., Rigon, R., Shen, C., Sulis, M., and Tarboton, D. 2016. An overview of current applications, challenges, and future trends in distributed process-based models in hydrology. *Journal of Hydrology*, **537**: 45-60. doi:<https://doi.org/10.1016/j.jhydrol.2016.03.026>.
- Fausett, L.V. 2006. Fundamentals of neural networks: architectures, algorithms and applications. Pearson Education India.
- Feng, S., Huo, Z., Kang, S., Tang, Z., and Wang, F. 2011. Groundwater simulation using a numerical model under different water resources management scenarios in an arid region of China. *ENVIRONMENTAL EARTH SCIENCES*, **62**: 961-971. doi:<https://doi.org/10.1007/s12665-010-0581-8>.
- Fukami, K., Fukagata, K., and Taira, K. 2020. Assessment of supervised machine learning methods for fluid flows. *Theoretical and Computational Fluid Dynamics*, **34**: 497-519. doi:[10.1007/s00162-020-00518-y](https://doi.org/10.1007/s00162-020-00518-y).
- Gadd, C., Xing, W., Nezhad, M.M., and Shah, A. 2019. A surrogate modelling approach based on nonlinear dimension reduction for uncertainty quantification in groundwater flow models. *Transport in porous media*, **126**: 39-77.

- Gagné, S., Larocque, M., Pinti, D.L., Saby, M., Meyzonnat, G., and Méjean, P. 2018. Benefits and limitations of using isotope-derived groundwater travel times and major ion chemistry to validate a regional groundwater flow model: example from the Centre-du-Québec region, Canada. Canadian Water Resources Journal / Revue canadienne des ressources hydriques, **43**: 195-213. doi:<https://doi.org/10.1080/07011784.2017.1394801>.
- Gao, H. 2011. Groundwater Modeling for Flow Systems with Complex Geological and Hydrogeological Conditions. Procedia Earth and Planetary Science, **3**: 23-28. doi:<https://doi.org/10.1016/j.proeps.2011.09.061>.
- Gebremicael, T.G., Mohamed, Y.A., Betrie, G.D., van der Zaag, P., and Teferi, E. 2013. Trend analysis of runoff and sediment fluxes in the Upper Blue Nile basin: A combined analysis of statistical tests, physically-based models and landuse maps. Journal of Hydrology, **482**: 57-68. doi:<https://doi.org/10.1016/j.jhydrol.2012.12.023>.
- Gelbrecht, M., White, A., Bathiany, S., and Boers, N. 2023. Differentiable programming for Earth system modeling. Geoscientific Model Development, **16**: 3123-3135.
- Gorgij, A.D., Moghaddam, A.A., and Kisi, O. 2017. Groundwater budget forecasting, using hybrid wavelet-ANN-GP modelling: A case study of Azarshahr Plain, East Azerbaijan, Iran. Hydrology Research, **48**: 455-467. doi:<https://doi.org/10.2166/nh.2016.202>.
- Green, T.R., Taniguchi, M., Kooi, H., Gurdak, J.J., Allen, D.M., Hiscock, K.M., Treidel, H., and Aureli, A. 2011. Beneath the surface of global change: Impacts of climate change on groundwater. Journal of Hydrology, **405**: 532-560. doi:<https://doi.org/10.1016/j.jhydrol.2011.05.002>.
- Guo, Q., Zhao, Y., Lu, C., and Luo, J. 2023. High-dimensional inverse modeling of hydraulic tomography by physics informed neural network (HT-PINN). Journal of Hydrology, **616**: 128828. doi:<https://doi.org/10.1016/j.jhydrol.2022.128828>.
- Gupta, R., Srivastava, D., Sahu, M., Tiwari, S., Ambasta, R.K., and Kumar, P. 2021. Artificial intelligence to deep learning: machine intelligence approach for drug discovery. Molecular Diversity, **25**: 1315-1360. doi:10.1007/s11030-021-10217-3.

- Haggerty, R., Sun, J., Yu, H., and Li, Y. 2023. Application of machine learning in groundwater quality modeling - A comprehensive review. *Water Research*, **233**: 119745. doi:<https://doi.org/10.1016/j.watres.2023.119745>.
- Halder, S., Roy, M.B., and Roy, P.K. 2020. Analysis of groundwater level trend and groundwater drought using Standard Groundwater Level Index: a case study of an eastern river basin of West Bengal, India. *SN Applied Sciences*, **2**: 507. doi:<https://doi.org/10.1007/s42452-020-2302-6>.
- Hashimoto, D.A., Rosman, G., Rus, D., and Meireles, O.R. 2018. Artificial intelligence in surgery: promises and perils. *Annals of surgery*, **268**: 70.
- Hautier, G., Fischer, C.C., Jain, A., Mueller, T., and Ceder, G. 2010. Finding nature's missing ternary oxide compounds using machine learning and density functional theory. *Chemistry of Materials*, **22**: 3762-3767. doi:<https://doi.org/10.1021/cm100795d>.
- Hirschberg, J., and Manning, C.D. 2015. Advances in natural language processing. *Science*, **349**: 261-266. doi:[doi:10.1126/science.aaa8685](https://doi.org/10.1126/science.aaa8685).
- Hoque, M.A., Hoque, M.M., and Ahmed, K.M. 2007. Declining groundwater level and aquifer dewatering in Dhaka metropolitan area, Bangladesh: causes and quantification. *Hydrogeology Journal*, **15**: 1523-1534. doi:<https://doi.org/10.1007/s10040-007-0226-5>.
- Hornik, K. 1991. Approximation capabilities of multilayer feedforward networks. *Neural Networks*, **4**: 251-257. doi:[https://doi.org/10.1016/0893-6080\(91\)90009-T](https://doi.org/10.1016/0893-6080(91)90009-T).
- Hou, Z., Lao, W., Wang, Y., and Lu, W. 2021. Homotopy-based hyper-heuristic searching approach for reciprocal feedback inversion of groundwater contamination source and aquifer parameters. *Applied Soft Computing*, **104**: 107191. doi:<https://doi.org/10.1016/j.asoc.2021.107191>.
- Huang, J.-C., Ko, K.-M., Shu, M.-H., and Hsu, B.-M. 2020. Application and comparison of several machine learning algorithms and their integration models in regression problems. *Neural Computing and Applications*, **32**: 5461-5469. doi:[10.1007/s00521-019-04644-5](https://doi.org/10.1007/s00521-019-04644-5).

- Huang, X., Gao, L., Crosbie, R.S., Zhang, N., Fu, G., and Doble, R. 2019. Groundwater recharge prediction using linear regression, multi-layer perception network, and deep learning. *Water*, **11**: 1879. doi:<https://doi.org/10.3390/w11091879>.
- Husic, A., Fox, J., Ford, W., Agouridis, C., Currens, J., and Taylor, C. 2017. Sediment carbon fate in phreatic karst (Part 2): Numerical model development and application. *Journal of Hydrology*, **549**: 208-219. doi:<https://doi.org/10.1016/j.jhydrol.2017.03.059>.
- Hussain, F., Wu, R.-S., and Shih, D.-S. 2022. Water table response to rainfall and groundwater simulation using physics-based numerical model: WASH123D. *Journal of Hydrology: Regional Studies*, **39**: 100988. doi:<https://doi.org/10.1016/j.ejrh.2022.100988>.
- Hussain, M., and Mahmud, I. 2019. pyMannKendall: a python package for non parametric Mann Kendall family of trend tests. *Journal of Open Source Software*, **4**: 1556.
- IBM. 2023. What is computer vision? Available from <https://www.ibm.com/topics/computer-vision2023>.
- Jeong, J., Park, E., Chen, H., Kim, K.-Y., Shik Han, W., and Suk, H. 2020. Estimation of groundwater level based on the robust training of recurrent neural networks using corrupted data. *Journal of Hydrology*, **582**: 124512. doi:<https://doi.org/10.1016/j.jhydrol.2019.124512>.
- Jiang, S., Zheng, Y., and Solomatine, D. 2020. Improving AI System Awareness of Geoscience Knowledge: Symbiotic Integration of Physical Approaches and Deep Learning. *Geophysical Research Letters*, **47**: e2020GL088229. doi:<https://doi.org/10.1029/2020GL088229>.
- John, B., and Das, S. 2020. Identification of risk zone area of declining piezometric level in the urbanized regions around the City of Kolkata based on ground investigation and GIS techniques. *Groundwater for Sustainable Development*, **11**: 100354. doi:<https://doi.org/10.1016/j.gsd.2020.100354>.
- Jyrkama, M.I., and Sykes, J.F. 2007. The impact of climate change on spatially varying groundwater recharge in the grand river watershed (Ontario). *Journal of Hydrology*, **338**: 237-250. doi:<https://doi.org/10.1016/j.jhydrol.2007.02.036>.

- Kadeethum, T., Jørgensen, T.M., and Nick, H.M. 2020. Physics-informed Neural Networks for Solving Inverse Problems of Nonlinear Biot's Equations: Batch Training. arXiv preprint arXiv:2005.09638.
- Kahana, A., Turkel, E., Dekel, S., and Givoli, D. 2020. Obstacle segmentation based on the wave equation and deep learning. Journal of Computational Physics, **413**: 109458. doi:<https://doi.org/10.1016/j.jcp.2020.109458>.
- Kalantar, B., Al-Najjar, H.A., Pradhan, B., Saeidi, V., Halin, A.A., Ueda, N., and Naghibi, S.A. 2019. Optimized conditioning factors using machine learning techniques for groundwater potential mapping. Water, **11**: 1909.
- Karimpouli, S., and Tahmasebi, P. 2020. Physics informed machine learning: Seismic wave equation. Geoscience Frontiers, **11**: 1993-2001. doi:<https://doi.org/10.1016/j.gsf.2020.07.007>.
- Karniadakis, G.E., Kevrekidis, I.G., Lu, L., Perdikaris, P., Wang, S., and Yang, L. 2021. Physics-informed machine learning. Nature Reviews Physics, **3**: 422-440. doi:<https://doi.org/10.1038/s42254-021-00314-5>.
- Karpatne, A., Atluri, G., Faghmous, J.H., Steinbach, M., Banerjee, A., Ganguly, A., Shekhar, S., Samatova, N., and Kumar, V. 2017. Theory-Guided Data Science: A New Paradigm for Scientific Discovery from Data. IEEE Transactions on Knowledge and Data Engineering, **29**: 2318-2331. doi:<https://doi.org/10.1109/TKDE.2017.2720168>.
- Kavvas, E.S., Yang, L., Monk, J.M., Heckmann, D., and Palsson, B.O. 2020. A biochemically-interpretable machine learning classifier for microbial GWAS. Nature communications, **11**: 1-11. doi:<https://doi.org/10.1038/s41467-020-16310-9>.
- Khakbaz, B., Imam, B., Hsu, K., and Sorooshian, S. 2012. From lumped to distributed via semi-distributed: Calibration strategies for semi-distributed hydrologic models. Journal of Hydrology, **418-419**: 61-77. doi:<https://doi.org/10.1016/j.jhydrol.2009.02.021>.
- Khalil, A., Almasri, M.N., McKee, M., and Kaluarachchi, J.J. 2005. Applicability of statistical learning algorithms in groundwater quality modeling. Water Resources Research, **41**. doi:<https://doi.org/10.1029/2004WR003608>.

Khandelwal, A., Mithal, V., and Kumar, V. Post Classification Label Refinement Using Implicit Ordering Constraint Among Data Instances. In 2015 IEEE International Conference on Data Mining. 14-17 Nov. 2015 2015, pp. 799-804.

Khanzode, K.C.A., and Sarode, R.D. 2020. Advantages and disadvantages of artificial intelligence and machine learning: A literature review. International Journal of Library & Information Science (IJLIS), **9**: 3.

Kingma, D.P., and Ba, J. 2014. Adam: A method for stochastic optimization. arXiv preprint arXiv:1412.6980.

Kiranyaz, S., Avci, O., Abdeljaber, O., Ince, T., Gabbouj, M., and Inman, D.J. 2021. 1D convolutional neural networks and applications: A survey. Mechanical Systems and Signal Processing, **151**: 107398. doi:<https://doi.org/10.1016/j.ymssp.2020.107398>.

Knoben, W.J.M., Freer, J.E., and Woods, R.A. 2019. Technical note: Inherent benchmark or not? Comparing Nash–Sutcliffe and Kling–Gupta efficiency scores. Hydrol. Earth Syst. Sci., **23**: 4323-4331. doi:<https://doi.org/10.5194/hess-23-4323-2019>.

Knoben, W.J.M., Freer, J.E., Peel, M.C., Fowler, K.J.A., and Woods, R.A. 2020. A Brief Analysis of Conceptual Model Structure Uncertainty Using 36 Models and 559 Catchments. Water Resources Research, **56**: e2019WR025975. doi:<https://doi.org/10.1029/2019WR025975>.

Kochhar, A., Singh, H., Sahoo, S., Litoria, P.K., and Pateriya, B. 2022. Prediction and forecast of pre-monsoon and post-monsoon groundwater level: using deep learning and statistical modelling. Modeling Earth Systems and Environment, **8**: 2317-2329. doi:<https://doi.org/10.1007/s40808-021-01235-z>.

Köksal, G., Batmaz, İ., and Testik, M.C. 2011. A review of data mining applications for quality improvement in manufacturing industry. Expert Systems with Applications, **38**: 13448-13467. doi:<https://doi.org/10.1016/j.eswa.2011.04.063>.

Konikow, L.F., and Kendy, E. 2005. Groundwater depletion: A global problem. Hydrogeology Journal, **13**: 317-320. doi:<https://doi.org/10.1007/s10040-004-0411-8>.

Krenker, A., Bešter, J., and Kos, A. 2011. Introduction to the artificial neural networks. Artificial Neural Networks: Methodological Advances and Biomedical Applications. InTech: 1-18.

- Kroes, J., van Dam, J., Supit, I., de Abelleyra, D., Verón, S., de Wit, A., Boogaard, H., Angelini, M., Damiano, F., Groenendijk, P., Wesseling, J., and Veldhuizen, A. 2019. Agrohydrological analysis of groundwater recharge and land use changes in the Pampas of Argentina. Agricultural water management, **213**: 843-857. doi:<https://doi.org/10.1016/j.agwat.2018.12.008>.
- Kumar, R., Dwivedi, S.B., and Gaur, S. 2021. A comparative study of machine learning and Fuzzy-AHP technique to groundwater potential mapping in the data-scarce region. Computers & Geosciences, **155**: 104855.
- Labrecque, G., Chesnaux, R., and Boucher, M.A. 2019. Water-table fluctuation method for assessing aquifer recharge: application to Canadian aquifers and comparison with other methods. Hydrogeology Journal, **28**: 521-533.
- Lampert, D.J., and Wu, M. 2015. Development of an open-source software package for watershed modeling with the Hydrological Simulation Program in Fortran. Environmental Modelling & Software, **68**: 166-174. doi:<https://doi.org/10.1016/j.envsoft.2015.02.018>.
- Larocque, M., Cloutier, V., Levison, J., and Rosa, E. 2018. Results from the Quebec Groundwater Knowledge Acquisition Program. Canadian Water Resources Journal / Revue canadienne des ressources hydriques, **43**: 69-74. doi:<https://doi.org/10.1080/07011784.2018.1472040>.
- Larocque, M., Levison, J., Martin, A., and Chaumont, D. 2019. A review of simulated climate change impacts on groundwater resources in Eastern Canada. Canadian Water Resources Journal / Revue canadienne des ressources hydriques, **44**: 22-41. doi:<https://doi.org/10.1080/07011784.2018.1503066>.
- Larson, M. 2005. Numerical Modeling. In Encyclopedia of Coastal Science. Edited by M.L. Schwartz. Springer Netherlands, Dordrecht. pp. 730-733.
- Lawrence, S., and Giles, C.L. Overfitting and neural networks: conjugate gradient and backpropagation. In Proceedings of the IEEE-INNS-ENNS International Joint Conference on Neural Networks. IJCNN 2000. Neural Computing: New Challenges and Perspectives for the New Millennium. 27-27 July 2000 2000. Vol. 1, pp. 114-119 vol.111.

- LeCun, Y., Boser, B., Denker, J.S., Henderson, D., Howard, R.E., Hubbard, W., and Jackel, L.D. 1989. Backpropagation applied to handwritten zip code recognition. *Neural computation*, **1**: 541-551. doi:<https://doi.org/10.1162/neco.1989.1.4.541>.
- Lee, J.-Y., Yi, M.-J., Yoo, Y.-K., Ahn, K.-H., Kim, G.-B., and Won, J.-H. 2007. A review of the National Groundwater Monitoring Network in Korea. *Hydrological Processes*, **21**: 907-919. doi:<https://doi.org/10.1002/hyp.6282>.
- Lee, S., Hyun, Y., Lee, S., and Lee, M.-J. 2020. Groundwater potential mapping using remote sensing and GIS-based machine learning techniques. *Remote Sensing*, **12**: 1200.
- Lehr, C., and Lischeid, G. 2020. Efficient screening of groundwater head monitoring data for anthropogenic effects and measurement errors. *Hydrol. Earth Syst. Sci.*, **24**: 501-513. doi:<https://hess.copernicus.org/articles/24/501/2020/>.
- Li, C., Han, Z., Li, Y., Li, M., Wang, W., Dou, J., Xu, L., and Chen, G. 2023. Physical information-fused deep learning model ensembled with a subregion-specific sampling method for predicting flood dynamics. *Journal of Hydrology*, **620**: 129465. doi:<https://doi.org/10.1016/j.jhydrol.2023.129465>.
- Li, H., and Jiao, J.J. 2002. Analytical solutions of tidal groundwater flow in coastal two-aquifer system. *Advances in Water Resources*, **25**: 417-426. doi:[https://doi.org/10.1016/S0309-1708\(02\)00004-0](https://doi.org/10.1016/S0309-1708(02)00004-0).
- Li, W., Bazant, M.Z., and Zhu, J. 2021. A physics-guided neural network framework for elastic plates: Comparison of governing equations-based and energy-based approaches. *Computer Methods in Applied Mechanics and Engineering*, **383**: 113933. doi:<https://doi.org/10.1016/j.cma.2021.113933>.
- Lijzen, J.P.A., Otte, P., and van Dreumel, M. 2014. Towards sustainable management of groundwater: Policy developments in The Netherlands. *Science of the Total Environment*, **485-486**: 804-809. doi:<https://doi.org/10.1016/j.scitotenv.2014.02.081>.
- Lin, Y.-F., Chang, C.-H., and Tsai, J.-P. 2022. Analytical solution for estimating transient vertical groundwater flux from temperature-depth profiles. *Journal of Hydrology*, **610**: 127920. doi:<https://doi.org/10.1016/j.jhydrol.2022.127920>.

- Ling, J., Kurzawski, A., and Templeton, J. 2016. Reynolds averaged turbulence modelling using deep neural networks with embedded invariance. *Journal of Fluid Mechanics*, **807**: 155-166. doi:<https://doi.org/10.1017/jfm.2016.615>[Opens].
- Lipton, Z.C. 2018. The mythos of model interpretability: In machine learning, the concept of interpretability is both important and slippery. *Queue*, **16**: 31-57.
- Liu, J., Wang, K., Ma, S., and Huang, J. 2013. 1 Accounting for Linkage Disequilibrium in Genome-Wide Association Studies: A Penalized Regression Method. *Statistics and its interface*, **6**: 99-115. doi:<https://doi.org/10.4310/SII.2013.v6.n1.a10>.
- Liu, Q., Gui, D., Zhang, L., Niu, J., Dai, H., Wei, G., and Hu, B.X. 2022. Simulation of regional groundwater levels in arid regions using interpretable machine learning models. *Science of the Total Environment*, **831**: 154902. doi:<https://doi.org/10.1016/j.scitotenv.2022.154902>.
- Lukoševičius, M., and Jaeger, H. 2009. Reservoir computing approaches to recurrent neural network training. *Computer Science Review*, **3**: 127-149. doi:<https://doi.org/10.1016/j.cosrev.2009.03.005>.
- Lundberg, S.M., and Lee, S.-I. 2017. A unified approach to interpreting model predictions. *Advances in neural information processing systems*, **30**.
- Luo, Q., Yang, Y., Qian, J., Wang, X., Chang, X., Ma, L., Li, F., and Wu, J. 2020. Spring protection and sustainable management of groundwater resources in a spring field. *Journal of Hydrology*, **582**: 124498. doi:<https://doi.org/10.1016/j.jhydrol.2019.124498>.
- Lykkegaard, M.B., Dodwell, T.J., and Moxey, D. 2021. Accelerating uncertainty quantification of groundwater flow modelling using a deep neural network proxy. *Computer Methods in Applied Mechanics and Engineering*, **383**: 113895.
- Ma, Y., Zheng, J., Liang, Y., Klemeš, J.J., Du, J., Liao, Q., Lu, H., and Wang, B. 2022. Deppipe: Theory-guided neural network method for predicting burst pressure of corroded pipelines. *Process Safety and Environmental Protection*, **162**: 595-609. doi:<https://doi.org/10.1016/j.psep.2022.04.036>.

- Marchant, B.P., Cuba, D., Brauns, B., and Bloomfield, J.P. 2022. Temporal interpolation of groundwater level hydrographs for regional drought analysis using mixed models. *Hydrogeology Journal*, **30**: 1801-1817. doi:<https://doi.org/10.1007/s10040-022-02528-y>.
- Martina, M.L.V., Todini, E., and Liu, Z. 2011. Preserving the dominant physical processes in a lumped hydrological model. *Journal of Hydrology*, **399**: 121-131. doi:<https://doi.org/10.1016/j.jhydrol.2010.12.039>.
- Martínez-Santos, P., Díaz-Alcaide, S., De la Hera-Portillo, A., and Gómez-Escaloniella, V. 2021. Mapping groundwater-dependent ecosystems by means of multi-layer supervised classification. *Journal of Hydrology*, **603**: 126873. doi:<https://doi.org/10.1016/j.jhydrol.2021.126873>.
- Mathon, B.R., Ozbek, M.M., and Pinder, G.F. 2008. Transmissivity and storage coefficient estimation by coupling the Cooper–Jacob method and modified fuzzy least-squares regression. *Journal of Hydrology*, **353**: 267-274. doi:<https://doi.org/10.1016/j.jhydrol.2008.02.004>.
- Maxwell, R.M., Condon, L.E., and Kollet, S.J. 2015. A high-resolution simulation of groundwater and surface water over most of the continental US with the integrated hydrologic model ParFlow v3. *Geosci. Model Dev.*, **8**: 923-937. doi:<https://doi.org/10.5194/gmd-8-923-2015>.
- Medsker, L.R., and Jain, L. 2001. Recurrent neural networks. *Design and Applications*, **5**: 64-67.
- Meehl, G.A., Boer, G.J., Covey, C., Latif, M., and Stouffer, R.J. 2000. The coupled model intercomparison project (CMIP). *Bulletin of the American Meteorological Society*, **81**: 313-318.
- Meggiorin, M., Passadore, G., Bertoldo, S., Sottani, A., and Rinaldo, A. 2023. Comparison of Three Imputation Methods for Groundwater Level Timeseries. *Water*, **15**: 801. doi:<https://doi.org/10.3390/w15040801>.
- Meixner, T., Manning, A.H., Stonestrom, D.A., Allen, D.M., Ajami, H., Blasch, K.W., Brookfield, A.E., Castro, C.L., Clark, J.F., Gochis, D.J., Flint, A.L., Neff, K.L., Niraula, R., Rodell, M., Scanlon, B.R., Singha, K., and Walvoord, M.A. 2016. Implications of projected climate change for groundwater recharge in the western United States. *Journal of Hydrology*, **534**: 124-138. doi:<https://doi.org/10.1016/j.jhydrol.2015.12.027>.

MELCCFP. 2023a. Programme d'acquisition de connaissances sur les eaux souterraines. Available from <http://www.mddelcc.gouv.qc.ca/eau/souterraines/programmes/acquisition-connaissance.htm> [accessed January 2023].

MELCCFP. 2023b. Normales climatiques 1981-2010. Available from <https://www.environnement.gouv.qc.ca/climat/normales/climat-qc.htm> [2023].

MELCCFP. 2023c. Réseau de suivi des eaux souterraines du Québec. Available from <https://www.environnement.gouv.qc.ca/eau/piezo/2023>.

Meng, X., Li, Z., Zhang, D., and Karniadakis, G.E. 2020. PPINN: Parareal physics-informed neural network for time-dependent PDEs. Computer Methods in Applied Mechanics and Engineering, **370**: 113250. doi:<https://doi.org/10.1016/j.cma.2020.113250>.

Merritt, W.S., Letcher, R.A., and Jakeman, A.J. 2003. A review of erosion and sediment transport models. Environmental Modelling & Software, **18**: 761-799. doi:[https://doi.org/10.1016/S1364-8152\(03\)00078-1](https://doi.org/10.1016/S1364-8152(03)00078-1).

Misyris, G.S., Venzke, A., and Chatzivasileiadis, S. Physics-Informed Neural Networks for Power Systems. In 2020 IEEE Power & Energy Society General Meeting (PESGM). 2-6 Aug. 2020 2020, pp. 1-5.

Moghaddam, D.D., Rahmati, O., Panahi, M., Tiefenbacher, J., Darabi, H., Haghizadeh, A., Haghghi, A.T., Nalivan, O.A., and Tien Bui, D. 2020. The effect of sample size on different machine learning models for groundwater potential mapping in mountain bedrock aquifers. Catena, **187**. doi:<https://doi.org/10.1016/j.catena.2019.104421>.

Mohamed, A., Dan, L., Kai, S., Mohamed, M., Aldaw, E., and Elubid, B. 2019. Hydrochemical Analysis and Fuzzy Logic Method for Evaluation of Groundwater Quality in the North Chengdu Plain, China. International Journal of Environmental Research and Public Health, **16**: 302. doi:<https://doi.org/10.3390/ijerph16030302>.

Montesinos López, O.A., Montesinos López, A., and Crossa, J. 2022. Overfitting, Model Tuning, and Evaluation of Prediction Performance. In Multivariate Statistical Machine Learning Methods for Genomic Prediction. Edited by O.A. Montesinos López and A. Montesinos López and J. Crossa. Springer International Publishing, Cham. pp. 109-139.

- Mosavi, A., Sajedi Hosseini, F., Choubin, B., Taromideh, F., Ghodsi, M., Nazari, B., and Dineva, A.A. 2021. Susceptibility mapping of groundwater salinity using machine learning models. Environmental Science and Pollution Research, **28**: 10804-10817. doi:10.1007/s11356-020-11319-5.
- Motiee, H., and McBean, E. 2017. Assessment of Climate Change Impacts on Groundwater Recharge for Different Soil Types-Guelph Region in Grand River Basin, Canada. Ecopersia, **5**: 1731-1744.
- Muralidhar, N., Bu, J., Cao, Z., He, L., Ramakrishnan, N., Tafti, D., and Karpatne, A. PhyNet: Physics Guided Neural Networks for Particle Drag Force Prediction in Assembly. *In* Proceedings of the 2020 SIAM International Conference on Data Mining. 2020. SIAM, pp. 559-567.
- Naghibi, S.A., Ahmadi, K., and Daneshi, A. 2017. Application of Support Vector Machine, Random Forest, and Genetic Algorithm Optimized Random Forest Models in Groundwater Potential Mapping. Water Resources Management : An International Journal - Published for the European Water Resources Association (EWRA), **31**: 2761-2775. doi:<https://doi.org/10.1007/s11269-017-1660-3>.
- Narkhede, M.V., Bartakke, P.P., and Sutaone, M.S. 2022. A review on weight initialization strategies for neural networks. Artificial Intelligence Review, **55**: 291-322. doi:10.1007/s10462-021-10033-z.
- Nath, B., Ni-Meister, W., and Choudhury, R. 2021. Impact of urbanization on land use and land cover change in Guwahati city, India and its implication on declining groundwater level. Groundwater for Sustainable Development, **12**: 100500. doi:<https://doi.org/10.1016/j.gsd.2020.100500>.
- Nearing, G.S., Kratzert, F., Sampson, A.K., Pelissier, C.S., Klotz, D., Frame, J.M., Prieto, C., and Gupta, H.V. 2021. What role does hydrological science play in the age of machine learning? Water Resources Research, **57**: e2020WR028091.
- Negm, A., Abdakhimova, P., Hayashi, M., and Rasouli, K. 2021. Effects of climate change on depression-focused groundwater recharge in the Canadian Prairies. Vadose Zone Journal, **20**: e20153. doi:<https://doi.org/10.1002/vzj2.20153>.

- Neuman, S.P. 1973. Calibration of distributed parameter groundwater flow models viewed as a multiple-objective decision process under uncertainty. *Water Resources Research*, **9**: 1006-1021. doi:<https://doi.org/10.1029/WR009i004p01006>.
- Nguyen, C., Hassner, T., Seeger, M., and Archambeau, C. Leep: A new measure to evaluate transferability of learned representations. *In International Conference on Machine Learning*. 2020a. PMLR, pp. 7294-7305.
- Nguyen, P.T., Ha, D.H., Jaafari, A., Nguyen, H.D., Van Phong, T., Al-Ansari, N., Prakash, I., Le, H.V., and Pham, B.T. 2020b. Groundwater Potential Mapping Combining Artificial Neural Network and Real AdaBoost Ensemble Technique: The DakNong Province Case-study, Vietnam. *International Journal of Environmental Research and Public Health*, **17**: 2473. doi:<https://doi.org/10.3390/ijerph17072473>.
- Nguyen, P.T., Ha, D.H., Nguyen, H.D., Van Phong, T., Trinh, P.T., Al-Ansari, N., Le, H.V., Pham, B.T., Ho, L.S., and Prakash, I. 2020c. Improvement of credal decision trees using ensemble frameworks for groundwater potential modeling. *Sustainability*, **12**: 2622. doi:<https://doi.org/10.3390/su12072622>.
- Nguyen, T.-T., Huang, J.Z., and Nguyen, T.T. 2015. Two-level quantile regression forests for bias correction in range prediction. *Machine Learning*, **101**: 325-343. doi:<https://doi.org/10.1007/s10994-014-5452-1>.
- Oberlack, M. 2002. Symmetries and invariant solutions of turbulent flows and their implications for turbulence modelling. *In Theories of Turbulence*. Springer. pp. 301-366.
- Ogundokun, R.O., Maskeliunas, R., Misra, S., and Damaševičius, R. Improved CNN based on batch normalization and adam optimizer. *In International Conference on Computational Science and Its Applications*. 2022. Springer, pp. 593-604.
- Ongsulee, P. Artificial intelligence, machine learning and deep learning. *In 2017 15th international conference on ICT and knowledge engineering (ICT&KE)*. 2017. IEEE, pp. 1-6.
- Osisanwo, F., Akinsola, J., Awodele, O., Hinmikaiye, J., Olakanmi, O., and Akinjobi, J. 2017. Supervised machine learning algorithms: classification and comparison. *International Journal of Computer Trends and Technology (IJCTT)*, **48**: 128-138.

- Oudin, L., Hervieu, F., Michel, C., Perrin, C., Andréassian, V., Anctil, F., and Loumagne, C. 2005. Which potential evapotranspiration input for a lumped rainfall–runoff model?: Part 2—Towards a simple and efficient potential evapotranspiration model for rainfall–runoff modelling. *Journal of Hydrology*, **303**: 290-306. doi:<https://doi.org/10.1016/j.jhydrol.2004.08.026>.
- Parent, M., and Occhietti, S. 2007. Late Wisconsinan Deglaciation and Champlain Sea Invasion in the St. Lawrence Valley, Québec. *Geographie Physique Et Quaternaire*, **42**: 215-246.
- Park, Y., Ligaray, M., Kim, Y.M., Kim, J.H., Cho, K.H., and Sthiannopkao, S. 2016. Development of enhanced groundwater arsenic prediction model using machine learning approaches in Southeast Asian countries. *Desalination and Water Treatment*, **57**: 12227-12236. doi:<https://doi.org/10.1080/19443994.2015.1049411>.
- Parra, V., Fuentes-Aguilera, P., and Muñoz, E. 2018. Identifying advantages and drawbacks of two hydrological models based on a sensitivity analysis: a study in two Chilean watersheds. *Hydrological Sciences Journal*, **63**: 1831-1843. doi:10.1080/02626667.2018.1538593.
- Pathak, A.A., and Dodamani, B.M. 2019. Trend Analysis of Groundwater Levels and Assessment of Regional Groundwater Drought: Ghataprabha River Basin, India. *Natural resources research*, **28**: 631-643. doi:<https://doi.org/10.1007/s11053-018-9417-0>.
- Patle, G.T., Singh, D.K., Sarangi, A., Rai, A., Khanna, M., and Sahoo, R.N. 2015. Time series analysis of groundwater levels and projection of future trend. *Journal of the Geological Society of India*, **85**: 232-242. doi:<https://doi.org/10.1007/s12594-015-0209-4>.
- Pazzani, M.J., and Brunk, C.A. 1991. Detecting and correcting errors in rule-based expert systems: an integration of empirical and explanation-based learning. *Knowledge Acquisition*, **3**: 157-173. doi:[https://doi.org/10.1016/1042-8143\(91\)90003-6](https://doi.org/10.1016/1042-8143(91)90003-6).
- Pham, D.T., and Afify, A.A. 2005. Machine-learning techniques and their applications in manufacturing. *Proceedings of the Institution of Mechanical Engineers, Part B: Journal of Engineering Manufacture*, **219**: 395-412. doi:10.1243/095440505x32274.
- Pham, Q.B., Kumar, M., Di Nunno, F., Elbeltagi, A., Granata, F., Islam, A.R.M.T., Talukdar, S., Nguyen, X.C., Ahmed, A.N., and Anh, D.T. 2022. Groundwater level prediction using machine

- learning algorithms in a drought-prone area. *Neural Computing and Applications*, **34**: 10751-10773. doi:10.1007/s00521-022-07009-7.
- Piccione, A., Berkery, J., Sabbagh, S., and Andreopoulos, Y. 2020. Physics-guided machine learning approaches to predict the ideal stability properties of fusion plasmas. *Nuclear Fusion*, **60**. doi:<https://doi.org/10.1088/1741-4326/ab7597>.
- Pogiatzis, A., and Samakovitis, G. 2021. An Event-Driven Serverless ETL Pipeline on AWS. *Applied Sciences*, **11**: 191. Available from <https://www.mdpi.com/2076-3417/11/1/191> [accessed].
- Pradhan, S., Kumar, S., Kumar, Y., and Sharma, H.C. 2019. Assessment of groundwater utilization status and prediction of water table depth using different heuristic models in an Indian interbasin. *Soft Computing : A Fusion of Foundations, Methodologies and Applications*, **23**: 10261-10285. doi:<https://doi.org/10.1007/s00500-018-3580-4>.
- Preziosi, L., and Farina, A. 2002. On Darcy's law for growing porous media. *International Journal of Non-Linear Mechanics*, **37**: 485-491.
- Qureshi, A.S., Gill, M.A., and Sarwar, A. 2010. Sustainable groundwater management in Pakistan: challenges and opportunities. *Irrigation and Drainage*, **59**: 107-116. doi:<https://doi.org/10.1002/ird.455>.
- Raazia, S., and Dar, A.Q. 2021. A numerical model of groundwater flow in Karewa-Alluvium aquifers of NW Indian Himalayan Region. *Modeling Earth Systems and Environment*: 1-12. doi:<https://doi.org/10.1007/s40808-021-01126-3>.
- Rackauckas, C., Ma, Y., Martensen, J., Warner, C., Zubov, K., Supekar, R., Skinner, D., Ramadhan, A., and Edelman, A. 2020. Universal differential equations for scientific machine learning. arXiv preprint arXiv:2001.04385.
- Rahman, A.T.M.S., Hosono, T., Quilty, J.M., Das, J., and Basak, A. 2020. Multiscale groundwater level forecasting: Coupling new machine learning approaches with wavelet transforms. *Advances in Water Resources*, **141**: 103595. doi:<https://doi.org/10.1016/j.advwatres.2020.103595>.
- Raiassi, M., Perdikaris, P., and Karniadakis, G.E. 2019. Physics-informed neural networks: A deep learning framework for solving forward and inverse problems involving nonlinear partial

differential equations. Journal of Computational physics, **378**: 686-707.

doi:<https://doi.org/10.1016/j.jcp.2018.10.045>.

Razavi, S., Hannah, D.M., Elshorbagy, A., Kumar, S., Marshall, L., Solomatine, D.P., Dezfuli, A., Sadegh, M., and Famiglietti, J. 2022. Coevolution of machine learning and process-based modelling to revolutionize Earth and environmental sciences: A perspective. *Hydrological Processes*, **36**: e14596.

Reddy, G.T., Reddy, M.P.K., Lakshmanna, K., Kaluri, R., Rajput, D.S., Srivastava, G., and Baker, T. 2020. Analysis of Dimensionality Reduction Techniques on Big Data. *IEEE Access*, **8**: 54776-54788. doi:10.1109/ACCESS.2020.2980942.

Reichstein, M., Camps-Valls, G., Stevens, B., Jung, M., Denzler, J., Carvalhais, N., and Prabhat. 2019. Deep learning and process understanding for data-driven Earth system science. *Nature*, **566**: 195-204. doi:<https://doi.org/10.1038/s41586-019-0912-1>.

Rey, N., Rosa, E., Cloutier, V., and Lefebvre, R. 2018. Using water stable isotopes for tracing surface and groundwater flow systems in the Barlow-Ojibway Clay Belt, Quebec, Canada. *Canadian Water Resources Journal / Revue canadienne des ressources hydriques*, **43**: 173-194. doi:<https://doi.org/10.1080/07011784.2017.1403960>.

Riahi, K., van Vuuren, D.P., Kriegler, E., Edmonds, J., O'Neill, B.C., Fujimori, S., Bauer, N., Calvin, K., Dellink, R., Fricko, O., Lutz, W., Popp, A., Cuaresma, J.C., Kc, S., Leimbach, M., Jiang, L., Kram, T., Rao, S., Emmerling, J., Ebi, K., Hasegawa, T., Havlik, P., Humpenöder, F., Da Silva, L.A., Smith, S., Stehfest, E., Bosetti, V., Eom, J., Gernaat, D., Masui, T., Rogelj, J., Strefler, J., Drouet, L., Krey, V., Luderer, G., Harmsen, M., Takahashi, K., Baumstark, L., Doelman, J.C., Kainuma, M., Klimont, Z., Marangoni, G., Lotze-Campen, H., Obersteiner, M., Tabeau, A., and Tavoni, M. 2017. The Shared Socioeconomic Pathways and their energy, land use, and greenhouse gas emissions implications: An overview. *Global Environmental Change*, **42**: 153-168. doi:<https://doi.org/10.1016/j.gloenvcha.2016.05.009>.

Rivard, C., Vigneault, H., Piggott, A.R., Larocque, M., and Anctil, F. 2009. Groundwater recharge trends in Canada. *Canadian Journal of Earth Sciences*, **46**: 841-854. doi:<https://doi.org/10.1139/E09-056>.

- Rivera, A. 2014. Canada's groundwater resources. Fitzhenry & Whiteside.
- Rodríguez, L., Vives, L., and Gomez, A. 2013. Conceptual and numerical modeling approach of the Guarani Aquifer System. *Hydrol. Earth Syst. Sci.*, **17**: 295-314. doi:10.5194/hess-17-295-2013.
- Rondeau-Genesse, G., and Braun, M. 2020. Production des scénarios climatiques pour les projets : Impact des changements climatiques sur les débits au Québec (cQ2) et la thématique Évolution du climat du projet de Soutien à INFO-Crue. Ouranos.
- Rudin, C. 2019. Stop explaining black box machine learning models for high stakes decisions and use interpretable models instead. *Nature Machine Intelligence*, **1**: 206-215. doi:<https://doi.org/10.1038/s42256-019-0048-x>.
- Sabat, L., and Kundu, C.K. 2020. History of finite element method: a review. *Recent Developments in Sustainable Infrastructure: Select Proceedings of ICRDSI 2019*: 395-404.
- Sahoo, S., and Jha, M.K. 2013. Groundwater-level prediction using multiple linear regression and artificial neural network techniques: a comparative assessment. *Hydrogeology Journal*, **21**. doi:<https://doi.org/10.1007/s10040-013-1029-5>.
- Sahoo, S., Russo, T.A., Elliott, J., and Foster, I. 2017a. Machine learning algorithms for modeling groundwater level changes in agricultural regions of the U.S. *Water Resources Research*, **53**: 3878-3895. doi:<https://doi.org/10.1002/2016WR019933>.
- Sahoo, S., Russo, T., Elliott, J., and Foster, I. 2017b. Machine learning algorithms for modeling groundwater level changes in agricultural regions of the US. *Water Resources Research*, **53**: 3878-3895.
- Sahour, H., Gholami, V., and Vazifedan, M. 2020. A comparative analysis of statistical and machine learning techniques for mapping the spatial distribution of groundwater salinity in a coastal aquifer. *Journal of Hydrology*, **591**: 125321. doi:<https://doi.org/10.1016/j.jhydrol.2020.125321>.
- Sajedi-Hosseini, F., Malekian, A., Choubin, B., Rahmati, O., Cipullo, S., Coulon, F., and Pradhan, B. 2018. A novel machine learning-based approach for the risk assessment of nitrate groundwater contamination. *Science of the Total Environment*, **644**: 954-962. doi:<https://doi.org/10.1016/j.scitotenv.2018.07.054>.

- Sanchez, P., Voisey, J.P., Xia, T., Watson, H.I., O'Neil, A.Q., and Tsafaris, S.A. 2022. Causal machine learning for healthcare and precision medicine. Royal Society Open Science, **9**: 220638.
- Satish Kumar, K., and Venkata Rathnam, E. 2019. Analysis and Prediction of Groundwater Level Trends Using Four Variations of Mann Kendall Tests and ARIMA Modelling. Journal of the Geological Society of India, **94**: 281-289. doi:<https://doi.org/10.1007/s12594-019-1308-4>.
- Schellekens, J. 2018. wflow Documentation. Detares, Delft.
- Schichl, H. 2004. Models and the history of modeling. Modeling languages in mathematical optimization: 25-36.
- Schwartz, M.O. 2006. Numerical modelling of groundwater vulnerability: the example Namibia. Environmental Geology, **50**: 237-249. doi:10.1007/s00254-006-0204-6.
- Secci, D., A. Godoy, V., and Gómez-Hernández, J.J. 2024. Physics-Informed Neural Networks for solving transient unconfined groundwater flow. Computers & Geosciences, **182**: 105494. doi:<https://doi.org/10.1016/j.cageo.2023.105494>.
- Secci, D., Giovanna Tanda, M., D'Oria, M., and Todaro, V. 2023. Artificial intelligence models to evaluate the impact of climate change on groundwater resources. Journal of Hydrology, **627**: 130359. doi:<https://doi.org/10.1016/j.jhydrol.2023.130359>.
- Sen, P.K. 1968. Estimates of the Regression Coefficient Based on Kendall's Tau. Journal of the American Statistical Association, **63**: 1379-1389. doi:<https://doi.org/10.1080/01621459.1968.10480934>.
- Shadab, M.A., Luo, D., Hiatt, E., Shen, Y., and Hesse, M.A. 2023. Investigating steady unconfined groundwater flow using Physics Informed Neural Networks. Advances in Water Resources, **177**: 104445. doi:<https://doi.org/10.1016/j.advwatres.2023.104445>.
- Shaham, U., Yamada, Y., and Negahban, S. 2018. Understanding adversarial training: Increasing local stability of supervised models through robust optimization. Neurocomputing, **307**: 195-204. doi:<https://doi.org/10.1016/j.neucom.2018.04.027>.
- Shamsuddoha, M., Chandler, R.E., Taylor, R.G., and Ahmed, K.M. 2009. Recent trends in groundwater levels in a highly seasonal hydrological system: the Ganges-Brahmaputra-

Meghna Delta. Hydrol. Earth Syst. Sci., **13**: 2373-2385. doi:<https://doi.org/10.5194/hess-13-2373-2009>.

Shen, C., Appling, A.P., Gentine, P., Bandai, T., Gupta, H., Tartakovsky, A., Baity-Jesi, M., Fenicia, F., Kifer, D., and Li, L. 2023. Differentiable modelling to unify machine learning and physical models for geosciences. *Nature Reviews Earth & Environment*: 1-16.

Shiri, J., Kisi, O., Yoon, H., Lee, K.-K., and Nazemi, A.H. 2013. Predicting groundwater level fluctuations with meteorological effect implications—A comparative study among soft computing techniques. *Computers & Geosciences*, **56**: 32-44. doi:<http://dx.doi.org/10.1016/j.cageo.2013.01.007>.

Singarimbun, R.N., Nababan, E.B., and Sitompul, O.S. Adaptive Moment Estimation To Minimize Square Error In Backpropagation Algorithm. *In* 2019 International Conference of Computer Science and Information Technology (ICoSNIKOM). 28-29 Nov. 2019 2019, pp. 1-7.

Singh, A., Thakur, N., and Sharma, A. A review of supervised machine learning algorithms. *In* 2016 3rd international conference on computing for sustainable global development (INDIACoM). 2016. Ieee, pp. 1310-1315.

Singha, S., Pasupuleti, S., Singha, S.S., Singh, R., and Kumar, S. 2021. Prediction of groundwater quality using efficient machine learning technique. *Chemosphere*, **276**: 130265. doi:<https://doi.org/10.1016/j.chemosphere.2021.130265>.

Slater, L.J., Arnal, L., Boucher, M.-A., Chang, A.Y.-Y., Moulds, S., Murphy, C., Nearing, G., Shalev, G., Shen, C., and Speight, L. 2023. Hybrid forecasting: blending climate predictions with AI models. *Hydrology and Earth System Sciences*, **27**: 1865-1889.

Sloan, W.T. 2000. A physics-based function for modeling transient groundwater discharge at the watershed scale. *Water Resources Research*, **36**: 225-241. doi:<https://doi.org/10.1029/1999WR900221>.

Solomatine, D.P., Dibike, Y.B., and Kukuric, N. 1999. Automatic calibration of groundwater models using global optimization techniques. *Hydrological Sciences Journal*, **44**: 879-894. doi:10.1080/02626669909492287.

- Sonali, P., and Nagesh Kumar, D. 2013. Review of trend detection methods and their application to detect temperature changes in India. *Journal of Hydrology*, **476**: 212-227. doi:<https://doi.org/10.1016/j.jhydrol.2012.10.034>.
- Song, T., Ding, W., Liu, H., Wu, J., Zhou, H., and Chu, J. 2020. Uncertainty quantification in machine learning modeling for multi-step time series forecasting: Example of recurrent neural networks in discharge simulations. *Water*, **12**: 912.
- Sousa, C.A.R.d. An overview on weight initialization methods for feedforward neural networks. In 2016 International Joint Conference on Neural Networks (IJCNN). 24-29 July 2016 2016, pp. 52-59.
- Srivastava, N., Hinton, G., Krizhevsky, A., Sutskever, I., and Salakhutdinov, R. 2014. Dropout: a simple way to prevent neural networks from overfitting. *The journal of machine learning research*, **15**: 1929-1958.
- Su, Y.-S., Ni, C.-F., Li, W.-C., Lee, I.-H., and Lin, C.-P. 2020. Applying deep learning algorithms to enhance simulations of large-scale groundwater flow in IoTs. *APPLIED SOFT COMPUTING*, **92**: 106298. doi:<https://doi.org/10.1016/j.asoc.2020.106298>.
- Sulis, M., Paniconi, C., Rivard, C., Harvey, R., and Chaumont, D. 2011. Assessment of climate change impacts at the catchment scale with a detailed hydrological model of surface-subsurface interactions and comparison with a land surface model [<https://doi.org/10.1029/2010WR009167>]. *Water Resources Research*, **47**. doi:<https://doi.org/10.1029/2010WR009167>.
- Sulis, M., Paniconi, C., Marrocù, M., Huard, D., and Chaumont, D. 2012. Hydrologic response to multimodel climate output using a physically based model of groundwater/surface water interactions [<https://doi.org/10.1029/2012WR012304>]. *Water Resources Research*, **48**. doi:<https://doi.org/10.1029/2012WR012304>.
- Sulis, M., Meyerhoff, S.B., Paniconi, C., Maxwell, R.M., Putti, M., and Kollet, S.J. 2010. A comparison of two physics-based numerical models for simulating surface water–groundwater interactions. *Advances in Water Resources*, **33**: 456-467. doi:<https://doi.org/10.1016/j.advwatres.2010.01.010>.

- Sun, A.Y. 2018. Discovering state-parameter mappings in subsurface models using generative adversarial networks. *Geophysical Research Letters*, **45**: 11,137-111,146. doi: <https://doi.org/10.1029/2018GL080404>.
- Sun, Y., Wang, X., and Tang, X. Deep learning face representation from predicting 10,000 classes. *In Proceedings of the IEEE conference on computer vision and pattern recognition*. 2014, pp. 1891-1898.
- Sun, Y., Wendi, D., Kim, D.E., and Lioung, S.Y. 2016. Technical note: Application of artificial neural networks in groundwater table forecasting – a case study in a Singapore swamp forest. *Hydrol. Earth Syst. Sci.*, **20**: 1405-1412. doi:10.5194/hess-20-1405-2016.
- Suzuki, K. 2011. Artificial neural networks: methodological advances and biomedical applications. BoD–Books on Demand.
- Sylvain, J.-D., Anctil, F., and Thiffault, É. 2021. Using bias correction and ensemble modelling for predictive mapping and related uncertainty: A case study in digital soil mapping. *Geoderma*, **403**: 115153. doi:<https://doi.org/10.1016/j.geoderma.2021.115153>.
- Tahmasebi, P., Kamrava, S., Bai, T., and Sahimi, M. 2020. Machine learning in geo- and environmental sciences: From small to large scale. *Advances in Water Resources*, **142**: 103619. doi:<https://doi.org/10.1016/j.advwatres.2020.103619>.
- Taillardat, M., Mestre, O., Zamo, M., and Naveau, P. 2016. Calibrated Ensemble Forecasts Using Quantile Regression Forests and Ensemble Model Output Statistics. *Monthly Weather Review*, **144**: 2375-2393. doi:<https://doi.org/10.1175/MWR-D-15-0260.1>.
- Tang, Y., Lu, C., and Luo, J. 2023. An Analytical solution for groundwater lens pumping in a three-dimensional rectangular island. *Journal of Hydrology*, **617**: 128928. doi:<https://doi.org/10.1016/j.jhydrol.2022.128928>.
- Tao, H., Hameed, M.M., Marhoon, H.A., Zounemat-Kermani, M., Heddam, S., Kim, S., Sulaiman, S.O., Tan, M.L., Sa'adi, Z., Mehr, A.D., Allawi, M.F., Abba, S.I., Zain, J.M., Falah, M.W., Jamei, M., Bokde, N.D., Bayatvarkeshi, M., Al-Mukhtar, M., Bhagat, S.K., Tiyasha, T., Khedher, K.M., Al-Ansari, N., Shahid, S., and Yaseen, Z.M. 2022. Groundwater level

- prediction using machine learning models: A comprehensive review. *Neurocomputing*, **489**: 271-308. doi:<https://doi.org/10.1016/j.neucom.2022.03.014>.
- Tapoglou, E., Trichakis, I.C., Dokou, Z., Nikolos, I.K., and Karatzas, G.P. 2014. Groundwater-level forecasting under climate change scenarios using an artificial neural network trained with particle swarm optimization. *Hydrological sciences journal = Journal des sciences hydrologiques.*, **59**: 1225-1239. doi:<http://dx.doi.org/10.1080/02626667.2013.838005>.
- Tartakovsky, A.M., Marrero, C.O., Perdikaris, P., Tartakovsky, G.D., and Barajas-Solano, D. 2020. Physics-Informed Deep Neural Networks for Learning Parameters and Constitutive Relationships in Subsurface Flow Problems. *Water Resources Research*, **56**: e2019WR026731. doi:<https://doi.org/10.1029/2019WR026731>.
- Tayfur, G., Nadiri, A.A., and Moghaddam, A.A. 2014. Supervised Intelligent Committee Machine Method for Hydraulic Conductivity Estimation. *Water Resources Management*, **28**: 1173-1184. doi:10.1007/s11269-014-0553-y.
- Taylor, K.E., Stouffer, R.J., and Meehl, G.A. 2012. An Overview of CMIP5 and the Experiment Design. *Bulletin of the American Meteorological Society*, **93**: 485-498. doi:<https://doi.org/10.1175/BAMS-D-11-00094.1>.
- Thiéry, D. 1990. Logiciel MARTHE. Modélisation d'Aquifère par un maillage Rectangulaire en régime Transitoire pour le calcul hydrodynamique des écoulements, version, **4**.
- Thomas, E.A., Needoba, J., Kaberia, D., Butterworth, J., Adams, E.C., Oduor, P., Macharia, D., Mitheu, F., Mugo, R., and Nagel, C. 2019. Quantifying increased groundwater demand from prolonged drought in the East African Rift Valley. *Science of the Total Environment*, **666**: 1265-1272. doi:<https://doi.org/10.1016/j.scitotenv.2019.02.206>.
- Tracy, F.T. 1995. 1-D, 2-D, and 3-D analytical solutions of unsaturated flow in groundwater. *Journal of Hydrology*, **170**: 199-214. doi:[https://doi.org/10.1016/0022-1694\(94\)02674-Z](https://doi.org/10.1016/0022-1694(94)02674-Z).
- Tran, D.A., Tsujimura, M., Ha, N.T., Nguyen, V.T., Binh, D.V., Dang, T.D., Doan, Q.-V., Bui, D.T., Anh Ngoc, T., Phu, L.V., Thuc, P.T.B., and Pham, T.D. 2021. Evaluating the predictive power of different machine learning algorithms for groundwater salinity prediction of multi-layer

- coastal aquifers in the Mekong Delta, Vietnam. Ecological Indicators, **127**: 107790. doi:<https://doi.org/10.1016/j.ecolind.2021.107790>.
- Tremblay, P. 2005. Étude hydrogéologique de l'aquifère de Saint-Honoré avec emphase sur son bilan hydrique [Hydrogeologic analysis of Saint-Honoré aquifer with emphasis on its water budget]. Applied Sciences, Université du Québec à Chicoutimi.
- Tutmez, B., Hatipoglu, Z., and Kaymak, U. 2006. Modelling electrical conductivity of groundwater using an adaptive neuro-fuzzy inference system. Computers and Geosciences, **32**: 421-433. doi:<https://doi.org/10.1016/j.cageo.2005.07.003>.
- Udrescu, S.-M., and Tegmark, M. 2020. AI Feynman: A physics-inspired method for symbolic regression. Science Advances, **6**: eaay2631. doi:<https://doi.org/10.1126/sciadv.aay2631>.
- Urolagin, S., kv, P., and Reddy, N.V.S. 2011. Generalization Capability of Artificial Neural Network Incorporated with Pruning Method.
- Vadyala, S.R., Betgeri, S.N., Matthews, J.C., and Matthews, E. 2022. A review of physics-based machine learning in civil engineering. Results in Engineering, **13**: 100316. doi:<https://doi.org/10.1016/j.rineng.2021.100316>.
- Valéry, A. 2010. Modélisation précipitations débit sous influence nivale : Elaboration d'un module neige et évaluation sur 380 bassins versants. Doctorat Hydrobiologie, Institut des Sciences et Industries du Vivant et de l'Environnement AgroParisTech.
- Valéry, A., Andréassian, V., and Perrin, C. 2014. 'As simple as possible but not simpler': What is useful in a temperature-based snow-accounting routine? Part 2 – Sensitivity analysis of the Cemaneige snow accounting routine on 380 catchments. Journal of Hydrology, **517**: 1176-1187. doi:<https://doi.org/10.1016/j.jhydrol.2014.04.058>.
- Van Geer, F., and Van Der Kloet, P. 1985. Two algorithms for parameter estimation in groundwater flow problems. Journal of Hydrology, **77**: 361-378.
- van Vuuren, D.P., Edmonds, J., Kainuma, M., Riahi, K., Thomson, A., Hibbard, K., Hurtt, G.C., Kram, T., Krey, V., Lamarque, J.-F., Masui, T., Meinshausen, M., Nakicenovic, N., Smith, S.J., and Rose, S.K. 2011. The representative concentration pathways: an overview. Climatic Change, **109**: 5. doi:<https://doi.org/10.1007/s10584-011-0148-z>.

- Vigiak, O., Sterk, G., Romanowicz, R.J., and Beven, K.J. 2006. A semi-empirical model to assess uncertainty of spatial patterns of erosion. *CATENA*, **66**: 198-210. doi:<https://doi.org/10.1016/j.catena.2006.01.004>.
- Vu, M.T., Jardani, A., Massei, N., and Fournier, M. 2021a. Reconstruction of missing groundwater level data by using Long Short-Term Memory (LSTM) deep neural network. *Journal of Hydrology*, **597**: 125776. doi:<https://doi.org/10.1016/j.jhydrol.2020.125776>.
- Vu, T.-D., Ni, C.-F., Li, W.-C., Truong, M.-H., and Hsu, S.M. 2021b. Predictions of groundwater vulnerability and sustainability by an integrated index-overlay method and physical-based numerical model. *Journal of Hydrology*, **596**. doi:10.1016/j.jhydrol.2021.126082.
- Wada, Y., van Beek, L.P.H., van Kempen, C.M., Reckman, J.W.T.M., Vasak, S., and Bierkens, M.F.P. 2010. Global depletion of groundwater resources. *Geophysical Research Letters*, **37**. doi:<https://doi.org/10.1029/2010GL044571>.
- Wagner, N., and Rondinelli, J.M. 2016. Theory-guided machine learning in materials science. *Frontiers in Materials*: 28. doi:<https://doi.org/10.3389/fmats.2016.00028>.
- Walter, J., Rouleau, A., Chesnaux, R., Lambert, M., and Daigneault, R. 2018. Characterization of general and singular features of major aquifer systems in the Saguenay-Lac-Saint-Jean region. *Canadian Water Resources Journal / Revue canadienne des ressources hydriques*, **43**: 75-91. doi:<https://doi.org/10.1080/07011784.2018.1433069>.
- Wanda, E., Monjerezi, M., Mwatseteza, J.F., and Kazembe, L.N. 2011. Hydro-geochemical appraisal of groundwater quality from weathered basement aquifers in Northern Malawi. *Physics and Chemistry of the Earth, Parts A/B/C*, **36**: 1197-1207. doi:<https://doi.org/10.1016/j.pce.2011.07.061>.
- Wang, B., Oldham, C., and Hipsey, M.R. 2016. Comparison of Machine Learning Techniques and Variables for Groundwater Dissolved Organic Nitrogen Prediction in an Urban Area. *Procedia Engineering*, **154**: 1176-1184. doi:<https://doi.org/10.1016/j.proeng.2016.07.527>.
- Wang, J., Li, Y., Zhao, R., and Gao, R.X. 2020a. Physics guided neural network for machining tool wear prediction. *Journal of Manufacturing Systems*, **57**: 298-310. doi:<https://doi.org/10.1016/j.jmsy.2020.09.005>.

- Wang, N., Chang, H., and Zhang, D. 2021a. Efficient uncertainty quantification for dynamic subsurface flow with surrogate by Theory-guided Neural Network. Computer Methods in Applied Mechanics and Engineering, **373**: 113492. doi:<https://doi.org/10.1016/j.cma.2020.113492>.
- Wang, N., Chang, H., and Zhang, D. 2021b. Theory-guided Auto-Encoder for surrogate construction and inverse modeling. Computer Methods in Applied Mechanics and Engineering, **385**: 114037. doi:<https://doi.org/10.1016/j.cma.2021.114037>.
- Wang, N., Zhang, D., Chang, H., and Li, H. 2020b. Deep learning of subsurface flow via theory-guided neural network. Journal of Hydrology, **584**: 124700. doi:<https://doi.org/10.1016/j.jhydrol.2020.124700>.
- Wang, R., Walters, R., and Yu, R. 2020c. Incorporating symmetry into deep dynamics models for improved generalization. arXiv preprint arXiv:2002.03061.
- Wang, S., Peng, H., and Liang, S. 2022. Prediction of estuarine water quality using interpretable machine learning approach. Journal of Hydrology, **605**: 127320. doi:<https://doi.org/10.1016/j.jhydrol.2021.127320>.
- Warde-Farley, D., Goodfellow, I.J., Courville, A., and Bengio, Y. 2013. An empirical analysis of dropout in piecewise linear networks. arXiv preprint arXiv:1312.6197.
- Wei, A., Chen, Y., Li, D., Zhang, X., Wu, T., and Li, H. 2022. Prediction of groundwater level using the hybrid model combining wavelet transform and machine learning algorithms. Earth Science Informatics, **15**: 1951-1962. doi:<https://doi.org/10.1007/s12145-022-00853-0>.
- Willard, J., Jia, X., Xu, S., Steinbach, M., and Kumar, V. 2020. Integrating physics-based modeling with machine learning: A survey. arXiv preprint arXiv:2003.04919.
- Wolpert, D.H., and Macready, W.G. 1997. No free lunch theorems for optimization. IEEE transactions on evolutionary computation, **1**: 67-82.
- Wu, J., and Zeng, X. 2013. Review of the uncertainty analysis of groundwater numerical simulation. Chinese Science Bulletin, **58**: 3044-3052. doi:10.1007/s11434-013-5950-8.
- Wu, Q., Zhou, W., Li, S., and Wu, X. 2005. Application of grey numerical model to groundwater resource evaluation. Environmental Geology, **47**: 991-999. doi:10.1007/s00254-005-1229-y.

- Wu, Y. 2004. Optimal design of a groundwater monitoring network in Daqing, China. *Environmental Geology*, **45**: 527-535. doi:<https://doi.org/10.1007/s00254-003-0907-x>.
- Wuest, T., Weimer, D., Irgens, C., and Thoben, K.-D. 2016. Machine learning in manufacturing: advantages, challenges, and applications. *Production & Manufacturing Research*, **4**: 23-45. doi:10.1080/21693277.2016.1192517.
- Wunsch, A., Liesch, T., and Broda, S. 2021. Groundwater level forecasting with artificial neural networks: a comparison of long short-term memory (LSTM), convolutional neural networks (CNNs), and non-linear autoregressive networks with exogenous input (NARX). *Hydrol. Earth Syst. Sci.*, **25**: 1671-1687. doi:<https://doi.org/10.5194/hess-25-1671-2021>.
- Wunsch, A., Liesch, T., and Broda, S. 2022. Deep learning shows declining groundwater levels in Germany until 2100 due to climate change. *Nature Communications*, **13**: 1-13. doi:<https://doi.org/10.1038/s41467-022-28770-2>.
- Xu, R., Zhang, D., Rong, M., and Wang, N. 2020. Weak Form Theory-guided Neural Network (TgNN-wf) for Deep Learning of Subsurface Single and Two-phase Flow.
- Xu, R., Zhang, D., Rong, M., and Wang, N. 2021. Weak form theory-guided neural network (TgNN-wf) for deep learning of subsurface single- and two-phase flow. *Journal of Computational physics*, **436**: 110318. doi:<https://doi.org/10.1016/j.jcp.2021.110318>.
- Xu, T., and Liang, F. 2021. Machine learning for hydrologic sciences: An introductory overview. *WIREs Water*, **8**: e1533. doi:<https://doi.org/10.1002/wat2.1533>.
- Yadav, B., Gupta, P.K., Patidar, N., and Himanshu, S.K. 2020. Ensemble modelling framework for groundwater level prediction in urban areas of India. *Science of the Total Environment*, **712**: 135539. doi:<https://doi.org/10.1016/j.scitotenv.2019.135539>.
- Yesertener, C. 2005. Impacts of climate, land and water use on declining groundwater levels in the Gnangara Groundwater Mound, Perth, Australia. *Australasian Journal of Water Resources*, **8**: 143-152. doi:<https://doi.org/10.1080/13241583.2005.11465251>.
- Ying, H.-w., Zhu, C.-w., Shen, H.-w., and Gong, X.-n. 2018. Semi-analytical solution for groundwater ingress into lined tunnel. *Tunnelling and Underground Space Technology*, **76**: 43-47. doi:<https://doi.org/10.1016/j.tust.2018.03.009>.

- Ying, X. An overview of overfitting and its solutions. In *Journal of Physics: Conference Series*. 2019. IOP Publishing. Vol. 1168, p. 022022.
- Yip, K.Y., and Gerstein, M. 2009. Training set expansion: an approach to improving the reconstruction of biological networks from limited and uneven reliable interactions. *Bioinformatics*, **25**: 243-250. doi:<https://doi.org/10.1093/bioinformatics/btn602>.
- Yira, Y., Diekkrüger, B., Steup, G., and Bossa, A.Y. 2016. Modeling land use change impacts on water resources in a tropical West African catchment (Dano, Burkina Faso). *Journal of Hydrology*, **537**: 187-199. doi:<https://doi.org/10.1016/j.jhydrol.2016.03.052>.
- Yoon, H., Jun, S.-C., Hyun, Y., Bae, G.-O., and Lee, K.-K. 2011. A comparative study of artificial neural networks and support vector machines for predicting groundwater levels in a coastal aquifer. *Journal of Hydrology*, **396**: 128-138. doi:<https://doi.org/10.1016/j.jhydrol.2010.11.002>.
- Yu, Z. 2015. HYDROLOGY, FLOODS AND DROUGHTS | Modeling and Prediction. In *Encyclopedia of Atmospheric Sciences* (Second Edition). Edited by G.R. North and J. Pyle and F. Zhang. Academic Press, Oxford. pp. 217-223.
- Yue, S., and Wang, C.Y. 2002. Applicability of prewhitening to eliminate the influence of serial correlation on the Mann-Kendall test. *Water Resources Research*, **38**: 4-1-4-7. doi:<https://doi.org/10.1029/2001WR000861>.
- Yue, S., Pilon, P., and Cavadias, G. 2002a. Power of the Mann-Kendall and Spearman's rho tests for detecting monotonic trends in hydrological series. *Journal of Hydrology*, **259**: 254-271. doi:[https://doi.org/10.1016/S0022-1694\(01\)00594-7](https://doi.org/10.1016/S0022-1694(01)00594-7).
- Yue, S., Pilon, P., and Phinney, B.O.B. 2003. Canadian streamflow trend detection: impacts of serial and cross-correlation. *Hydrological Sciences Journal*, **48**: 51-63. doi:<https://doi.org/10.1623/hysj.48.1.51.43478>.
- Yue, S., Pilon, P., Phinney, B., and Cavadias, G. 2002b. The influence of autocorrelation on the ability to detect trend in hydrological series. *Hydrological Processes*, **16**: 1807-1829. doi:<https://doi.org/10.1002/hyp.1095>.
- Zakaria, N., Anornu, G., Adomako, D., Owusu-Nimo, F., and Gibrilla, A. 2021. Evolution of groundwater hydrogeochemistry and assessment of groundwater quality in the Anayari

catchment. Groundwater for Sustainable Development, **12**: 100489.

doi:<https://doi.org/10.1016/j.gsd.2020.100489>.

Zhang, A., Lipton, Z.C., Li, M., and Smola, A.J. 2021. Dive into deep learning. arXiv preprint arXiv:2106.11342.

Zhang, P. 2010. Industrial control system simulation routines. pp. 781-810.

Zhang, W., Gu, X., Tang, L., Yin, Y., Liu, D., and Zhang, Y. 2022. Application of machine learning, deep learning and optimization algorithms in geoengineering and geoscience: Comprehensive review and future challenge. Gondwana Research, **109**: 1-17. doi:<https://doi.org/10.1016/j.gr.2022.03.015>.

Zhao, C., Wang, Y., Chen, X., and Li, B. 2005. Simulation of the effects of groundwater level on vegetation change by combining FEFLOW software. Ecological Modelling, **187**: 341-351. doi:<https://doi.org/10.1016/j.ecolmodel.2004.10.019>.

Zobeiry, N., and Humfeld, K.D. 2021. A physics-informed machine learning approach for solving heat transfer equation in advanced manufacturing and engineering applications. Engineering Applications of Artificial Intelligence, **101**: 104232. doi:<https://doi.org/10.1016/j.engappai.2021.104232>.

Zobeiry, N., Reiner, J., and Vaziri, R. 2020a. Theory-guided machine learning for damage characterization of composites. Composite Structures, **246**. doi:<https://doi.org/10.1016/j.compstruct.2020.112407>.

Zobeiry, N., Stewart, A., and Poursartip, A. Applications of Machine Learning for Process Modeling of Composites *In* SAMPE Virtual Conference. 2020b.

## **ANNEXES**

Dans le cadre de cette thèse, une quatrième étude a été réalisée et a donné lieu à un manuscrit actuellement en phase de production dans Environmental Earth Sciences. Cette étude est exposée en détail ci-dessous.

### **TOWARD A METHODOLOGY TO EXPLORE HISTORICAL GROUNDWATER LEVEL TRENDS AND THEIR ORIGIN: THE CASE OF QUEBEC, CANADA**

Adoubi Vincent De Paul Adombi<sup>a\*</sup>, Romain Chesnaux<sup>a</sup>, Marie-Amélie Boucher<sup>b</sup>

- a. Research Group R2Eau, Centre d'études sur les ressources minérales, Université du Québec à Chicoutimi, 555 boulevard de l'Université, Chicoutimi, Québec G7H 2B1, Canada.  
Email : [adombi.vincentdepaul@gmail.com](mailto:adombi.vincentdepaul@gmail.com)
- b. Department of Civil Engineering, Université de Sherbrooke, 2500 boulevard de l'Université, Sherbrooke, Québec J1R 2R2, Canada

Reçu le 17 mai 2023 - Accepté le 30 janvier 2024 dans la revue Environmental Earth Sciences.

#### **1.1 ABSTRACT**

In this study, a methodology combining some state-of-the-art methods for the analysis of groundwater monitoring networks is proposed to test the hypothesis that it can be successfully used to assess trends in groundwater levels and their origin with minimal hydrogeological data requirements. The methodology first employs trend detection methods, namely the trend-free

prewhitening Mann-Kendall test and a bootstrap test, to explore trends; then it uses the reference hydrograph method, land-use change maps and consultation with groundwater resource managers to understand the origin of the trends. The methodology was tested on the groundwater monitoring network of the province of Quebec, Canada. This study focuses on short-term trends, given the length of the data available. The results showed that all but one of the observation wells in the monitoring network exhibited significant upward (38%) and downward (62%) trends at the 5% statistical significance level, but that the majority of observation wells (77%) exhibited a trend amplitude of less than 3 cm/year in absolute value, the threshold below which the rate of upward or downward change is considered stable. Application of the bootstrap test validated the representativeness of the trends calculated at well scale. For 33% of the observation wells with moderate to large trends (amplitude greater than or equal to 3 cm/year in absolute value), changes in the field around the wells were identified and could explain the observed trends for half of them. For the remaining 67% of wells, no changes in the field were reported.

**Keywords:** Groundwater monitoring · Trend analysis · TFPW-MK · Groundwater management · Quebec

## 1.2 INTRODUCTION

Groundwater accounts for the largest proportion of the world's fresh water. Because it is generally better protected from pollution than surface water, groundwater is mostly of good quality (Akakuru et al. 2021; Wanda et al. 2011; Zakaria et al. 2021) and often inexpensive to treat, making it the primary source of drinking water in many parts of the world. In recent decades, economic development and agricultural innovation have led to an increased demand for groundwater (Awadh et al. 2021; Famiglietti 2014; Qureshi et al. 2010; Thomas et al. 2019). As a result, a decline in groundwater levels has been reported in different regions of the world (Nath et al. 2021; Wada et al. 2010). The anthropogenic effects combine with the long-term effects of climate change to alter

groundwater dynamics. In some contexts, altered groundwater dynamics, in addition to having significant environmental consequences such as land subsidence or ecosystem degradation, may contribute to the scarcity of groundwater for consumption. This alarming fact has led many countries to adopt concrete action plans to ensure rational management of groundwater resources, notably by developing groundwater level monitoring networks with sufficient spatial and temporal resolution (e.g., Bhat et al. 2014; Farrell and Whiteman 2023; Lee et al. 2007; Wu 2004). Monitoring networks are a valuable source of data because they can be used to provide a picture of the past and present state of the groundwater resource in a region and to identify anomalies in its evolution so that informed decisions can be made regarding its management. In particular, one of the key questions for decision makers is what the trend in groundwater levels is, i.e., whether groundwater levels are stable, increasing, or decreasing, what the magnitude of the trend is, and, most importantly, why the trend is occurring (Gebremicael et al. 2013). Characterizing the trends in groundwater levels has raised particular attention and concerns during the last decades with climate change (e.g., Halder et al. 2020; Pathak and Dodamani 2019; Patle et al. 2015; Shamsudduha et al. 2009). Here, the focus is on the historical evolution of groundwater levels and the origin of this evolution.

Trend detection has been a topic of continuing interest since the 1970s and has resulted in a considerable literature on trend detection techniques in the environmental and hydrological fields (Sonali and Nagesh Kumar 2013). These techniques can be grouped into two categories: a first category of slope-based tests (or parametric tests), such as linear least squares regression, and a second category of rank-based tests (or non-parametric), namely Mann-Kendall (MK) and Spearman rank correlation. Parametric tests are applicable provided that the data satisfy both the distribution and independence hypotheses, whereas for non-parametric tests, only the second hypothesis must be satisfied. Because of their highly serial and generally non-stationary structure, neither category of trend detection methods can be strictly applied to daily groundwater level series. Indeed, the erroneous assumption of independent observations can lead to erroneous conclusions (Sonali and Nagesh Kumar 2013). The effect of serial correlation must therefore be taken into consideration when analyzing trends in groundwater level time series. To account for the effect of serial correlation, Yue

et al. (2002a) proposed a procedure, called the trend free pre-whitening Mann-Kendall test (TFPW-MK) (Yue et al. 2002b). The TFPW-MK provides the ability to handle the serial structure of the data without altering the power of the MK test, making it particularly well suited for time series analysis of groundwater levels at the observation well scale. However, the existence of a trend at the scale of the observation well does not necessarily guarantee its regional representativeness. In order to assess the regional representativeness of the trends calculated at the local scale, Yue et al. (2003) proposed a bootstrap test with the use of the TFPW-MK procedure. Thus, the coupling of the TFPW-MK procedure and the bootstrap test allows for a rigorous spatiotemporal analysis of trends in time series. Globally, no studies have used the coupling of the bootstrap and TFPW-MK tests for groundwater level trend analysis, with the exception of Rivard et al. (2009).

Trends in groundwater level series, whether increasing or decreasing, are the result of the coupling, in varying proportions, of perennial or seasonal anthropogenic effects such as changes in land use and water demand, and cyclic or persistent fluctuations in climatic drivers (Green et al. 2011; Yesertener 2005). The determination of the origin of the observed trends, whether of direct anthropogenic or climatic origin, has been the subject of different approaches that are well documented in the literature.

A first approach consists in using physics-based models to simulate the effect of an explanatory variable on the evolution of groundwater levels (e.g., Kroes et al. 2019; Yira et al. 2016). For example, Yira et al. (2016) used a physics-based model and land use scenarios to study the impacts of historical land use changes on water resources in the Dano catchment, Burkina Faso. The physics-based model, the Water flow and balance Simulation Model (WaSiM), was calibrated and validated using observed discharge, soil moisture and groundwater level with good agreement between observed and simulated variables. The model was then ran under land use scenarios that show a decrease in savannah at an annual rate of 2% since 1990 and an increase in cultivated land and urban areas. The results showed a clear increase in total discharge (+17%) and a decrease in

evapotranspiration (-5%), suggesting an increase in water resources that are not available for plant growth and human consumption. Kroes et al. (2019) used long-term weather data to assess the effects of land-use change on groundwater recharge and crop yields using regionally distributed modeling. Results showed that threats arise from continuous monotonic land use, but opportunities arise when groundwater supply and demand are appropriately balanced through greater land use differentiation. Although this physics-based model is fairly robust, its complexity and the amount of data it requires can be significant. In addition to climate data, a physics-based model requires a good knowledge of the hydrogeology and hydraulic properties of the study area, as well as land use and pumping data at a reasonable spatial resolution, which makes the implementation of such a model far too cost prohibitive, especially on very large spatial scales.

Another approach is to use empirical models to simulate the effect of one or more explanatory variables on the evolution of groundwater levels (Banadkooki et al. 2020; Collenteur et al. 2021; Sahoo et al. 2017a). These models can range from simple and easily interpretable models such as reservoir models or linear regression to much more complex models such as those based on machine learning. The advantage of empirical models is that they are easy and quick to implement, generally not time consuming, and require less spatial data than their physics-based counterparts.

Recently, Lehr and Lischeid (2020) proposed a method based on a bootstrap principal component analysis to derive a reference hydrograph at the scale of observation well, which is then used to investigate anomalies in the observed hydrograph at the observation well. By consulting groundwater resource managers or taking advantage of land-use change maps, it is then possible to attribute these anomalies to targeted field observations. For instance, this could help identify wells that are influenced by pumping or other anthropogenic activities. The reference hydrograph method does not require additional data beyond the groundwater level time series and is easy to implement and interpret compared to empirical models.

In this study, we propose to test the hypothesis that a methodology combining statistical approaches, namely the TFPW-MK procedure, the bootstrap test and the reference hydrograph method, could be successful in exploring groundwater level trends and their origin with minimal hydrogeological data requirements. The data used for the methodology are GWL time series, climate variables (vertical inflow and potential evapotranspiration), land-use change maps and consultation with groundwater resource managers. To the best of the authors' knowledge, such a methodology has never been proposed in the literature and could serve as a starting point for the development of a more general methodology for the analysis of groundwater monitoring networks. In the following, the methodology is described in detail, followed by a case study of the groundwater monitoring network of the province of Quebec, Canada. Finally, a discussion of our results, the methodology, its limitations, and potential improvements is presented.

As the data used to test the hypothesis is limited to ten years, only short-term trends and their origins are investigated. However, the methodology can be applied to longer time series. It should also be noted that the main contribution of this work lies in the methodology proposed.

### **1.3 METHODOLOGY**

To explore historical groundwater level trends in a monitoring network and understand their origin with minimal hydrogeological data requirements, a three-step methodology has been proposed. The first step is to assess the groundwater level trend at the scale of the observation well using the TFPW-MK method: this is known as the “site trend significance”, because it involves determining trends for a given observation well without considering trends for the other observation wells in the network. The second step is to assess the regional representativeness of local trends: this is called the field trend significance. This step consists of a bootstrap test, which means that  $N$  virtual monitoring networks are generated by random time sampling from the original monitoring network. This allows for the determination of a cumulative probability distribution which is then used to test the

regional significance of the observed local trends of the original network. Finally, the third step consists in defining for each observation well in the original network a reference hydrograph which is, by definition, the expected behavior of an observation well in the absence of local deviation. Consequently, this reference hydrograph makes it possible to identify if and when the well deviates from the expected behavior.

### **1.3.1 LOCAL GROUNDWATER LEVEL TRENDS: SITE SIGNIFICANCE**

#### **1.3.1.1 MANN-KENDALL TEST**

The non-parametric Mann-Kendall test is used on time series to test the validity of the null hypothesis, i.e. the non-existence of a monotonic trend in the series, at a given statistical significance level  $\alpha$ . The test is performed on the Mann-Kendall S-statistic which represents the number of negative and positive changes of successive pairs of values in the time series. On the one hand, when  $S = 0$  at significance level  $\alpha$ , the null hypothesis cannot be rejected. On the other hand, when  $S > 0$  or  $S < 0$  at significance level  $\alpha$ , the null hypothesis is irrelevant, meaning that the statistical series has a monotonic upward or downward trend, respectively. A formal definition of the Mann-Kendall test with details of the equations can be found in Satish Kumar and Venkata Rathnam (2019).

#### **1.3.1.2 TREND-FREE PREWHITENING MANN-KENDALL PROCEDURE**

Yue et al. (2002a) showed that the serial structure of time series, such as GWL daily time series, weakens the power of the Mann-Kendall test and proposed the trend-free prewhitening Mann-Kendall (TFPW-MK) test procedure to overcome this problem. The procedure assumes that the time series is a composition of an autoregressive series and a linear trend series with slope  $\beta$  obtained by the Sen (1968) method. The procedure consists first in removing the detrended component from the

original time series. Second, the detrended series, which is the autoregressive component, is pre-whitened, i.e., it is cleared of serial correlation. Third, a new time series is constructed, which is the sum of the pre-whitened time series and the linear-trend time series. Finally, the traditional MK test is applied to the time series of the third step. More formal details are given in Yue and Wang (2002). Trend evaluation using the TFPW-MK procedure was performed using the python package "pyMannKendall" (Hussain and Mahmud 2019).

### 1.3.2 REGIONAL GROUNDWATER LEVEL TRENDS: FIELD SIGNIFICANCE

The field significance of detected trends is of utmost importance because it allows to check whether the number of observation wells showing an increasing or decreasing trend respectively is not overestimated or underestimated. To do this, a probabilistic approach is adopted. The procedure consists in determining separately for each type of trend (upward or downward) an empirical cumulative distribution of the regional average of the Mann-Kendall statistic (S-slope). The cumulative distribution is obtained by bootstrapping the data. This is performed according to the four steps described in Yue et al. (2003). Consider a network of  $N$  observation wells. Each well is represented by its time series, which data points are indexed on the time axis.

**Step 1:** Resampling the time axis randomly with replacement in order to obtain a bootstrapped time series. During the resampling, the time indexes are also accumulated in a vector, meaning that there also exists a bootstrapped series of the original time indexes. This new series of temporal indexes is reused in step 2.

**Step 2:** Rearranging the groundwater level values for each of the  $N$  observation wells according to the new, bootstrapped, temporal indexes. This step makes it possible to obtain a new

"fictitious" network of  $N$  observation wells in which time series are ordered according to the bootstrapped indexes.

**Step 3:** Applying trend detection methods for each observation well in the bootstrapped network of Step 2 to determine, at the significance level  $\alpha = 0.05$ , the number of stations with an increasing trend ( $N_{up}$ ) versus the number of stations with a decreasing trend ( $N_{down}$ ).

**Step 4:** Steps 1 to 3 are repeated  $B$  times.  $B$  is chosen equal to 1000, as in Yue et al. (2003) and Rivard et al. (2009). At the end of the procedure, two sets are obtained, the first of which is made up of the number of stations with an upward trend ( $N_{up} = \{N_{up}^1, \dots, N_{up}^B\}$ ) and the second is made up of the number of stations with a downward trend ( $N_{down} = \{N_{down}^1, \dots, N_{down}^B\}$ ) in the successive bootstrapped networks. Next, the bootstrapped empirical cumulative distributions (BECD) of the upward and downward trend numbers are estimated by Equation (1.1).

$$P(N^* < N^r) = \frac{r}{B+1}, \quad (N^* = N_{up}, N_{down}) \quad (1.1)$$

where  $r \in [1, \dots, B]$  is the rank of  $N^r$  in the bootstrap sample data in ascending order. For example, for the upward trend,  $N^r = N_{up}^r$ . Using the results obtained with the real network, i.e. the number of significant upward (resp. downward) trends ( $N_{up}^{real}$ ), the probability value associated with  $N_{up}^{real}$  in the BECD distribution as well as its corresponding p-value can be calculated via Equations (1.2) and (1.3) respectively.

$$P_{up}^{real} = P(N_{up}^{real} < N^r) \quad (1.2)$$

$$p = \begin{cases} P_{up}^{real} & \text{for } P_{up}^{real} \leq 0.5 \\ 1 - P_{up}^{real} & \text{for } P_{up}^{real} > 0.5 \end{cases} \quad (1.3)$$

Thus, at the significance level of 0.05, the upward (resp. downward) trend is considered field-significant, i.e., this trend is regional, if  $p \leq 0.05$ . If this is not the case, it means that the trend detection method is detecting an abnormal number of upward and/or downward trends. The bootstrap approach and all other methods were coded in Python (Adombi 2023a).

### 1.3.3 ORIGIN OF TRENDS: THE REFERENCE HYDROGRAPH METHOD

The reference hydrograph method for identifying local anomalies in groundwater level time series was proposed by Lehr and Lischeid (2020). The method is summarized here.

**Step 1:** First, stable regional GWL behaviors from a bootstrap principal component analysis (10 000 runs) on the observation well network data are determined.

The stable regional GWL behaviors are the principal components (PCs) that are stable in time and space. To determine stable PCs, the first step is to normalize the GWL time series and then to perform a principal component analysis (PCA) on a random subsample at a rate of 70% on the temporal axis (spatial stability) or 70% of the observation wells (temporal stability) and to retain only the PCs that have an eigenvalue greater than 1. These PCs constitute the potential candidates from which the stable PCs will be selected. This operation is performed 10000 times for temporal stability and 10000 times for spatial stability. Then, separately for spatial stability and temporal stability, the squared Pearson correlation coefficient ( $R^2$ ) of all combinations between the 10000 PC1s is calculated, then that between the 10000 PC2s and so on for all candidate PCs. The PCs stable in time and space are those for which the median of  $R^2$  is greater than a criterion (for example, 0.9).

**Step 2:** Then, the scores corresponding to the stable PCs are used to calculate the reference hydrographs for each observation well using multiple linear regression.

**Step 3:** Third, the reference hydrograph is used to derive a residual hydrograph whose dynamics are attributed to local deviations from regional behavior.

The residual hydrograph is the difference between the observed hydrograph (GWL time series) and the reference hydrograph.

**Step 4:** Finally, in consultation with the monitoring network managers and/or the use of land-use change maps, an informed interpretation of the causes of the anomalies could be made based on the changes observed in the immediate environment of the observation wells.

The reference hydrograph method could be particularly useful when a large network is available, as it reduces the time required to analyze GWL hydrographs. The methodology presented is summarized in **Figure 34**.

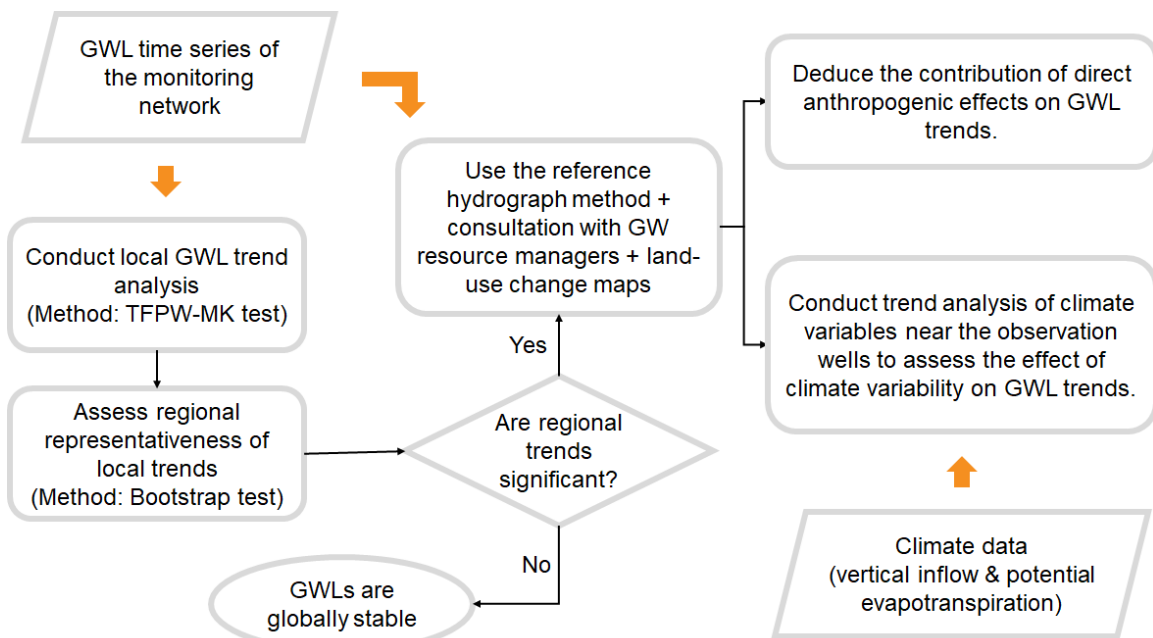


**Figure 34** Flowchart of the methodology.

In the reference hydrograph method, since local deviations are attributed to direct anthropogenic effects, local climate variability, or human and technical errors in groundwater level measurements, a trend analysis of climate variables (vertical inflow and potential evapotranspiration) near all the observation wells is necessary to assess their contribution to the computed GWL trends and to identify the contribution of anthropogenic effects and possibly human and technical errors.

## 1.4 CASE STUDY: THE GROUNDWATER MONITORING NETWORK OF QUEBEC, CANADA

### 1.4.1 STUDY AREA

The study area is approximately 612,000 km<sup>2</sup> and lies between 45° – 51°N and 60° – 80°W, covering most of southern Quebec (**Figure 35**).



**Figure 35** Location of the study area including the main cities

The territory is marked by a cold and humid continental climate with an average temperature of 2°C with large variations between the different regions of the area, falling below average in the extreme west towards Rouyn-Noranda and increasing to 3°C towards Gaspé and Chicoutimi and up to 7°C towards Montreal (MELCCFP 2023b). Temperature differences between the warm and cold seasons also vary greatly, with temperatures reaching an average of 17°C in July, while in January the average is about -15°C. Solid and liquid precipitation totals an average of 1,000 millimeters per year, of which nearly 75% is rain, with significant snowfall generally occurring between December and March (MELCCFP 2023b). Several important geological domains in Quebec are covered in the area, including the Superior and Grenville Provinces, the St. Lawrence Platform and the Appalachian Province (Larocque et al. 2018; Rivera 2014). The deposition of unconsolidated sediment and the formation of proglacial lakes following marine invasions during the last glaciation/deglaciation cycle had a decisive impact on the geology and hydrogeology of the current aquifer systems in the study area (Larocque et al. 2018). For example, in the western part of the study area, around Val d'Or, there is a clay belt composed of numerous esker and moraine aquifers (Rey et al. 2018) whereas between Trois-Rivières and Quebec City, the main aquifer is located in the fractured sedimentary basement and is covered by till, sand and clay (Gagné et al. 2018). In the vicinity of Chicoutimi, it can be noted the presence of a multilayered aquifer system composed of glaciofluvial sediments covered by a marine clay-silt aquitard, deltaic and shore deposits and finally fractured rock aquifers (Walter et al. 2018). In terms of land use, with the exception of residential and urban areas, the study area is mainly covered by forest, followed by agricultural and agroforestry areas.

In the study area, groundwater supplies 90% of the inhabited area and 25% of the population. Although 10% of Quebec's territory is covered by freshwater, with tens of thousands of rivers and more than three million bodies of water, the groundwater resource is often the only economically exploitable source because of its generally good quality and its proximity to the place of consumption; this is why the sound management of this resource and its adequate protection is a major issue for the Quebec Ministry of the Environment (MELCCFP 2023a).

#### **1.4.2 GROUNDWATER MONITORING NETWORK AND DATA USED**

The groundwater monitoring network of the Quebec Ministry of the Environment was developed to monitor the changes in groundwater levels and temperatures in the context of climate change. Although some observation wells were active as early as 1968, most of the network has been developed since 2008 and counts 263 observation wells to date. Each well is provided with a hydrostatic pressure sensor and a temperature sensor. Some wells have a second pressure sensor placed on the surface of the water to correct the groundwater level according to changes in atmospheric pressure. These sensors are connected to a data logger. The data are synthesized in the form of daily time series. While there are a large number of observation wells, data from most of them are not usable for this study, either because there is not enough data (< 5 years) or because there is a very large proportion of missing data (> 10 years). Here, only wells with less than 2% missing data, with a length of at least 10 years and coinciding with the period 2011 - 2021 were selected. There are a number of imputation methods that could be used to obtain better spatial coverage of GWL data (Bikše et al. 2023; Marchant et al. 2022; Meggiorin et al. 2023; Vu et al. 2021a). The use of these methods could be the subject of further study.

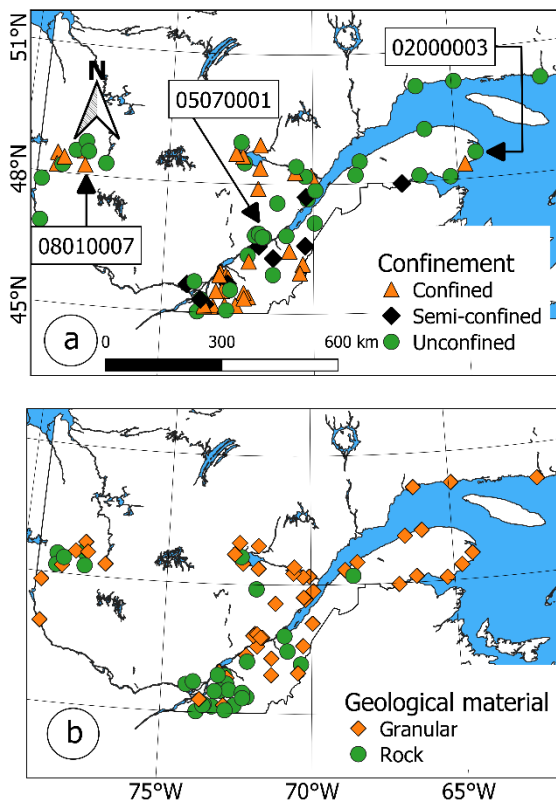


**Figure 36** Location of the groundwater level observation stations analyzed in this study, as well as (a) the state of confinement and (b) the nature of the geological material. The three observation wells that will be used as illustrations in the rest of this work are located by their identifiers

The location of the selected observation wells (79 wells) is shown in **Figure 36**. The period 2011-2021 provides the greatest number of observation wells with usable data. For wells with missing data, extrapolation was performed using data from wells with which they are sufficiently correlated. The wells are located in different types of aquifers with a depth of up to 43 m (**Figure 36a**): 37 wells are located in unconfined aquifers, 9 in semi-confined aquifers, 31 in confined aquifers, and 2 wells with unknown confinement state. 63% of the observation wells are in a granular context, while the remaining 37% are in rock (**Figure 36b**).

Given the short duration of the GWL time series (10 years), only short-term trends are evaluated in this study. The existence of short-term trends may be related to anthropogenic effects but also to local climate variability. To account for the latter, climate data near the observation wells were retrieved. Climate data, namely precipitation and temperature were obtained from the Info-Climat service of the *Ministère de l'Environnement, de la Lutte contre les changements climatiques, de la Faune et des Parcs* (MELCCFP), on daily  $0.1^\circ \times 0.1^\circ$  grids covering the period 1961-2018 (Bergeron 2016). The grid points closest to the observation wells (< 5 km on average) were selected and data from 2010 to 2018 were used (period of data availability). Vertical inflow and potential evaporation were calculated from precipitation and temperature data.

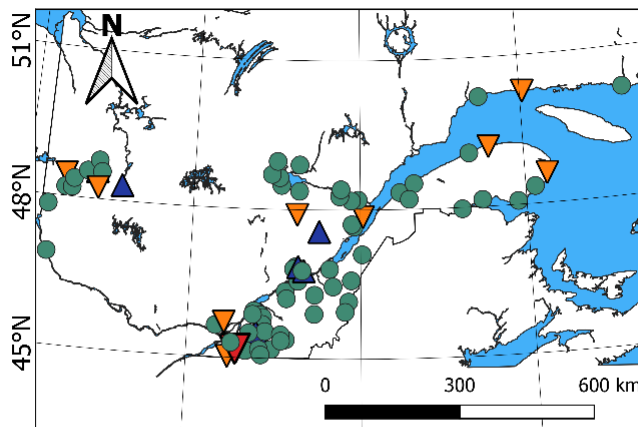
To calculate potential evapotranspiration, the simple and efficient model proposed by Oudin et al. (2005) was used. The model of Oudin et al. (2005) receives as input the minimum and maximum temperatures and provides as output the potential evapotranspiration. The calculation of vertical inflow was performed using the CemaNeige snow accumulation and melt model described in Valéry (2010) and Valéry et al. (2014). In this study, vertical inflow, refers to the amount of water originating from snowmelt and rainfall. The CemaNeige model receives as input precipitation as well as minimum, mean and maximum temperatures and provides the vertical inflow as the only output. CemaNeige is a simple degree-day model that has two parameters that must normally be calibrated jointly with those of a hydrological model, against streamflow data. The calibrated average of these parameters over the analyzed Quebec watersheds was used in this study (see Valéry et al. 2014).

To account for anthropogenic effects, the managers of the monitoring network were consulted, as well as land use change maps. The land use change maps were obtained from the Environment Canada database (Ministry of Environment of Canada).

## 1.5 RESULTS

### 1.5.1 LOCAL GROUNDWATER LEVEL TRENDS: SITE SIGNIFICANCE

The TFPW-MK procedure was applied to each of the 79 observation wells selected for this study to test the existence of a general monotonic trend in groundwater levels with different statistical significance (1%, 5%, 10% and 15%). Since the results are the same for the different statistical significance values, only the results at the 5% statistical significance are presented. **Figure 37** shows the spatial distribution of trends in the monitoring network.



#### Trend categories (slope in cm/year)

- ▼ Large rate of decline ( $\text{slope} \leq -10$ )
- ▲ Moderate rate of decline ( $-10 < \text{slope} \leq -3$ )
- Stable ( $-3 < \text{slope} < 3$ )
- ▲ Moderate rate of increase ( $3 \leq \text{slope} < 10$ )

**Figure 37** Spatial distribution of trends in the monitoring network. Based on the absolute value of the slope, three trend categories can be defined: (1) stable when  $|\text{S}| < 3 \text{ cm/year}$ , (2) moderate rate when  $3 \text{ cm/year} \leq |\text{S}| < 10 \text{ cm/year}$ , and (3) significant rate when  $|\text{S}| \geq 10 \text{ cm/year}$ . This classification is based on a combination of statistical and environmental significance criteria, developed by Environmental Reporting BC (2019) and used to focus further investigations on wells where trends are considered more critical ( $|\text{S}| > 3 \text{ cm/year}$ ).

The results show that all but one of the 79 observation wells show a significant monotonic trend using the TFPW-MK procedure. Of all the stations, 30 show an upward trend and 48 a downward trend. However, the majority of observation wells (77%) show a trend of less than 3 cm/year, independently of aquifer type (**Table 5**). For these wells, the groundwater level can be considered stable during the study period based on the trend magnitude classification proposed by

Environmental Reporting BC (2019). The trend slope for each of the observation wells is available in **Online Resource 1** (Adombi 2023c).

**Table 5** Distribution of the number of observation wells by trend magnitude and aquifer type. UC: unconfined, SC: semi-confined, C: confined, UNK: unknown. Based on the absolute value of the slope, three trend categories have been defined: (1) stable when  $|S| < 3 \text{ cm/year}$ , (2) moderate rate when  $3 \text{ cm/year} \leq |S| < 10 \text{ cm/year}$ , and (3) significant rate when  $|S| \geq 10 \text{ cm/year}$

	UC	SC	C	UNK
Large rate of decline	-	1	2	-
Moderate rate of decline	6	-	3	-
Stable	27	8	24	2
Moderate rate of increase	4	-	2	-
Large rate of increase	-	-	-	-

7.6% of observation wells have a moderate rate of increase versus 11.4% that have a moderate rate of decrease in GWL. Finally, 4% of observation wells have a large rate of decrease and are located in confined or semi-confined aquifer. Proportionally, there are almost as many observation wells located in unconfined aquifers (27%) as observation wells located in confined aquifers (22.6%) that show a moderate to large GWL trend. Therefore, both confined and unconfined aquifer are equally vulnerable to the influence of exogenous factors capable of significantly altering the dynamics of the groundwater table. Regarding the geological nature of the aquifers (table not shown), there are as many observation wells with a moderate to large trend located in granular aquifers (11.4%) as in bedrock aquifers (11.4%). However, proportionally, twice as many observation wells located in bedrock aquifers show a moderate to large trend (42.85%) than those located in

granular aquifers (18%). Thus, bedrock aquifers are twice as vulnerable to the influence of exogenous factors as granular aquifers. The 23% of observation wells (18 / 79) with moderate to large trends require further investigation to understand the origin of these significant trend magnitudes.

### 1.5.2 REGIONAL GROUNDWATER LEVEL TRENDS: FIELD SIGNIFICANCE

In order to ensure that the TFPW-MK method does not detect an anomalous number of observation wells with a monotonically increasing or decreasing trend and thus assess the representativeness of trends calculated at the scale of observation wells, the bootstrap test proposed by Yue et al. (2003) was applied. The approach involved applying the TFPW-MK method to 1000 random temporal resamples from the original groundwater level monitoring network (Yue et al. 2003). For each of the 1000 simulations, the number of stations with an increasing trend versus those with a decreasing trend is evaluated. By combining the results of the simulations, a cumulative distribution for increasing trends and another for decreasing trends are defined. The cumulative distributions are presented in **Figure 38**.

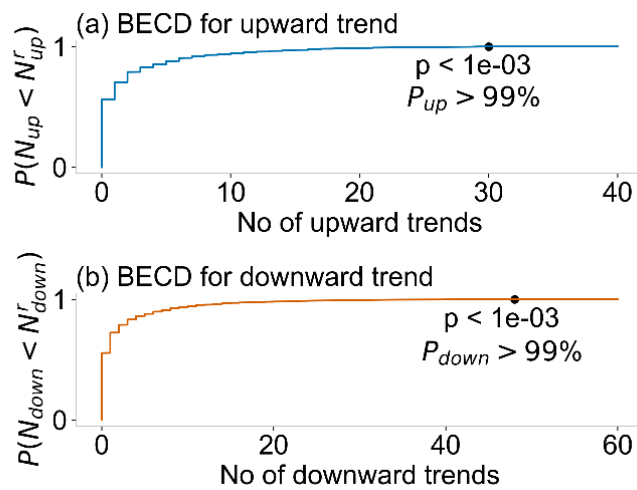


**Figure 38** Bootstrap empirical cumulative distributions (BECD) of upward (a) and downward (b) trend numbers from the TFPW-MK method

In **Figure 38**, the probability that the number of observation wells with increasing (respectively decreasing) trend in the actual monitoring network is equal to that obtained (i.e., 30 wells with increasing trend and 48 wells with decreasing trend) is represented by a black dot. The corresponding p-value is also displayed. The probability that the number of observation wells with an increasing or decreasing trend is equal to 30 and 48 respectively in the actual monitoring network is greater than 99% with p-values far smaller than 0.05. At the chosen statistical significance level of 5% (resp., 1%, 10% and 15%), it can be inferred that the number of observation wells with an increasing or decreasing trend detected by the TFPW-MK method in the actual monitoring network is statistically consistent. Consequently, the trends calculated at the observation well scale are regionally representative at the significance level of 5% (resp., 1%, 10% and 15%).

### 1.5.3 ORIGIN OF THE TRENDS

Changes in groundwater levels depend on several factors. In the short term, groundwater dynamics are modified by climate variability, changes in land use, and groundwater withdrawals. Due to the lack of detailed groundwater extraction data, a two-step statistical methodology has been adopted to understand the possible origins of the moderate to large trends in groundwater levels. The first step was to assess the trends in climate variables (vertical inflow and potential evapotranspiration) near the observation wells. In that way, it is possible to establish a causal relationship between the trends observed in the climate variables and those of GWLs. The second step was to apply the reference hydrograph method to identify local anomalies attributed to direct anthropogenic effects, climate variability and, eventually, human and technical errors in taking GWL measurements. The calculated trends in climate variables was then used to infer the contribution of direct anthropogenic effects and possible human and technical errors on GWL trends.

#### Trends in climate variables

Vertical inflow and potential evapotranspiration calculated near the observation wells over the period of climate data availability (2010 - 2018) were subjected to the TFPW-MK procedure. The spatial distribution of trends in vertical inflow and potential evapotranspiration are shown in **Figure 39a** and **Figure 39b** respectively.

Vertical inflow shows no significant trend except for a few stations (3 / 79) in the east of the study area where a decreasing trend (-65 to -40 mm/year) is observed (**Figure 39a**). This implies that from one year to the next during the study period, the vertical inflows remain globally stable except for the three eastern stations. Two of the three stations with a decrease in vertical inflow are associated with observation wells with moderate decreases in groundwater levels. Under unchanged initial conditions and if aquifer diffusivity is sufficiently significant, a decrease in vertical inflow could contribute to a decrease in groundwater level and explain the computed downward trend.

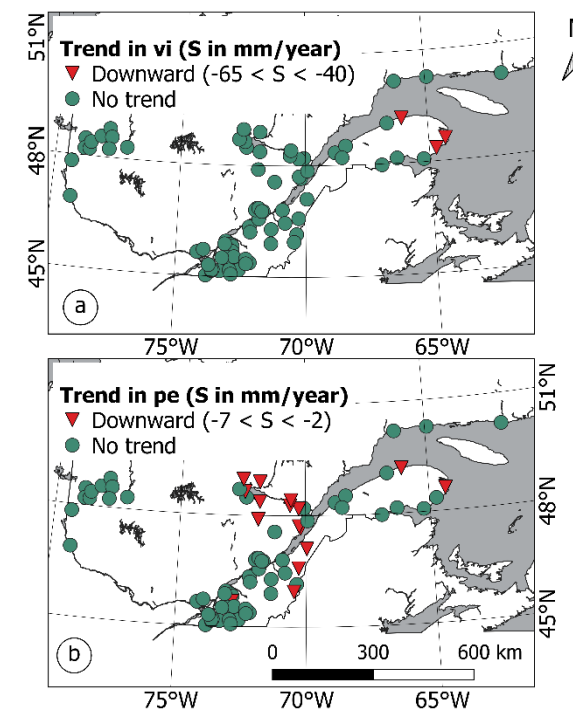


**Figure 39** Spatial distribution of trends in (a) vertical inflow (vi) and (b) potential evapotranspiration (pe)

Potential evapotranspiration shows a decreasing trend (-7 to -2 mm/year) mainly near the observation wells located in the center part of the study area. Elsewhere, potential evapotranspiration shows no significant trend (**Figure 39b**). However, the magnitude of potential evapotranspiration trends remains very small, so that its impact on groundwater levels can be considered very limited or insignificant.

#### **Analysis of local anomalies in groundwater level hydrograph**

The hydrograph method was used to identify local deviations from the observed hydrograph at the observation well. The method consists of searching for stable hydrodynamic behaviors (i.e., principal components) in time and space within the monitoring network using a bootstrap principal component analysis. Then, the stable principal components (PCs) were used to calculate the reference hydrograph for each observation well. **Figure 40** shows the distribution of potential hydrodynamic behaviors and their level of spatial and temporal stability represented by the squared  $R^2$  Pearson correlation coefficient whisker box.

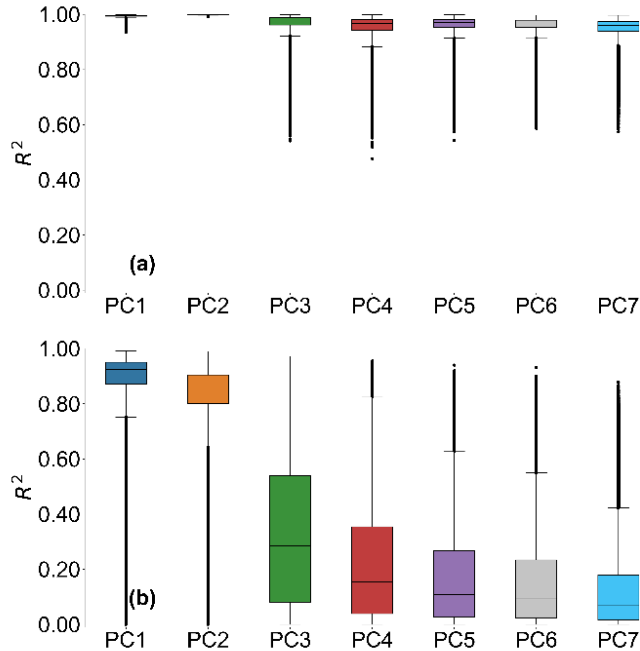


**Figure 40** Spatial and temporal stability analysis of PCs. **(a)** Correlation of eigen vector based on the random subsampling of the measurement dates to assess the stability of spatial patterns. **(b)** Correlation of scores based on the random selection of observation wells, i.e. complete series, to assess the stability of temporal patterns

The more the  $R^2$  median value of a PC tends to 1, both in time and space, the more stable it is. **Figure 40** shows that spatial stability is satisfied for all 7 candidate PCs. Indeed, the median value of  $R^2$  is greater than 0.9 for all PCs. However, in terms of temporal stability, it can be seen that except for PC1 and PC2 which have a median value close to 1, the median value of the other PCs is very low (less than 0.4) with a very large dispersion. Thus, PC3 to 7 do not show temporal stability. Finally, only PC1 and PC2 are both spatially and temporally stable. The scores of PC1 and PC2 thus represent the two stable hydrodynamic behaviors of the monitoring network. **Figure 41** shows the results of the hydrograph method for one of the observation wells (id: 02000003) located in an unconfined aquifer, showing a moderate rate of decrease in GWL.

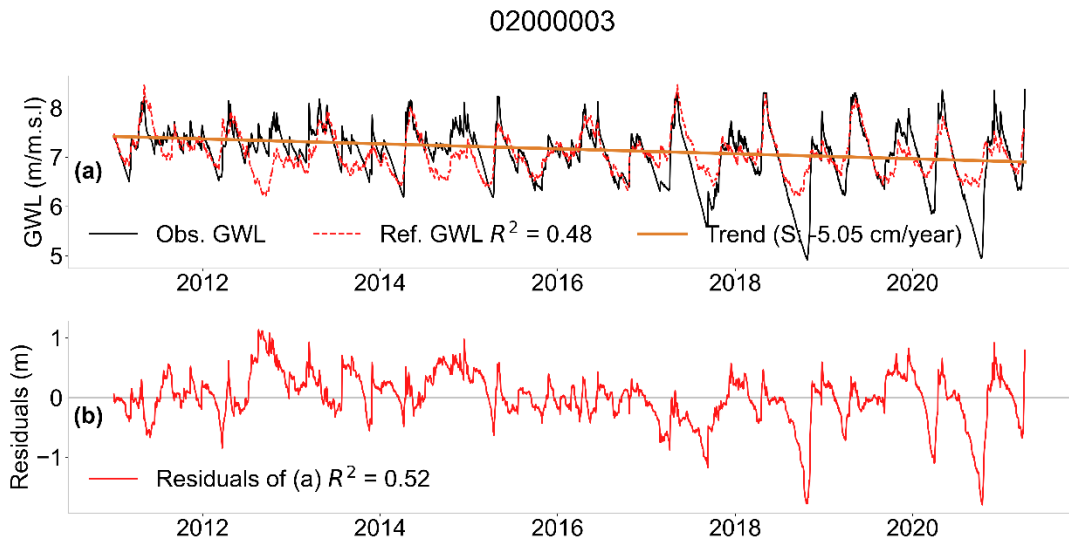


**Figure 41** (a) Time series of GWL and reference hydrograph for well 02000003 located near Gaspé (see [Figure 36](#)). (b) Time series of residuals. The correlation of the observed series with the reference hydrograph and with the residuals is given by  $R^2$ . The trend line and slope of the trend are also shown

Analysis of the residual hydrograph shows that prior to 2017, local deviations hover around 0. After 2017, the average residual is significantly less than 0, expressing the fact that observed groundwater levels are well below what should be expected. Declining groundwater levels occur when aquifer recharge is less than its discharge. The Quebec Ministry of Environment noted that around 2018, a lot of backfilling was done on the land upstream of the observation well. Backfilling results in soil compaction and can lead to sealing. Soil sealing limits water infiltration and reduces the potential recharge of the aquifer. As a result, a decrease in groundwater levels can be observed. This probably explains the recession observed since 2017 at observation well 02000003.

**Table 6** summarizes the residual hydrograph analysis as well as field observations for the 18 observation wells where the GWL trend magnitude is not stable (amplitude equal or greater than 3 cm/year). The reference hydrograph for each of the 18 observation wells is available in [Online Resource 2](#) (Adombi 2023b). For all observation wells, a change in GWL dynamics was identified. These dynamics are expressed as an increase or decrease in the average GWL over a given period

and corroborate the calculated trends. However, changes in the immediate environment were identified for only 33% of the observation wells (6/18), half of which are in unconfined aquifers. Changes in the immediate environment of the 3 wells located in unconfined aquifers could explain the observed GWL trends. For example, for well 05070001 (see **Figure 36** for location) where an increasing trend in GWL is calculated, a cyclicity of GWL residuals is observed with an increase in average GWL since 2014. In 2014, logging took place (from MELCCFP). The logging reduces the amount of water intercepted by vegetation and provides more available water for potential aquifer recharge. Also, the analysis of the residual hydrograph of well 08010007 (see **Figure 36** for location) revealed that it has an atypical hydrodynamic behavior that most likely reflects erroneous GWL measurements due to human or technical errors for example. For the remaining 67% (12/18) of observation wells, no change was observed in their immediate environment. Therefore, it is not possible to attribute a potential origin to the observed trends. Further field investigation is necessary.

**Table 6** Analysis of residual hydrographs and corresponding field observations for the 18 observation wells with moderate to large trends

id	x	y	slope (cm/year)	Residual hydrograph analysis	Field observation (MELCCFP or change in land use)
02000003	-64.32	48.60	-5.05	GW recession after 2017	Backfill around 2018
02120001	-66.06	49.21	-4.95	Average GWL lower after 2017	No change
03030006	-73.02	45.52	3.02	Constant increase in GWL since 2011	No change
03070002	-73.57	45.19	-13.61	Average GWL lower after 2017	No change
03090008	-73.82	45.02	-9.50	Average GWL lower after 2015	No change
03090012	-73.61	45.14	-19.38	Decline in average GWL after 2016 and exacerbation after 2018.	Increase of cropland between 2015 and 2020
03090015	-73.60	45.17	-27.18	Decline in average GWL after 2016 and exacerbation after 2018.	Increase of cropland between 2015 and 2020

04300002	-78.87	48.46	-7.86	Average GWL lower after 2017	Increase of mixed forest between 2015 and 2020
04640001	-73.95	45.71	-5.12	Average GWL lower after 2019	Increase of the urban area between 2015 and 2020
05070001	-71.84	46.85	6.49	Cyclicity of GWL residues with increase of average GWL since 2014	Logging in 2014
05080001	-71.67	46.77	3.20	Increase of average GWL since 2014	No change
05080002	-71.23	47.56	4.70	Increase of average GWL after 2018	No change
05170001	-69.92	47.86	-4.25	Average GWL lower after 2014	No change
06150001	-71.89	47.90	-4.37	Average GWL lower after 2017	No change
07000004	-64.91	50.27	-4.79	Constant decrease in GWL since 2011	No change
08010001	-77.95	48.55	5.36	Constant increase in GWL since 2011	No change
08010007	-77.89	48.23	-5.08	Atypical behavior	No change
08070002	-77.17	48.31	3.48	Cyclicity of GWL residues with increase of average GWL between 2014 and 2016	No change

## 1.6 DISCUSSION: LIMITATIONS OF THE PROPOSED METHODOLOGY AND FUTURE WORK

This work demonstrated the utility of coupling the TFPW-MK procedure with a bootstrap test to assess trends and their magnitudes in a GWL monitoring network. The limitations of applying the traditional MK test to daily groundwater level series, due to their highly serial structure, were overcome by using the TFPW-MK procedure. The bootstrap test did, however, make it possible to assess the regional representativeness of trends calculated at the scale of observation wells. Subsequently, the use of the reference hydrograph method, combined with analysis of land-use change maps and consultation with groundwater resource managers, enabled local anomalies to be

analyzed and identified in order to understand the origin of the calculated trends. The methodology used in this work is easy to implement and requires little data, which limits the effort that could be devoted to the analysis of groundwater level monitoring networks compared to traditional hydrogeological modeling. However, several limitations can be pointed out that could be the subject of future work.

### 1.6.1 THE MANN-KENDALL TEST

The main contribution of the TFPW-MK method to the analysis of trends in groundwater level time series is the consideration of the effect of serial correlation. The TFPW-MK method applied to groundwater level time series allows to obtain a new series without the serial structure of the original series and on which the traditional MK test is applied. However, the Mann-Kendall S-statistic has a fundamental weakness that can be illustrated by the following hypothetical example. Let three vectors  $X$ ,  $Y$  and  $Z$  be composed of 7 elements.  $X$  is a vector composed of 1,  $Y$  is a vector whose elements are equal to  $1 + 10^{-6} \cdot i$  and  $Z$  is a vector whose elements are equal to  $1 - 10^{-6} \cdot i$  with  $i$  going progressively from 0 to 6. For engineering purposes, the three vectors are equal to each other, but their Mann-Kendall S-statistics, which are 0, 21 and -21 respectively, are radically different. This means that a small change in the time series can lead to an incorrect MK test. This weakness of the MK test has not been addressed in this work. One perspective would be to compare the results obtained by the TFPW-MK procedure with other methods that make no assumptions about the distribution or independence of the time series. Another possibility is to apply parametric trend detection methods, such as linear regression, to the time series without serial structure, as in the TFPW-MK procedure. This way, the independence assumption imposed by parametric methods is circumvented.

### **1.6.2 EFFECTS OF CLIMATE VARIABLES ON GROUNDWATER LEVEL TRENDS**

To establish a causal relationship between the climate variables and the trends observed in GWL, a trend analysis of vertical inflow and potential evapotranspiration was performed. In this study, and probably due to the very small data set covering only 10 years, almost no significant trends were observed in the climate variables. However, vertical inflow and evapotranspiration are not the most appropriate indicators of changes in aquifer recharge. Indeed, aquifer recharge is a complex process that depends on other processes such as infiltration, runoff or capillary rise. Recharge is also conditioned by the diffusivity of the aquifer. Therefore, using trends in vertical inflow and evapotranspiration to establish a causal relationship with GWL trends is a far too simplistic model of reality. Ideally, and if the necessary data are available, a numerical model would better investigate the relationship between changes in climate variables and changes in GWL. An alternative, in the absence of sufficient data, is the use of reservoir models with transfer functions to study the response of the aquifer under the effect of a climate variable or a combination of climate variables.

### **1.6.3 LIMITATIONS OF FIELD OBSERVATIONS**

The reference hydrograph method, combined with consultation with groundwater resource managers, was used to analyze and identify local anomalies to understand the origin of the calculated trends. Although the reference hydrograph method identified periods during which groundwater dynamics were altered to induce the calculated trends, field observations serving as a possible explanation were identifiable for only 33% of the observation wells that exhibited moderate to large trends. For the remaining 67% of observation wells, no conclusions were drawn as to the origin of the trends. This indicates either that significant changes in the immediate environment of the concerned observation wells were not reported or that the reference hydrograph method is very sensitive to local GWL variations. In the first case, additional field investigations should be conducted to detect any significant changes not previously identified. In the second case, a comparison with other methods should be performed.

#### **1.6.4 QUESTIONING THE BASIS OF THE REFERENCE HYDROGRAPH METHOD**

Using the reference hydrograph method, the main hydrodynamic behaviours in a GWL monitoring network can be determined. A comparison of these reference hydrodynamic behaviours individually with those of the network's wells enables to identify local hydrodynamic deviations attributable to climatic variability or anthropogenic activities. Let us consider an ideal GW monitoring network for which all observation wells show the same hydrodynamic signatures with increasing trend due to a continuous recharge for example. Applying the hydrograph method to such a monitoring network will identify an absence of local deviation at individual observation well, which would mean that neither climatic variability nor anthropogenic activities has any effect on this monitoring network, which is not true. The reference hydrograph method is based on the idea that the absence of deviation implies the absence of natural or anthropogenic effect on groundwater dynamics. This hypothesis, which is not necessarily realistic, is probably one of the reasons why a cause-and-effect relationship between anthropogenic changes in the wells' immediate environment and the anomalies identified by the hydrograph method has not been trivially established. How to reconsider the fundamental assumption of the reference hydrograph method so that it better describes actual hydrodynamic behaviors is a question that would be worth investigating in future research.

#### **1.7 CONCLUSION**

In this study, a statistical methodology was proposed to test the hypothesis that it can be successfully used to explore historical trends in groundwater levels and understand their origin. Using the TFPW-MK procedure and a bootstrap test, trends at the scale of observation wells and their regional representativeness were examined. The use of the reference hydrograph method, combined with analysis of land-use change maps and consultation with groundwater resource managers, makes it possible to identify local anomalies in the GWL time series and attribute to them a possible

explanation based on changes observed in the immediate environment of the corresponding wells. The methodology, which requires only time series of groundwater levels, precipitation and temperature, has been tested using the Quebec groundwater monitoring network.

The results show that all but one of the observation wells in the monitoring network exhibited significant upward (38%) and downward (62%) trends at the 5% statistical significance level. However, the majority of observation wells (77%) have a trend magnitude of less than 3 cm/year in absolute value, the threshold below which the upward or downward rate of change is considered stable. The results also show that, proportionally, confined and unconfined aquifers are equally vulnerable to the influence of exogenous factors capable of significantly altering the dynamics of groundwater levels, while bedrock aquifers are twice as vulnerable to the influence of exogenous factors as granular aquifers.

The application of the bootstrap test confirmed the existence of a regional upward and downward trend, respectively, as the probability of the upward trend percentage being 38% and the downward trend percentage being 62% is estimated to be over 99% with a p-value well below 0.05. Thus, the Bootstrap test enabled to validate the regional representativeness of the trends calculated at the scale of the observation well. Trend analysis of vertical inflow and potential evapotranspiration show virtually no significant trends. Therefore, it was inferred that the trends in GWL are due to anthropogenic effects. The reference hydrograph method is used to identify periods when groundwater dynamics were altered to induce the calculated trends. Consultation with groundwater resource managers and analysis of land-use change maps enabled the identification of changes in the immediate environment of 33% of the observation wells with moderate to large trends. The changes observed in the wells' immediate environment could explain the GWL trends calculated in half of the 33% wells with moderate to large trends. For the remaining 67% of wells, no field changes are reported.

Although the methodology presented was easy to implement, it was not able to validate the initial hypothesis, probably due to its various limitations. First, although the TFPW-MK procedure circumvents the independence assumption of the time series, this procedure does not correct the fundamental weakness of the MK test which, for two almost identical time series, does not provide comparable S-statistic values. Thus, it is necessary to use multiple trend detection methods and compare their results to account for uncertainties and to better characterize trends in the monitoring network. Secondly, establishing a cause-and-effect relationship between changes in climate variables (vertical inflow and potential evapotranspiration) and trends in GWL is a far too simplistic model. Therefore, a more rigorous study of the relationships between climatic factors and groundwater levels can be performed using conceptual bucket-type hydrological models. Third, effective use of the hydrograph method to detect changes in groundwater level time series attributable to possible anthropogenic effects depends on the availability of field observations by groundwater resource managers and the reliability of land-use change maps. In addition, the assumption on which the reference hydrograph method is based should be re-examined in order to better describe actual hydrodynamic behaviors and reach meaningful inferences. Despite all these limitations, this study has highlighted the potential of the proposed methodology for the analysis of groundwater level monitoring networks. The proposed methodology could serve as a starting point for the development of a more mature methodology.

#### **CRediT authorship contribution statement**

**AVDP Adombi:** Conceptualization, Methodology, Data curation, Software, Visualization, Validation, Writing- Original draft preparation, Investigation. **Romain Chesnaux:** Conceptualization, Supervision, Resources, Reviewing and Editing. **Marie-Amélie Boucher:** Conceptualization, Supervision, Reviewing and Editing.

### **Acknowledgements**

The authors would like to thank the Quebec Ministry of the Environment for the data provided.

### **Funding sources**

The authors acknowledge the financial support of the Natural Sciences and Engineering Research Council (NSERC-federal funding) of Canada in the framework of the Individual Discovery Grant Program held by Prof. Romain Chesnaux. The financial support of Fondation de l'Université du Québec à Chicoutimi (FUQAC), Rio Tinto through its Excellence Scholarships program and Fonds de Recherche du Québec - Nature et Technologie (FRQNT-provincial funding) are also acknowledged.

### **Declaration of Competing Interest**

On behalf of all authors, the corresponding author states that there is no conflict of interest.

## REFERENCES

- Adombi, A.V.D.P. 2023a. Groundwater Monitoring Network Analysis Tool. doi:<https://doi.org/10.5281/zenodo.7933551>.
- Adombi, A.V.D.P. 2023b. Online Resource 2. Available from [https://github.com/avadombi/SupplementaryMaterial/blob/main/Article3/Supplementary\\_material\\_2.docx](https://github.com/avadombi/SupplementaryMaterial/blob/main/Article3/Supplementary_material_2.docx).
- Adombi, A.V.D.P. 2023c. Online Resource 1. Available from [https://github.com/avadombi/SupplementaryMaterial/blob/main/Article3/Supplementary\\_material\\_1.xlsx](https://github.com/avadombi/SupplementaryMaterial/blob/main/Article3/Supplementary_material_1.xlsx).
- Akakuru, O.C., Akudinobi, B., Opara, A.I., Onyekuru, S.O., and Akakuru, O.U. 2021. Hydrogeochemical facies and pollution status of groundwater resources of Owerri and environs, Southeastern Nigeria. Environmental monitoring and assessment, **193**: 623. doi:<https://doi.org/10.1007/s10661-021-09364-9>.
- Awadh, S.M., Al-Mimar, H., and Yaseen, Z.M. 2021. Groundwater availability and water demand sustainability over the upper mega aquifers of Arabian Peninsula and west region of Iraq. Environment, Development and Sustainability, **23**: 1-21. doi:<https://doi.org/10.1007/s10668-019-00578-z>.
- Banadkooki, F.B., Ehteram, M., Ahmed, A.N., Teo, F.Y., Fai, C.M., Afan, H.A., Sapitang, M., and El-Shafie, A. 2020. Enhancement of groundwater-level prediction using an integrated machine learning model optimized by whale algorithm. Natural resources research, **29**: 3233-3252. doi:<https://doi.org/10.1007/s11053-020-09634-2>.
- Bergeron, O. 2016. Guide d'utilisation 2016 - Grilles climatiques quotidiennes du Programme de surveillance du climat du Québec. Ministère du Développement durable, de l'Environnement et de la Lutte contre les changements climatiques, Direction du suivi de l'état de l'environnement version 1.2, Québec.
- Bhat, S., Motz, L.H., Pathak, C., and Kuebler, L. 2014. Geostatistics-based groundwater-level monitoring network design and its application to the Upper Floridan aquifer, USA.

Environmental monitoring and assessment, **187**: 4183. doi:<https://doi.org/10.1007/s10661-014-4183-x>.

Bikše, J., Retike, I., Haaf, E., and Kalvāns, A. 2023. Assessing automated gap imputation of regional scale groundwater level data sets with typical gap patterns. Journal of Hydrology, **620**: 129424. doi:<https://doi.org/10.1016/j.jhydrol.2023.129424>.

Collenteur, R.A., Bakker, M., Klammler, G., and Birk, S. 2021. Estimation of groundwater recharge from groundwater levels using nonlinear transfer function noise models and comparison to lysimeter data. Hydrol. Earth Syst. Sci., **25**: 2931-2949. doi:<https://hess.copernicus.org/articles/25/2931/2021/>.

Environmental Reporting BC. 2019. Long-term Trends in Groundwater Levels in B.C. Available from <https://www.env.gov.bc.ca/soe/indicators/water/groundwater-levels.html2023>.

Famiglietti, J.S. 2014. The global groundwater crisis. Nature Climate Change, **4**: 945-948. doi:<https://doi.org/10.1038/nclimate2425>.

Farrell, R.P., and Whiteman, M. 2023. The Environment Agency Chalk groundwater level monitoring network in England. Geological Society, London, Special Publications, **517**: 163-182. doi:<https://www.lyellcollection.org/doi/abs/10.1144/SP517-2022-274>.

Gagné, S., Larocque, M., Pinti, D.L., Saby, M., Meyzonnat, G., and Méjean, P. 2018. Benefits and limitations of using isotope-derived groundwater travel times and major ion chemistry to validate a regional groundwater flow model: example from the Centre-du-Québec region, Canada. Canadian Water Resources Journal / Revue canadienne des ressources hydriques, **43**: 195-213. doi:<https://doi.org/10.1080/07011784.2017.1394801>.

Gebremicael, T.G., Mohamed, Y.A., Betrie, G.D., van der Zaag, P., and Teferi, E. 2013. Trend analysis of runoff and sediment fluxes in the Upper Blue Nile basin: A combined analysis of statistical tests, physically-based models and landuse maps. Journal of Hydrology, **482**: 57-68. doi:<https://doi.org/10.1016/j.jhydrol.2012.12.023>.

Green, T.R., Taniguchi, M., Kooi, H., Gurdak, J.J., Allen, D.M., Hiscock, K.M., Treidel, H., and Aureli, A. 2011. Beneath the surface of global change: Impacts of climate change on groundwater. Journal of Hydrology, **405**: 532-560. doi:<https://doi.org/10.1016/j.jhydrol.2011.05.002>.

Halder, S., Roy, M.B., and Roy, P.K. 2020. Analysis of groundwater level trend and groundwater drought using Standard Groundwater Level Index: a case study of an eastern river basin of West Bengal, India. *SN Applied Sciences*, **2**: 507. doi:<https://doi.org/10.1007/s42452-020-2302-6>.

Hussain, M., and Mahmud, I. 2019. pyMannKendall: a python package for non parametric Mann Kendall family of trend tests. *Journal of Open Source Software*, **4**: 1556.

Kroes, J., van Dam, J., Supit, I., de Abelleira, D., Verón, S., de Wit, A., Boogaard, H., Angelini, M., Damiano, F., Groenendijk, P., Wesseling, J., and Veldhuizen, A. 2019. Agrohydrological analysis of groundwater recharge and land use changes in the Pampas of Argentina. *Agricultural water management*, **213**: 843-857. doi:<https://doi.org/10.1016/j.agwat.2018.12.008>.

Larocque, M., Cloutier, V., Levison, J., and Rosa, E. 2018. Results from the Quebec Groundwater Knowledge Acquisition Program. *Canadian Water Resources Journal / Revue canadienne des ressources hydriques*, **43**: 69-74. doi:<https://doi.org/10.1080/07011784.2018.1472040>.

Lee, J.-Y., Yi, M.-J., Yoo, Y.-K., Ahn, K.-H., Kim, G.-B., and Won, J.-H. 2007. A review of the National Groundwater Monitoring Network in Korea. *Hydrological Processes*, **21**: 907-919. doi:<https://doi.org/10.1002/hyp.6282>.

Lehr, C., and Lischeid, G. 2020. Efficient screening of groundwater head monitoring data for anthropogenic effects and measurement errors. *Hydrol. Earth Syst. Sci.*, **24**: 501-513. doi:<https://hess.copernicus.org/articles/24/501/2020/>.

Marchant, B.P., Cuba, D., Brauns, B., and Bloomfield, J.P. 2022. Temporal interpolation of groundwater level hydrographs for regional drought analysis using mixed models. *Hydrogeology Journal*, **30**: 1801-1817. doi:<https://doi.org/10.1007/s10040-022-02528-y>.

Meggiorin, M., Passadore, G., Bertoldo, S., Sottani, A., and Rinaldo, A. 2023. Comparison of Three Imputation Methods for Groundwater Level Timeseries. *Water*, **15**: 801. doi:<https://doi.org/10.3390/w15040801>.

MELCCFP. 2023a. Programme d'acquisition de connaissances sur les eaux souterraines. Available from <http://www.mddelcc.gouv.qc.ca/eau/souterraines/programmes/acquisition-connaissance.htm> [accessed January 2023].

MELCCFP. 2023b. Normales climatiques 1981-2010. Available from <https://www.environnement.gouv.qc.ca/climat/normales/climat-qc.htm> [2023].

Nath, B., Ni-Meister, W., and Choudhury, R. 2021. Impact of urbanization on land use and land cover change in Guwahati city, India and its implication on declining groundwater level. *Groundwater for Sustainable Development*, **12**: 100500. doi:<https://doi.org/10.1016/j.gsd.2020.100500>.

Oudin, L., Hervieu, F., Michel, C., Perrin, C., Andréassian, V., Anctil, F., and Loumagne, C. 2005. Which potential evapotranspiration input for a lumped rainfall–runoff model?: Part 2—Towards a simple and efficient potential evapotranspiration model for rainfall–runoff modelling. *Journal of Hydrology*, **303**: 290-306. doi:<https://doi.org/10.1016/j.jhydrol.2004.08.026>.

Pathak, A.A., and Dodamani, B.M. 2019. Trend Analysis of Groundwater Levels and Assessment of Regional Groundwater Drought: Ghataprabha River Basin, India. *Natural resources research*, **28**: 631-643. doi:<https://doi.org/10.1007/s11053-018-9417-0>.

Patle, G.T., Singh, D.K., Sarangi, A., Rai, A., Khanna, M., and Sahoo, R.N. 2015. Time series analysis of groundwater levels and projection of future trend. *Journal of the Geological Society of India*, **85**: 232-242. doi:<https://doi.org/10.1007/s12594-015-0209-4>.

Qureshi, A.S., Gill, M.A., and Sarwar, A. 2010. Sustainable groundwater management in Pakistan: challenges and opportunities. *Irrigation and Drainage*, **59**: 107-116. doi:<https://doi.org/10.1002/ird.455>.

Rey, N., Rosa, E., Cloutier, V., and Lefebvre, R. 2018. Using water stable isotopes for tracing surface and groundwater flow systems in the Barlow-Ojibway Clay Belt, Quebec, Canada. *Canadian Water Resources Journal / Revue canadienne des ressources hydriques*, **43**: 173-194. doi:<https://doi.org/10.1080/07011784.2017.1403960>.

- Rivard, C., Vigneault, H., Piggott, A.R., Larocque, M., and Anctil, F. 2009. Groundwater recharge trends in Canada. Canadian Journal of Earth Sciences, **46**: 841-854. doi:<https://doi.org/10.1139/E09-056>.
- Rivera, A. 2014. Canada's groundwater resources. Fitzhenry & Whiteside.
- Sahoo, S., Russo, T.A., Elliott, J., and Foster, I. 2017a. Machine learning algorithms for modeling groundwater level changes in agricultural regions of the U.S. Water Resources Research, **53**: 3878-3895. doi:<https://doi.org/10.1002/2016WR019933>.
- Satish Kumar, K., and Venkata Rathnam, E. 2019. Analysis and Prediction of Groundwater Level Trends Using Four Variations of Mann Kendall Tests and ARIMA Modelling. Journal of the Geological Society of India, **94**: 281-289. doi:<https://doi.org/10.1007/s12594-019-1308-4>.
- Sen, P.K. 1968. Estimates of the Regression Coefficient Based on Kendall's Tau. Journal of the American Statistical Association, **63**: 1379-1389. doi:<https://doi.org/10.1080/01621459.1968.10480934>.
- Shamsuddoha, M., Chandler, R.E., Taylor, R.G., and Ahmed, K.M. 2009. Recent trends in groundwater levels in a highly seasonal hydrological system: the Ganges-Brahmaputra-Meghna Delta. Hydrol. Earth Syst. Sci., **13**: 2373-2385. doi:<https://doi.org/10.5194/hess-13-2373-2009>.
- Sonali, P., and Nagesh Kumar, D. 2013. Review of trend detection methods and their application to detect temperature changes in India. Journal of Hydrology, **476**: 212-227. doi:<https://doi.org/10.1016/j.jhydrol.2012.10.034>.
- Thomas, E.A., Needoba, J., Kaberia, D., Butterworth, J., Adams, E.C., Oduor, P., Macharia, D., Mitheu, F., Mugo, R., and Nagel, C. 2019. Quantifying increased groundwater demand from prolonged drought in the East African Rift Valley. Science of the Total Environment, **666**: 1265-1272. doi:<https://doi.org/10.1016/j.scitotenv.2019.02.206>.
- Valéry, A. 2010. Modélisation précipitations débit sous influence nivale : Elaboration d'un module neige et évaluation sur 380 bassins versants. Doctorat Hydrobiologie, Institut des Sciences et Industries du Vivant et de l'Environnement AgroParisTech.

- Valéry, A., Andréassian, V., and Perrin, C. 2014. 'As simple as possible but not simpler': What is useful in a temperature-based snow-accounting routine? Part 2 – Sensitivity analysis of the Cemaneige snow accounting routine on 380 catchments. *Journal of Hydrology*, **517**: 1176-1187. doi:<https://doi.org/10.1016/j.jhydrol.2014.04.058>.
- Vu, M.T., Jardani, A., Massei, N., and Fournier, M. 2021a. Reconstruction of missing groundwater level data by using Long Short-Term Memory (LSTM) deep neural network. *Journal of Hydrology*, **597**: 125776. doi:<https://doi.org/10.1016/j.jhydrol.2020.125776>.
- Wada, Y., van Beek, L.P.H., van Kempen, C.M., Reckman, J.W.T.M., Vasak, S., and Bierkens, M.F.P. 2010. Global depletion of groundwater resources. *Geophysical Research Letters*, **37**. doi:<https://doi.org/10.1029/2010GL044571>.
- Walter, J., Rouleau, A., Chesnaux, R., Lambert, M., and Daigneault, R. 2018. Characterization of general and singular features of major aquifer systems in the Saguenay-Lac-Saint-Jean region. *Canadian Water Resources Journal / Revue canadienne des ressources hydriques*, **43**: 75-91. doi:<https://doi.org/10.1080/07011784.2018.1433069>.
- Wanda, E., Monjerezi, M., Mwatseteza, J.F., and Kazembe, L.N. 2011. Hydro-geochemical appraisal of groundwater quality from weathered basement aquifers in Northern Malawi. *Physics and Chemistry of the Earth, Parts A/B/C*, **36**: 1197-1207. doi:<https://doi.org/10.1016/j.pce.2011.07.061>.
- Wu, Y. 2004. Optimal design of a groundwater monitoring network in Daqing, China. *Environmental Geology*, **45**: 527-535. doi:<https://doi.org/10.1007/s00254-003-0907-x>.
- Yesertener, C. 2005. Impacts of climate, land and water use on declining groundwater levels in the Gnangara Groundwater Mound, Perth, Australia. *Australasian Journal of Water Resources*, **8**: 143-152. doi:<https://doi.org/10.1080/13241583.2005.11465251>.
- Yira, Y., Diekkrüger, B., Steup, G., and Bossa, A.Y. 2016. Modeling land use change impacts on water resources in a tropical West African catchment (Dano, Burkina Faso). *Journal of Hydrology*, **537**: 187-199. doi:<https://doi.org/10.1016/j.jhydrol.2016.03.052>.

Yue, S., and Wang, C.Y. 2002. Applicability of prewhitening to eliminate the influence of serial correlation on the Mann-Kendall test. *Water Resources Research*, **38**: 4-1-4-7.  
doi:<https://doi.org/10.1029/2001WR000861>.

Yue, S., Pilon, P., and Cavadias, G. 2002a. Power of the Mann–Kendall and Spearman's rho tests for detecting monotonic trends in hydrological series. *Journal of Hydrology*, **259**: 254-271.  
doi:[https://doi.org/10.1016/S0022-1694\(01\)00594-7](https://doi.org/10.1016/S0022-1694(01)00594-7).

Yue, S., Pilon, P., and Phinney, B.O.B. 2003. Canadian streamflow trend detection: impacts of serial and cross-correlation. *Hydrological Sciences Journal*, **48**: 51-63.  
doi:<https://doi.org/10.1623/hysj.48.1.51.43478>.

Yue, S., Pilon, P., Phinney, B., and Cavadias, G. 2002b. The influence of autocorrelation on the ability to detect trend in hydrological series. *Hydrological Processes*, **16**: 1807-1829.  
doi:<https://doi.org/10.1002/hyp.1095>.

Zakaria, N., Anornu, G., Adomako, D., Owusu-Nimo, F., and Gibrilla, A. 2021. Evolution of groundwater hydrogeochemistry and assessment of groundwater quality in the Anayari catchment. *Groundwater for Sustainable Development*, **12**: 100489.  
doi:<https://doi.org/10.1016/j.gsd.2020.100489>.